STRUCTURE AND REACTIVITY OF TITANIA-SUPPORTED MOLYBDENUM AND VANADIUM OXIDES

A THESIS SUBMITTED FOR THE DEGREE OF DOCTOR OF PHILOSOPHY

BY

SAAD FLAMERZ TAHIR

MAY 1987

CHEMISTRY DEPARTMENT
BRUNEL UNIVERSITY
UXBRIDGE, MIDDLESEX
UNITED KINGDOM

ALL MISSING PAGES ARE BLANK

IN

ORIGINAL

TO MY FAMILY

ABSTRACT

Vanadium and molybdenum oxide catalysts have been prepared on different TiO_2 supports by a variety of methods. Solutions of $VOCl_3$, $VO(O^iBu)_3$ and $MoOCl_4$ were used to graft VO_X and MoO_X monolayers onto the supports in a single treatment. The other methods were intended to produce more than one monolayer (i.e. aqueous impregnation and multiple treatments of $VOCl_3$ and $VO(O^iBu)_3$).

TPR and Raman spectroscopy showed the formation above the monolayer of a phase denoted as disordered vanadium oxide, which has the same reducibility as the monolayer species but which has a band in the Raman spectrum at 995 cm^{-1}. Raman spectroscopy also showed the formation of a disordered molybdenum oxide phase. With supports which contained phosphorus and potassium as impurities, TPR and Raman spectoscopy indicated a potassium-containing vanadium oxide, which was difficult to reduce and which showed no band at 995 cm^{-1}. "Paracrystalline" V_2O_5 and MoO_3 are formed when the oxide content exceeds four monolayers. XPS measurements confirm the dispersion of MO_X species (M = V, Mo) on the surface of the support in the monolayer region; they also show that disordered and paracrystalline oxide phases occupy a limited area of the monolayer surface, but could not distinguish between them. ESR results showed 95% of the supported vanadium in the oxidation state +5.

Phosphorus and potassium impurities in (or on) the TiO_2 support influence the structure and catalytic properties of the VO_X monolayer phase.

In the case of catalysts made on supports with low

impurities, activities in butadiene oxidation and isopropanol decomposition are principally due to the monolayer species and little contribution is made by the disordered or paracrystalline V_2O_5, while in the catalysts made on the supports with relatively high level of impurities, the activities in both reactions increase with V_2O_5 content in the region of one to four monolayers. MoO_x catalysts showed low activities and selectivities in butadiene oxidation.

ACKNOWLEDGEMENTS

I wish to express my sincere gratitude to Professor G.C. Bond for his guidance and continuous encouragement throughout my research.

I am grateful to Dr. J.G. van Ommen and Mr. H. Bosch (Twente University of Technology, The Netherlands) for valuable discussions.

I am also grateful to Dr. Michael Gelsthorpe for his advice and discussions on temperature-programmed reduction and Mr. Edward Aidam for his help in using the Wordwise.

My sincere thanks to all the technical staff at Brunel. I also wish to thank University of Mosul, Iraq for providing the financial support.

I am grateful to my colleagues Dr. Raj Rajaram, Dr. Brian Riley, Stephen Namijo and Miss Rosiyah Yahya for informal discussion, friendship and also for creating a very pleasant atmosphere in which to work. I wish to thank Mrs Rita James for all her help.

Moral support from my brother, Mr. Hussein Tahir is greatly acknowledged.

Last but not least, I am grateful to my wife, Fouziea, for her continuous moral support and encouragement throughout my work.

CONTENTS

CHAPTER 1

INTRODUCTION

1.1 Catalysts based on vanadium oxide

Vanadium oxides have been intensively studied because of their importance as catalysts. Vanadium oxide-based catalysts are used extensively for the selective oxidation of hydrocarbons in the chemical industry for the production of monomers (acrylic acid and styrene), compounds for polyester resins (maleic anhydride) and dyes (anthraquinone). Table 1.1 lists the usage and typical catalysts involved in the processes(1).

Table 1.1

Industrial applications of vanadia-based catalysts.

catalyst	reaction
V_2O_5-Sb_2O_5-MoO_3	$H_3C-CH=CH_2 + 3/2O_2 \rightarrow H_2C=CH-C(=O)OH$ propene → acrylic acid
V_2O_5-P_2O_5	$H_3C-CH_2-CH=CH_2 + 3O_2 \rightarrow$ 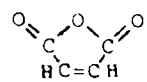 $+ 3H_2O$ butene → maleic anhydride
V_2O_5, V_2O_5-MoO_3, V_2O_5-Sb_2O_3	 $+ 9/2O_2 \rightarrow$ maleic anhydride $+ 2CO_2 + 2H_2O$ benzene
V_2O_5-MgO	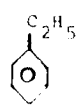 $+ 1/2O_2 \rightarrow$ 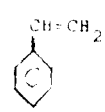 $+ H_2O$ ethyl benzene
V_2O_5 (dopants:K,Sn,Nb)	 $+ 3O_2 \rightarrow$ 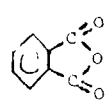 $+ 3H_2O$ o-xylene → phthalic anhydride
V_2O_5(dopants:K,Na)	 $+ 9/2O_2 \rightarrow$ phthalic anhydride $+ 2CO_2 + 2H_2O$
V_2O_5, V_2O_5-MoO_3	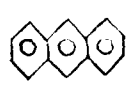 $+ 3/2O_2 \rightarrow$ 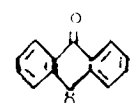 $+ H_2O$ anthraquinone

1.1.1 Unsupported V_2O_5

V_2O_5 has a complicated orthorhombic structure. The severly distorted octahedral coordination of oxygen ions around a vanadium ion is shown in Figure 1.1.

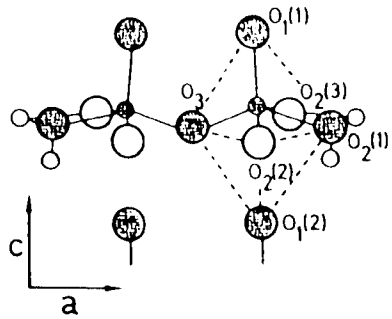

interatomic distance(Å)(2)	
$V-O_1(1)$	1.586
$V-O_1(2)$	2.788
$V-O_2(1)$	2.022
$V-O_2(2)$	1.889
$V-O_2(3)$	2.029
$V-O_3$	1.780

Figure 1.1 Oxygen coordination of vanadium in V_2O_5 (based on data from Rŭzicka(3)).

The length of bond $V-O_1(1)$ is indicative of a doubly bonded "vanadyl" oxygen, V=O. This V=O species is present on the ab-plane. Since the $V-O_1(2)$ bond is very long, it is probably a weak van der Waals bond. V_2O_5 has a layered structure with a cleavage plane parallel to ab-plane.

The activity of V_2O_5 is related to the number of oxygen vacancies, or the equivalent number of V^{4+} ions. Generally(4-7) it is assumed that the oxygen vacancies are preferentially formed at the vanadyl-oxygen ions.

It is generally accepted that the lower oxides derived from V_2O_5, i.e. V_4O_9, V_6O_{13} and VO_2 also play an important role: they can be understood in terms of the formation of vanadyl-oxygen vacancies. Different opinions about these active and selective species have appeared in the literature(8,9). The origin of the differences in activity and selectivity of the various oxides is thought to

reside in the structure. V_2O_3 is not considered because it is not present in the steady state under catalytic reaction conditions(9).

1.1.2 Vanadates

A relatively common compound that contains an isopolyanion is the cream-coloured solid, NH_4VO_3. The compound contains infinite chains of VO_4 tetrahedra. Due to this polymeric structure of the anion, NH_4VO_3 is not particularly soluble in cold water. However, when the compound is heated with water, the isopolyanion is broken up and the solid readily dissolves. Control of temperature and acidity of this solution permits isolation of other ammonium isopolyvanadates such as $NH_4V_3O_8$ and $(NH_4)_6V_{10}O_{28}.6H_2O$. These transformations all involve protonation-condensation reactions of V(V). VO_4^{3-} exists only in very basic solution and VO^{2+} only in very acidic solution(10).

Another class of vanadate compounds is the vanadium bronzes(11-16). In these compounds V^{4+} ions are stabilised in the V_2O_5 lattice: this provides the possibility to study the effect of a known concentration of V^{4+} ions. In this way, it is possible to test the hypothesis that the catalytic activity of vanadia is improved by an enhanced concentration of V^{4+}.

Vanadium bronzes are non-stoichiometric interstitial solid-solutions of a singly ionised metal M in V_2O_5 with the formula $M_xV_2O_5 (0<x<1)$. To maintain electrical neutrality, a fraction x of the V^{5+} ions has been converted into V^{4+} (for $0<x<1$). Therefore, the composition is more accurately

designated

$$M_x^{1+}V_x^{4+}V_{2-x}^{5+}O_5 \qquad 0<x<1$$

where M = Ag, K and Na.

ESR(17) and NMR(18) studies have indicated the metal to be singly ionised (M^+). β-phase vanadium bronzes are found to exist for almost all univalent metals.

1.1.3 Vanadium-phosphorus oxide(VPO_X)

Maleic anhydride (MA) is an important intermediate in a large number of chemical processes. Two processes are currently used to product MA on the industrial scale. The first is benzene oxidation over V_2O_5-MoO_3 catalysts (19); the second is oxidation of C_4 feedstocks over VPO_X catalysts (20). For economic and technical reasons, enormous strides have been made in recent years to produce MA from C_4 (butane, butene and butadiene) hydrocarbons. The number of patents published bear witness to this. It will be wise to assume therefore that industry intends to switch from benzene to C_4 hydrocarbons as the starting material for MA synthesis in the 1980's (19-21). Catalysts that are active and selective in the oxidation of C_4 hydrocarbons include VPO_X based catalysts.

This type of catalyst is normally prepared in one of two ways: first, by reducing V_2O_5 with HCl, or NH_4VO_3 with $H_2C_2O_4$ (22), or V_2O_5 with N_2H_4 (23), followed by addition of the appropriate amount of phosphorus, usually as H_3PO_4, to give the desired P:V ratio. Secondly, they are prepared in

non aqueous media: V_2O_5 is reduced using a mixture of isobutyl and benzyl alcohols (24) followed by addition of H_3PO_4 to give the desired P:V ratio. The precursor is isolated by precipitation or by evaporation of the solvent. If a supported catalyst is required, the evaporation method is chosen; then the support material is added, followed by the evaporation of the solvent to obtain a uniform deposition of the mixed oxides on the support (25,26).

Many attempts have been made to increase the activity, selectivity and lifetime of these catalysts. These include adding small quantities of a third metal as a modifier. The role of some additives, such as alkaline earth metals, is to suppress sublimation of phosphorus at the high temperatures at which these catalysts are used. However, these modifying substances, which include Fe, Cu, Zn, Zr, Ti, U, Si or Co, have been claimed to increase the selectivity of these catalysts (22,27-29). Activation is usually carried out by slowly heating the precursor in a flow of air or an air-hydrocarbon mixture identical to that which is eventually used as feed (30,31).

The P:V ratio exceeds 1.1:1 in the vast majority of patents. The role of phosphorus in diminishing the activity but increasing the selectivity for partial oxidation of C_4 hydrocarbons on mixed VPO_x catalysts has been known for many years. Information abstracted from some of the published patents is given in Table 1.2.

Table 1.2

Information from patents on oxidation of C_4-hydrocarbons to maleic anhydride (MA) using VPO_x catalysts.

catalyst (P/V)	feed	contact time(s)	temp.°C	yield %	select. %	conv. %	ref.
1.2:1	1% $n\text{-}C_4H_{10}$ in air	7.2	425	20	--	34	32a
1:1	1.5% $n\text{-}C_4H_{10}$ in air	3.6	446	--	47	--	32b
1.2:1	$n\text{-}C_4H_{10}$	2	389	62	69	89	32c
3:1	0.5% $1\text{-}C_4H_8$ in air	0.6	425	49	--	100	32d
PVO_x/Al_2O_3 P/V:0.6	0.5% C_4H_8 in air	---	450	62.4	--	--	32e
1:1	1.5% $n\text{-}C_4H_{10}$ in air	7	440	64	--	93	32f
$VO(PO_3)_2$	1% $1,3\text{-}C_4H_6$ in air	1.2	375	--	67.5	--	32g

It has been shown that the nature of the compounds obtained after calcination is influenced by the P:V ratio, the method and the atmosphere of calcination. In many studies strong emphasis has been placed on trying to identify which phase or phases are present in these catalysts. Some of these phases, such as α-$VOPO_4$ (33,34) and β-$VOPO_4$ (34,35) are the most commonly cited phases containing V in the +5 oxidation state. Phases containing V in the +4 oxidation state include a phase variously labelled as β (36), $(VO)_2P_2O_7$ (30,34) and a β^*-phase, a poorly crystalline material which transforms slowly into β-$VOPO_4$ upon heating in air (37). Other phases have been detected, such as B (31), $(VO)_2P_2O_7 \cdot 2H_2O$ or the α-phase (31)

and a $VOHPO_4 . 1/2H_2O$ phase (38-40).

It has been mentioned in the literature that since selective oxidation on heterogeneous catalysts is a redox process (26), the presence of V in two different oxidation states is important. The oxidation state in which V is present determines the selectivity of this system. A large concentration of V^{4+} favours selective oxidation, whereas V^{5+} is believed to favour total oxidation processes (25). Bordes and Courtine (30) have suggested that the "active phase" for 1-butene oxidation to maleic anhydride is the interface between two phases ($(VO)_2P_2O_7$ and β-$VOPO_4$). Varma and Saraf (26) studied the same reaction and they proposed a two-stage redox mechanism. They also concluded that maleic anhydride is hardly oxidized to CO and CO_2, which are mainly formed in a side reaction from the original hydrocarbon. Brkic and Trifiro (41) studied the reaction of 1-butene and 1,3-butadiene over VPO_X catalysts and have proposed a reaction pathway involving conversion of 1-butene to 1,3-butadiene by a redox mechanism utilizing lattice oxygen. Subsequent conversion of butadiene to maleic anhydride was believed to occur on another site involving an adsorbed oxygen species. The role of the partial pressure of O_2 in the oxidation of 1-butene and butadiene to maleic anhydride for VPO_X catalysts has been examined by Cavani et al.(42). Their model for the reaction pathway involves butadiene and furan as intermediate products. Ai (43) proposed the same reaction scheme for butene, butadiene and furan oxidation over V_2O_5 and V_2O_5-P_2O_5 catalysts. He also indicated the formation of side products (mainly CO, CO_2 and some polymers) for each step and concluded that each intermediate

step had different rates for the conversion to partially oxygenated products as compared to the conversion to side products. Ai and Suzuki (44) discussed the same reaction pathway involving consecutive steps

$$C_4H_8 \rightarrow C_4H_8(ads) \rightarrow C_4H_6(ads) \rightarrow C_4H_4O(ads) \rightarrow MA$$

for their studies of butene, butadiene and furan oxidation over MoO_3-P_2O_5 catalysts containing Bi_2O_3. Cavani et al. (45) found that, in the oxidation of 1-butene on VPO_x catalysts, the first step of the reaction is the dehydrogenation of 1-butene to butadiene which is accompanied by the formation of V(III) ions. The second step of the reaction, i.e., the oxidation of the adsorbed intermediate to maleic anhydride and to CO and CO_2, requires V(V) ions, as found by Hodnett and Delmon (37), Brkic and Trifiro (41) and Ai(43). Centi et al. (46) reported results showing that the rate-limiting step for n-butane oxidation to maleic anhydride is the formation of the corresponding olefins.

Numerous side products are formed in parallel reactions. Bordes and Courtine (30) reported acetaldehyde, acrolein, methacrolein, acetic, propionic and acrylic acids and in smaller amounts, methyl ethyl ketone, methyl vinyl ketone and crotonaldehyde. Varma and Saraf (26) found acetic acid, acetaldehyde, acrolein and butyraldehyde.

Cavani et al. (47) studied the influence of P on the selectivity of n-butane oxidation to maleic anhydride. They found that the deficiency of P with respect to a P:V atomic ratio of 1.0 enhances the rate of maleic anhydride

decomposition, leading to lower yields of maleic anhydride at high conversion. An excess of P limits the rate of maleic anhydride decomposition,but decreases both the activity of the catalyst and the ratio of the two parallel rates of maleic anhydride and carbon oxides formation from n-butane. Hodnett and Delmon (48) found that VPO_X catalysts (range 0.94-1.10:1) gave higher activity and selectivity for n-butane oxidation to maleic anhydride when calcined at 650°C and reduced in H_2 at 450°C than when just calcined in air at 500°C. Cavani et al. (24) studied C_4 oxidation to maleic anhydride by VPO_X catalysts prepared in organic and aqueous media. The VPO_X catalyst prepared in an organic medium makes it possible to oxidise n-butane at lower temperatures than with VPO_X catalyst prepared in aqueous medium. Busca et al. (49) prepared $(VO)_2P_2O_7$ in both aqueous and an organic media. They found that $(VO)_2P_2O_7$ prepared in an organic medium is much more active in n-butane selective oxidation than the one prepared in aqueous medium , whereas no significant differences are found in butene oxidation. Buchanan et al. (50) studied butane oxidation to maleic anhydride on VPO_X catalyst prepared using an organic medium. They found that the catalyst washed with boiling methanol gives high activity and yield of maleic anhydride due to removal of a surface phase rich in P and V(V).

Recently Hodnett (51) has published a review on the VPO_X catalysts for the selective oxidation of C_4 hydrocarbons to maleic anhydride.

1.1.4 Supported vanadium oxide

Supported vanadium oxide catalysts are used in industrial processes such as the selective oxidation (52-60) and ammoxidation (61,62) reactions. Most of these catalysts are doped with promoters to improve their activity and/or selectivity. The supports are used to improve the mechanical strength, the thermal stability and lifetime of the catalytic system (63). For a long time these supports were believed to be inert in the chemical reaction. It is now known, however, that the structure and the composition of the materials used as supports offers a means for influencing the catalytic activities and selectivities of the active phase applied (64-67). The vanadium oxide is most efficiently used when it is present as a layer applied as thinly as possible over the surface of the support. The active component is present as a monolayer or monomolecular dispersion and is maximally influenced by the support. Such an influence can considerably affect the activity and selectivity of the active species in the oxidation reactions (56, 68-71).

A large number of supported V_2O_5 catalysts are used in the selective oxidation of hydrocarbons; typical catalyst supports in common use are Al_2O_3 and SiO_2. The most effective catalyst for the process has proved to be a combination of V_2O_5 and TiO_2(anatase). The effect of TiO_2 supports in the selective oxidation of hydrocarbons is currently a topic of investigation. A catalyst consisting of V_2O_5 and TiO_2(anatase) has been used in the selective oxidation of butadiene, 1-butene and benzene to maleic anhydride (MA), and naphthalene and o-xylene to phthalic

anhydride (PA). There have been numerous investigations of V_2O_5/TiO_2 catalysts: some of the research is summarised in Table 1.3.

Table 1.3

Selective oxidation on V_2O_5/TiO_2 catalysts

reactant	product	reaction temp.°C	reference
o-xylene	PA	320-380	56
n-butene	acetic acid acetaldehyde	180-300	72
benzene	MA	389	73
butadiene	MA, Furan	250-300	74
methanol	formaldehyde	274	75

It appears that the use of the V_2O_5/TiO_2 catalyst may result in improved activity or selectivity for hydrocarbons oxidation reactions. This means that the TiO_2 plays a role, not only as a support, but also has a distinct promoting influence on the catalytic properties of the V_2O_5 phase. Since V_2O_5 by itself or supported on the other oxides (e.g. Al_2O_3 or SiO_2) is rather an indifferent catalyst for these reactions, the improvements shown by V_2O_5/TiO_2 may be connected with the close structural similarities between V_2O_5 and TiO_2(anatase) as suggested by Vejux and Courtine (76).

1.1.4.1 Monolayer catalysts

As explained in the beginning of the Section 1.1.4, the metal oxides are most efficiently used and also maximally influenced if they are present as a thin layer on the support.This arrangement has several advantages over the bulk oxides, e.g. a higher mechanical strength, a better

thermal stability and a large surface area.

The concept of a monolayer in oxidic catalysts is not new: Russell and Stokes (77) observed, when measuring the dehydrogenation activity of MoO_3/Al_2O_3 catalysts, that maximum activity occured when the Al_2O_3 surface was covered completely by a monolayer of Mo(VI)-oxide. Their catalysts were prepared by impregnation of the Al_2O_3 with a solution of ammonium paramolybdate. In most cases, Mo, W and V oxides on several supports like Al_2O_3, SiO_2, ZrO_2, MgO and TiO_2 are prepared by the impregnation method (78-89). This method has the disadvantage that metal oxide crystallites may already be formed at low surface coverages in addition to a monolayer or monomolecular dispersion. It is observed that in catalyst preparation by impregnation, contact between the active component solution and support material, a monolayer or monomolecular dispersion of the active component is deposited on the support first. This interacts chemically with the outer layer of the support material. It is obvious that such catalytic systems can have properties that different from bulk metal oxide.

Several methods were used to put the metal oxide onto the surface of the support as a monolayer or monomolecular dispersion. These methods involve a specific chemical reaction between surface hydroxyl groups of the support and a metal compound. One of these methods was used by Yermakov (90). He adsorbed organometallic compounds of V, Mo, Cr, Ni, Pd, Pt, W and Zr on the supports. He claimed to have a well-dispersed metal oxide on supports like SiO_2 and Al_2O_3. Buiten (91) described a method for preparing a Mo(VI)-oxide monolayer catalyst by chemisorbing gaseous

$MoO_2(OH)_2$ at 600°C on SnO_2. The Mo(VI) compound is though to react with the hydroxyl groups on the support surface. A similar method to that above was used to prepare Mo(VI)-oxide monolayer on Al_2O_3 (92), and on Al_2O_3, TiO_2 and SiO_2 (93). Roozeboom et al. (94) also prepared a V(V)-oxide monolayer catalyst by chemisorbing gaseous $V_2O_3(OH)_4$ at 600°C on Al_2O_3. Monolayer catalysts of V, Mo and W oxides on a number of supports (Al_2O_3, TiO_2, SiO_2, Cr_2O_3 and CeO_2) were prepared by adsorption of vanadate, molybdate and tungstate ions from acidic aqueous solutions respectively (92-96). This technique is called ion-exchange. Wang and Hall (97) prepared Mo, W, Cr and V oxides monolayer on a number of supports (Al_2O_3, TiO_2, MgO and SiO_2) using an equilibrium adsorption technique. Ng and Gulari (83) prepared a Mo(VI)-oxide monolayer catalyst using an equilibrium adsorption at pH = 2 using TiO_2(P-25) as support. Leyrer et al. (98) have prepared $Mo(VI)O_x$ monolayer catalysts on different supports like Al_2O_3, CeO_2 and TiO_2 by the incipient wetness method using paramolybdate solutions at pH = 6 as the impregnating solution, while crystallites of MoO_3 were detected on SiO_2 and ZrO_2. Yoshida et al. (80) impregnated the Al_2O_3 or SiO_2 with a solution of NH_4VO_3 followed by dissolution of the "isolated massive V_2O_5" with NH_4OH. After the dissolution process, they obtained a residual V(V)-oxide which was chemically interacting with the support, i.e. a monolayer.

Another method used to prepare monolayer catalysts involves chemical reaction of the surface hydroxyl groups of the support with the vanadium halide. Chien (99) used VCl_4 in gaseous form to prepare a well-dispersed V(V)-oxide on

SiO_2 and Al_2O_3. Malygin et al. (100) prepared a similar catalyst using $VOCl_3$ in gaseous form instead of VCl_4. Bond and Konig (101) however went a step further. They prepared the catalyst like Malygin et al. (100) using a TiO_2 as support but they increased the amount of VO_x on the surface by rehydroxylating the prepared catalyst and contacting the product with $VOCl_3$ in gaseous form again. This process was repeated in a cyclic manner. Murakami et al. (102) used the same technique as Bond and Konig (101) but utilized Al_2O_3. $VOCl_3$ dissolved in CCl_4 was used to prepare monolayer catalysts on various supports (103-106). Bond and Bruckman (68) and Busca et al. (74) used $VOCl_3$ dissolved in benzene and TiO_2 as support to prepare VO_x monolayer catalysts. Kijenski et al. (107,108) have described a method for preparation of VO_x monolayers on Al_2O_3, SiO_2, MgO and TiO_2. In this method $VO(O^iBu)_3$ in an organic solvent reacts with hydroxyl groups on the surface of the support, but an incomplete monolayer is obtained in case of a TiO_2 support. van Hengstum et al. (109,110) have described three methods to prepare monolayer catalysts using metal acetylacetonates dissolved in toluene and ethanol. The first method is called continuous adsorption which basically is that used by Sonnemans and Mars (92) involving the adsorption of the active component from the liquid phase. The second method, called batch adsorption, involves a metal acetylacetonate complex dissolved in toluene or ethanol. The third method, wet impregnation, involves the dissolution of the metal acetylacetonate in an excess of ethanol or toluene. This solution is then added to the support followed by slow evaporation of the solvent. The resulting catalyst is washed

throughly with pure solvent. These methods have been applied for the preparation of V, Mo and Fe monolayer catalysts on various supports.

1.1.4.2 Characterisation

In recent years there has been a growing emphasis on the study of the structure and composition of catalytically active surface phases containing V ions, their dependence on the method of preparation and on the degree of surface coverage, nature of the support and their relation to catalytic properties. The existence of different surface vanadium oxides on various supports has been the subject of several studies (7,84,85,109,111-117). For the characterisation of supported V(V)-oxide catalysts, a large number of analytical techniques are available such as temperature programmed reduction (TPR), laser Raman spectroscopy, X-ray photoelectron spectroscopy (XPS), Fourier transform infrared spectroscopy (FTIR) and electron spin resonance (ESR).

Laser Raman spectroscopy

Raman spectroscopy is a valuable technique in catalytic research because different surface and bulk phases of vanadium oxide on surface of catalyst can be investigated. As reported (118) bulk V_2O_5 exhibits Raman peaks at 997, 700 and 485 cm^{-1}. The peak at 997 cm^{-1} is associated with the symmetrical stretching mode of the terminal oxygen atom (V=O). The VO_x catalysts supported on Al_2O_3, SiO_2 and TiO_2 prepared by wet impregnation (84,111) examined by Raman spectroscopy showed that at low V content, isolated $VO4^{2-}$

tetrahedra (830 cm^{-1}) and a two dimensional polymeric network of distorted octahedra (970 and shoulder at 995 cm^{-1}) exist. At higher concentrations crystalline V_2O_5 is formed. The same authors (84,111) studied the Raman spectra of VO_x monolayer catalysts supported on Al_2O_3, SiO_2 and TiO_2 prepared by ion-exchange. These did not exhibit lines due to crystalline V_2O_5. The dominant species is the two dimensional network of distorted vanadate octahedra, together with a minor amount of isolated $VO4^{2-}$ tetrahedra. An exception was SiO_2 on which crystalline V_2O_5 was formed by both preparation techniques. In the case of TiO_2, the authors experienced difficulties in detecting the $VO4^{2-}$ tetrahedra peak due to overlap with the strong anatase bands. van Hengstum (95) studied the Raman spectrum of VO_x/TiO_2 catalyst prepared by adsorption of vanadate ions from an acidic aqueous solution. He found a relatively broad weak band in the region of 1030 cm^{-1} and proposed that the breadth of the band pointed to the presence of a crystallographically ill-defined VO_x complex on the surface of the TiO_2 support. van Hengstum et al. (109) also prepared a series of VO_x/TiO_2 catalysts by adsorption of vanadium acetylacetonate on the TiO_2 surface and examined them by Raman spectroscopy. They found that crystalline V_2O_5 formed when the VO_x monolayer was complete. The same group studied (119) the Raman spectra for two series of VO_x/TiO_2"1" and VO_x/TiO_2"2" catalysts prepared by successive impregnation of vanadium acetylacetonate from ethanol or by adsorption from toluene. The TiO_2"1" support contained 0.24% K_2O and 0.38% P_2O_5 as impurities while TiO_2"2" support contained 0.07% K_2O and 0.14% P_2O_5 as impurities. Crystalline V_2O_5 was detected

in the case of VO_x/TiO_2"2" above the formation of the monolayer. In the case of VO_x/TiO_2"1" catalysts above the monolayer, crystalline V_2O_5 is not formed as is usually observed for VO_x/TiO_2"2" catalysts, but some kind of amorphous structure not detectable with Raman spectroscopy. Crystalline V_2O_5 is formed only at a V_2O_5 concentration which is equivalent to three monolayers. Chan et al. (117) studied the Raman spectrum for 7 wt.% V_2O_5/TiO_2(anatase, low area) in the range 750-1250 cm^{-1}. They found two bands: the symmetrical stretching mode of the terminal oxygen atom (V=O) of crystalline V_2O_5 at 997 cm^{-1} and the weak second-order feature of TiO_2(anatase) at 794 cm^{-1}. Heating the sample in dry air to 400°C and cooling back to room temperature showed that there were no significant structural changes in the crystalline V_2O_5 and TiO_2 phases due to the thermal treatment and that the change (broadening) with temperature was due to thermal broadening. Wachs et al. (112) studied the difference in Raman spectra of a 1.9% V_2O_5/TiO_2 monolayer catalyst before and after use in o-xylene oxidation. They found in both cases a broad Raman band between 850 and 1050 cm^{-1} characteristic of surface vanadia; this means that the surface vanadia species on the TiO_2 are essentially in the same state in the fresh and spent catalysts. The same authors (112) also studied the Raman spectra of fresh and spent 7% V_2O_5/TiO_2 catalysts which contained both a monolayer of the surface vanadia species and crystalline V_2O_5. The Raman spectrum of the fresh catalyst exhibited a sharp band at 997 cm^{-1} due to symmetrical stretch of terminal V=O in crystalline V_2O_5 while the spectrum for the spent sample did not show it.

They concluded that crystalline V_2O_5 may be reduced partially to V_2O_4 and V_2O_3 during the reaction: the lower oxides do not possess Raman bands in the region 750-1200 cm^{-1} and the very weak Raman signals from these lower V-oxide phases cannot be distinguished from the strong TiO_2(anatase) Raman bands below 750 cm^{-1}. Wachs et al. (56,120) also studied by Raman spectroscopy a series of V_2O_5/TiO_2(low area) catalysts which were prepared by impregnation. They found that the lowest loading of vanadia that exhibited the crystalline V_2O_5 Raman band at 997 cm^{-1} is 2% V_2O_5. Below 2% V_2O_5, the peak associated with crystalline V_2O_5 is replaced by a broad Raman band between 850-1000 cm^{-1}. They thought that this broad band was due to a surface vanadia species coordinated to the TiO_2(anatase) surface. Saleh et al. (121) studied the effect of calcination temperature on the 7% V_2O_5/TiO_2(anatase) catalyst. They found that with increasing calcination temperature, the surface area of the catalyst decreased and TiO_2(anatase) transformed to TiO_2(rutile). They also found that the anatase to rutile transformation was accompanied by a decrease in the content of crystalline V_2O_5 and formation of $V_XTi_{1-X}O_2$ solid solution. Similar results were found by Bond et al. (54).

TPR

The TPR technique has proven to be a quite appropriate tool for quantitative analysis. Moreover, this technique gives information about the reducibility of the different supported phases as well as of the support itself. TPR also has been used to investigate the different types of oxygen

present in vanadium oxide, and which may be involved in the oxidation process over such catalysts. Roozeboom et al. (84) obtained the TPR profile for pure V_2O_5 and they found one single reduction peak at 530°C. Bosch et al. (122) obtained TPR profiles for pure V_2O_5, consisting of three or four peaks, the first two peaks being resolved, but the last of these not being resolved. They concluded that the reduction probably proceeds as follows:

$$V_2O_5 \rightarrow 1/3V_6O_{13} \rightarrow 2VO_2 \rightarrow V_2O_3$$

the last two peaks together representing the last step. Roozeboom et al. (84) studied the TPR profiles for a series of VO_x/Al_2O_3, VO_x/SiO_2 and VO_x/TiO_2 catalysts which were prepared by wet impregnation. In the case of VO_x/Al_2O_3 catalysts, they found that below 6.6% V_2O_5, the profiles showed a peak at about 380°C which was assigned to a two dimensional octahedral polyvanadate surface structure, and the extra peak or shoulder at about 330°C to a tetrahedral vanadate structure. Above 6.6% V_2O_5, they found a third peak beyond 430°C due to crystalline V_2O_5. With increasing V-coverage, the peak due to crystalline V_2O_5 shifted to higher temperatures up to the reduction temperature of pure V_2O_5. In the case of VO_x/SiO_2 catalysts, two peaks were observed again, one at about 430°C and another at 430-510°C which can be assigned to some surface phases and a crystalline V_2O_5 phase respectively. In the case of the VO_x/TiO_2 catalysts, they found that at lower coverages one peak and shoulder at 330-380°C may due to surface polyvanadate while at 7.5% V_2O_5, a peak at about 430-480°C

was found, due to crystalline V_2O_5. The same authors (84) studied the TPR profiles for VO_x/Al_2O_3, VO_x/SiO_2 and VO_x/TiO_2 monolayer catalysts which were prepared by an ion-exchange method. They found a dispersed vanadia monolayer species on the surface of the supports but with VO_x/SiO_2 catalyst, the crystalline V_2O_5 was present even though the concentration of V_2O_5 was below monolayer coverage. van Hengstum et al. (75) studied the TPR profiles for VO_x monolayer catalysts supported on α-Al_2O_3, TiO_2(rutile), TiO_2(anatase, 0.28% K_2O and 0.38% P_2O_5 as impurities) and TiO_2(anatase, 0.07% K_2O and 0.14% P_2O_5 as impurities). The results show just one peak (related to the reduction of V(V) to V(III) in one step), in contrast to the behavior of bulk V_2O_5 for which three or four peaks are obtained. The authors also found that the structure and the composition of the support has a great influence on the reducibility: the order of reducibility is VO_x/Al_2O_3 > VO_x/TiO_2(rutile) > VO_x/TiO_2(anatase,low impurities) > VO_x/TiO_2(anatase,high impurities). van Hengstum et al. (119) studied the effect of K_2O and P_2O_5 impurities separately on the reducibility of VO_x/TiO_2(anatase) monolayer catalysts. They found that when K_2O content increases, the reducibility of VO_x phase decreased and was only slightly affected by presence of P_2O_5. Wachs et al. (56,120,123) prepared a series of V_2O_5/TiO_2 catalysts by the impregnation method and tested them by the TPR technique. They found that surface vanadia monolayer species and crystalline V_2O_5 are reduced more readily than unsupported V_2O_5. They concluded that the rate of reduction increased with decreasing the thickness of the V_2O_5 crystal in the C direction. Monti et al. (124)

studied the TPR profiles for unsupported V_2O_5 catalysts containing between 0 and 40 mol.% K_2SO_4 and found that the starting temperatures for catalyst reduction by H_2 were lowered by more than 150°C when the K_2SO_4 content was increased from 0 to 40%. They also found that the TPR profiles separated into a low- and a high-temperature region. They concluded from the H_2 consumption that the low-temperature part can be ascribed to the reduction of V(V) to V(IV), whereas the high-temperature peak shows further reduction of the V(IV) to V(III) and partial reduction of the sulfate. Wachs et al. (112) studied the fresh and spent VO_x/TiO_2 monolayer catalysts by the TPR technique. Both catalysts exhibited a peak at 430°C characteristic of surface vanadia. They concluded that the surface vanadia species on the TiO_2 support are essentially in the same state in the fresh and spent catalysts. Iwamoto et al. (85) studied the TPR profile for 5.1% V_2O_5/MgO catalyst. They found that there are two kinds of supported V_2O_5 and each kind is reduced by two steps, i.e. $V_2O_5 \rightarrow V_2O_4$ and $V_2O_4 \rightarrow V_2O_3$.

Recently Haber et al. (106) prepared VO_x monolayer catalysts by using TiO_2, Al_2O_3 and SiO_2 as supports. They found that the VO_x/TiO_2 sample loses one oxygen atom for each V ion on reduction whereas in the case of VO_x supported on Al_2O_3 and SiO_2 only about 0.5 oxygen atom per V ion. Kijenski et al. (108) studied the TPR profiles for VO_x/TiO_2, VO_x/Al_2O_3, VO_x/SiO_2 and VO_x/MgO monolayer catalysts. They found that the catalysts exhibited one peak and indicated that reducibility of the VO_x species depended mainly on the support and T_{max} increased in the sequence $TiO_2 < Al_2O_3 < SiO_2 < MgO$.

XPS

X-ray photoelectron spectroscopy (XPS) is another technique which allows the determination of the oxidation state of the V species; some structural information can be inferred by comparing binding energies with that of known chemical compounds.

The literature gives the V $2p_{3/2}$ binding eneries reported for V_2O_5 (61,72,114,125-128), V_6O_{13} (72), V_2O_4 (127,128), V_2O_3 (127) and VO (127). These represent all the oxidation states of V with the exception of V metal. The V $2p_{3/2}$ binding energy value reported for V_2O_5 and were about 516.4-517.4 eV (125-128). The next oxidation state, V(IV), represented by V_2O_4, showed binding energy values in the range 515.4 - 515.7 eV (127,128). Binding energy values have revealed that the vanadium in VO_x/Al_2O_3, VO_x/SiO_2 and VO_x/TiO_2 catalysts are present as V(V) (52,114,115,123,129).

It has been shown that the XPS metal-to- support intensity ratio can be provide important information regarding the dispersion and crystalline size of supported metal particles (52,130-134).

Mendialdua (125) used XPS to study V_2O_5 deposited on TiO_2(anatase) and TiO_2(rutile). He assumed some models of deposition such as the model of the homogenous layers, the model of blocks and the model of solid solution. Recently Gil-Llambías et al. (115) studied VO_x/Al_2O_3 and VO_x/TiO_2 catalysts by XPS. They found that the V 2p/Ti 2p intensity ratio increased monotonically with V_2O_5 contents up to a certain level and then declined for higher surface concentration. They concluded that the formation of a less well dispersed phase above the monolayer " the appearance of

multilayered V structures". Jonson et al. (52) studied VO_x/Al_2O_3 catalysts by the XPS technique. They found that at low V content, the surface was enriched with V of high dispersion but, at high V content, the V $2p_{3/2}$ / Al 2p intensity ratio was too low, probably caused by the partial occurrence of vanadium oxides of low dispersion.

FTIR

Infrared spectra is a useful technique in the field of heterogeneous catalysis (135). Information can be obtained from FTIR in the case of supported V_2O_5, MoO_3 and WO_3 catalysts, bulk VPO_x and the interaction with absorbate (136-139).

Nakagawa et al. (140) studied V_2O_5/TiO_2 catalysts by IR. They found a shift from 1020 (pure V_2O_5) to 980 cm^{-1} of the V=O bond stretching frequency in the infrared spectra for the vanadium oxide monolayer species on TiO_2. They concluded that the vanadium on the surface is present as amorphous V_2O_5 at low vanadium coverage and amorphous and crystalline V_2O_5 at high surface vanadium coverage. Busca et al. (136) suggested that overtone bands observable in the IR spectra of mixed and supported oxide catalysts,may give information on the state of the active phases. They found in the case of V_2O_5/TiO_2, MoO_3/Al_2O_3 and WO_3/Al_2O_3 catalysts that the single uncoupled M=O bonds are exposed on the surface. Busca et al. (141,142) examined the surface of monolayer V-Ti-O catalyst by FTIR. They have shown that vanadate species have a very strong Lewis acid site identified as coordinatively unsaturated VO^{2+} vanadyl and medium-strong Brönsted V-OH sites. Recently Miyata et al. (143) examined the V_2O_5 catalysts supported on TiO_2, Al_2O_3,

ZrO_2 and SiO_2 which were prepared by wet impregnation and $VOCl_3$-gas phase methods. They found similar result to those obtained by Nakagawa et al. (140) for V_2O_5/TiO_2 catalysts prepared by impregnation. In the case of the $VOCl_3$ method, they found three vanadate phases. At low V content, there is a band at 983 cm^{-1} due to amorphous V_2O_5. Above 2 wt.% V_2O_5, the 982 cm^{-1} band was still present and a new band at 992 cm^{-1} appeared due to a new phase which reached a maximum at $\sim$5% V_2O_5. Thereafter new bands appeared at 1010 and 1020 cm^{-1} due to crystalline V_2O_5. In the case of the V_2O_5 catalysts supported on the Al_2O_3, ZrO_2 and SiO_2, they found that at low V content (except V_2O_5/SiO_2 sample) the catalysts show only one band around 970 cm^{-1} while at higher V content the spectra consist of two peaks.

ESR

ESR specroscopy has proved to be a powerful method to detect the presence of the paramagnatic V(IV) species with great accuracy in vanadium based catalysts. It has also been found that fresh supported VO_x samples, slightly reduced, undergo further reduction in the hydrocarbon/air mixture, the extent of reduction depending on the type of support used and the reaction temperature. The low content of vanadia did not permit, however, identification of the reduced phases, e.g., lower vanadium oxides, by conventional phase analysis. The ESR was used as a better method for the characterisation of the reduced vanadia phase in contact with support.

Bond et al. (54) studied VO_x/TiO_2 catalysts calcined at

450°C by ESR. They found that the catalysts at low V loading have a few percent of V(IV) in the form of VO^{2+} ions. Inomata et al. (6) used ESR to study VO_x catalysts supported on different types of TiO_2 calcined at 500°C. They concluded that the amount of V(IV) on the surface of the catalysts was small. Rusiecka et al. (144,145) studied the ESR of the VO_x catalysts deposited in different quantities on the surface of anatase and rutile. They found that reduced vanadia on both types of TiO_2 is present in the form of VO^{2+} groups dispersed on the TiO_2 surface and V(IV) ions in the V_2O_5 phase. They also concluded that VO^{2+} groups on anatase containing samples are more densely placed than those on rutile. Glinski and Kijenski (107) studied the ESR spectrum for a VO_x/Al_2O_3 monolayer catalyst and found that about 5% of the total V content was V(IV); this increased with reduction at higher temperature. Busca et al. (142) found by chemical analysis that V(IV) is indeed the predominant valence state present in V_2O_5/TiO_2 catalysts. Furthermore, the evacuation pretreatment used for ESR experiments caused a strong further lowering of the content of V(V) with formation of V(IV) and to some extent also to V(III). Jonson et al. (52) studied the ESR spectra for VO_x/Al_2O_3 catalysts. They concluded that at low V content, the V(IV) is present as VO^{2+} while at high V content, V(IV) was also present due to crystalline V_2O_5 as well as VO^{2+}. Nowinska (96) examined fresh VO_x/Al_2O_3 catalysts by ESR. He found V(IV) in the form of VO^{2+} and in the ranges from 5 to 10% of the total V content in the catalysts, where the surface coverage with V ions which does not exceed a monolayer.

1.1.4.3 Catalytic applications

1.1.4.3.1 Selective oxidation of o-xylene

Oxidation of o-xylene is the major industrial process for the production of phthalic anhydride (PA). V_2O_5 is a well-known catalyst for the oxidation of o-xylene into PA. Higher activities and selectivities in this reaction can be obtained if TiO_2 is the support (53,75). Products beside PA include o-tolualdehyde, o-toluic acid, phthalide, together with minor amounts of maleic anhydride (MA), and the products of total combustion, CO and CO_2.

There is little information on the forms of oxygen involved in the oxidation of o-xylene, or on the optimum oxidation state of the V ions. The oxidation of o-xylene over oxidic catalysts is believed to occur by the Mars-van Krevelen mechanism (146) which involves sequential oxidation and reduction of the active oxide component of the catalyst.

Yabrov and Ivanov (147) studied the mechanism of o-xylene oxidation over a V_2O_5/TiO_2 catalyst. They indicated that the products are formed through the introduction of O_2 with o-xylene molecules adsorbed strongly on the surface. Hauffe and Raveling (65) studied the oxidation of o-xylene using V_2O_5 catalysts on a number of supports, and of these TiO_2 showed the high activity and selectivity to PA, followed by SnO_2 and ZrO_2. They explained these results on the basis of the influence of the support on the defect structure of the vanadium oxide. Boreskov et al. (148) studied the influence of the alkali metals on the catalytic properties of the V_2O_5/TiO_2 catalyst in the oxidation of o-xylene. They concluded that when introducing the promoter into the catalyst, and as the alkaline nature of the metals

increases, the initial selectivity to partial oxidation products also increases. They observed a correlation between the selectivity and the acidity of the surface. The most acidic sites of the surface are assumed to be responsible for the destructive oxidation of o-xylene. Bond and Brückman (68) have studied VO_x/TiO_2 catalysts in the oxidation of o-xylene. They found that the catalytic properties of these catalysts did not improve continuously with increasing V content, but were constant above 1.2 wt.% V_2O_5.

Gąsior et al. (78) studied o-xylene oxidation on V_2O_5/TiO_2 catalysts prepared by decomposition of a vanadia phase on anatase (AN) and rutile (RT) modifications of TiO_2 under conditions which excluded possible solid-state reactions resulting in the formation of solid solutions of V in TiO_2(RT). A comparison of the catalytic oxidation behaviour of V_2O_5/TiO_2(AN) and V_2O_5/TiO_2(RT) catalysts showed that the promoting effect of TiO_2 on V_2O_5 was limited only to the TiO_2(AN). The activity and selectivity to PA for V_2O_5/TiO_2(AN) was higher than both V_2O_5/TiO_2(RT) and pure V_2O_5. The promoting effect for the V_2O_5/TiO_2(AN) in o-xylene oxidation was observed at low concentration ($\sim$1 mol% V_2O_5) at 623K. This concentration corresponds to 1 monolayer of VO_x, and above this the selectivity remains constant. Similar results were obtained by Wachs et al. (56) by using V_2O_5/TiO_2(anatase) catalysts for the same reaction. van Hengstum et al. (119) used TiO_2(Tioxide,anatase,10 m^2g^{-1}) as a support for the VO_x catalysts. This TiO_2 contained P and K as impurities, which the authors washed out with deionized water. They used these catalysts to study the selective oxidation of o-xylene to PA. Catalysts made with the

contaminated support were found to be less active for this oxidation reaction. The activity and yield of PA for catalysts with or without P and K impurities were constant above a certain V content. At low V content, there was a distinct negative effect of these impurities on the catalytic behaviour of the VO_x phase. At higher V content, however, catalysts containing P and K were more active and gave higher yields of PA than catalysts without these impurities. TiO_2(anatase) is superior to TiO_2(rutile) as a support for the V_2O_5 in the oxidation of o-xylene (78). The promoting effect of a TiO_2 support on the oxidation of o-xylene on V_2O_5 has been ascribed to an increase in the number of V=O bonds on the V_2O_5/TiO_2 catalysts (73). Saleh et al. (121) studied the effect of calcination temperature on 7% V_2O_5/TiO_2(anatase) in the o-xylene oxidation. They found that catalyst performance were active when calcined at 350-575°C, where a complete monolayer of surface vanadia exists on the TiO_2(anatase) support. Reviews on the o-xylene oxidation by catalysts containing V were published (58,149).

1.1.4.3.2 Selective oxidation of 1,3-butadiene

As mentioned in the literature, one of the developments that has made the C_4 route to maleic anhydride (MA) more attractive is the fact that VPO_x catalysts are well studied for the oxidation of C_4 hydrocarbons (see Section 1.1.3). The supported V catalysts are able to catalyse the selective oxidation of 1-butene, 1,3-butadiene, furan and benzene to maleic anhydride. When V is supported over TiO_2, the activity and selectivity vary from those observed in pure V_2O_5.

Bond et al. (54) studied the oxidation of butadiene using

VO_x/TiO_2(anatase,10 m^2g^{-1}) catalysts. They showed that the activity as well as the selectivity to MA increased with increasing vanadium content up to ~ 10 wt.% V_2O_5. Busca et al. (150) studied the n-butane oxidation on the VO_x/TiO_2. They found that n-butane is not selectively oxidised to MA and when the amount of V deposited largely exceeds the monolayer amount, low yields of acetic acid are obtained. They concluded that the formation of MA from n-butane occurs through the successive formation of butadiene, 2,5-dihydrofuran and furan. Mori et al. (151-154) studied the oxidation of 1-butene, 1,3-butadiene, furan and benzene over V_2O_5 supported on Al_2O_3 and TiO_2 supports. They found a relationship between selectivity to MA (S_{MA}) and number of layers (N) in both V_2O_5/TiO_2 and V_2O_5/Al_2O_3, while the structures of the V_2O_5/TiO_2 catalysts differed significantly from those of the V_2O_5/Al_2O_3 catalysts.They concluded that when N is 1 or 2, S_{MA} is very low, while it increases markedly with an increase in N to N = 5 and attains a constant value above N = 5 (46% for 1-butene, 60% for 1,3-butadiene, 80% for furan and 50% for benzene).

1.1.4.3.3 Decomposition of isopropanol

The two basic modes for the decomposition of isopropanol are: a) dehydrogenation to form acetone and H_2 and b) dehydration to form propylene and water. At high temperatures (300-600^{o}C), severe decomposition of an alcohol may occur to the cleavage of C-C bonds and the resultant formation of paraffins, CO and CO_2 (155).

Transition metal oxide catalysts for oxidation processes also exhibit acid-base properties, being capable

of sorption of acids and/or bases, as well as of catalysing some acidic reactions such as the dehydration of alcohols and isomerization of hydrocarbons. Many works, in particular on mixed oxide catalysts for the selective oxidation of hydrocarbons, have been concerned with searching for correlation between the acid-base properties of these systems and activity/selectivity in the oxidation reaction(55,156,157). Miyata et al. (158) studied the decomposition of isopropanol on V-Ti-oxide catalysts and found high activity for the dehydrogenation of isopropanol to acetone. They concluded that the Lewis-acid (V ion) and base site (oxygen in the surface V=O species) played a significant role in the dehydrogenation.

Grzybowska et al. (78,159) tested the V_2O_5/TiO_2(AN) and V_2O_5/TiO_2(RT) catalysts for isopropanol decomposition: V_2O_5/TiO_2(AN) at 1 wt.% V_2O_5 showed that special structure formed on the TiO_2(AN) exhibited dehydrogenating properties to a much higher extent than those inherent for pure V_2O_5. The lower dehydrating rate (lower acidity) of this structure could account for the lower selectivity to total oxidation observed on V_2O_5/TiO_2(AN) as compared with V_2O_5/TiO_2(RT) or pure V_2O_5. The acid centres capable of strong adsorption of an aromatic hydrocarbon may lead to the processes of hydrocarbon destruction.

1.2 Catalysts based on the other metal oxides

1.2.1 Supported molybdenum oxide

Mo catalysts play an important role in a large range of reactions. Bulk MoO_3 and several molybdates are used in selective oxidation (44,55,57,160-162). Supported Mo oxide

and sulfide catalysts are applied in the oil-refining industry for hydrodesulfurization(HDS) (163-165), hydrodenitrogenation(HDN) (166,167), hydrogenation (168) and alkene metathesis (169-171). The Mo catalysts used in industry are usually promoted with Co or Ni (172,173).

Supported MoO_3 catalysts are prepared by different methods which were discussed in Section 1.1.4.1. It is clear, in general, that the molybdate species when dispersed on the support (monolayer) differ from bulk MoO_3 (174,175). It had been reported that the tetrahedral/octahedral molybdate ratio depended on the molybdate concentration; the lower Mo content, the higher this ratio (176). At high Mo content, bulk MoO_3 and $Al_2(MoO_4)_3$ had been observed (83,173,177,178).

Surface morphology has a major effect on the activity and selectivity of heterogeneous catalysts especially for multicomponent catalysts. There is an abundance of papers dealing with structural and catalytic aspects of Mo-containing catalysts (169,179-182). The information of fundamental importance is often obtained when the catalytic behaviour of a catalyst can be connected with its chemical and/or physical properties. Therefore, several techniques giving structural information have been applied to study the structure of the catalysts, such as X-ray photoelectron spectroscopy(XPS), Raman spectroscopy and temperature programmed reduction(TPR).

1.2.1.1 MoO_x/Al_2O_3 catalysts

Laser Raman spectroscopy

Raman spectroscopy was used to follow the morphology of surface and crystalline species as a function of metal

loading, metal impregnation sequence and method of impregnation. In general, the spectra of MoO_3/Al_2O_3 catalysts reported by various research groups are comparable. The most marked band is that at 940-970 cm^{-1}. This band shifts to higher wavenumbers with increasing Mo content (176,183-185); this can be attributed to the presence of a polymeric octahedrally coordinated surface species. The position and the intensity of this band can be modified by the presence of H_2O on the sample (177). Recent Raman spectroscopy studies of a series of MoO_x/Al_2O_3 catalysts have shown that highly dispersed MoO_x readily interacts with H_2O and O_2 causing large shifts in the metal-oxygen stretching frequencies associated with surface oxide (186,187).

Thomas (188) found that the Raman spectra of Mo catalysts prepared by liquid phase adsorption (pH = 1 and 6) and by gas phase adsorption were essentially similar to the spectra of catalysts prepared by impregnation of Al_2O_3 (188). From the presence of weak bands at 295, 665, 820 and 998 cm^{-1}, he concluded that a small amount of MoO_3 was present in the catalyst prepared by liquid phase adsorption at pH = 1. Dufresne et al. (173) studied catalysts prepared via impregnation using high and low surface area Al_2O_3. Raman spectra show that MoO_4^{2-} ions were present in catalysts with low Mo loading. For higher Mo concentrations, polymeric aggregates or two-dimensional polymolybdates are thought to be the major species, with Mo-O octahedra being the dominant species. For very high Mo contents, Raman spectra were assigned to bulk MoO_3. Depending on the preparation conditions, the $Al_2(MoO_4)_3$ phase can also be detected. They concluded that the dispersion of Mo species is very similar

between the two Al_2O_3 supports. They also found that at low Mo loading, many more Mo species in the tetrahedral environmemt were detected on the low surface area Al_2O_3.

Iannibello et al. (189) and Wang and Hall (190), suggested that the band at 950 cm^{-1} corresponds to the Mo=O frequency of a tetrahedral molybdate group bonded to the surface. In addition, Wang and Hall (176) suggested that the ratio of intensities at the 950 and 970 cm^{-1} bands can then be taken as a measure of the ratio of tetrahedral monomeric to octahedrally coordinated polymolybdate species. They found that this ratio decreased with increasing loading. Leyrer et al. (98) prepared a MoO_x/Al_2O_3 monolayer catalyst by the incipient wetness method at pH = 6. The occurence of low frequency bands in the Raman spectrum indicated the presence of a small percentage ($\sim$10%) of Mo as the tetrahedral monomeric species, while the other species were thought to be polymolybdates.

TPR

The TPR profile for bulk MoO_3 shows that MoO_3 is reduced to Mo metal by two steps passing through MoO_2 as the intermediate (95,191). Fransen et al. (192) studied the reduction of bulk MoO_3 and MoO_x/Al_2O_3 monolayer catalyst by measuring the valence state of Mo after 16h of reduction at constant temperature. It was observed that MoO_3 is reduced to MoO_2 at a temperature of 330°C but for MoO_x/Al_2O_3 at 450°C. It was concluded that the higher valence state of Mo was stabilized by a strong interaction with the support. However, Yao (193) found that at 500°C the reducibility of a series of MoO_x/Al_2O_3 catalyst samples was higher than for bulk MoO_3. The reducibility for higher Mo loading was

greater than low Mo loading. Calcination at higher temperature for low Mo loading decreas the reducibility of MoO_x/Al_2O_3. He also found that a complete reduction to Mo metal occured rapidly at 900°C for pure MoO_3 while an additional hour at this temperature was required for complete reduction of the catalyst samples.

Many reduction studies show that the average Mo valence after reduction is +4 or higher, which is interpreted as being caused by the presence of mixtures of Mo(VI), Mo(V) and Mo(IV) ions (194,195). Thomas et al. (181,196), and Arnoldy et al. (197), applied TPR to a series of MoO_x/Al_2O_3 catalyst samples. They found that the Mo(VI) monolayer species, which interacted strongly with the support, were reduced at higher temperatures (at 610-880°C) while the Mo(VI) bilayer/multilayer was reduced in one step to Mo metal at lower temperatures (between 380 and 460°C). Burch and Collins (179) observed that the TPR profiles for MoO_x/Al_2O_3 catalysts heated to 730°C show just one peak at 500-520°C which is due to reduction of Mo(VI) to Mo(IV). Caceres et al. (198) obtained TPR results for a series of MoO_3/Al_2O_3 prepared by equilibrium adsorption and found that supported MoO_3 is reduced first to MoO_2 (at 415-590°C) and then to Mo metal (between 740-770°C). The authors concluded that strong interaction with the support at low Mo content may be due to high dispersion.

XPS

A large number of studies on MoO_3/Al_2O_3 catalysts have been made using XPS. Zingg et al. (87) studied MoO_3/Al_2O_3 catalyst samples by XPS and found the presence of only Mo(VI) on the oxidic catalyst. They also studied the

reduction of MoO_3/Al_2O_3 catalyst samples at 500°C and found that the Mo(VI) intensity decreased rapidly with time, resulting in Mo(V) and Mo(IV). They explained that octahedral Mo(VI)(MoO_3) was reduced completely to Mo(IV) after 12h of reduction at 500°C in H_2 while tetrahedral Mo(VI)($Al_2(MoO_4)_3$) was reduced only to Mo(V). Thomas et al. (196) studied MoO_x/Al_2O_3 catalyst samples by XPS and found that the XPS intensity ratios (IMo_{3d}/IAl_{2p}) were in good agreement with the theoretical monolayer prediction. The authors concluded that the MoO_3 is highly dispersed and a small deviation at the highest concentration was probably due to a non-uniform distribution of the MoO_3 phase over the catalysts. Dufresne et al. (173) studied MoO_3/Al_2O_3 catalysts prepared using both high and low surface area Al_2O_3 by XPS. The authors plotted the intensity ratio (IMo_{3d}/IAl_{2p}) as a function of Mo content expressed as the molar ratio Mo/Al and obtained two straight lines in the low Mo content range. This was explained by a monolayer coverage of Al_2O_3 by MoO_x species. They found that deviations from a straight line began at Mo/Al ratio, of 4×10^{-2} and 9×10^{-2}-10×10^{-2}, which corresponded to completion of the monolayer for low- and high-surface area Al_2O_3 respectively. The dispersion of MoO_x species was similar between the two Al_2O_3 supports. Kasztelan et al. (199) applied XPS to MoO_3/Al_2O_3 catalysts prepared using an equilibrium adsorption method. They found that the increases in the XPS intensity ratio (IMo_{3d}/IAl_{2p}) after calcining the sample were a consequence of a modification of dispersion, i.e. the migration of Mo from multilayer dispersion at the drying step to a monolayer dispersion at the calcination step. Leyrer et al. (98) heated a MoO_x/Al_2O_3 monolayer catalyst to

400°C in H_2(2h) and the XPS results showed that the degree of reduction was low, but some Mo(IV) and Mo(V) were formed.

1.2.1.2 MoO_x/SiO_2 catalysts

Laser Raman spectroscopy

By Raman spectroscopy both bulk MoO_3 and Mo surface species have been detected (185,200,201). The nature of the surface phase was subject to the same discussion as has been described for MoO_3/Al_2O_3 catalysts, since it concerns the same Raman bands. Qualitatively, the structure of MoO_3/SiO_2 catalysts thus resembles the structure of MoO_3/Al_2O_3 catalysts. From the presence of crystalline MoO_3 at surface coverages considerably lower than the theoretical monolayer coverage, it was concluded that the adsorption capacity of SiO_2 is lower than that of Al_2O_3. The behaviour of SiO_2 is quite different from that of the other supports. In this case, adsorption of molybdate ions from acid solution is not effective for the formation of a complete MoO_x monolayer (93). The SiO_2 surface is also incompletely covered with MoO_x via adsorption of $MoO_2(OH)_2$ from the gas phase (93). MoO_x-surface species/SiO_2 interactions will therefore be weak. As a consequence, the weakly held molybdate will largely decompose on SiO_2 during calcination to form crystalline MoO_3 even below monolayer coverage (184,202). Raman spectra of a series of MoO_3/SiO_2 catalysts prepared by impregnation showed a weak broad band appearing at 970 cm^{-1} at 2.8% MoO_3; it shifts to 956 cm^{-1} in 6.7% MoO_3/SiO_2 with an additional broad band at 884 cm^{-1}. Following the band assignments as in MoO_3/Al_2O_3, these bands can be ascribed to

a molybdena interaction species which must be considered as an analogue of a polyanion chemically interacting with support surface. The formation of crystalline MoO_3 was first detected in a sample having 6.7% MoO_3 as indicated by the occurence of the two narrow bands at 996 and 821 cm^{-1}; these increase with increasing Mo loading of the sample (202). The Raman spectrum for a MoO_x/SiO_2 catalyst (loading near the monolayer capacity) prepared by the incipient wetness method at pH = 6 and calcined at 500°C showed that crystalline MoO_3 is the dominant species. A weak and broad band near 930 cm^{-1} was detected which also indicaties the formation of some surface molybdate (98). Recently Stencel et al. (203) studied $Mo(VI)O_x/SiO_2$ catalysts by Raman spectroscopy and found that the surface of MoO_x/SiO_2 samples depended on the state of hydration/dehydration of the catalysts.

TPR

Fransen et al. (192) prepared $Mo(VI)O_x/SiO_2$ catalysts by adsorption of molybdate ions from acid solution and by adsorption of $MoO_2(OH)_2$ from the gas phase; incomplete monolayers were formed. Valence measurements showed that the $Mo(VI)O_x$ surface species was reduced to $Mo(IV)O_x$ at 330°C as if it were pure MoO_3 while $Mo(VI)O_x/Al_2O_3$ was reduced to $Mo(IV)O_x$ only at 450°C. Thomas et al. (181) prepared two series of MoO_3/SiO_2 catalysts by wet and dry impregnation. They found that the major part of the molybdate species in the catalysts was reduced at lower temperature than pure MoO_3. At the lowest Mo contents, only one peak at about 480°C was observed. With increasing Mo content, the

intensity of the peak at 630°c and the sharpness of 480°C peak both increased. The two reduction peaks pointed to the presence of two Mo phases, namely $Mo(VI)O_x$ monolayer species and crystalline MoO_3. The $Mo(VI)O_x$ monolayer species reduced completely to Mo metal in the low-temperature peak, whereas the crystalline MoO_3 reduced in two steps, viz. to MoO_2 and further to Mo metal in the low- and high-temperature peaks, respectively. Arnoldy et al. (197) prepared a series of MoO_x/SiO_2 catalysts by pore volume impregnation. The TPR results were similar to those of Thomas et al. (181).

XPS

Thomas et al. (181) studied MoO_3/SiO_2 catalysts by the XPS technique. The results show that the intensity ratio ($I_{Mo\ 3d}/I_{Si\ 2p}$) was lower compared to the theoretical monolayer prediction and the deviation of the experimental points from the monolayer line occurs at a lower Mo content than expected on the basis of the appearance of bulk MoO_3.

1.2.1.3 MoO_x/TiO_2 catalysts

Few studies on MoO_3/TiO_2 catalysts have been carried out. van Hengstum (95) reported that the Raman spectrum of a MoO_x/TiO_2 monolayer catalyst produced a relatively broad, weak band at 980 cm^{-1}, which indicated that the supported species is not isostructural with the species present in the bulk MoO_3. The breadth of the band was attributed to the presence of crystallographically ill-defined Mo complexes on the surface of TiO_2. Ng and Gulari (83) studied by Raman spectroscopy a series of MoO_x/TiO_2 catalysts prepared by wet impregnation. They observed a shift in frequency from 945 to

964 cm^{-1} for a Raman mode for an octahedral molybdate surface species on TiO_2 as the concentration of MoO_3 was increased from 1 to 5 wt.%; there was no more change with further increases in loading. The intensity of the band also remained the same once the monolayer coverage was reached. When the monolayer coverage was exceeded, crystalline MoO_3 appeared. The same authors (83) studied the spectrum of MoO_x/TiO_2 catalysts prepared by equilibrium adsorption and found that only well-dispersed monolayer species were formed; similar conclusions were reached by Wang and Hall (190). Liu et al. (177) prepared a series of MoO_3/TiO_2 catalysts by the impregnation method; they observed the same behaviour as Ng and Gulari (83) in that surface molybdate species reached a saturation limit at a Mo loading of about 4 wt.% MoO_3 (monolayer catalyst). Leyrer et al. (98) prepared a MoO_x/TiO_2 monolayer catalyst by the incipient wetness method (the impregnation solution contained the amount of paramolybdate required for loading near the monolayer capacity, pH = 6). The Raman spectrum of the calcined catalyst showed that the surface polymolybdate is the dominant species as indicated by the strong band at 967 cm^{-1} and the shoulders at 323 and 247 cm^{-1}. There was no indication of crystalline MoO_3 formation. Raman spectroscopy studies of a series of MoO_x/TiO_2 catalysts have shown that highly dispersed MoO_x readily interacts with H_2O and O_2 causing large shifts in the Mo=O stretching frequency (186). Xian-Chun et al. (202) studied Raman spectra of MoO_x/TiO_2(anatase) catalysts prepared by impregnation. They found for low Mo content catalysts that the predominant species on the surface were octahedral polymolybdate and

tetrahedral MoO_4^{2-} . Increasing the loading of MoO_3 showed the crystalline MoO_3 begining to emerge, and becoming the main species at high loading.

Thermal analysis results show that MoO_x on TiO_2 is reduced in two steps to Mo metal (95). Tanaka et al. (170) found that MoO_x/TiO_2 catalysts with loadings of 10 wt.% MoO_3 or less could be reduced nearly to Mo metal with H_2 at 500°C after 1h, while the loading greater than 10 wt.% MoO_3 was harder to reduce to Mo metal. The XPS spectrum for a MoO_x/TiO_2 monolayer catalyst reduced at 400°C (2h) showed Mo(IV) (98).

1.2.2 Supported tungsten oxide

WO_x catalysts

W-catalysts are used for the same reactions mentioned in Section 1.2.1 (57,160,169,180,181,196,205). The methods of preparation were discussed in Section 1.1.4.1. The supported WO_x system has been examined with many different characterisation techniques such as TPR, laser Raman spectroscopy and XPS.

Laser Raman spectroscopy

Thomas et al. (184,196) assigned the Raman bands observed to polymeric surface species consisting of octahedrally coordinated W(VI) ions. At increasing W content the band for WO_x/Al_2O_3 catalysts shifted from 960 to 995 cm^{-1}, which was correlated with an increase of the degree of polymerization of the surface compound. Iannibello et al. (189) assigned the band observed at 960 cm^{-1} for WO_x/Al_2O_3 to the stretching vibration of the W(VI) ion tetrahedrally coordinated by oxygen. Salvati et al. (79) observed in Raman

spectra for WO_x/Al_2O_3 catalysts below 15 wt.% WO_3, bands at 973 and 333 cm^{-1}, which could be assigned to tetrahedral WO_4^{2-} interaction species. With increasing W loading octahedral WO_3 interaction species were formed producing bands at 807, 715 and 272 cm^{-1}. Stencel et al. (206) studied a series of WO_3/Al_2O_3 catalysts (1-30 wt.% WO_3) by Raman spectroscopy. They found that the frequencies of bands due to surface tungstate species can be shifted reversibly during alternate O_2 calcination and H_2O exposure cycles. Chan et al. (207) studied the influence of calcination temperature upon the solid state chemistry of WO_3 and Al_2O_3 by means of Raman spectroscopy. Raman spectroscopy revealed that a close-packed monolayer of $W(VI)O_x$ surface complex on Al_2O_3 was formed as the surface area of Al_2O_3 decreased at high calcination temperatures. The lower $W(VI)O_x$ loading, the more severe the calcination temperature must be to reach the close-packed monolayer. The close-packed $W(VI)O_x$ monolayer accommodated the further loss of surface area at still higher temperatures, forming the bulk WO_3 and $Al_2(WO_4)_3$ phases. Soled et al. (82) studied WO_3/Al_2O_3 catalysts by Raman spectroscopy. The spectra showed a band around 970 cm^{-1} at loadings of 10 wt.% WO_3 which was assigned to the W=O symmetrical stretch of the surface tungsten oxide species. The 10 wt.% WO_3 catalyst calcined above 650°C exhibited Raman peaks at 972, 809 and 718 cm^{-1}. The peak near 970 cm^{-1} was associated with a tungsten oxide surface complex and shifted to about 1000 cm^{-1} as the calcination temperature was increased to 950°C. Samples calcined at 1000 and 1050°C displayed bulk WO_3 and $Al_2(WO_4)_3$ phases.

In the case of WO_3/SiO_2 catalysts, the same bands as observed in WO_3/Al_2O_3 catalysts at high W contents, viz. at 715 and 805 cm^{-1}, were observed also at lower W-contents. In the catalysts with low W-content only a band at 970 cm^{-1} was present (188).

TPR

Thomas et al. (169,196) found that bulk WO_3 reduced essentially in one step to W metal. van Hengstum (95) found the thermal analysis result showed that the bulk WO_3 was reduced in two steps to W metal. He thought that WO as the intermediate. Germain et al. (208) found that WO_2 as the intermediate in reduction of bulk WO_3.

Sondag et al. (209) found that the reducibility decreased in the order $WO_3 > WO_3/SiO_2 > WO_3/Al_2O_3$. Thomas et al. (180,196) studied WO_3/Al_2O_3 catalysts which were prepared by wet and dry impregnation by TPR. They found only one broad reduction peak for all catalysts. Reduction, being very difficult at low W contents may be due to the high dispersion of $W(VI)O_x$ on the surface of the support (monolayer catalyst). With increasing W content, the reduction became easier. The WO_3/Al_2O_3 catalysts were reduced in one step to W metal without the formation of intermediate oxides. They also found that bulk WO_3 was reduced more easily than the catalysts. Thomas et al. (181) found that the reducibility of WO_3/SiO_2 catalysts was much higher than the reducibility of the corresponding WO_3/Al_2O_3 catalysts which means that a stronger interaction existed between $W(VI)O_x$ species and Al_2O_3 than $W(VI)O_x$ and SiO_2. In most WO_3/SiO_2 catalysts, a peak can be observed at the same temperature for reduction of the bulk WO_3 which indicated

the presence of crystalline WO_3. Soled et al. (82) found that thermal analysis results indicated that the surface $W(VI)O_x$ phase on Al_2O_3 was difficult to reduce. With increasing W loading and at 900°C (2h), WO_3/Al_2O_3 catalysts were extensively reduced. Using thermal analysis, van Hengstum (95) showed that WO_x/TiO_2 monolayer catalyst was reduced to W(IV)-oxide and not to the metal as was observed for bulk WO_3. Hence, the WO_2 phase was stabilized by the TiO_2 support, suppressing further reduction.

XPS

Thomas et al. (188,196) studied WO_3/Al_2O_3 catalysts by XPS. They found that the calculated intensity ratio ($I_{W\ 4f}/I_{Al\ 2p}$) is in good agreement with the experimental data and they can be considered as monolayer catalysts. In the case of WO_3/SiO_2 catalysts (188), at low surface coverage, the deviation of the experimental points from the theoretical monolayer line occur at a lower W content which may due to the formation of an aggregated W(VI)-oxide phase. Biloen and Pott (210) found by XPS that unsupported WO_3 was reduced to W metal at temperatures of 430°C and higher, WO_3/SiO_2 reduced only to intermediate valences and WO_3/Al_2O_3 does not reduce at all. Several studies of the reduction of WO_3/Al_2O_3 using XPS have been made (79,82,211). The studies showed that below the monolayer coverage, $W(VI)O_x$ is reduced at very high temperature to W metal in one step, while WO_3 in excess of the monolayer coverage was reduced at lower temperature and may exhibit intermediate W oxidation states.

1.2.3 Supported rhenium oxide

Re-catalysts showed high activity for metathesis

(212-214), HDS (188,215) and HDN (216). Re also increased the stability of Pt reforming catalysts (217,218). Re appeared to be a selective hydrogenation catalyst (219).

Thomas (188) prepared Re_2O_7/Al_2O_3 catalysts by the impregnation method. The TPR profiles showed that at very low loading, the Re-compounds were reduced at higher temperatures, two peaks were present which may show a strong interaction between the support and the Re-surface species. The TPR profile for high surface coverage showed that the Re species in the catalyst strongly resembled the profile of the reference compound NH_4ReO_4. No Raman spectrum could be obtained from the catalyst with low Re-content, but a catalyst with high surface coverage showed bands at 340 and 980 cm^{-1} and was similar to spectra of this type of catalyst reported in the literature (220). The bands have been ascribed to a monomeric tetrahedrally coordinated ReO_4^- species. Arnoldy et al. (221) studied the reducibility of Al_2O_3-, SiO_2- and C-supported Re_2O_7 catalysts, over a wide range of Re contents. They found that the dried catalysts contained a monolayer type $Re(VII)O_x$ surface phase, as well as crystalline NH_4ReO_4. Calcined catalysts contained a $Re(VII)O_x$ surface phase and Re_2O_7 clusters. They also found that the reducibility decreased in the order $Re_2O_7/C \rangle Re_2O_7/SiO_2 \rangle Re_2O_7/Al_2O_3$.

1.3 Scope of this work

The aim of the investigations described in this thesis was to obtain information on some fundmental aspects concerning the following:

- the preparation of supported oxide catalysts by using

different methods (aqueous impregnation, $VOCl_3$, $VO(O^iBu)_3$ and $MoOCl_4$ methods) to apply the active phases, and their characterisation in relation to properties of the catalysts in the selective oxidation of 1,3-butadiene and the decomposition of isopropanol;
- the influence of the impurities on (or in) the TiO_2 support on the properties of the vanadium oxide applied.

Chapter 2 contains an overview of the experimental techniques which were employed to characterise the catalysts and to measure the catalytic activities.

Chapter 3 deals with the preparation of supported oxide catalysts by different methods. The monolayer catalysts prepared by reaction from organic solutions of $VOCl_3$, $VO(O^iBu)_3$ and $MoOCl_4$ with the surface hydroxyl groups of the support, and the aqueous impregnation method which was used to produce catalysts having more than one monolayer of oxide.

Chapter 4 deals with characterisation of vanadium oxide catalysts supported on different types of titania and prepared by different techniques, and their catalytic properties.

Chapter 5 gives the results of the influence of small amounts of P and K, both often present as additives in commercial TiO_2 samples, on the properties of vanadium oxide catalysts.

Chapter 6 deals with the characterisation of molybdenum oxide catalysts and their catalytic properties.

Finally, Chapter 7 comprises the general discussion and conclusions.

1.4 References

1. D.B. Dadyburjor, S.S. Jewur and E. Ruckenstein, Catal. Rev.-Sci. Eng., 19, 293 (1979).
2. J. van den Berg, Ph.D. Thesis, Utrecht Institute, The Netherlands (1984).
3. M. Rβzicka, Kristall und Technik, 9, 969 (1974).
4. A. Miyamoto, Y. Yamazaki, M. Inomata and Y. Murakami, J. Phys. Chem., 85, 2366 (1981).
5. M. Inomata, A. Miyamoto and Y. Murakami, J. Phys. Chem., 85, 2372 (1981).
6. M. Inomata, K. Mori, A. Miyamoto, T. Ui and Y. Murakami, J. Phys. Chem., 87, 754 (1983).
7. M. Inomata, K.Mori, A. Miyamoto and Y. Murakami, J. Phys. Chem., 87, 761 (1983).
8. G.L. Simard, J.F. Steger, R.J. Arnott and L.A. Siegel, Ind. Eng. Chem., 47, 1424 (1955).
9. S.L.T. Andersson, Ph.D. Thesis, Lund Institute of Technology, Lund, Sweden (1982).
10. G.G. Long, R.L. Stanfield and F.C. Hentz, J. Chem. Education, 56, 195 (1979).
11. E. Dziluma, S. Giller, V. Slavinska, V. Evgrashim, D. Kreile, A. Strautina and I. Milman, in " Preparation of Catalysts", B. Delmon, P.A. Jacobs and G. Poncelet, eds., Elsevier, Amsterdam, 187 (1976).
12. D.K. Chakrabarty, D. Guha, I.K. Bhatnagar and A.B. Biswas, J. Catal., 45, 305 (1976).
13. R.K. Grasselli, in " Surface Properties and Catalysis by Non-Metals ", J.P. Bonnelle, B. Delmon and E. Derouane, eds., NATO ASI Series C. No. 105, D. Reidal Publishing Company, Dordrecht, p. 273 (1983).

14. D.K. Chakrabarty, D. Guha and A.B. Biswas, J. Solid State Chem., 22, 263 (1977).

15. A.A. Fotiev, A.P. Palkin, A.A. Soboleva and L.A. Perelyaeva, Zhur. Neorg. Khim., 26, 1062 (1981).

16. U.S. Patent 3987080 (1976).

17. A. Polaczek, K. Dyrek and E. Polaczkowa, Bull. Acad. Pol. Sci. Ser. Sci. Chem., 20, 705 (1972).

18. J. Gendell, R.M. Cotts and M.J. Sienko, J. Chem. Phys., 37, 220 (1962).

19. M. Malow, Hydrocarbon Processing, Nov., 149 (1980).

20. K. Wohlfart and G. Emig, Hydrocarbon Processing, June, 83 (1980).

21. D.A. de Maio, Chem. Eng., 104 (1980).

22. R.L. Varma and D.N. Saraf, Ind. Eng. Chem. Prod. Res. Dev., 18, 7 (1979).

23. F. Garbassi, J.C.J. Bart, F. Montino and G. Petrini, Appl. Catal., 16, 271 (1985).

24. F. Cavani, G. Centi and F. Trifiro, Appl. Catal., 9, 191 (1984).

25. M. Nakamura, K. Kawai and Y. Fujiwara, J. Catal., 34, 345 (1974).

26. R.L. Varma and D.N. Saraf, J. Catal., 55, 361 (1978).

27. B.K. Hodnett and B. Delmon, Appl. Catal., 6, 245 (1983).

28. M. Brutovsky and S. Gerej, Collection Czechoslovak Chem. Commun., 47, 403 (1982).

29. M. Brutovsky, S. Gerej, F. Vasilco and J. Gerejova, Collection Czechoslovak Chem. Commun., 47, 1290 (1982).

30. E. Bordes and P. Courtine, J. Catal., 57, 236 (1979).

31. G. Centi, I. Manenti, A. Riva and F. Trifiro, Appl. Catal., 9, 177 (1984).

32. a) U.S. Patent 4209423 (1980), b) Mitsubishi Chemical Industries Co. Ltd., Jpn. Kokai 8141816 (1981), c) U.S. Patent 4315864 (1982), d) Jpn. Kokai 75131921 (1975), e) Jpn. Kokai 7441291 (1974), f) Jpn. Kokai 8145815 (1981) and g) Jpn. Kakai 7648615 (1976).

33. B. Jordan and C. Calvo, Can. J. Chem., 51, 2621 (1973).

34. I. Matsuura, "Proc. 8th Internat. Congr. Catalysis", Dechema, Frankfurt-am-Main, IV 473 (1984).

35. B. Jordan and C. Calvo, J. Solid State Chem., 5,432 (1972).

36. G. Poli, I. Resta, O. Ruggeri and F. Trifiro, Appl. Catal., 1, 395(1981).

37. B.K. Hodnett and B. Delmon, Appl. Catal., 9, 203 (1984).

38. E. Bordes, P. Courtine and J.W. Johnson, J. Solid State Chem., 55, 270 (1984).

39. F. Cavani, G. Centi, F. Trifiro and G. Poli, J. Thermal Analysis, 30, 1241 (1985)

40. G. Centi, F. Trifiro and G. Poli, Appl. Catal., 19, 225 (1985).

41. D. Brkic and F. Trifiro, Ind. Eng. Chem. Prod. Res. Dev., 18, 333 (1979).

42. F. Cavani, G. Centi, I. Manenti, A. Riva and Trifiro, Ind. Eng. Chem. Prod. Res. Dev., 22, 565 (1983).

43. M. Ai, Bull. Chem. Soc. Jpn., 43, 3490 (1970).

44. M. Ai and S. Suzuki, J. Catal., 26, 202 (1972).

45. F. Cavani, G. Centi, I. Manenti and F. Trifiro, Ind. Eng. Chem. Prod. Res. Dev., 24, 221 (1985).

46. G. Centi, G. Fornasari and F. Trifiro, J. Catal., 89, 44 (1984).

47. F. Cavani, G. Centi and F. Trifiro, Appl. Catal., 15, 151 (1985).

48. B.K. Hodnett and B. Delmon, Appl. Catal., 15, 141 (1985).

49. G. Busca, G. Centi and F. Trifiro, J. AM. Chem. Soc., 107, 7757 (1985).

50. J.S. Buchanan, J. Apostolakis and S. Sundaresan, Appl. Catal., 19, 65 (1985).

51. B.K. Hodnett, Catal. Rev.- Sci. Eng., 27, 373 (1985).

52. B. Jonson, B. Rebenstorf, R.Larsson, S.L.T. Andersson and S.T. Lundin, J. Chem. Soc., Faraday Trans. 1, 82, 767 (1986).

53. R. Grabowski, B. Grzybowska, J. Haber and J. Sloczynski, React. Kinet. Catal. Lett., 2, 81 (1975).

54. G.C. Bond, J. Sarkany and G.D. Parfitt, J. Catal., 57, 476 (1979).

55. J. Haber, "Proc. 8th Internat. Congr. Catalysis", Dechema, Frankfurt-am-Main, I85 (1984).

56. I.E. Wachs, R.Y. Saleh, S.S. Chan and C.C. Chersich, Appl. Catal., 15, 339 (1985).

57. J.C. Volta and J.L. Portefaix, Appl. Catal., 18, 1 (1985).

58. M.S. Wainwright and N.R. Foster, Catal. Rev.-Sci. Eng., 19, 211 (1979).

59. G. Lischke, W. Hanke, H.-G. Jerschkewitz and G. Ohlmann, J. Catal., 91, 54 (1985).

60. M. Gasior, B. Grzybowska and J. Haber, React. Kinet. Catal. Lett., 15, 395 (1980).

61. S.L.T. Andersson, J. Chem. Soc., Faraday Trans. 1, 75, 1356 (1979).

62. A. Andersson and S.T. Lundin, J. Catal., 65, 9 (1980).

63. P.L. Villa, in " Catalyst Deactivation", eds. B. Delmon and G.F. Froment, Elsevier, Amsterdam, 103 (1980).

64. M. Akimoto and E. Echigoya, J. Catal., 29, 191 (1973).

65. K. Hauffe and H. Raveling, Ber. Bunsenges. Phys. Chem., 84, 912 (1980).

66. D. Vanhove and M. Blanchard, J. Catal., 36, 6 (1976).

67. M.S. Wainwright and T.W. Hoffman, Canad. J. Chem., 55, 552 (1977).

68. G.C. Bond and K. Brückman, Faraday Disc. Chem. Soc., 72, 235 (1981).

69. A.J. van Hengstum, J.G. van Ommen, H. Bosch and P.J. Gellings, Appl. Catal., 8, 369 (1983).

70. F. Roozeboom, A.J. van Dillen, J.W. Geus and P.J. Gellings, Ind. Eng. Chem. Prod. Res. Dev., 21, 304 (1981).

71. F. Roozeboom, P.D. Cordingley and P.J. Gellings, J. Catal., 68, 464 (1981).

72. W.E. Slinkard and P.B. deGroot, J. Catal., 68, 423 (1981).

73. Y. Murakami, M. Inomata, A. Miyamoto and K. Mori, "Proc. 7th Internat. Cong. Catalysis", Tokyo, B 1344 (1981).

74. G. Busca, L. Marchetti, G. Centi and F. Trifiro, J. Chem. Soc., Faraday Trans. 1, 81, 1003 (1985).

75. A.J. van Hengstum, J.G. van Ommen, H. Bosch and P.J. Gellings, "Proc. 8th Internat. Cong. Catalysis", Dechema, Frankfurt-am-Main, IV 297 (1984).

76. A. Vejux and P. Courtine, J. Solid State Chem., 23, 93 (1978).

77. A.S. Russell and J.J. Stokes, Ind. Eng. Chem., 38, 1071 (1946).

78. M. Gąsior, I. Gąsior and B. Grzybowska, Appl. Catal., 10, 87 (1984).

79. L. Salvati, L.E. Makovsky, J.M. Stencel, F.R. Brown and D.M. Hercules, J. Phys. Chem., 85, 3700 (1981).

80. S. Yoshida, T. Iguchi, S. Ishida and K. Tarama, Bull. Chem. Soc. Jap., 45, 376 (1972).

81. M.V. Mathieu and H. Praliaud, J. Chim. Phys.-Chim. Biol., 73, 689 (1976).

82. S. Soled, L.L. Murrell, I.E. Wachs, G.B. McVicker, L.G. Sherman, S. Chan, N.C. Dispenziere and R.T.K. Baker,in "Solid State Chemistry in Catalysis", eds., R.K. Grasselli and J.F. Brazdil, ACS Symposium Series, 279, 103 (1985).

83. K.Y.S. Ng and E. Gulari, J. Catal., 92, 340 (1985).

84. F. Roozeboom, M.C. Mittelmeijer-Hazeleger, J.A. Moulijn, J. Medema, V.H.J. deBeer and P.J. Gellings, J. Phys. Chem., 84, 2783 (1980).

85. M. Iwamoto, T. Takenaka, K. Matsukami, J. Hirata, S. Kagawa and J. Izumi, Appl. Catal., 16, 153 (1985).

86. A. Castellan, J.C.J. Bart, A. Vaghi and N. Giordano, J. Catal., 42, 162 (1976).

87. D.S. Zingg, L.E. Makovsky, R.E. Tischer, F.R. Brown and D.M. Hercules, J. Phys. Chem., 84, 2898 (1980).

88. L.L. Murrell, D.C. Grenoble, R.T.K. Baker, E.B. Prestridge, S.C. Fung, R.R. Chianelli and S.P.Cramer, J. Catal., 79, 203 (1983).

89. V.A. Shvets and V.B. Kazansky, J. Catal., 25, 123 (1972).

90. Yu.I. Yermakov, Catal. Rev.-Sci. Eng., 13, 77 (1976).

91. J. Buiten, J. Catal., 36, 81 (1975).

92. J. Sonnemans and P. Mars, J. Catal., 31, 209 (1973).

93. T. Fransen, P.C. van Berge and P. Mars, in" Preparation of Catalysts", Eds., B. Delmon, P.A. Jacobs and G. Poncelet, Elsevier, Amsterdam, 405 (1976).

94. F. Roozeboom, T. Fransen, P. Mars and P.J. Gellings, Z. anorg. allg. Chem., 449, 25 (1979).

95. A.J. van Hengstum, Ph.D. Thesis, Twente University of Technology, Enschede, The Netherlands (1984).

96. K. Nowinska, Bull. Ac. Pol. Chim., 32, 393 (1984).

97. L. Wang and W.K. Hall, J. Catal., 77, 232 (1982).

98. J. Leyrer, B. Vielhaber, M.I. Zaki, Z. Shuxian, J. Weitkamp and H. Knozinger, Materials Chemistry and Physics, 13,301 (1985).

99. J.C.W. Chien, J. Am. Chem. Soc., 93, 4675 (1971).

100. A.A. Malygin, A.N. Volkova, S.I. Kol"tsov and V.B. Aleskovskii, Zh. Obsh. Khim., 43, 1436 (1973).

101. G.C. Bond and P. Koñig, J. Catal., 77, 309 (1982).

102. Y. Murakami, M. Inomata, K. Mori, T. Ui, K. Suzuki, A. Miyamoto and T. Hattori,"Preparation of Catalysts III", Elsevier, Amsterdam, 531 (1983).

103. W. Hanke, K. Heise, H.G. Jerschkewitz, G. Lischke, G. Öhlmann and B. Parlitz, Z. anorg. allg. Chem., 438, 176 (1978).

104. R. Fricke, W. Hanke, H.-G. Jerschkewitz, B. Parlitz and G. Öhlmann, Appl. Catal., 9, 235 (1984).

105. R. Kozlowski, R.F. Pettifer and J.M. Thomas, J. Phys. Chem., 87, 5176 (1983).

106. J. Haber, A. Kozlowska and R. Kozlowski, J. Catal., 102, 52 (1986).

107. M. Glinski and J. Kijenski, in "Preparation of Catalysts", Eds., G. Poncelet, P. Grange and P.A. Jacobs, Elsevier, Amsterdam, 553 (1983).

108. K. Kijenski, A. Baiker, M. Glinski, P. Dollenmeier and A. Wokaun, J. Catal., 100, 1 (1986).

109. A.J. van Hengstum, J.G. van Ommen, H. Bosch and P.J. Gellings, Appl. Catal., 5, 207 (1983).

110. J.G. van Ommen, K. Hoving, H. Bosch, A.J. van Hengstum and P.J. Gellings, Z. Phys. Chem., N.F., 134, 99(1983).

111. F. Roozeboom, J. Medema and P.J. Gellings, Z. Phys. Chem., N.F., 111, 215 (1978).

112. I.E. Wachs, S.S. Chan and R.Y. Saleh, J. Catal., 91, 366 (1985).

113. A. Miyamoto, A. Hattori and Y. Murakami, J. Solid State Chem., 47, 373 (1983).

114. J. Haber and J. Stoch, React. Kinet. Catal. Lett., 9, 319(1978).

115. F.J. Gil-Llambías, A.M. Escudey, J.L.G. Fierro and A.L. Agudo, J. Catal., 95, 520 (1985).

116. S.L.T. Andersson and S. Järås, J. Catal., 64, 51 (1980).

117. S.S. Chan, I.E. Wachs, L.L. Murrell, L. Wang and W.K. Hall, J. Phys. Chem., 88, 5831 (1984).

118. I.R. Beattie and T.R. Gilson, J. Chem. Soc. (A), 2322 (1969); Proc. Roy. Soc. A, 307, 407 (1968).

119. A.J. van Hengstum, J. Pranger, J.G. van Ommen and P.J. Gellings, Appl. Catal., 11, 317 (1984).

120. I.E. Wachs, S.S. Chan and C.C. Chersich, Mater. Sci. Monoger, 28B, 1047 (1985).

121. R.Y. Saleh, I.E. Wachs, S.S. Chan and C.C. Chersich, J. Catal., 98, 102 (1986).

122. H. Bosch, B.J. Kip, J.G. van Ommen and P.J. Gellings, J. Chem. Soc., Faraday Trans. 1, 80, 2479 (1984).

123. I.E. Wachs, R.Y. Saleh, S.S. Chan and C.C. Chersich, CHEMTECH, Dec., 756 (1985).

124. D. Monti, A. Reller and A. Baiker, J. Catal., 93, 360 (1985).

125. J. Mendialdua, Ph.D. Thesis, University of Science and Technology of Lille, France (1983).

126. L. Fiermans and J. Verunick, Surf. Sci., 35, 42 (1973).

127. C.R.N. Rao, D.D. Sarma, S. Vasudenvan and M.S. Hegde, Proc. Roy. Soc. Lond. Ser. A., 367, 239 (1979).

128. C. Blaauw, F. Lecnhouts, F. van der Woude and G.A. Sawatsky, J. Phys. C, 8, 459 (1975).

129. B. Howath, J. Strutz, J. Geyer-Lippmann and E.G. Horvath, Z. Anorg. All. Chem., 483, 181 (1981).

130. J.S. Brinen, J.L. Schmitt, W.R. Doughman, P.J. Achorn and L.A. Siegel, J. Catal., 40, 295 (1975).

131. D. Briggs, J. Elec. Spec. Relat. Phenom., 9, 487 (1976).

132. F.P.J.M. Kerkhof and J.A. Moulijn, J. Phys. Chem., 83, 1612 (1979).

133. S.C. Fung, J. Catal., 58, 454 (1979)

134. M.A. Stranick, M. Houalla and D.M. Hercules, J. Catal., 103, 151 (1987).

135. J.B. Peri, in Catalysis, Science and Technology, eds., J.R. Anderson and M. Boudart, Springer, Berlin, Vol. 5, p. 171 (1984).

136. G. Busca and J.C. Lavalley, Spectrochimica Acta, 42A, 443 (1986).

137. R.W. Wenig and G.C. Schrader, J. Phys. Chem., 91, 1911 (1987).

138. R.W. Wenig and G.C. Schrader, J. Phys. Chem., 90, 6480 (1986).

139. S.J. Puttock and C.H. Rochester, J. Chem. Soc., Faraday Trans. 1, 82, 3033 (1986).

140. Y. Nakagawa, T. Ono, H. Miyata and Y. Kubokawa, J. Chem. Soc., Faraday Trans. 1, 79, 2929 (1983).

141. G. Busca, Langmuir, 2, 577 (1986).

142. G. Busca, G. Centi, L. Marchetti and F. Trifiro, Langmuir, 2, 568 (1986).

143. H. Miyata, K. Fujii, T. Ono, Y. Kubokawa, T. Ohno and F. Hatayama, J. Chem. Soc., Faraday Trans. 1, 83, 675 (1987).

144. M. Rusiecka, Radio Microwave Spectrosc., 53, 265 (1985).

145. M. Rusiecka, B. Grzybowska and M. Gąsior, Appl. Catal., 10, 101 (1984).

146. P. Mars and D.W. van Krevelen, Chem. Eng. Sci. (Special Suppl.), 3, 41 (1954).

147. A.A. Yabrov and A.A. Ivanov, React. Kinet. Catal. Lett., 14, 347 (1980).

148. G.K. Boreskov, A.A. Ivanov, O.M. Ilyinich and V.G. Ponomareva, React. Kinet. Catal. Lett., 3, 1 (1975).

149. P.J. Gellings, in "Catalysis", eds., G.C. Bond and G. Webb, Specialist Periodical Report, Vol. 7, the Royal Society of Chemistry, London, p. 105 (1985).

150. G. Busca, G. Centi and F. Trifiro, Appl. Catal., 25, 265 (1986).

151. K. Mori, M. Inomata, A. Miyamoto and Y. Murakami, J. Chem. Soc., Faraday Trans. 1, 80, 2655 (1984).

152. K. Mori, A. Miyamoto and Y. Murakami, J. Catal., 95, 482 (1985).

153. K. Mori, A. Miyamoto and Y. Murakami, J. Chem. Soc., Faraday Trans. 1, 82, 13 (1986).

154. K. Mori, M. Inomata, A. Miyamoto and Y. Murakami, J. Phys. Chem., 87, 4560 (1983).

155. O.V. Krylov, "Catalysis by Nonmetals", Academic Press, New York (1970).

156. M. Ai and S. Suzuki, J. Catal., 30, 362 (1973).

157. M. Ai, J. Catal., 49, 305 (1977).

158. H. Miyata, Y. Nakagawa, T. Ono and Y. Kubokawa, J. Chem. Soc., Faraday Trans. 1, 79, 2343 (1983).

159. B. Grzybowska-Swierkosz, in " Catalysis by Acids and Bases", eds., B. Imelik, C. Naccache, G. Coudurier, Y. Ben Taarit and J. C. Védrine, Elsevier, Amsterdam, 45 (1985).

160. C.J. Machiels, U. Chowdhry, W.T.A. Harrison and A.W. Sleight, in "Solid State Chemistry in Catalysis", eds., R.K. Grasselli and J.F. Brazdil, ACS Symposium Series, 207, 103 (1985).

161. U. Ozkan and G.L. Schrader, J. Catal., 95, 137 (1985).

162. K. van der Wiele and P.J. van den Berg, J. Catal., 39, 437 (1975).

163. N. Yamagata, Y. Owada, S. Okazaki and K. Tanabe, J. Catal., 47, 358 (1977).

164. K.Y.S. Ng and E. Gulari, J. Catal., 95, 33 (1985).

165. R. Burch and A. Collins, Appl. Catal., 18, 373 (1985).

166. A. Olalde and G. Perot, Appl. Catal., 13, 373 (1985).

167. M. J. Ledoux, A. Bouassida and R. Benazouz, Appl. Catal., 9, 41 (1984).

168. J. Sonnemans, G.H. van den Berg and P. Mars, J. Catal., 31, 220 (1973).

169. R. Thomas, J.A. Moulijn, V.H.J. de Beer and J. Medema, J. Mol. Catal., 8, 161 (1980).

170. K. Tanaka, K. Miyahara and K.-I. Tanaka, Bull. Chem. Soc. Jpn., *54, 3106 (1981)*.

171. J. Engelhardt, D. Kallo and I. Zsinka, J. Catal., 88, 317 (1984).

172. J. Abart, E. Delgado, G. Ertl, H. Jeziorowski, H. Knozinger, N. Thiele and X.ZH. Wang, Appl. Catal., 2, 155 (1982).

173. P. Dufresne, E. Payen, J. Grimblot and J.P. Bonnelle, J. Phys. Chem., 85, 2344 (1981).

174. F.E. Massoth, J. Catal., 36, 164 (1975).

175. F.E. Massoth, J. Catal., 30, 204 (1973).

176. L. Wang and W.K. Hall, J. Catal., 66, 251 (1980).

177. Y.C. Liu, G.L. Griffin, S.S. Chan and I.E. Wachs, J. Catal., 94, 108 (1985).

178. F.R. Brown, L.E. Makovsky and K.H. Rhee, J. Catal., 50, 162 (1977).

179. R. Burch and A. Collins, Appl. Catal., 18, 389 (1985).

180. R. Thomas, E.M. van Oers, V.H.J. de Beer, J. Medema and J.A. Moulijn, J. Catal., 76, 241 (1982).

181. R. Thomas, E.M. van Oers, V.H.J. de Beer and J.A. Moulijn, J. Catal., 84, 275 (1983).

182. M. Houalla, C.L. Kibby, L. Petrakis and D.M. Hercules, J. Catal., 83, 50 (1983).

183. B. Sombert, P. Dhamelincourt, F Wallart, A.C. Muller, M. Bouquet and J. Grosmangin, J. Raman Spectrosc., 9, 291 (1980).

184. R. Thomas, M.C. Mittelmeijer-Hazeleger, F.P.J.M. Kerkhof, J.A. Moulijn, J. Medema and V.H.J. de Beer, in "Proc. 3rd Internat. Conf. on Chemistry Uses of Molybdenum", eds., H.F. Barry and P.C. Mitchell, Climax Molybdenum Co., Ann Arbor, Michigan, 85 (1979).

185. J. Medema, C. van Stam, V.H.J. de Beer, A.J.A. Konings and D.C. Koningsberger, J. Catal., 53, 386 (1978).

186. E. Payen, S. Kasztelan, J. Grimblot and J.P. Bonnelle, J. Raman Spectrosc., 17, 233 (1986).

187. J.M. Stencel, L.E. Makovsky, T.A. Sarkus, J. de Vries, R. Thomas and J.A. Moulijn, J. Catal., 90, 314 (1984).

188. R. Thomas, Ph.D. Thesis, university of Amsterdam, Amsterdam, The Netherlands (1981).

189. A. Iannibello, S. Marengo, F. Trifiro and P.L. Villa, in "Preparation of Catalysts. II. Scientific Bases for the Preparation of Heterogeneous Catalysts", Proceedings of the Second Internat. Symp., eds., B. Delmon, P. Grange, P. Jacobs and G. Poncelet, Elsevier, Amsterdam, 65 (1979).

190. L. Wang and W.K. Hall, J. Catal., 83, 242 (1983).

191. P. Arnoldy, J.C.M. de jonge and J.A. Moulijn, J. Phys. Chem., 89, 4517 (1985).

192. T. Fransen, P.C. van Berge and P. Mars, React. Kinet. Catal. Lett., 5, 445 (1976).

193. H.C. Yao, J. Catal., 70, 440 (1981).

194. W.K. Hall and F.E. Massoth, J. Catal., 34, 41 (1974).

195. T. Fransen, O. van der Meer and P. Mars, J. Phys. Chem., 80, 2103 (1978).

196. R. Thomas, V.H.J. de Beer and J.A. Moulijn, Bull. Soc. Chim. Belg., 90, 1349 (1981).

197. P. Arnoldy, Ph.D. Thesis, University of Amsterdam, The Netherlands (1985).

198. C.V. Caceres, J.L.G. Fierro, A.L. Agudo, M.N. Blanco and H.J. Thomas, J. Catal., 95, 501 (1985).

199. S. Kasztelan, J. Grimblot, J.P. Bonnelle, E. Payen, H. Toulhoat and Y. Jacquin, Appl. Catal., 7, 91 (1983).

200. C.P. Cheng and G.L. Schrader, J. Catal., 60, 276 (1979).

201. P. Gajardo, D. Pirotte, P. Grange and B. Delmon, J. Phys. Chem., 83, 1780 (1979).

202. H. Jeziorowski, H. Knozinger, P. Grange and P. Gajardo, J. Phys. Chem., 84, 1825 (1980).

203. J.M. Stencel, J.R. Diehl, J.R. D'Este, L.E. Makovsky, L. Rodrigo, K. Marcinkowska, A. Adnot, P.C. Roberge and S. Kaliaguine, J. Phys. Chem., 90, 4739 (1986).

204. Y. Xian-chun, C. Jian-wen and L. Da-dong., J. Catalysis (Chinese), 5, 240 (1985).

205. A. Andreini and J.C. Mol, J. Chem. Soc., Faraday Trans. 1, 81, 1705 (1985).

206. J.M. Stencel, L.E. Makovsky, J.R. Diehl and T.A. Sarkus, J. Raman Spectrosc., 15, 282 (1984).

207. S.S. Chan, I.E. Wachs, L.L. Murrell and N.C. Dispenziere, J. Catal., 92, 1 (1985).

208. J.E. Germain and R. Laugier, Bull. Soc. Chim. Fr., 2, 541 (1972).

209. P. Sondag, D. Q. Kim and F. Marion, Compt. Rend., 259, 4704 (1964)

210. P. Biloen and G.T. Pott, J. Catal., 30, 169 (1973).

211. I.E. Wachs, C.C. Chersich and J.H. Hardenbergh, Appl. Catal., 13, 335 (1985).

212. J.C. Mol and J.A. Moulijn, Adv. Catal., 24, 131 (1975).

213. A.A. Olsthoorn and C.Boelhouwer, J. Catal., 44, 207 (1976).

214. P. Arnoldy, O.S.L. Bruinsma and J.A. Moulijn, J. Mol. Catal., 30, 111 (1985).

215. T.A. Pecoraro and R.R. Chianelli, J. Catal., 67, 430 (1981).

216. E.W. Stern, J. Catal., 57, 390 (1979).

217. P. Biloen, J.M. Helle, H. Verbeek, F.M. Dautzenberg and W.M.H. Sachtler, J. Catal., 63, 112 (1980).

218. R.J. Bertolacini and R.J. Pellet, in " Catalyst Deactivation", eds., B. Delmon and G.F. Froment, Elsevier, Amsterdam, 73 (1980).

219. W.H. Davenport, V. Kollonitsch and C.H. Kline, Ind. Eng. Chem., 60, 11 (1968).

220. F.P.J.M. Kerkhof, J.A. Moulijn and R. Thomas, J. Catal., 56, 279 (1979).

221. P. Arnoldy, E.M. van Oers, O.S.L. Bruinsma, V.H.J. deBeer and J.A. Moulijn, J. Catal., 93, 231 (1985).

CHAPTER 2

EXPERIMENTAL TECHNIQUES

2.1 Introduction

Many of the studies described in this thesis have been made using a common set of experimental techniques and apparatus. The purpose of this chapter is to collate the descriptions of these, thus avoiding repetition in the subsequent chapters.

2.2 Characterization methods

2.2.1 Chemical analysis

The V and Mo contents of the catalysts are expressed as Wt.% V_2O_5 and MoO_3 respectively. These were measured by Inductively Coupled Plasma Spectroscopy using a SPEX spectrometer. Samples were dissolved in HF/H_2SO_4 and after removing the HF, the sample analysed to an accuracy of $\pm$0.1%. Phosphorus and potassium contents are expressed as wt.% P_2O_5 and wt.% K_2O respectively. These were determined by X-ray fluorescence using the Philips 1270 automatic simultaneous XRF spectrometer. I wish to thank Dr. D. Urwin of Tioxide International Ltd. for arranging for these analyses to be carried out.

2.2.2 Surface area measurements

Physical adsorption (1) is a phenomenon which may be used for the surface area determination of solids. It is generally non-specific and occurs by means of van der Waals forces when a gas is brought into contact with an outgassed

solid surface.

The specific surface areas of the catalysts have been determined by nitrogen adsorption at 77 K (in a Carlo Erba Sorptomatic), using the BET equation (2). For the calculation of S_{BET}, the area of an adsorbed N_2 molecule was taken to be 0.162 nm^2.

Application

In the present work, surface areas were determined for:

(i) TiO_2 supports;

(ii) VO_x/TiO_2 catalysts;

and (iii) MoO_x/TiO_2 catalysts.

I wish to thank Mr. R.A. Roberts for carrying out the surface area measurements.

2.2.3 Laser Raman spectroscopy

Laser Raman spectroscopy is a vibration-analysis technique, which gives information on the nature of the compounds present in a sample. The use of Laser Raman spectroscopy in chemical applications has been reviewed (3-5). In the interpretation of the spectra, it should be kept in mind that not all vibrations of a molecule are Raman active: only when the polarizability of the molecule changes during a vibration, is it Raman active.

The Laser Raman spectra of the samples were recorded on a SPEX RAMALAB spectrometer and an EMI 9862B photomultiplier. The green (514.5 nm) emission line from a Coherent Radiation model 52 M.G. Ar^+ Laser was used for excitation. The output power of the Laser was always about 100 mW and 60 mW at the sample. The spectral slit width was 6 cm^{-1} and the scanning

speed was 50 cm^{-1} min^{-1}. A cylindrical lens was used just before the sample to image the Laser beam as a line rather than a point and thus minimise the decomposition of the sample. Catalysts were ground into a very fine powder, pelletized and placed in the sample holder for analysis. The spectrometer was calibrated by reference to the known lines of CCl_4. The wavenumber obtained from the spectra are accurate to within about 2 cm^{-1}.

Application

In the present work, the laser Raman spectroscopy technique has been applied to the structure of the following catalysts and pure compounds:

(i) VO_x/TiO_2 catalysts prepared by different methods;

(ii) MoO_x/TiO_2 catalysts prepared by different methods; and (iii) unsupported V_2O_5, MoO_3 and TiO_2 samples.

2.2.4 Fourier transform infrared spectroscopy (FTIR)

Infrared spectroscopy is a well accepted technique for the study of catalysts and surface reactions. The systems studied include amorphous support material such as silica, silica-alumina and titania and also crystalline solids such as metal oxides, molecular sieves, and metal dispersions supported on most of the above materials (4, 6-14).

These studies include the nature of the catalysts themselves (e.g., nature, quantity and acidity of hydroxyl groups present on the catalyst surface), the nature and quantity of the adsorbed species, the strength of adsorption, the detection of new species formed by surface reaction and occasionally the kinetics of surface reactions.

FTIR instruments offer higher sensitivity and higher resolution than conventional IR instruments: for these reasons FTIR is employed in studying the surfaces of materials (15,16).

Experimental

The IR spectra of VO_x/TiO_2 (P-25), TiO_2(P-25) and unsupported V_2O_5 samples were recorded in air using a Perkin-Elmer model 1710 Infrared Fourier - Transform Spectrometer. The spectra for the above samples were recorded after evacuation at 100°C for 3h. Pressed discs were prepared by mixing KBr and the oxide (ca. 2.0%) with a thickness 0.2 mm.

Application

In the present work, the FTIR technique has been used in preliminary studies on the following catalysts and pure compounds:

(i) VO_x/TiO_2(P-25) catalysts prepared by the $VOCl_3$ methods;

and (ii) unsupported V_2O_5 and TiO_2(P-25) samples.

2.2.5 X-ray photoelectron spectroscopy (XPS)

XPS is a technique which provides elemental and chemical information about a solid surface. When X-ray photons of energy $h\nu$ hit a solid surface, photoelectrons are ejected having a kinetic energy depending on the wavelength of the incident photon and on the energy which binds the electrons to the nucleus.

The binding energy (B.E.), which is the ionization

potential of the electron, is calculated from the equation:

$$B.E. = h\nu - K.E.$$

where $h\nu$ is the energy of the incident photon and K.E. is the kinetic energy of the ejected electron (17,18). Generally, a contact potential exists between the sample and the spectrometer which causes a slight change in the kinetic energy of the photoelectrons due to the charging effect. A factor ϕ, which includes the work function of the sample surface, is introduced into the above equation to compensate for the kinetic energy change, and the resulting equation is:

$$B.E. = h\nu - K.E. - \phi$$

Ejection of electrons may occur from any orbital for which the binding energy is less than the energy of the incident photon (18).

The difference in the oxidation states, and in the chemical environment of a given atom, determine the binding energy shift (19); while peak intensity, modified by the photoionization cross-section and the escape depth factor, determines the surface composition (20).

Following the creation of a hole in the core shell (K), the atom relaxes by filling the hole via a transition from an outer level(L_1). As a result of that transition the energy difference becomes available as excess kinetic energy, and this excess energy can be used by the atom in either of two ways. It can appear as a characteristic X-ray photon at that energy, and is called X-ray fluorescence, or it can be given to another electron either in the same level ($L_{2,3}$) or in a more shallow level, where upon the second electron is

ejected; this process is called Auger emission, Figure 2.1 (18). Clearly, both can not take place from the same initial core hole, so that they compete and their relative rates depend upon the atomic number of the element involved. High atomic numbers favour fluorescence, while Auger emission predominates with atoms of very low atomic numbers.

Equipment

The XPS-spectra were recorded on a Kratos ES 300 electron spectrometer, using an X-ray source comprising an aluminum anode (Al K_{α} = 1486.6 eV) operated at 14 KV and 11 mA. The pressure of the spectrometer was better than 5 x 10^{-7} Torr. Usually the samples were powdered in a mortar before the measurement and mounted on double-sided adhesive tape. Peaks corresponding to electron ejection from the C 1s, O 1s, Ti 2p, V 2p and Mo 3d were recorded.

Binding energies

A serious disadvantage of the fact that the V and Mo species were deposited on a semi-conductor oxidic carrier (TiO_2) is charging of the sample. Due to accumulation of surface charge during the measurement, a shift is observed in the binding energy of the atoms. In order to be able to determine the true energy of the atoms studied, it is necessary to correct for this effect, which has been reported by many others (21-27).

The energy of the C 1s level, due to surface contamination with hydrocarbons, has been used, as the reference line. It is then assumed that the shift of the C 1s line is the same as the shift of all other lines and that the nature of the carbon containing species is the same for

all samples.

Another method, namely, use of XPS lines of the support as a reference, can be considered. An advantage is that they are part of the sample.

In this study, the binding energies of standard compounds were determined by referencing to the C 1s line at 284.6 eV. The Ti $2p_{3/2}$ photoelectron line of the support (458.5 eV) served as the reference for catalyst samples on the grounds that most of this signal will originate from the Ti^{+4} ions within the bulk, and that any shifts due to modification of the surface layer will be minimal (27).

Calculation

In this work, the variation in the intensity of the V or Mo signals relative to the Ti signal was determined as a function of V or Mo content. The areas of the peaks of interest (V $2p_{1/2}$, V $2p_{3/2}$, Mo $3d_{3/2}$, Mo $3d_{5/2}$, Ti $2p_{1/2}$ and Ti $2p_{3/2}$) were measured. These areas were adjusted by photoelectron sensitivity factors (V, 2.69; Mo, 3.73; Ti, 2.39) (28). An example of this calculation can be seen on Figure 2.2 for the VO_x/TiO_2 catalyst. The areas of the four peaks of interest (V $2p_{1/2}$, V $2p_{3/2}$, Ti $2p_{1/2}$ and Ti $2p_{3/2}$) were measured by triangulation, using the average of the widths at 1/3, 1/2 and 2/3 of full peak height. These areas were divided by sensitivity factors (V, 2.69; Ti, 2.39) and the four intensity ratios calculated:

$$R_1 = V\ 2p_{1/2} / Ti\ 2p_{1/2};\ R_2 = V\ 2p_{1/2} / Ti\ 2p_{3/2};$$
$$R_3 = V\ 2p_{3/2} / Ti\ 2p_{1/2};\ R_4 = V\ 2p_{3/2} / Ti\ 2p_{3/2}.$$

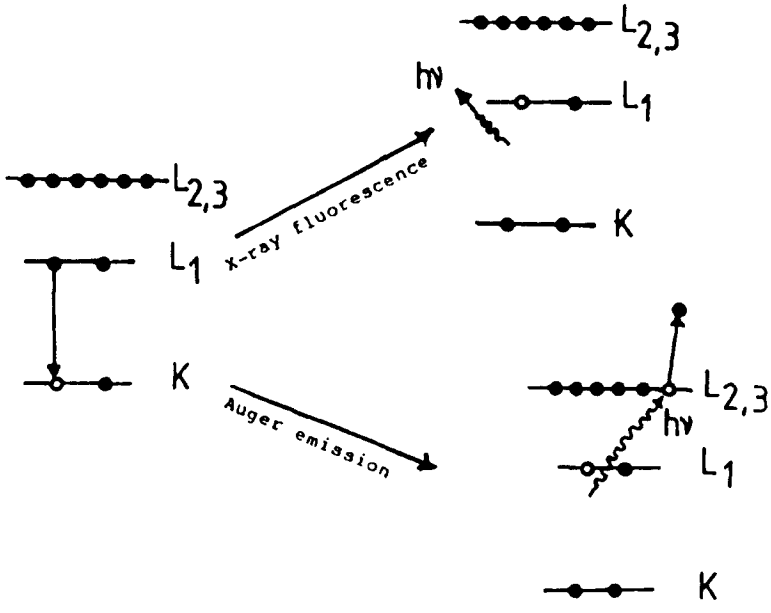

Figure 2.1 Schematic diagram of the Auger emission and X-ray fluorescence processes in a solid.

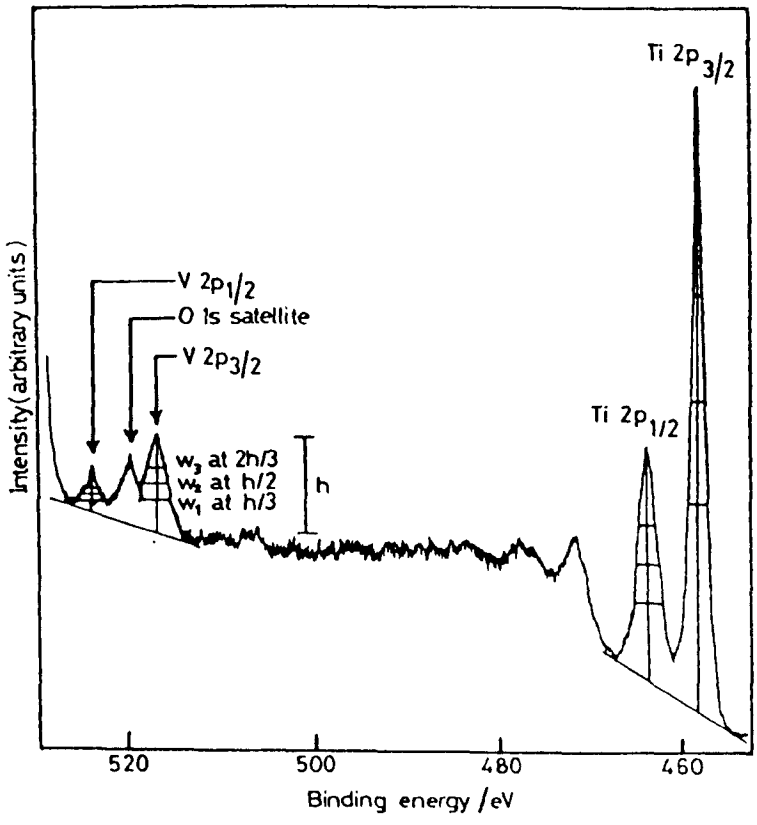

Figure 2.2 A typical XP spectrum indicating the base-lines used in estimating peak heights (5.0% V_2O_5 on washed low-area anatase (CLD 939) prepared by the aqueous impregnation method).

The ratios R_1 and R_2 are therefore generally less accurate than R_3 and R_4, for this reason R_3 and R_4 are used only in this work. The value of R_4 has been scaled to that of R_3 at the highest V content measured; the adjusted R_4 values and the R_3 values were then averaged, it being assumed that R_3 and R_4 values are comparably accurate. In most cases the values of this mean ($\bar{R}_{3,4}$) are reliable to about ±5%. Although the intensities of the two V peaks increases, and those of the two Ti peaks decrease, with increasing V content, it was impossible to obtain satisfactory reproducibility of absolute intensities from sample to sample, because the amount of sample exposed to the X-ray beam could not be controlled. The same calculations were carried out for MoO_x/TiO_2 catalysts.

Application

In the present work, the XPS technique has been applied for the following catalysts and pure compounds:

(i) VO_x/TiO_2 catalysts prepared by different methods;

(ii) MoO_x/TiO_2 catalysts prepared by impregnation methods;

and (iii) unsupported V_2O_5, MoO_3, TiO_2 and $(NH_4)_2\ VO(C_2O_4)_2 \cdot 2H_2O$ samples.

2.2.6 Electron spin resonance (ESR)

This is a branch of spectroscopy which is applicable specifically to the study of paramagnetic species, i.e. ones containing unpaired electrons (29,30).

The principles of ESR belong to fundamental physics. Essentially, an electron, which has a negative charge,

possesses a spin magnetic moment which can take up one of two possible orientations, because of quantisation, in an applied magnetic field. The magnetic field lifts the degeneracy of the $\pm 1/2$ states of the electron with the formation of two separated energy levels, the lower of which corresponds to $m_s = -1/2$ and the upper to $m_s = +1/2$. The lower energy state is more highly populated than the upper as given by the Boltzmann equation. Resonance is said to occur when the applied magnetic field induces a separation between these two levels that is equal in energy ($h\nu$) to that of an applied microwave field, with the electron absorbing energy from the microwave field and flipping its spin orientation from -1/2 to +1/2.

The resonance equation is:

$$h\nu = g_e \times \beta_e \times B$$

where g_e is the g-value of the electron, an experimental parameter that depends upon the chemical nature of the species under investigation, β_e is the Bohr magneton ($eh/4\pi m_e$) and B is the applied magnetic field.

A paramagnetic species can frequently be identified from its g-value and from hyperfine structure in the spectrum arising from the interaction of the unpaired electron(s) with a nucleus possessing a magnetic moment (I) when the resonance line splits into (2I + 1) hyperfine lines.

Calculation

The ESR spectra in this study were measured on a Varian E3 X-band spectrometer working at 9.5 GHz frequency and 100 kHz modulation. The samples were placed in standard 3mm internal diameter quartz tubes and the spectra run at room

temperature. The g-values were measured by comparison against DPPH (g_s = 2.0036) as standard using the equation

$$g_u = g_s \left(1 - \pm \Delta B_{sep} / B \right)$$

where ΔB is the field separation between the signal of the standard at a field value B and that of the sample.

Application

In the present work, the ESR technique has been applied to a study of two fresh VO_x/TiO_2(P-25) catalysts which were prepared by the $VOCl_3$ method containing 4.0% and 13.0% V_2O_5 loading as well as TiO_2(P-25). Quantitative estimates of the amounts of V(IV) were made using a sample of $(NH_4)_2VO(C_2O_4)_2.2H_2O$ for comparison. I wish to thank Dr. K.A.K. Lott for his assistance in recording the ESR spectra.

2.2.7 Temperature programmed reduction (TPR)

TPR provides information on the composition of mixtures of reducible compounds. As in gas chromatography (GC) the amount of the reduced materials, and thus the composition of the sample, can be derived from the areas of the TPR peaks. The assignment of the various peaks can often be accomplished by comparison with the reduction behaviour of the pure reference compounds (like retention time analysis in GC) (31). The basic idea was suggested first by Holm and Clark (32).

In the case of heterogeneous catalysts, the compounds to be reduced are present on the surface or are potentially

available to the surface. This method is a convenient tool to obtain "finger print" characterizations of the reducibility of catalysts. Hurst et al. (33) have recently give an excellent review of both the theoretical background and the applications of the technique.

The reduction is measured by monitoring H_2 consumption from a 6% H_2 / N_2 mixture while increasing the temperature of the sample at a constant heating rate. In this way, if one or more reduction peaks occur at different temperatures, the reduction profile or "spectrum" can be easily obtained.

The temperatures of the peak maxima (T_{max}) are characteristic of different reduction processes and may be used for "finger-print" identification.

Gentry et al. (34) have given a method for calculating the apparent activation energy of the reduction. They arrive at the equation:

$$\ln(T_m^2 / \beta) = E / RT_m + \text{constant}$$

where T_m is the temperature of the peak maximum (K), β is the heating rate ($K\ s^{-1}$) and E is the apparent activation energy ($kJ\ mol^{-1}$). In the derivation of the above equation, the assumptions are that a purely chemical process is described, its rate being governed by an Arrhenius equation.

Monti and Baiker (35) found that the only parameter affecting the peak shape is the apparent activation energy (E) and that the asymmetric peaks become sharper as the value of E increase.

The total area under one or more peaks corresponds to the total amount of H_2 consumed in the reduction process, from

which the final oxidation state of the reduced product can be determined. In the case of reduction of a V(V)-oxide / TiO_2 catalyst, two mole of H_2 are consumed per mole of V(V)-oxide surface species, which means, that V^{+5} is reduced to V^{+3} (36).

If the catalyst contains at least two or three different V-containing compounds that differ significantly in their ease of reduction, it is possible, by deconvolution of the split peaks, to calculate the amount of H_2 consumed by each species.

Apparatus and experimental procedure

The TPR apparatus used in the present work is shown in Figure 2.3. The catalyst sample, contained in a quartz reaction (inner diameter 10 mm), was surrounded by a tubular electric furnace whose temperature was controlled by a linear temperature programmer. The reducing gas, which is a mixture of 6% H_2 / N_2, was passed over 0.5% Pd/Al_2O_3 catalyst (for deoxygenation) and also through a trap of molecular sieve 4A for drying. The gas then flowed through the reference side of the thermal conductivity cell and then through the reactor to the cold trap kept at $-78^{\circ}C$ (to remove water and other reduction products that otherwise would interfere with the H_2 analysis). The gas then flowed to the sample side of the thermal conductivity cell.

The change in H_2 concentration before and after the reactor was monitored by the thermal conductivity cell. When the concentration of H_2 in the gas stream remained constant, the response displayed on the recorder is the base line. Any change in hydrogen concentration will cause the base line to

shift, indicating the start of reduction, until a peak is reached and the base line returns to its normal position showing that reduction is complete. The area under the peak represents the amount of hydrogen needed for the reduction of the sample. The detector response is calibrated by injecting a known volume of pure H_2 into the system at the end of the experiment, using a gas sampling valve.

The amount of H_2 in cm^3 consumed for the reduction per gram of sample is calculated by the following equation:

$$cm^3\ H_2 \text{ consumed / g} = \frac{WPS \times L \times SS \times CC \times F}{WPC \times SC \times CS \times WS}$$

where: WPS= weight of area under sample peak;

WPC= weight of area under calibration peak;

SS = sensitivity used for the sample;

SC = sensitivity used for the calibration;

CS = chart speed used for the sample;

CC = chart speed used for the calibration;

WS = weight of sample;

L = volume of H_2 injected (0.125 cm^3);

F = temperature correction factor converting volumes of gas from room temperature to STP (0.9381).

Small samples (18 - 960 mg) of catalyst were reduced in a 6% H_2 + 94% N_2 mixture (flow rate 40 $cm^3\ min^{-1}$). The temperature was raised from room temperature (25°C) to 950°C at constant heating of 5°C min^{-1}.

Application

In the present work, the TPR technique was used to study oxidation state changes and to detect and identify different

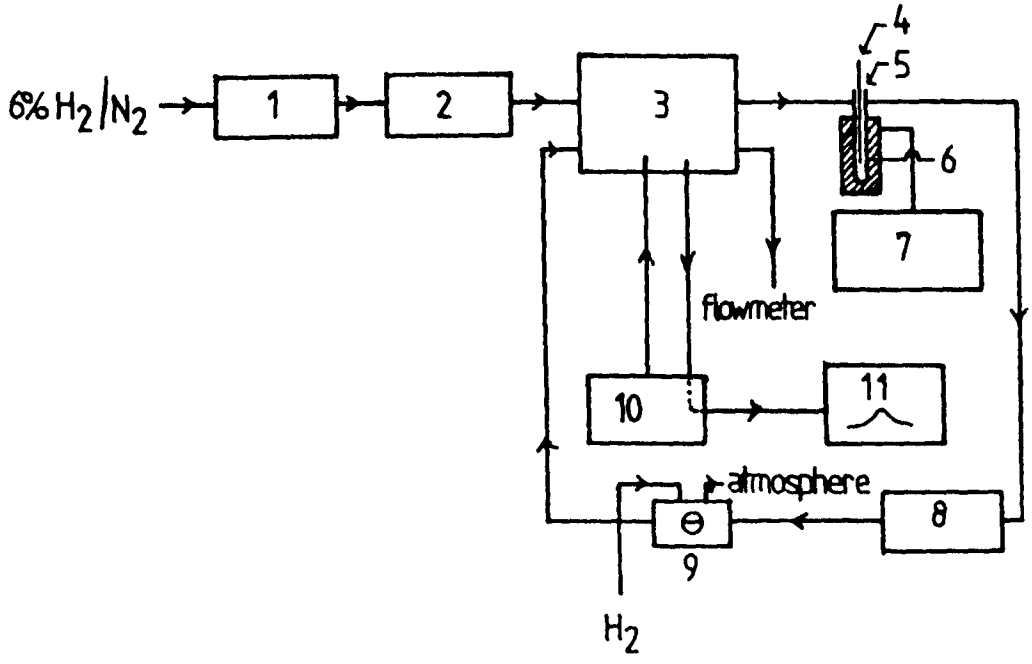

Figure 2.3 Flow diagram of apparatus for the TPR. 1: tube with Pd/Al_2O_3; 2: tube with molecular sieve; 3: detector; 4: thermocouple; 5: reactor; 6: furnace; 7:temperature programmer; 8: cold trap; 9: injection valve (for calibration); 10: power supply; 11: chart recorder.

V and Mo species for the following catalysts and pure compounds:

(i) VO_x/TiO_2 catalysts prepared by differents methods;

(ii) MoO_x/TiO_2 catalysts prepared by different methods;

and (iii) unsupported V_2O_5, MoO_3 and TiO_2 samples.

In addition, the effect of impurities such as P_2O_5, K_2O and SO_3 in the TiO_2 on the reducibility of the VO_x catalysts were also investigated.

2.3 Catalytic activity measurements

2.3.1 Selective oxidation of 1,3-butadiene to maleic anhydride

In order to assess the catalytic properties of the materials which had been prepared and characterised,the selective oxidation of 1,3-butadiene to produce maleic anhydride has been studied.

Apparatus

The apparatus is outlined in figure 2.4. Butadiene oxidation was carried out in a conventional flow apparatus at atmospheric pressure. The experiments were performed with a mixture containing about 1 mol% butadiene in air, made by mixing gas flows from the two cylinders (Both gases were dried with molecular sieves).The gases passed through pressure controllers (PC) and pressure indicators (PI), then through flow controllers (FC) and flow indicators (FI) before mixing. The reactor was a glass U-tube (1 cm inner diameter and about 16.5 cm long) and in one arm was a quartz sinter supporting the catalyst bed. The reactor temperature was controlled by connection to a temperature controller with a Chromel-Alumel feedback thermocouple. The outlet tube

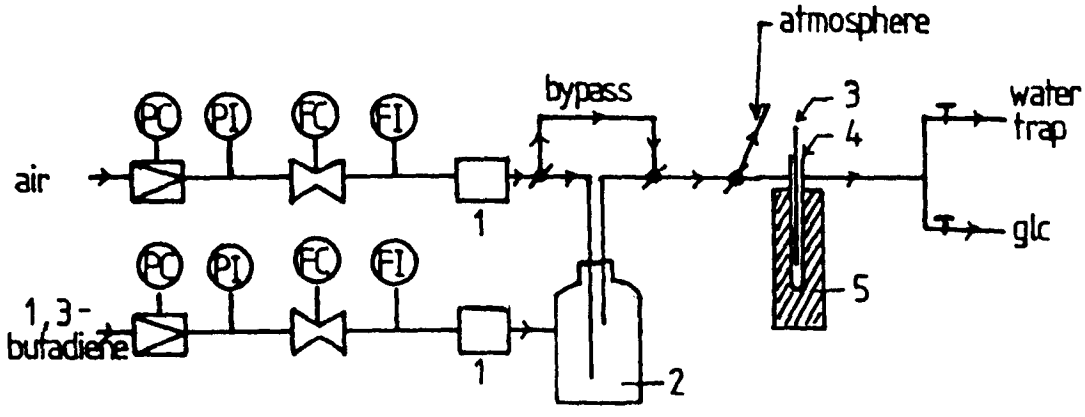

Figure 2.4 Flow diagram of apparatus for selective oxidation reaction of 1,3-butadiene. 1: tube with molecular sieve; 2: gas mixer; 3: thermocouple; 4: reactor; 5: furnace.

of the reactor was heated with an heating tape (170°C) to prevent condensation of the maleic anhydride which was subsequently collected in a water trap kept at ambient temperature for a measured time (15 to 60 min). The product was then titrated with standard 0.1M NaOH solution. 1,3-Butadiene was analysed using a Perkin-Elmer F11 GLC with a chart recorded connected. The GLC has a flame ionization detector and the carrier gas was N_2. The 1,3-butadiene was separated from untrapped products on a stainless steel column (2 mm i.d. x 3 m) packed with 20% Silicone fluid on Chromosorb P (80 - 100 mesh) at 170°C.

Experimental Procedure

0.2 g of the catalyst was placed on the quartz sinter in the U-tube. Air was passed through and the temperature was raised to 330°C and kept at this value for 1h. After this time, 1,3-butadiene was added and the reaction was left running overnight. After 18h, a complete steady state was reached, and the catalytic measurements were carried out at many different temperatures . As the reaction proceeded, samples were taken and analysed.

Calculation

The conversion and selectivities were calculated as a % and were defined as:

$$\%\text{Conversion} = \frac{\text{Mole of 1,3-butadiene removed}}{\text{Mole of 1,3-butadiene total}} \times 100$$

$$\%\text{Selectivity} = \frac{\text{Mole of maleic anhydride formed}}{\text{Mole of 1,3-butadiene removed}} \times 100$$

Apparent activation energies of the catalysts for butadiene removal (E_a), for maleic anhydride formation (E_{MA})

and for carbon oxides formation (E_{CO_x}) were calculated for the temperature range (283 - 374°C), refer Figure 2.5.

Application

In the present work, the selective oxidation of 1,3-butadiene to maleic anhydride has been used for the catalysts and pure compounds:

(i) VO_x/TiO_2 catalysts prepared by different methods;

(ii) MoO_x/TiO_2 catalysts prepared by different methods;

and (iii) unsupported V_2O_5 and TiO_2 samples.

2.3.2 Decomposition of isopropanol (37,38)

Decomposition of isopropanol to propylene was used as a test reaction for the determination of acidity of VO_x/TiO_2 catalysts. The isopropanol dehydrogenation product (acetone) was also analysed. Apart from propylene and acetone, only diisopropyl ether was found in the product, but the amount of this ether was very small compared with the amount of the other two compounds.

Apparatus

The apparatus is outlined in Figure 2.6. The reaction was carried out in a conventional flow apparatus at atmospheric pressure. The experiments were performed with a mixture containing about 1.08 mol % isopropanol in N_2 made by passing N_2 through a saturator filled with isopropanol at zero°C. The N_2 gas was dried with molecular sieves. The dried gas was then passed through a pressure controller (PC), then a pressure indicator (PI), followed by a flow controller (FC) and flow indicator (FI) before entering the saturator. The reactor was a glass U-tube (1 cm inner diameter and about 16.5 cm long) and in one arm was a quartz

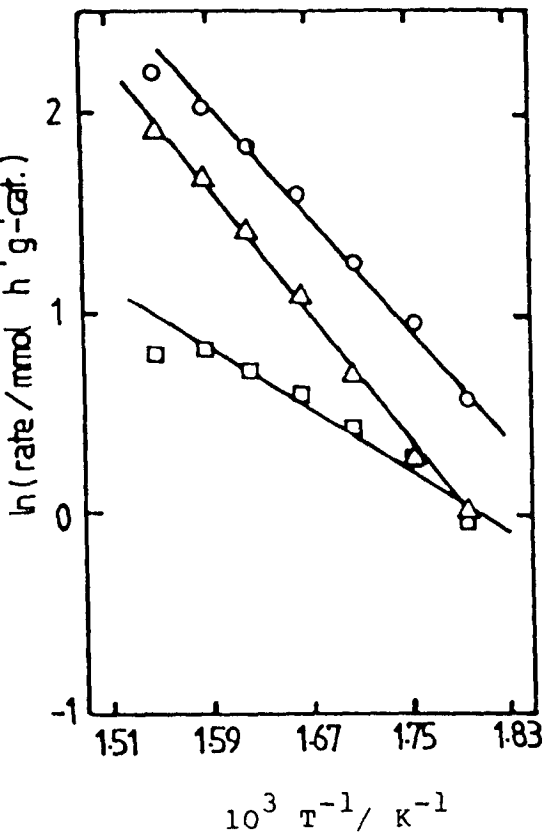

Figure 2.5 Typical plot for the calculation of E_t (○), E_{MA} (□) and E_{CO_x} (△) for VO_x/TiO_2(unwashed) catalyst containing 0.9% V_2O_5 prepared by wet impregnation method.

sinter supporting the catalyst bed. The reactor temperature was controlled by a Chromel-Alumel thermocouple (located with its tip in the catalyst bed) connected to a temperature controller. The outlet tube of the reactor was heated with a heating tape 70°C. The analysis of all the products being performed by a Perkin-Elmer F11 GLC with a chart recorded connected. The GLC has a flame ionization detector and the carrier gas was N_2. Propylene, diisopropyl ether, acetone and unreacted isopropanol were separated on a stainless steel column (2 mm i.d. x 3 m) packed with 5% Carbowax on 60 - 100 AW.H.M.D.S. treated Chromosorb W at 50°C.

Experimental procedure

0.1 g of catalyst was placed on the quartz sinter in the U-tube. The temperature was raised to 170°C. With the gaseous mixture flowing over the catalyst, this temperature was held for 4h. After this time activity measurements were made for the catalyst. The temperature was then changed and the above procedure repeated.

Calculation

%Conversion for isopropanol and %selectivities for propylene (S_{pr}) and acetone (S_{ac}) formation were calculated. The apparent activation energies of the catalysts for isopropanol removal (E_t), for propylene formation (E_{pr}) and for acetone formation (E_{ac}) were also calculated for the temperature range (189 - 252°C), refer Figure 2.7.

Application

In the present work, the isopropanol decomposition has been used for the following catalysts and pure compounds:

(i) VO_x/TiO_2 prepared by different methods;

and (ii) unsupported V_2O_5 and TiO_2 samples.

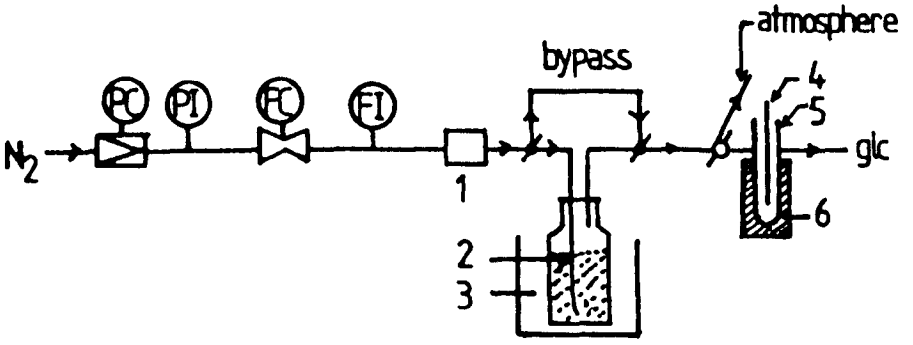

Figure 2.6 Flow diagram of apparatus for isopropanol decomposition. 1: tube with molecular sieve; 2: saturator filled with isopropanol; 3: thermostat; 4: thermocouple; 5: reactor; 6: furnace.

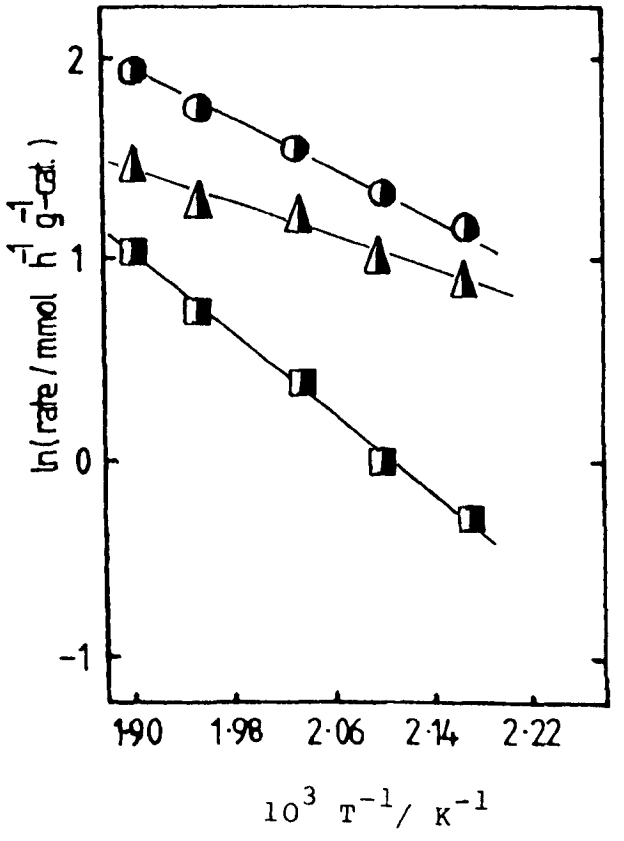

Figure 2.7 Typical plot for the calculation of E_t (◑), E_{ac} (◭) and E_{pr} (◧) for VO_x/TiO_2(P-25) monolayer catalyst containing 4.0% V_2O_5 prepared by the $VO(O^iBu)_3$ method.

2.4 Chemicals used

For operating the TPR apparatus and the GLC, cylinders of 6% H_2 / N_2 mixture, air, H_2 and N_2 were supplied by the British Oxygen Company.

1,3-Butadiene and propylene were supplied by Cambrian Gases Ltd. Isopropanol, acetone and diisoprpyl ether were obtained from Fisons Products (laboratory reagent grade).

2.5 References:

1. S.J. Gregg and K.S.W. Sing, "Adsorption surface area and porosity" Academic Press, London (1982).
2. S. Brunauer, P.H. Emmett and E. Teller, J. Amer. Chem. Soc., 60, 309 (1938).
3. J. Loader, Basic Laser Raman Spectroscopy, Heyden-Sadtler (1970).
4. T.T. Nguyen, J. Singapore National Acad. Sci., 10-12,84 (1983).
5. P.P. Shorygin, Russ. Chem. Rev., 47, 907 (1978).
6. G. Connell and J.A. Dumesic, J. Catal., 101, 103 (1986).
7. G. Connell and J.A. Dumesic, J. Catal., 102, 216 (1986).
8. M. Inomata, K. Mori, A. Miyamoto, T. Ui and Y. Murakami, J. Phys. Chem., 87, 754 (1983).
9. M. Inomata, K. Mori, A. Miyamoto and Y. Murakami, J. Phys. Chem., 87, 761 (1983).
10. G. Busca and J.C. Lavalley, Spectrochimica Acta, 42A, 443 (1986).
11. G. Busca, L. Marchetti, G. Centi and F. Trifiro, J. Chem. Soc., Faraday Trans. 1, 81, 1003 (1985).
12. G. Busca, H. Saussey, O. Saur, J.C. Lavalley and V. Lorenzelli, Appl. Catal., 14, 245 (1985).
13. G. Busca, Langmuir, 2, 577 (1986).
14. A. J. van Hengstum, Ph.D. Thesis, Twente University of Technology, Enschede, The Netherlands (1984).
15. C.L. Angell, Chapter 1 in Fourier Transform Infrared Spectroscopy: Techniques using Fourier Transform Interferometry, Vol. 3 (J.R. Ferraro and L.J. Basile, eds.), Academic Press, New York (1982).

16. P.R. Griffiths and J.A. de Haseth," Fourier Transform Infrared Spectroscopy", John Wiley & Sons, New York (1986).

17. P. Biloen and G.T. Pott, J. Catal., 30, 169 (1973).

18. D. Briggs and M.P. Seah, "Practical Surface Analysis by Auger and X-ray Photoelectron Spectroscopy", John Wiley & Sons, New York (1983).

19. M.W. Roberts, Chemistry in Britain, 17, 510 (1981).

20. C.D. Wagner, Anal. Chem., 44, 1050 (1972).

21. A. Cimino and B.A. De Angelis, J. Catal., 36, 11 (1975).

22. J. Haber and J. Stoch, React. Kinet. Catal. Lett., 9(3), 319 (1978).

23. D.S. Zingg, L.E. Makovsky, R.E. Tischer, F.R. Brown and D.M. Hercules, J. Phys. Chem., 84, 2898 (1980).

24. L. Salwati, L.E. Makovsky, J.M. Stencel, F.R. Brown and D. M. Hercules, J. Phys. Chem., 85, 3700 (1981).

25. P. Dufresne, E. Payen, J. Grimblot and J.P. Bonnelle, J. Phys. Chem., 85, 2344 (1981).

26. C. Ping Li and D. M. Hercules, J. Phys. Chem., 88, 456 (1984).

27. J. Mendialdua, Ph.D. Thesis, University of Science and Technology of Lille, France (1983).

28. Theoretical photoionization cross sections from 1 to 1500 eV. J. H. Scofield (Lawrence Livermore Lab., Univ. of California), 376 (1973).

29. K.A. Mclauchlan,"Magnetic Resonance", Oxford Chemistry Series (P.W. Atkins, J.S.E. Holker and A.K. Holliday, Eds.) Clarendon Press, Oxford (1972).

30. W.N. Delgass, G.L. Haller, R.Kellerman and J.H. Lunsford,"Spectroscopy in Heterogenous Catalysis", Academic Press, New York (1979).

31. J.W. Jenkins, B.D. McNicol and S.D. Robertson, Chem. Tech., 1977, 316 (1977).

32. V.C.F. Holm and A. Clark, J. Catal., 11, 305 (1968).

33. N.W. Hurst, S.J. Gentry, A. Jones and B.D. McNicol, Catal. Rev. Sci. Eng., 24, 233 (1982).

34. S.J. Gentry, N.W. Hurst and A. Jones, J. Chem. Soc. Faraday Trans. 1, 75, 1688 (1979).

35. D.A.M. Monti and A. Baiker, J. Catal., 83, 323 (1983).

36. A.J. van Hengstum, J.G. van Ommen, H. Bosch and P.J. Gellings, Proc. 8th Internat. Congr. Catalysis, Dechema, Frankfurt-am-Main, IV, 297 (1984).

37. M. Ai, Bull. Chem. Soc. Jpn., 49, 1328 (1976).

38. M. Gasior, I. Gasior and B. Grzybowska, Appli. Catal., 10, 87 (1984).

CHAPTER 3

PREPARATION OF CATALYSTS

3.1 Introduction

This Chapter deals with the preparation of series of supported V and Mo oxide catalysts by different methods. Several types of TiO_2 (mainly anatase) were used as supports in these preparations.

3.2 Titania supports

The supports used in the present work were supplied by Tioxide International Ltd. and their characteristic properties are shown in Table 3.1. In order to remove the impurities listed in Table 3.1, some of the supports were washed with water as described below.

3.3 Reagents

NH_4VO_3, $(NH_4)_6Mo_7O_{24}.4H_2O$, KOH and oxalic acid were obtained from Fisons Products (laboratory reagent grade).

$VOCl_3$ was obtained from Aldrich, $MoOCl_4$ from Lancaster Synthesis and vanadyl triisobutoxide ($VO(O^iBu)_3$) was prepared as described below (1):

Purified isobutanol (in excess) and NH_4VO_3 mixture was refluxed rapidly under a 300 mm fractionating column. The water was removed as formed by the azeotropic system (The H_2O-n-heptane azeotrope was removed at 79.0°C). After 32h, the majority of the excess isobutanol was distilled off. The clear solution was decanted from the unreacted solid and the remaining isobutanol was removed by vacuum distillation. The

Table 3.1

Characteristic properties of the TiO_2 samples used as support

TiO_2	support washing	surface area/m^2g^{-1}	phase	impurities (wt.%) Al_2O_3	SiO_2	P_2O_5	K_2O	SO_3
CLD 939	unwashed	~9.6	anatase	<0.01	<0.01	0.45	0.28	0.02
CLD 939-W	washed	~9.6	anatase	n.d.	n.d.	0.15	0.05	n.d.
Degussa P-25	unwashed	~55.0	anatase(76%)	<0.3	<0.2	<0.02	<0.02	----
CLD 1117/2	unwashed	~48.6	anatase	<0.01	<0.01	0.4	<0.005	2.6
CLD 1117/2-W	washed	~48.6	anatase	n.d.	n.d.	0.6	<0.001	n.d.
1-Eurotitania	unwashed	~45.5	anatase	<0.002	----	<0.0046	----	<0.025
CLD 782	unwashed	~9.6	anatase	<0.01	<0.01	0.50	0.28	0.08

n.d. = not determined

final solution was purified by two consecutive vacuum distillations (b.p. 87°C under 0.55 Torr) to get a pale yellow liquid ($VO(O^{i}Bu)_3$ in a yield of 56.6%.

The solvents used were benzene, toluene, carbon tetrachloride, ethanol, cyclohexane, n-heptane, and isobutanol. All solvents were obtained from Fisons Products (laboratory reagent grade).

3.4 Pretreatment of TiO_2

3.4.1 Washing of TiO_2 to remove the P and K impurities

Before using the TiO_2 as a support in some preparations of the catalysts, a preliminary washing was carried out to remove impurities such as P and K. 25 g of TiO_2 (9.6 m^2g^{-1}, anatase) was washed with deionized water by refluxing for 24h in a Soxhlet apparatus. After washing, the material was then dried in an air oven at 120°C and designated as TiO_2 (washed).

Using this treatment, it was found that P and K were partially removed from the TiO_2 (Table 3.1).

3.4.2 Addition to TiO_2 of some impurities including P and K

Addition of P and K to the unwashed and washed supports (9.6 m^2g^{-1}, anatase) by wet impregnation:

Samples of unwashed and washed support (5 g) were each impregnated with 15 cm^3 aliquots of an aqueous solution containing H_3PO_4 and KOH respectively, followed by drying in an air oven at 120°C overnight (18h). The concentrations of $H_3PO_4$and KOH were chosen to increase the level of P_2O_5 by 0.25 and 0.75 wt.% in the unwashed support and the level of K_2O by 0.15 and 0.35 wt.% in the washed support.

The supports doped with P_2O_5 and K_2O were used in some catalyst preparations.

3.5 Preparation of V catalysts

Three methods were used to prepare the supported vanadium oxide (VO_x) catalysts.

3.5.1 Wet impregnation method

Catalyst preparation

5 g of the support was first wetted with doubly-distilled water and dried for 18h at 120°C in an air oven. The desired amount of NH_4VO_3 (series A, B, C, D and E, Table 3.2) was added to 20 cm^3 of 1M oxalic acid solution, which on heating provided the deep blue $(NH_4)_2VO(C_2O_4)_2$ complex.

In the case of high V contents ($\geq$ 14 wt.%), stoichiometric amounts of NH_4VO_3 and oxalic acid were dissolved in 20 cm^3 water (to produce a blue solution on heating). The resulting solution was added to the support, and the water evaporated slowly on a hot-plate while stirring continuously until the material was apparently dry. The resulting solid was dried overnight in an air oven at 120°C and a portion calcined in an air furnace at 450°C for 5h.

Results and discussion

Using the impregnation method, the percentage of VO_x deposited on the TiO_2 support depends on the amount of V-complex in the solution (Table 3.2). Because the impregnation method does not involve a specific reaction

with the surface hydroxyl groups, it is not possible to prepare a monolayer catalyst by this technique.

The surface areas of the catalysts prepared by this method are equal to those of the supports. Only relatively high VO_x contents resulted in a lower surface area, and only in the case of high surface area supports: this is probably due to sintering of the support.

Table 3.2

Results for the preparation of VO_x/TiO_2 catalysts by wet impregnation method.

Catalyst*	V_2O_5%	Colour
Series A,		
VO_x/TiO_2 CLD 939	0.4	very pale yellow
"	0.9	yellow
"	1.8	"
"	3.7	"
"	4.2	"
"	5.3	"
"	7.6	"
"	8.8	"
Series B,		
VO_x/TiO_2 CLD 939-W	0.4	very pale yellow
"	0.9	yellow
"	1.8	"
"	4.1	"
"	5.0	"
"	5.4	"
"	7.5	"
"	8.8	"
Series C,		
VO_x/TiO_2 CLD 939-A	1.0	"
VO_x/TiO_2 CLD 939-B	1.1	"
Series D,		
VO_x/TiO_2 CLD 939-WD	1.0	"
VO_x/TiO_2 CLD 939-WE	0.9	"
Series E,		
VO_x/TiO_2 P-25	2.0	"
"	4.0	brown
"	8.2	"
"	14.0	"
"	22.0	"
"	32.0	"

* W = washed
A and B = 0.25 and 0.75 wt.% P_2O_5 were added to the support CLD 939 respectively by wet impregnation.
WD and WE = 0.15 and 0.35 wt.% K_2O were added to the support CLD 939-W respectively by wet impregnation.

3.5.2 $VOCl_3$ mothod

Catalyst preparation

The procedure for preparing catalysts using $VOCl_3$ is an improved version of that described by Bond and Brückman (2).

5 g of TiO_2 was placed in a two-necked flask to which doubly-distilled water is added. The TiO_2 was dried under a slow flow of N_2 (150^oC for 18h).

A solution of $VOCl_3$ in dry benzene was added, and after fitting a reflux condenser the flask was heated at 70^oC for 5h with stirring (Figure 3.1). The solid was then filtered under N_2, washed with pure solvent and dried for 1h in an air oven. The hot solid was subsequently hydrolysed by passing moist air over it, after which it was dried (120^oC, 18h) and calcined (450^oC, 5h).

In the standard preparation, 0.2 cm^3 $VOCl_3$ in 50 cm^3 benzene was used for 9.6 m^2g^{-1} TiO_2, and 0.8 cm^3 $VOCl_3$ in 70 cm^3 benzene for 50 $\pm$ 5 m^2g^{-1} TiO_2. This represents a 2.5 and a 2.0 $\pm$ 0.2-fold excess of V respectively, over that estimated needed to form a monolayer (Table 3.3). Half quantities of $VOCl_3$ was used to make a half-monolayer catalyst.

To obtain the equivalent of two or more monolayers, the catalysts were re-impregnated using the same procedure (as described above in this section) as many times as required, finally producing 3.8 monolayers.

Results and discussion

In $VOCl_3$ method, the monolayer is formed by a specific chemical reaction of $VOCl_3$ with surface hydroxyl groups, with the elimination of HCl. The pretreatment conditions

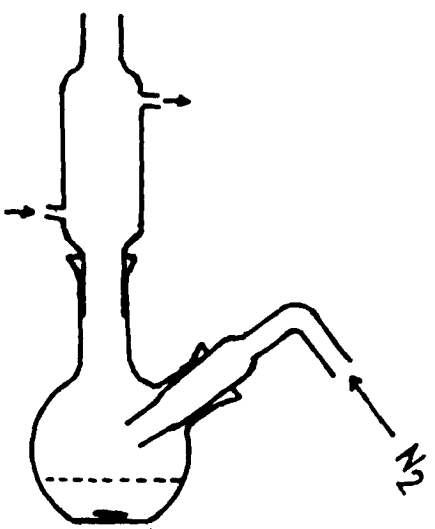

Figure 3.1 Schematic representation of the apparatus used for the preparation of the catalyst by the $VOCl_3$, $VO(O^iBu)_3$ and $MoOCl_4$ methods.

described above were designed to remove physisorbed water but not to dehydroxylate the surface. The exact stoichiometry of the reactions is not known, but there is qualitative evidence for the release of HCl in the hydrolysis stage.

In previous publications (2-4), the basis for a single theoretical monolayer has been taken as a lamella of the V_2O_5 structure, which if laid upon a TiO_2 surface would correspond to 0.145 wt.% V_2O_5 per m^2 of surface (see Appendix IA). The results of chemical analysis for V_2O_5 on a support of given area may be converted into a fraction of the theoretical monolayer (actual V_2O_5 / theoretical V_2O_5 x 100).

However, it now seems more appropriate to employ an empirical definition of monolayer capacity based on observation. Application of the surface-specific methods noted above to anatase of 9.6 m^2g^{-1} usually leads to a V_2O_5 content of 0.85 $\pm$ 0.05 wt.% (Table 3.3), i.e. about 55 - 62% of a theoretical monolayer. For the high surface area anatase (48.6 m^2g^{-1}), a single treatment affords 4.8 $\pm$ 0.6 wt.% V_2O_5, i.e. (0.08 - 0.1) wt.% V_2O_5 per m^2 as the monolayer capacity for anatase. Busca et al. (5) and Haber et al. (6) found that the monolayer capacity for anatase high areas (117 and 120 m^2g^{-1}) were 8.3% and 13.3% V_2O_5 respectively using the $VOCl_3$ method. Degussa P-25 gives somewhat lower V_2O_5 contents, i.e. 0.07 wt.% V_2O_5 per m^2. This latter figure may be due either to the fact that the Degussa P-25 particles comprise a rutile coating on an anatase core, or to the existence of surface impurities, especially of SiO_2. The monolayer capacity for P-25 of surface 55 m^2g^{-1} was 4.0

wt.% V_2O_5(Table 3.3). van Hengstum et l. (4,7) found similar results for VO_X/TiO_2 monolayer catalysts using vanadate adsorption from acidic solution and vanadium acetylacetonate methods.

Table 3.3

Results for the preparation of monolayer catalysts by the $VOCl_3$ method.

Catalyst	V_2O_5%	Colour	% of theoretical monolayer of V_2O_5
VO_X/TiO_2 CLD 939	0.9	yellow	62
VO_X/TiO_2 CLD 939-W	0.8	"	55
VO_X/TiO_2 P-25	4.0	brown	50
VO_X/TiO_2 CLD 1117/2	5.4	yellow	76
VO_X/TiO_2 CLD 1117/2-W	4.2	"	60

The experimental results of vanadium content in the VO_X/TiO_2 monolayer catalysts (Table 3.3) support the results of the calculations of VO_X monolayer based on two methods of calculation. In the first method, the number of Ti-OH group nm^{-2} is taken as 4.9 nm^{-2} (8,9) giving 0.71 wt.% V_2O_5 per 9.6 m^2g^{-1} (see Appendix IIA). In the second method, the number of $Ti_{surface}$ atoms is taken as 6.25 nm^{-2} for the (010) anatase surface and at a 1:1 V:Ti ratio of 0.091 wt.% V_2O_5 per m^2 (see Appendix IIIA).

In order to increase the VO_X content of the support surface, successive treatments were applied and it was found

that each gave almost equal increments in the amounts of VO_X (Figure 3.2) (4). From the nature of the reaction between $VOCl_3$ and surface hydroxyl groups, it is expected that during the first treatment the vanadium complex would be well dispersed on the surface of the support. By calcining at 450°C for 5h, all Cl^- ions are removed, possibly leading to the formation of VO_X containing OH groups with which further $VOCl_3$ can react. Concerning the VO_X species present in the monolayer (first layer), a detailed EXAFS study (10) has concluded that they are dioxo-vanadium species linked to the surface by two bridging oxygens, and arranged in a disordered fashion. Haber et al. (6,11) suggested the following structure (A) on the (010) anatase surface:

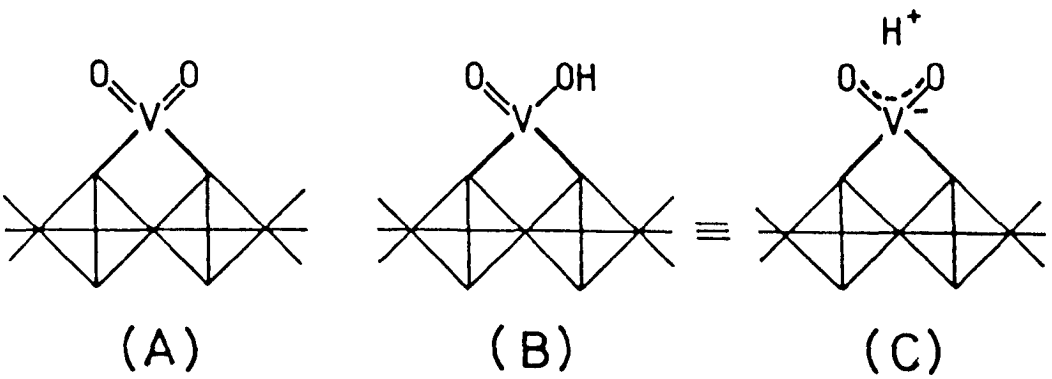

this representation is however inadequate on several grounds. This V=O bond order cannot be as high as two, and is more probably about 1.5 (10); the structure does not have the facility to react with a further vanadium precursor to form a second layer. For this reason, the structure suggested for this VO_X species is the oxohydroxy formulation (B) or a structure (C) in which the electrons are delocalised. Structure (B) received support from the FTIR results of Busca et al. (5,12). In the following treatment, the $VOCl_3$ can react with these OH groups, forming an over growth

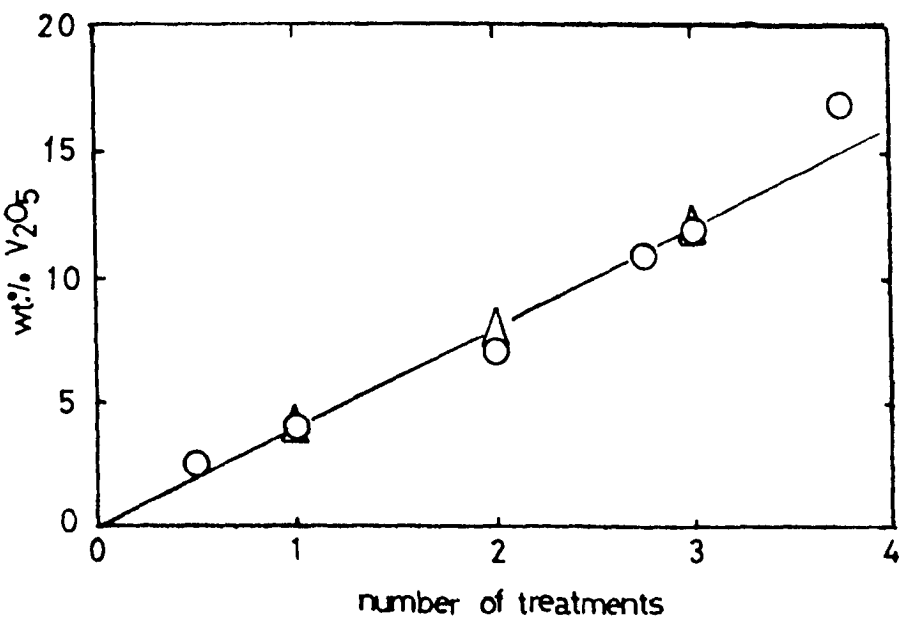

Figure 3.2 Results of the preparation of catalysts by successive treatment of $VOCl_3$ from benzene; ○, VO_x/TiO_2(P-25); △, VO_x/TiO_2 CLD 1117/2.

of VO_x upon calcination and the process repeated. The experimental results are presented in Figure 3.2.

The same effect appears here for the surface area measurements of these catalysts as is the case of impregnated catalysts (see Section 3.5.1).

3.5.3 $VO(O^iBu)_3$ method (13)

Catalyst preparation

The general procedure described in Section 3.5.2 for $VOCl_3$ was used for the $VO(O^iBu)_3$ method. The reaction temperature was 75°C, toluene as a solvent, and after filtration the solid was washed, dried and calcined as before.

In the standard preparation, 0.62 cm^3 $VO(O^iBu)_3$ in 50 cm^3 toluene was used for 9.6 m^2g^{-1} TiO_2, and 2.5 cm^3 $VO(O^iBu)_3$ in 70 cm^3 toluene for 50 $\pm$ 5 m^2g^{-1} TiO_2. This represents a 2.7 and 2.2 $\pm$ 0.2-fold excess of V respectively, over that estimated to be needed to form a monolayer. Half quantities of $VO(O^iBu)_3$ were used to make a half-monolayer catalyst.

To obtain higher VO_x coverages of the support, the procedure was repeated several times and samples were prepared designed to have 1.3, 1.5, 2, 2.3, 2.5, 3, 4 and 5 monolayers.

Results and discussion

In this method, the influence of the pretreatment of the support, the adsorption temperature, the reaction time and the solvent used was investigated.

Because the $VO(O^iBu)_3$ is moisture sensitive, supports

used without pretreatment (i.e. without drying under inert atmosphere N_2) result in more hydrolysis of $VO(O^iBu)_3$ than is necessary to form a VO_x monolayer. To avoid this problem, the supports were dried at 150°C (18h) under an inert atmosphere (N_2). Drying under these conditions removes physisorbed water molecules but does not dehydroxylate the surface of the support.

Three solvents were tried for the preparation method, namely ethanol, cyclohexane and toluene. For the dried support (9.6 m^2g^{-1}) a solution containing 0.62 cm^3 of $VO(O^iBu)_3$ in 50 cm^3 solvent was used and a reaction temperature of 75°C for 5h. It appeared that cyclohexane and toluene were better solvents than ethanol in the preparation using this method because higher V contents were obtained using the first two solvents (Table 3.4).

Table 3.4

Results for the preparation of monolayer catalysts by the $VO(O^iBu)_3$ method using different solvents.

Catalyst	Solvent	V_2O_5%	Colour
VO_x/TiO_2 CLD 939	cyclohexane	0.8	yellow
"	toluene	0.8	yellow
"	ethanol	0.3	very pale yellow

The use of ethanol as a solvent resulted in a lower V content of the catalyst (0.3 wt.% V_2O_5), caused either by a

better solvation of the $VO(O^iBu)_3$ in ethanol, or by strong adsorption of ethanol on the support surface (14) or by a combination of the two.

The influence of the adsorption temperature is presented in Figure 3.3, showing that the V content increases slightly with temperature. $VO(O^iBu)_3$ is believed to react with the surface hydroxyl groups of the support, with elimination of ^iBuOH.

The effect of varying the time of reaction of $VO(O^iBu)_3$ with the surface hydroxyl was also examined and the results are given in Table 3.5, which shows that after 5h, the V content remains constant.

Table 3.5

Results for the preparation of monolayer catalysts as a function of time for the adsorption of $VO(O^iBu)_3$ on TiO_2 (9.6 m^2g^{-1}).

Catalyst	time(hr)	V_2O_5%	Colour
VO_x/TiO_2 CLD 939	1	0.5	yellow
"	3	0.7	"
"	5	0.8	"
"	7	0.8	"

The result for a single treatment by this method show that the actual amount of V_2O_5 formed on an anatase support of given area is a fraction of the theoretical monolayer (0.145 wt.% V_2O_5 per m^2 of surface).

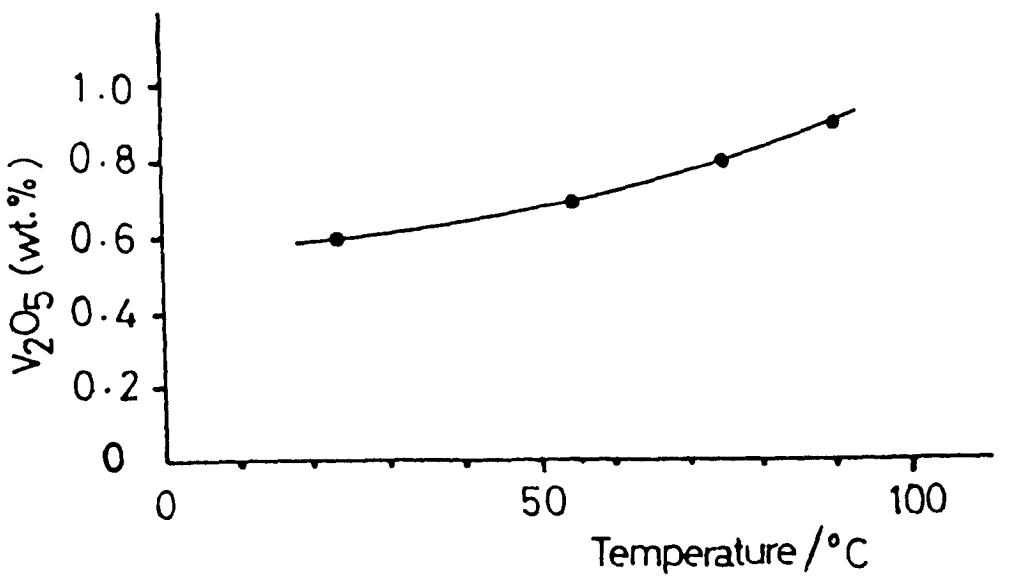

Figure 3.3 Influence of the temperature during the adsorption of $VO(O^iBu)_3$ from toluene on the vanadium content of supported catalysts.

Anatase (9.6 m^2g^{-1}) leads to a V_2O_5 content of 0.85 ± 0.05 wt.% (Table 3.6), a similar result to the $VOCl_3$ method (Table 3.3). For anatase of high surface area (48.6 m^2g^{-1}) a single treatment affords 4.95 ± 0.15 wt.% V_2O_5 and the Eurotitania (45.5 m^2g^{-1}) gave 4.4 wt.% V_2O_5. These figures indicate 0.08-0.1 wt.% V_2O_5 per m^2 to be the monolayer capacity for anatase.

Like the $VOCl_3$ method, P-25 again gives lower V_2O_5 contents, i.e. 0.07 wt.% V_2O_5 per m^2 (Table 3.6). From the above results it appear that the structure of VO_x monolayer species is similar to that obtained using the $VOCl_3$ method (structure B or C, Section 3.5.2).

Table 3.6

Results for the preparation of monolayer catalysts by the $VO(O^iBu)_3$ method.

Catalyst	V_2O_5%	Colour	% of Theoretical monolayer of V_2O_5
VO_x/TiO_2 CLD 939	0.8	yellow	55
VO_x/TiO_2 CLD 939-W	0.8, 0.9*	"	55, 62*
VO_x/TiO_2 (P-25)	3.9, 4.0*	brown	49, 50*
VO_x/TiO_2 CLD 1117/2	4.8	yellow	67
VO_x/TiO_2 CLD 1117/2-W	5.1	"	72
VO_x/TiO_2 Eurotitania	4.4	"	66

*Duplicate preparations

Kijenski et al. (15) obtained an incomplete VO_x monolayer (i.e. 0.45% V_2O_5) by the reaction of $VO(O^iBu)_3$ dissolved in n-hexane with OH groups present on the surface of TiO_2(P-25) with surface area 38 m^2g^{-1}. They suggested that part of the OH groups on the surface of TiO_2 were unreactive toward the alkoxide, and thus the coverage stays below one monolayer with the first impregnation. They suggested also that the vanadyl species are doubly bound to the surface of titania.

However, after the calcination stage (450°C,5h) to remove the residual organic materials, a second and subsequent treatment leads to the deposition of about the same amount of VO_x as deposited in the first treatment. The experimental results are presented in Figure 3.4 (4). From these results it appears that the structure of VO_x layers is similar to that obtained using the $VOCl_3$ method and the mechanism of overgrowth in subsequent treatments is the same.

The surface area of the catalysts is equal to the surface area of the supports: only at high loadings is there a decrease which is due to sintering of the supports.

3.6 Preparation of Mo catalysts

Two methods were used to prepare the supported MoO_x catalysts.

3.6.1 Wet impregnation method

The same procedure described in Section 3.5.1 for V catalysts preparation was employed, but using $(NH_4)_6Mo_7O_{24}.4H_2O$ instead of NH_4VO_3. Mo catalysts were prepared in the range 0.25-9.5 wt.% MoO_3 with TiO_2 CLD782

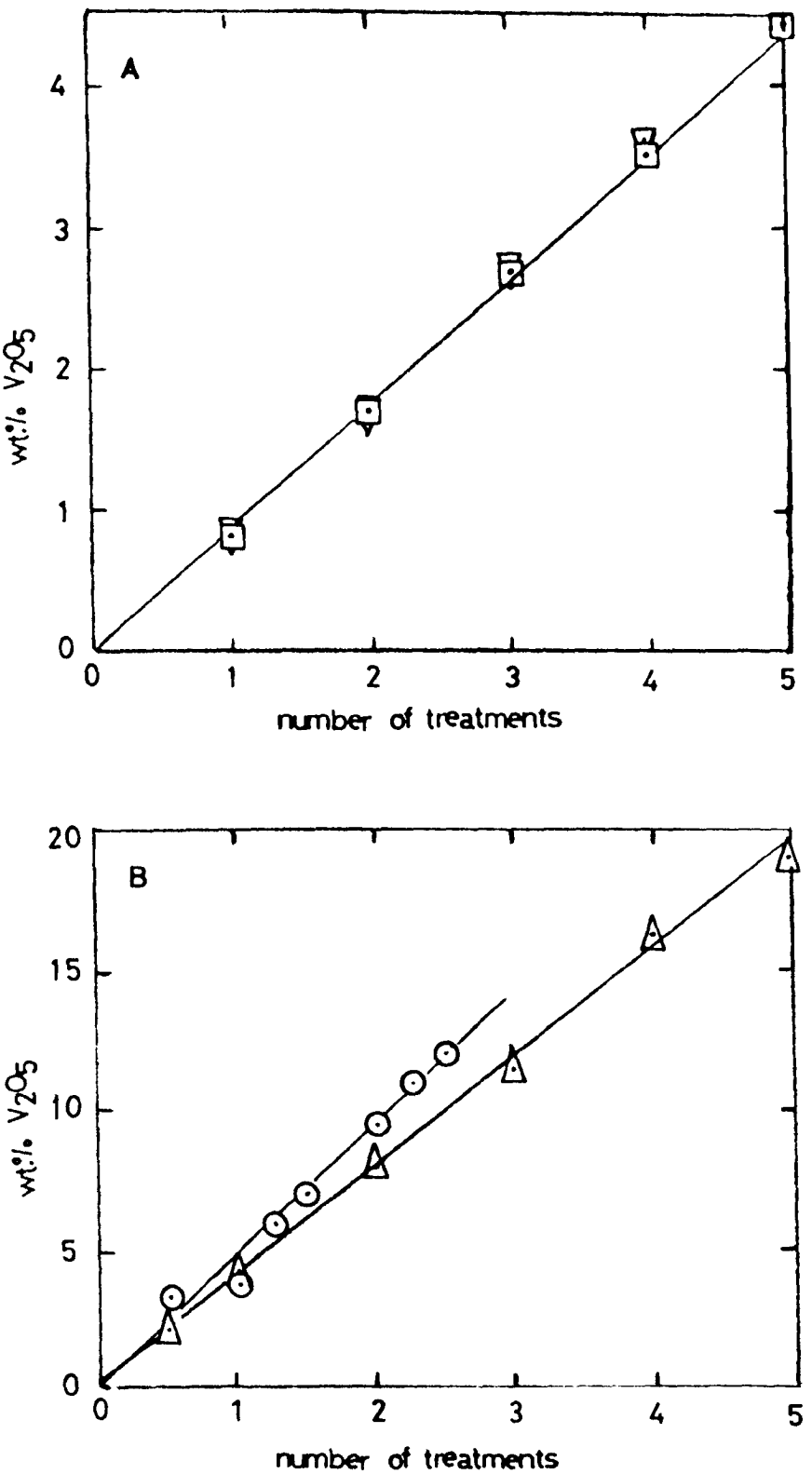

Figure 3.4 Results of the preparation of catalysts by successive treatment of $VO(O^{i}Bu)_3$ from toluene; (A) ▽, VO_x/TiO_2 CLD 939; ⊡, VO_x/TiO_2 CLD 939-W. (B) ⊙, VO_x/TiO_2(P-25); △, VO_x/TiO_2(Eurotitania).

(see Table 3.7).

Using the impregnation method, the percentage of MoO_x deposited on the TiO_2 support depends on the amount of Mo-complex in the solution (Table 3.7).

Table 3.7

Results for the preparation of MoO_x/TiO_2 catalysts by wet impregnation method.

Catalyst	MoO_3%	Colour
MoO_x/TiO_2 CLD 782	0.25	white
"	0.40	"
"	0.80	"
"	1.30	"
"	1.80	yellow
"	3.30	yellow-green
"	5.10	green
"	7.30	"
"	9.50	"

3.6.2 $MoOCl_4$ method

The same procedure described in Section 3.5.2 for V catalysts preparation was employed, but using a solution of $MoOCl_4$ in CCl_4 instead of $VOCl_3$ in benzene. CCl_4 was used as the solvent for $MoOCl_4$ because benzene reacts with $MoOCl_4$ (16).

In the standard preparation, 0.36 g $MoOCl_4$ in 50 cm^3 CCl_4 was used for 9.6 m^2g^{-1} TiO_2(anatase) and 1.6 g $MoOCl_4$ in 70 cm^3CCl_4 for 55 m^2g^{-1} TiO_2(P-25). This represents a 2.5 and a 2.0-fold excess of Mo respectively, over that estimated to form a monolayer (Table 3.8).

Results and discussion

In this method, the MoO_x monolayer catalyst is formed by a reaction of $MoOCl_4$ with surface OH groups, with the elimination of HCl.

The basis for a single theoretical monolayer has been taken as a single layer of the MoO_3 structure, which if laid upon a TiO_2 surface would correspond to 0.164 wt.% MoO_3 per m^2 of surface (4)(see Appendix IB). The results of chemical analysis are expressed as MoO_3 on a support of given area as a fraction of this theoretical monolayer (see Table 3.8). Using anatase (9.6 m^2g^{-1}) gives a MoO_3 content of 0.8 wt.%, i.e. about 49% of a theoretical monolayer, and 0.08 wt.% MoO_3 per m^2 as the monolayer capacity. TiO_2(P-25) gives 4.1 wt.% MoO_3, i.e. about 45% of a theoretical monolayer (0.075 wt.% MoO_3 per m^2). Monolayer contents for MoO_x/TiO_2 catalysts have been estimated by many workers, employing various preparative techniques. For low-area anatase, a value of 0.9 wt.% MoO_3 has been reported using the molybdenum acetylacetonate method (4), while for TiO_2(P-25) values of between 3.9 and 6.3 wt.% MoO_3 have been given (4,7,17,18). These are in fair agreement with the results reported in this work.

Table 3.8
Results for the preparation of monolayer catalysts by the $MoOCl_4$ method.

Catalyst	MoO_3%	Colour	% of theoretical monolayer of MoO3
MoO_X/TiO_2 CLD 782	0.8,0.8*	white	49
MoO_X/TiO_2 (P-25)	4.1	pale-yellow	45

*Duplicate preparations

The experimental results of Mo content in the MoO_X/TiO_2 monolayer catalysts (Table 3.8) are lower comparing with the results of the calculations of MoO_X monolayer based on two methods of calculation. In the first method, the number of Ti-OH groups nm^{-2} is taken as 4.9 nm^{-2} (8,9) giving 1.12 wt.% MoO_3 per 9.6 m^2g^{-1} (Appendix IIB). In the second method, the number of $Ti_{surface}$ atoms is taken as 6.25 nm^{-2} for the (010) anatase surface and at a 1:1 Mo:Ti ratio of 0.143 wt.% MoO_3 per m^2 (Appendix IIIB). These results may imply a structure such as (A) or a mixture of structures (A) and (B), with the former predominating.

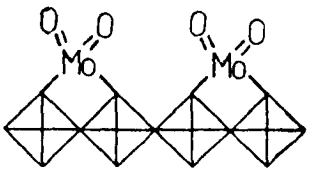

(A)

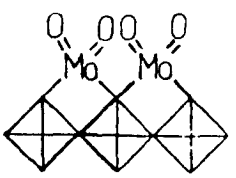

(B)

3.7 Conclusions

The $VOCl_3$, $VO(O^iBu)_3$ and $MoOCl_4$ methods were used to prepare supported VO_X and MoO_X catalysts by reaction with the surface hydroxyl groups of the support. All three methods were capable of giving a significant fraction of a monolayer catalysts by a single treatment. The other methods were intended to produce more than one monolayer (i.e. the aqueous impregnation and multiple treatment of $VOCl_3$ or $VO(O^iBu)_3$ methods).

3.8 References

1. F. Cartan and C.N. Caughlan, J. Phys. Chem., 64, 1756 (1960).
2. G.C. Bond and K. Brückman, Faraday Disc. Chem. Soc., 72, 235 (1981).
3. F. Roozeboom, M.C. Mittelmeijer-Hazeleger, J.A. Moulijn, J. Medema, V.H.J. de Beer and P.J. Gellings, J. Phys. Chem., 84, 2783 (1980).
4. A.J. van Hengstum, J.G. van Ommen, H. Bosch and P.J. Gellings, Appl. Catal., 5, 207 (1983).
5. G. Busca, G. Centi, L. Marchetti and F. Trifrio, Langmuir, 2, 568 (1986).
6. J. Haber, A. Kozlowska and R. Kozłowski, J. Catal., 102, 52 (1986).
7. A.J. van Hengstum, Ph.D. Thesis, Twente University of Technology, Enschede, The Netherlands (1984).
8. H.P. Boehm and M. Herrmann, Z. Anorg. Allg. Chem., 352, 156 (1967).
9. G.D. Parfitt, in"Progress in Surface and Membrane Science", Vol. 11 (D.A. Cadenhead and J.F. Danielli, eds.), 181 (1976).
10. R. Kozłowski, R.F. Pettifer and J.M. Thomas, J. Phys. Chem., 87, 5176 (1983).
11. J. Haber, Proc. 8th Internat. Congr. Catalysis, Dechema, Frankfurt-am-Main, I85 (1984).
12. G. Busca, Langmuir, 2, 577 (1986).
13. M. Gliński and J. Kijeński, in"Preparation of Catalysts", (G. Poncelet, P. Grange and P.A. Jacobs, eds.), Elsevier, Amsterdam, 553 (1983).

14. I. Carrizosa and G. Munuera, J. Catal., 49, 174 (1977).

15. J. Kijenski, A. Baiker, M. Glinski, P. Dollenmeier and A. Wokaun, J. Catal., 101, 1 (1986).

16. M.L. Larson and F.W. Moore, Inorg. Chem., 5, 801 (1966).

17. K.Y.S. Ng and E. Gulari, J. Catal., 92, 340 (1985).

18. Y.C. Liu, G.L. Griffin, S.S. Chan and I.E. Wachs, J. Catal., 94, 108 (1985).

CHAPTER 4

TITANIA-SUPPORTED VANADIUM OXIDE CATALYSTS

4.1 Introduction

The catalysts studied in this chapter were prepared as described in Chapter 3. It is unclear at present how the surface species resulting from the impregnation of the support with an aqueous solution of $(NH_4)_2VO(C_2O_4)_2$ obtained by dissolving NH_4VO_3 in water with oxalic acid may differ from those obtained with the grafting method ($VOCl_3$ and $VO(O^iBu)_3$ methods). In this Chapter, various techniques were used (Temperature programmed reduction (TPR), laser Raman spectroscopy, X-ray photoelectron spectroscopy (XPS), electron spin resonance (ESR) and Fourier transform infrared spectroscopy (FTIR)) to characterise the VO_x species formed by different preparative methods. Several types of TiO_2 have been used as supports. Catalytic oxidation of 1,3-butadiene and decomposition of isopropanol have been studied with some of these catalysts. The Arrhenius parameters both for the decomposition of isopropanol and for the oxidation of 1,3-butadiene show the compensation effect which are summarized in Figures 4.92 and 4.93 in the Discussion Section respectively.

4.2 Results

4.2.1 Unsupported V_2O_5

4.2.1.1 Characterisation

The specific surface area of the pure V_2O_5(Merck) is 8.5 m^2g^{-1}. This material was studied by TPR and laser Raman spectroscopy.

TPR

The TPR profile (Figure 4.1) of pure V_2O_5 has three peaks with T_{max} values of 662, 694 and 765°C. The quantity of H_2 consumed corresponds to that required for the reduction of V(V) to V(III) (i.e. 2 mol H_2/mol V_2O_5).

Laser Raman spectroscopy

The Raman spectrum of pure V_2O_5 shows bands at 995, 700 and 485 cm^{-1} as was also observed by others (1). The band at 995 cm^{-1} is the most intense and is attributed to the V=O····V vibration (2).

4.2.1.2 Oxidation of 1,3-butadiene

Selectivity to maleic anhydride (S_{MA}) increased with increasing temperature (S_{MA} = 44% at 73% conversion at 375°C). Figure 4.2 shows the S_{MA}% versus 1/T. Figure 4.2 shows also the plots of ln(rate of butadiene removal/r_B), ln(rate of formation of maleic anhydride/r_{MA}) and ln(rate of formation of carbon oxides/r_{CO_x}) versus 1/T giving the apparent activation energies for butadiene removal (E_B), for formation of maleic anhydride (E_{MA}) and for formation of carbon oxides (E_{CO_x}). The parameters (E_B, E_{MA} and E_{CO_x}) were measured at conversions up 30%. Table 4.1 shows E_B, E_{MA} and E_{CO_x} and the corresponding values of lnA.

4.2.1.3 Decomposition of isopropanol

The value of selectivity to propylene(S_{pr}) is always 93% through out the range of the reaction temperature (163 - 221°C). Figure 4.3 shows the plots of ln(rate of isopropanol removal/r_t), ln(rate of formation of acetone/r_{ac}) and

ln(rate of formation of propylene/r_{pr}) versus 1/T, giving the apparent activation energies for isopropanol removal (E_t), for formation of acetone (E_{ac}) and for formation of propylene (E_{pr}). Table 4.2 shows E_t, E_{ac} and E_{pr} and the corresponding values of lnA.

Table 4.1

The Arrhenius parameters of unsupported V_2O_5 catalyzed oxidation of 1,3-butadiene.

E_B[1]	lnA[2]	c.c.	E_{MA}[1]	lnA[2]	c.c.	E_{CO_x}[1]	lnA[2]	c.c.
69.4	16.92	0.987	148.1	31.2	0.967	55.6	13.9	0.968

1 = E/ kJ mol^{-1};

2 = ln(A/ mmol $h^{-1}g^{-1}$cat.);

c.c. = correlation coefficient.

Table 4.2

The Arrhenius parameters of unsupported V_2O_5 catalyzed decomposition of isopropanol.

E_t[1]	lnA[2]	c.c.	E_{ac}[1]	lnA[2]	c.c.	E_{pr}[1]	lnA[2]	c.c.
41.0	12.27	0.982	49.0	11.67	0.952	40.1	12.08	0.972

1 = E/ kJ mol^{-1};

2 = ln(A/mmol $h^{-1}g^{-1}$cat.);

c.c. = correlation coefficient.

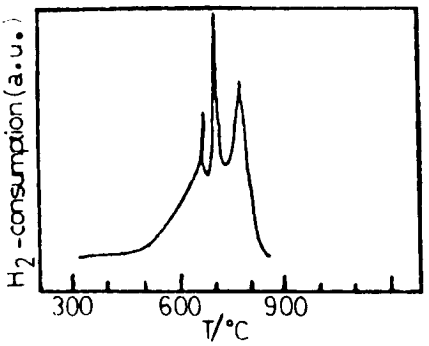

Figure 4.1 TPR profile of pure V_2O_5.

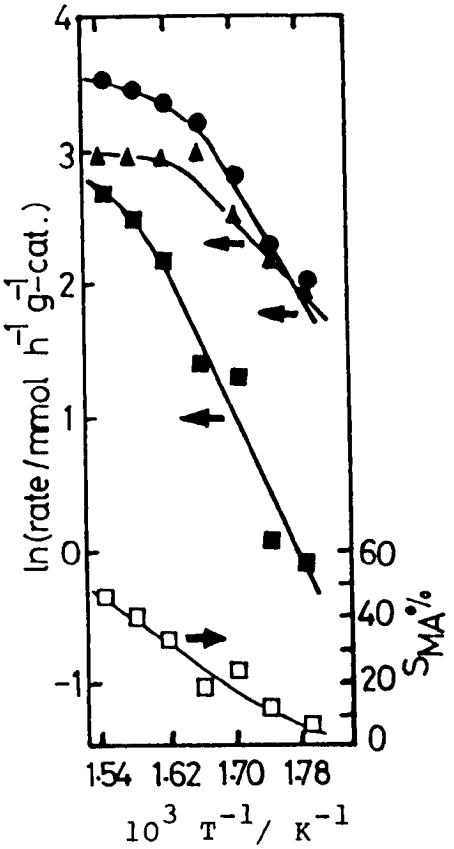

Figure 4.2 Ln(rate/r_B(●), r_{MA}(■) and r_{CO_x}(▲)) and S_{MA}% versus 1/T for unsupported V_2O_5 catalyzed oxidation of 1,3-butadiene.

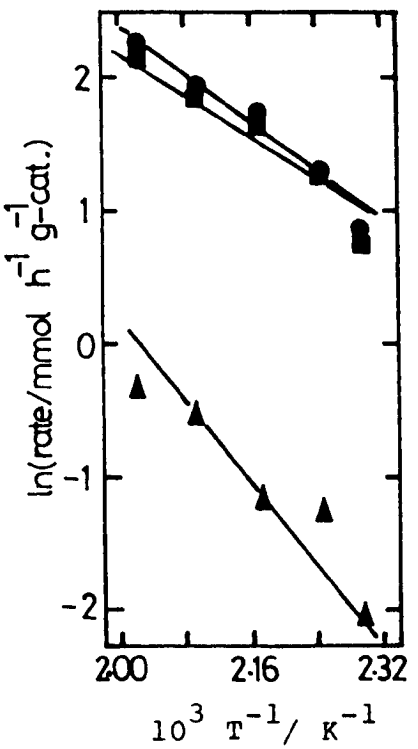

Figure 4.3 Ln(rate/r_t(●), r_{ac}(▲) and r_{pr}(■)) versus 1/T for unsupported V_2O_5 catalyzed decomposition of isopropanol.

4.2.2 VO_x/TiO_2(CLD 939, anatase, unwashed, 9.6 m^2g^{-1})

Unwashed TiO_2 CLD 939 was used as a support for these catalysts. It contained P_2O_5 and K_2O as impurities (see Table 3.1, Chapter 3).

4.2.2.1 Catalysts prepared by the wet impregnation method

The VO_x/TiO_2(unwashed) catalysts containing 0.4 - 8.8 wt.% V_2O_5 were prepared by this method as described in Section 3.5.1 of Chapter 3.

4.2.2.1.1 Characterisation

The catalysts were studied by TPR, laser Raman spectroscopy and XPS. The results are given below.

TPR

Figure 4.4 shows the TPR profiles for catalysts containing 0.4 - 8.8% V_2O_5, for the support and for pure V_2O_5. Figure 4.5 shows the dependence of T_{max}, and Figure 4.6 shows the H_2 consumption per g catalyst, as a function of V_2O_5 content.

The TPR profiles for samples containing 0.4 - 1.8% V_2O_5 consist of a single peak. It is difficult to estimate precisely the value of T_{max} in the submonolayer region, as the peak is broad, but it is in the range 530 - 538°C (Figure 4.5). This is well below the T_{max} of the first of the three peaks seen with pure V_2O_5. At 3.7% V_2O_5, a small shoulder appears on the high temperature side of the main peak, the T_{max} of which shifts to lower temperature up to 4.2% V_2O_5, then increases to higher temperature with increasing V_2O_5 content. The shoulder becomes a peak at 5.3%

V_2O_5 and increases in size with increasing V_2O_5 content (Figure 4.4). The quantity of H_2 consumed corresponds to that required for reduction of V(V) to V(III) (Figure 3.6)(i.e. 2 mol H_2/mol V_2O_5). Approximate manual deconvolution of the split peaks appears to show that the first peak attains a constant size after the second starts to appear. Above 5.3% V_2O_5, however, the size of the first peak starts to increase. Deconvolution may be inaccurate due to the extensive overlap of the two peaks, the broadening of which may arise from the presence of K_2O and P_2O_5 impurities in or on the TiO_2.

Laser Raman spectroscopy

Laser Raman spectra were obtained for the same series of catalysts, as well as for the support and for pure V_2O_5 (Figure 4.7). The band at 995 cm^{-1}, due to the V=O····V vibration, suffers least interference by the bands due to anatase (640, 515 and 385 cm^{-1}). For samples containing up to 5.3% V_2O_5, the portion of the spectrum above 850 cm^{-1} was also run at a higher sensitivity: some of these results are shown in greater detail in Figure 4.8. The important feature of these spectra is that the 995 cm^{-1} band is not detectable at V_2O_5 loadings of less than 3.7% V_2O_5. From the variation of the intensity of the 995 cm^{-1} band with V_2O_5 content (Figure 4.9), it is clearly associated with the second and subsequent monolayers, although its intensity does not increase above 5% V_2O_5. The intensities of the bands due to anatase are severely weakened by even the lowest V_2O_5 contents, an effect which has been remarked on before (1,3) and which is almost certainly due to the Raman scattering

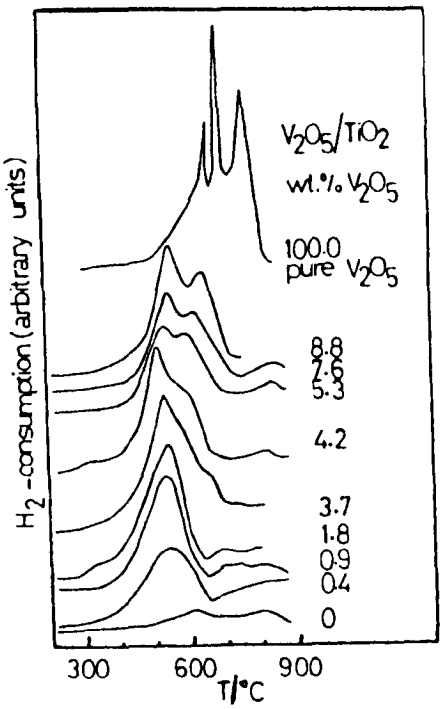

Figure 4.4 TPR profiles for catalysts prepared by aqueous impregnation of TiO_2 anatase(unwashed), and for the support and for pure V_2O_5. The wt.% V_2O_5 is given for each curve.

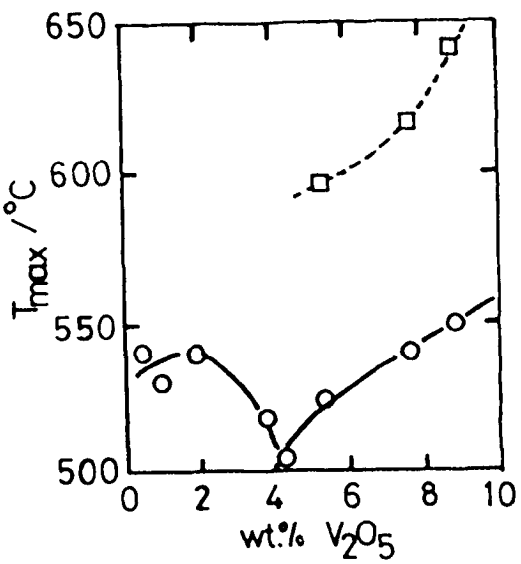

Figure 4.5 Dependence of T_{max} on V_2O_5 content for catalysts shown in Figure 4.4. Circles, first peak; squares, second peak.

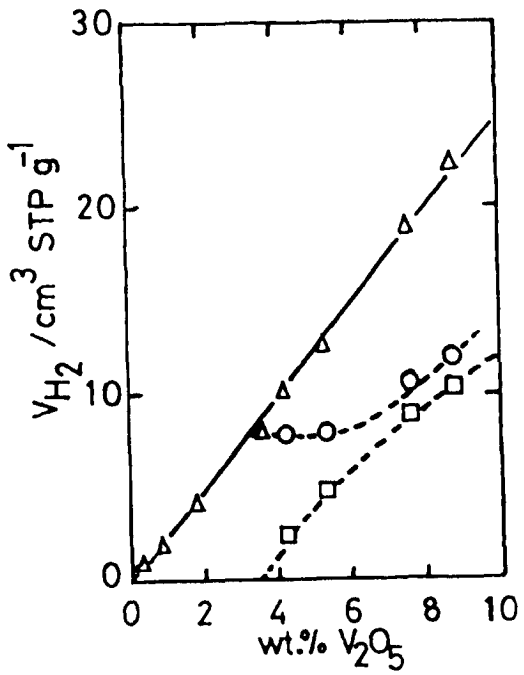

Figure 4.6 Dependence of volume of H_2 consumed in TPR on V_2O_5 content for catalysts shown in Figure 4.5. Symbols as before; triangles represent total H_2 volume.

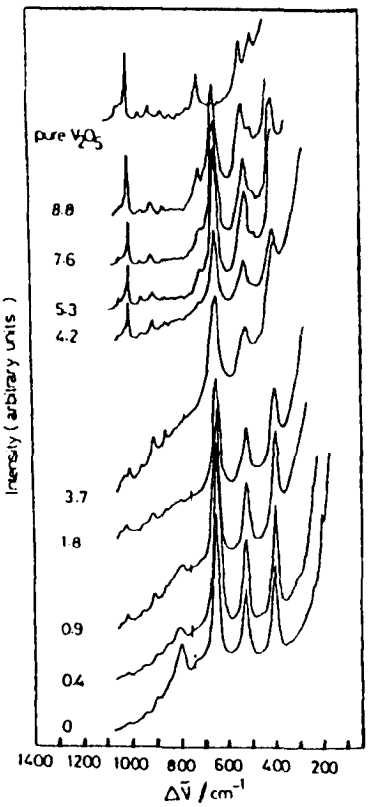

Figure 4.7 Laser Raman spectra for the catalysts shown in Figure 4.4: the V_2O_5 content (wt.%) is given by each spectrum. Above 700 cm^{-1}, sensitivities are the same; below 700 cm^{-1} the sensitivities varied to bring the 640 cm^{-1} band on scale.

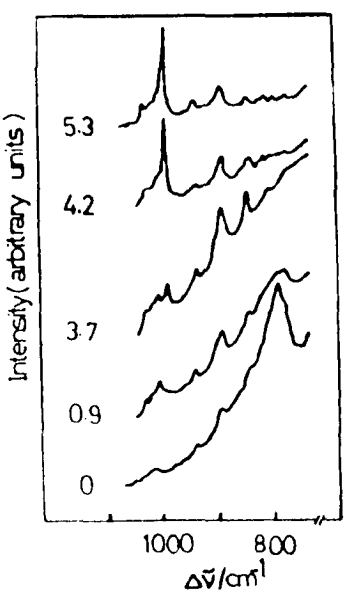

Figure 4.8 Laser Raman spectra of low V_2O_5 content catalysts (as in Figure 4.7) at higher sensitivity.

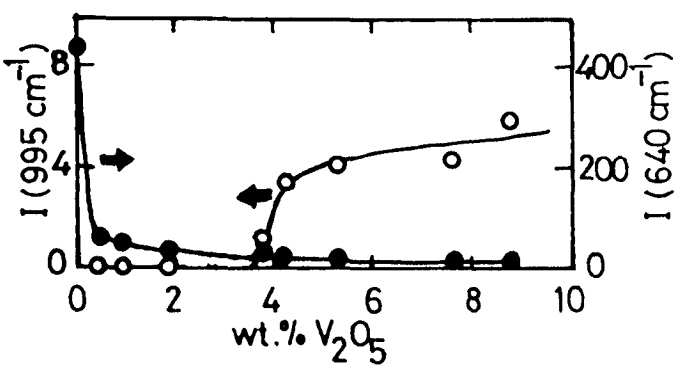

Figure 4.9 Variation in intensities (in cm) of 995 cm^{-1} band (V=O····V) and 640 cm^{-1} (anatase) band with V_2O_5 content for catalysts shown in Figure 4.7.

process becoming less efficient as the colour deepens with increasing amount of V_2O_5. This may also explain why the 995 cm^{-1} band does not continue to increase in intensity.

XPS

Figure 4.10 shows the XP spectra for the same series of catalysts, covering the range in which the V 2p and Ti 2p bands appear. The XP spectra of pure TiO_2 and V_2O_5 are also included in Figure 4.10 for comparative purposes. The binding energies of the V $2p_{1/2}$ and V $2p_{3/2}$ levels in all samples are observed at 524.3 $\pm$ 0.26 and 517.2 $\pm$ 0.27 eV respectively; these values are similar to the values for pure V_2O_5 (524.5 and 517.2 eV)(Table 4.3). This indicates the presence of only V(V) in the calcined samples. The binding energy values of the Ti $2p_{1/2}$ and O 1s satellite levels in the catalysts and in the TiO_2 are the same, viz. 464.2 $\pm$ 0.16 and 464.3 eV, and 520.1 $\pm$ 0.15 and 519.9 eV respectively. The O 1s satellite binding energy for unsupported V_2O_5 is 520.2 eV.

Figure 4.11 shows the R_1, R_2, R_3 and R_4 ratio values (for ratio calculations , see Section 2.2.5, Chapter 2) as a function of V_2O_5 content. Each ratio varies in much the same way. The ratios R_1 and R_2 are generally less accurate than R_3 and R_4, so the averaged $\bar{R}_{3,4}$ values are used to summarise these results (see Section 2.2.5, Chapter 2). Figure 4.12 shows the averaged $\bar{R}_{3,4}$ values as a function of V_2O_5 content. The V/Ti ratio increases rapidly as the first monolayer is formed. It is thought to be at about 0.9% V_2O_5, and thereafter remains essentially constant up to the equivalent of some ten monolayers.

Figure 4.13 shows the XP spectra for the same series of catalysts (at the dried stage), for TiO_2 and for $(NH_4)_2VO(C_2O_4)_2.2H_2O$. They show that the V $2p_{1/2}$ level overlaps with O 1s satellite to a much greater extent than with the calcined catalysts while the V $2p_{3/2}$ level remains the same. The binding energies of Ti $2p_{1/2}$, V $2p_{3/2}$ and O 1s satellite levels are 464.2 $\pm$ 0.16, 515.9 $\pm$ 0.34 and 520.4 $\pm$ 0.17 eV, respectively (Table 4.3). The pure oxalate (Figure 4.13) shows binding energy values for V $2p_{3/2}$ and O 1s satellite levels; 515.1 and 520.1 eV respectively (Table 4.3). The V $2p_{3/2}$ value in pure oxalate (due to V(IV)) is similar to those of the dried catalysts already stated in Figure 4.13. This indicates the presence of V(IV) in the dried samples. Figure 4.14 shows the averaged $\bar{R}_{3,4}$ values as a function of the V_2O_5 content for the dried catalysts. The V/Ti ratio initially increases in proportion to the V_2O_5 content up to o.9% V_2O_5 (equivalent to one monolayer of VO_x) and passes through a plateau in the region 2.0 - 4.0% V_2O_5. The V/Ti intensity ratio in this range is about half that for the calcined materials. Above 4.0% V_2O_5, the V/Ti intensity ratio increases again up to 6% V_2O_5, and thereafter remains constant with values similar to those for calcined catalysts.

4.2.2.1.2 Oxidation of 1,3-butadiene

Only the VO_x/TiO_2 catalyst containing 0.9% V_2O_5 was tested in this reaction (temperature range 283 - 374°C). The value of S_{MA} was high only at low temperature (S_{MA} = 50% at 6% conversion at 297°C) (see Figure 4.15, S_{MA}% versus 1/T). At high temperature further oxidation to carbon oxides

Table 4.3

XPS results of VO_x/TiO_2(anatase, unwashed, 9.6 m^2g^{-1}) catalysts prepared by wet impregnation, TiO_2, $(NH_4)_2VO(C_2O_4)_2.2H_2O$ and unsupported V_2O_5.

wt.% V_2O_5	sample preparation	Binding energy (FWHM) V $2p_{1/2}$	V $2p_{3/2}$	O 1s[a]	Ti $2p_{1/2}$	FWHM(eV)[b] Ti $2p_{3/2}$
0.4	powd.,calcined	524.1(1.6)	516.7(2.8)	520.1(1.8)	464.1(2.4)	1.8
0.9	"	524.5(1.4)	517.3(2.4)	520.0(1.8)	464.4(2.6)	1.8
1.8	"	524.1(1.4)	517.0(2.4)	519.9(--)	463.9(2.4)	1.7
4.2	"	524.8(2.6)	517.3(2.4)	520.3(--)	464.2(2.8)	1.8
5.3	"	524.3(2.4)	517.3(2.6)	520.1(2.6)	464.3(2.8)	2.0
7.6	"	524.3(1.6)	517.5(2.2)	520.2(2.4)	464.1(2.4)	1.6
8.8	"	524.1(2.0)	517.4(2.8)	520.3(--)	464.2(2.4)	1.8
0.4	powd., not calcined		516.3(--)	520.4(--)	464.3(2.8)	1.8
0.9	"		516.2(2.4)	520.7(--)	464.5(2.8)	1.8
1.8	"		516.1(2.6)	520.4(--)	464.2(2.6)	1.8
4.2	"		515.7(2.2)	520.6(2.4)	464.2(2.6)	1.9
5.3	"		515.9(2.4)	520.2(--)	464.2(2.4)	1.7
7.6	"		515.8(2.0)	520.5(--)	464.1(2.6)	1.8
8.8	"		515.3(2.4)	520.3(--)	464.0(2.7)	1.9
TiO_2†c				519.9(1.9)	464.3(2.6)	458.4(1.5)
V_2O_5†c		524.5(2.7)	517.2(1.9)	520.2(--)		
$(NH_4)_2VO(C_2O_4)_2.2H_2O$†c			515.1(1.8)	520.1(--)		

FWHM = Full width at half of the maximum height;
a = Oxygen satellite;
b = Binding energies of the catalysts were determined by referencing to the Ti $2p_{3/2}$ line at 458.5 eV;
c = Binding energies of the standard compounds were determined by referencing to the C 1s line at 284.6 eV.

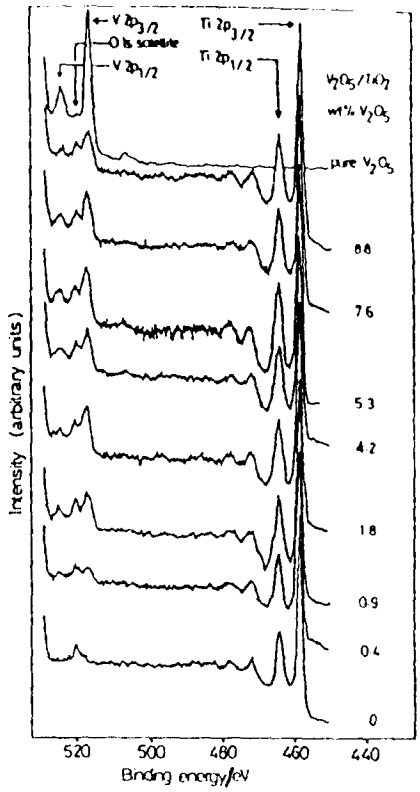

Figure 4.10 XPS spectra of catalysts made by aqueous impregnation of TiO_2 anatase(unwashed), and for the support and for pure V_2O_5. The wt.% V_2O_5 is given for each curve.

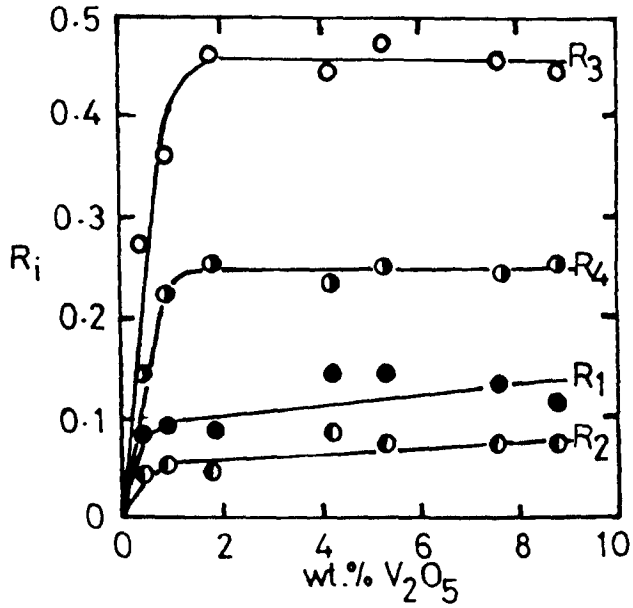

Figure 4.11 Dependence of V/Ti ratios R_1 - R_4 on wt.% V_2O_5 for catalysts prepared by aqueous impregnation of TiO_2 anatase(unwashed) low-area. R_1(●) = V $2p_{1/2}$ / Ti $2p_{1/2}$; R_2(◐) = V $2p_{1/2}$ / Ti $2p_{3/2}$; R_3(○) = V $2p_{3/2}$ / Ti $2p_{1/2}$; R_4(◑) = V $2p_{3/2}$ / Ti $2p_{3/2}$.

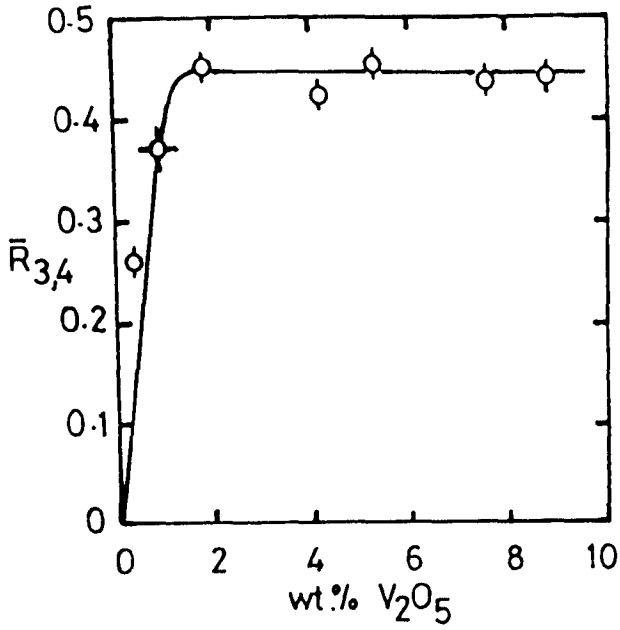

Figure 4.12 Dependence of V/Ti ratio $\bar{R}_{3,4}$(○) on wt.% V_2O_5 for the catalysts depicted in Figure 4.11. The curve is that calculated for $f_1 = f_2 = 0.3$, $x = 0.05$; $\bar{R}_{3,4}$ taken as 0.37 at the one monolayer point.

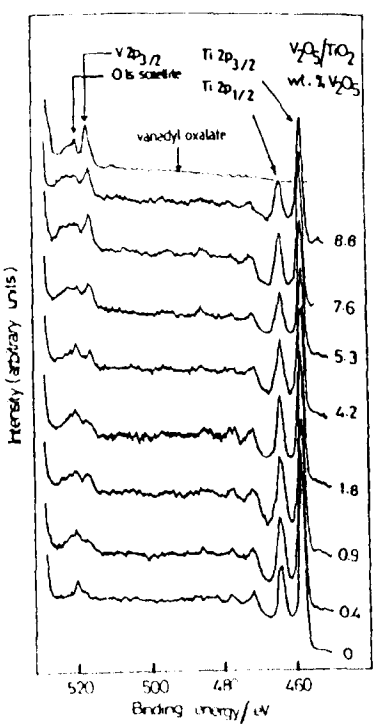

Figure 4.13 XPS spectra for the same catalysts in Figure 4.10, but in the dried stage.

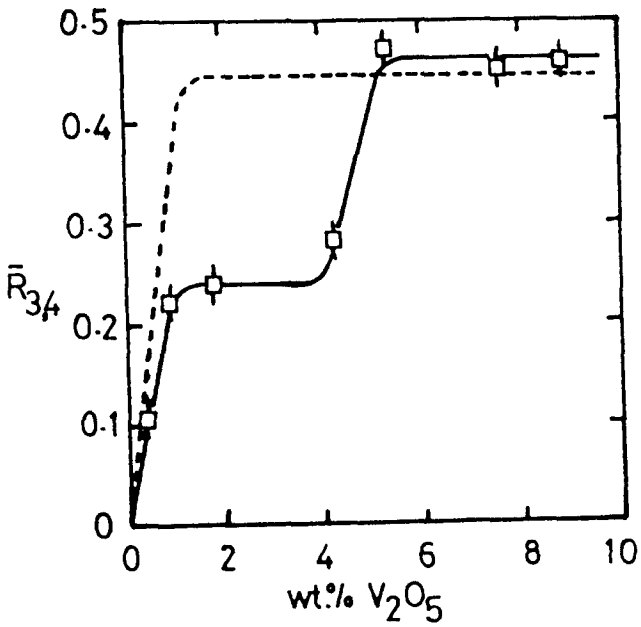

Figure 4.14 Dependence of V/Ti ratio $\bar{R}_{3,4}$(□) on wt.% V_2O_5 for the dried catalysts depicted in Figure 4.13. The broken line represents the $\bar{R}_{3,4}$ for the calcined catalysts for the same series (see Figure 4.12) are shown for comparison.

occured. Figure 4.15 shows also the plots of ln(r_B, r_{MA} and r_{CO_x}) versus 1/T for the same catalyst, giving the E_B, E_{MA} and E_{CO_x}. These were measured at conversions up to 30%. Table 4.4 shows the values of E_B, E_{MA} and E_{CO_x} and the corresponding values of lnA.

Table 4.4

The Arrhenius parameters of VO_x/TiO_2(unwashed) catalyst containing 0.9% V_2O_5 catalyzed oxidation of 1,3-butadiene.

E_B[1]	lnA[2]	c.c.	E_{MA}[1]	lnA[2]	c.c.	E_{CO_x}[1]	lnA[2]	c.c.
52.7	12.0	0.994	32.2	7.0	0.92	64.4	13.9	0.997

1 = E/ kJ mol^{-1};

2 = ln(A/ mmol h^{-1} g^{-1}cat.).

4.2.2.1.3 Decomposition of isopropanol

In contrast to pure V_2O_5, for which dehydration to propylene is the predominant reaction, the decomposition of isopropanol on TiO_2 and VO_x/TiO_2 samples also yield the dehydrogenation product (acetone) in considerable quantities. In Figure 4.16, conversion, S_{ac} and S_{pr}% measured at 220°c, are plotted against the V_2O_5 content. Figure 4.16 shows that S_{ac} is higher than S_{pr} on the unwashed TiO_2. The value of S_{ac} increases up to 80% at 0.9% V_2O_5, then decreases gradually with increasing V_2O_5 content. The value of S_{pr}, taken as a measure of acidity, therefore increases gradually above 0.9% V_2O_5. The conversion also increases gradually with V_2O_5 content. Similar results were found at 210 and 230°C. Figure 4.17 shows r_t, r_{ac} and r_{pr} at 220°C are plotted as a function of the V_2O_5 content. The

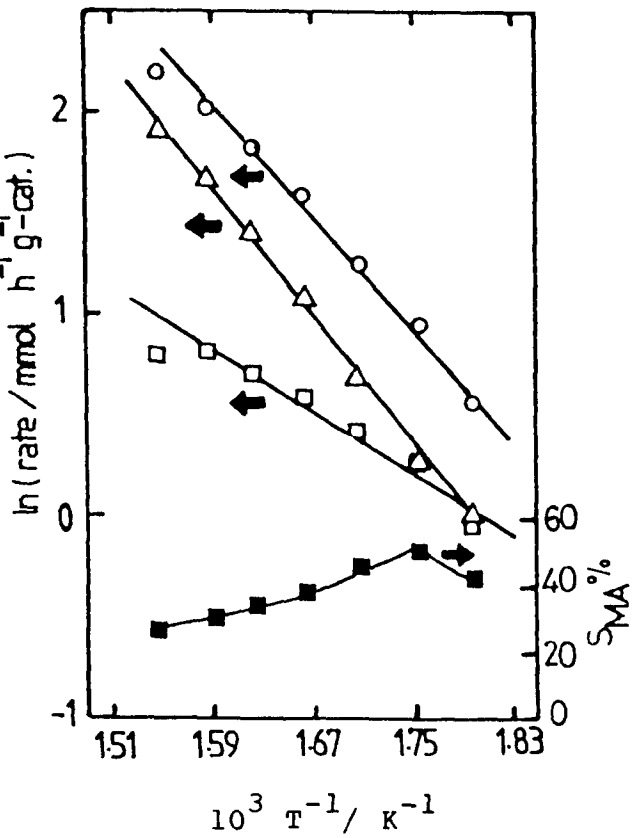

Figure 4.15 Ln(rate/ r_B(O), r_{MA}(□) and r_{CO_x}(△)) and S_{MA}%(■) versus 1/T for the VO_x/TiO_2 (unwashed) catalyst containing 0.9% V_2O_5 prepared by aqueous impregnation catalyzed oxidation of 1,3-butadiene.

values of r_t and r_{ac} increase linearly up to 5.3% V_2O_5 then increase gradually. The value of r_{pr} increases linearly above o.9% V_2O_5. Below 0.9% V_2O_5, r_{pr} does not vary (see Figure 4.17).

Figure 4.18 shows the plots of ln(r_t, r_{ac} and r_{pr}) versus 1/T for the catalyst containing 8.8% V_2O_5 from which E_t, E_{ac} and E_{pr} are derived. Table 4.5 shows the values of E_t, E_{ac} and E_{pr} and the corresponding values of lnA for the catalysts and for TiO_2(unwashed) which were alsoshown in Figure 4.16.

Table 4.5
The Arrhenius parameters of VO_x/TiO_2(unwashed) catalysts, prepared by wet impregnation, for the catalyzed decomposition of isopropanol.

Wt.% V_2O_5	E_t[1]	lnA[2]	c.c.	E_{ac}[1]	lnA[2]	c.c.	E_{pr}[1]	lnA[2]	c.c.
pure TiO_2	89.5	21.43	0.999	84.1	19.57	0.999	100.9	22.95	0.996
0.9	61.5	15.20	0.973	48.1	11.67	0.986	86.6	20.1	0.982
1.8	31.8	8.31	0.982	23.0	5.87	0.959	76.5	17.63	0.971
5.3	25.1	7.33	0.964	18.0	5.24	0.960	40.1	9.89	0.959
8.8	35.5	10.00	0.968	31.4	8.57	0.978	45.6	11.44	0.941

1 = E/kJ mol $^{-1}$;

2 = ln(A/mmol h^{-1} g^{-1}-cat.).

Figure 4.19 shows the values of E_t, E_{ac} and E_{pr} (Table 4.5) as a function of the V_2O_5 content. The value of E_t falls sharply with the V_2O_5 content and passes through a minimum in the 3 - 5% V_2O_5 region. The value of E_t for TiO_2 is higher than for the VO_x/TiO_2 catalysts and for unsupported V_2O_5. The value of E_t for unsupported V_2O_5 is

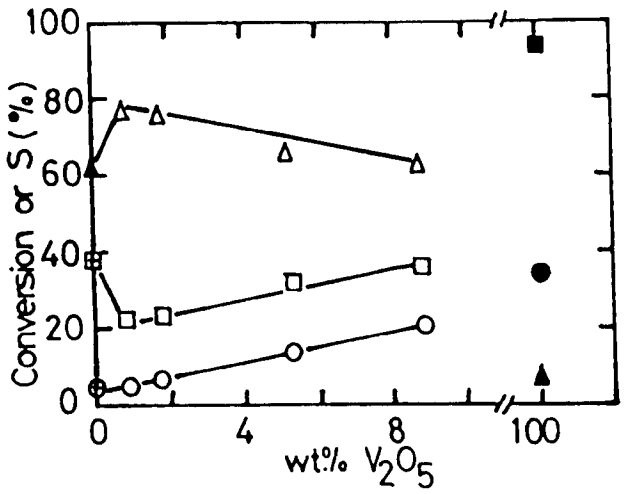

Figure 4.16 Decomposition of isopropanol on VO_x/TiO_2(unwashed) catalysts, TiO_2(unwashed) and unsupported V_2O_5 at 220°C: ○, isopropanol conversion; □, S_{pr}; △, S_{ac}. Isopropanol conversion(●), S_{pr}(■) and S_{ac}(▲) for unsupported V_2O_5. Isopropanol conversion(⊕), S_{pr}(⊞) and S_{ac}(⊿) for TiO_2(unwashed).

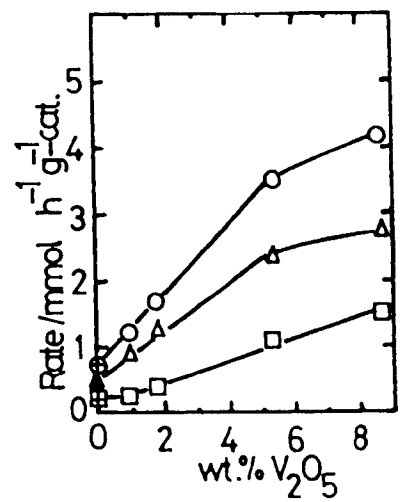

Figure 4.17 The rate of decomposition of isopropanol (r_t(○), r_{ac}(△) and r_{pr}(□)) at 220°C as a function of the V_2O_5 content for samples shown in Figure 4.16.

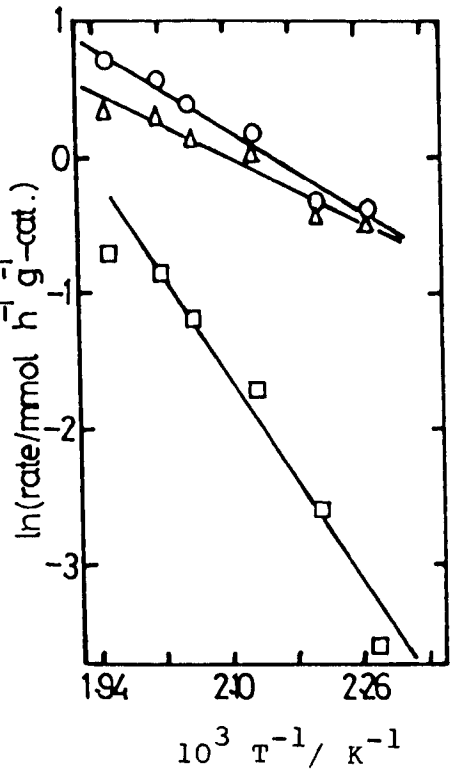

Figure 4.18 Ln(rate/r_t(○), r_{ac}(△) and r_{pr}(□)) versus 1/T for the catalyst containing 8.8% V_2O_5: the decomposition of isopropanol (this catalyst used in Figure 4.16).

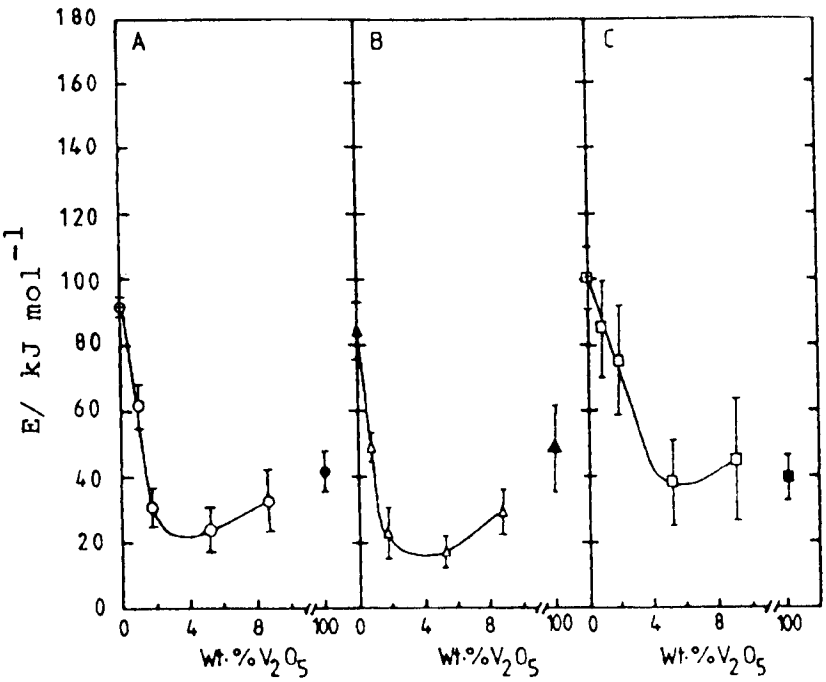

Figure 4.19 E_t(○), E_{ac}(△) and E_{pr}(□) as a function of V_2O_5 content for samples shown in Figure 4.16. E_t(●), E_{ac}(▲) and E_{pr}(■) for unsupported V_2O_5. E_t(⊕), E_{ac}(⊕) and E_{pr}(⊞) for TiO_2(unwashed).

higher than E_t for VO_x/TiO_2 catalysts at 1.8 - 8.8% V_2O_5. Similar results are shown for E_{ac} with V_2O_5 content. The value of E_{pr} for TiO_2 is higher than those of VO_x/TiO_2 catalysts and unsupported V_2O_5. The VO_x/TiO_2 catalysts at 5.2 - 8.8% V_2O_5 have about the same E_{pr} as for unsupported V_2O_5. In general, E_{pr} values for TiO_2 and the catalysts are higher than the E_t and E_{ac} values.

4.2.2.2 Catalyst prepared by the $VOCl_3$ method

The VO_x/TiO_2(unwashed) monolayer catalyst was prepared as described in Section 3.5.2 of Chapter 3 and contained 0.9% V_2O_5.

4.2.2.2.1 Characterisation

VO_x/TiO_2(unwashed) monolayer catalyst was studied by TPR and laser Raman spectroscopy.

TPR

Figure 4.20A shows the TPR profile which has only one peak with T_{max} = 503°C. This is lower than T_{max} for the 0.9% V_2O_5 catalyst prepared by the impregnation method (see Figure 4.4), and much lower than for bulk V_2O_5. The quantity of H_2 consumed corresponds to that required for reduction of V(V) to V(III) (i.e. 2 mol H_2/mol V_2O_5).

Laser Raman spectroscopy

The laser Raman spectrum of the same monolayer catalyst did not exhibit bands due to crystalline V_2O_5 and showed only those due to TiO_2 (Figure 4.20B).

4.2.2.2.2 Oxidation of 1,3-butadiene

The VO_x/TiO_2(unwashed) monolayer catalyst was tested in this reaction in the temperature range 278 - 335°C. The value of S_{MA}% increased with temperature and became constant above 290°C (S_{MA} = 28% at 11% conversion at 290°C). Figure 4.21 shows the S_{MA}% versus 1/T. Figure 4.21 shows also the plots of ln(r_B, r_{MA} and r_{CO_x}) versus 1/T, giving E_B, E_{MA} and E_{CO_x}. The above parameters were measured at conversions up to 30%. Table 4.6 shows the values of E_B, E_{MA} and E_{CO_x} and the corresponding values of lnA.

Table 4.6

The Arrhenius parameters of VO_x/TiO_2(unwashed) monolayer catalyst, prepared by the $VOCl_3$ method, catalyzed oxidation of 1,3-butadiene.

E_B[1]	lnA[2]	c.c.	E_{MA}[1]	lnA[2]	c.c.	E_{COx}[1]	lnA[2]	c.c.
58.1	13.9	0.994	72.8	15.6	0.969	53.1	12.7	0.998

1 = E/ kJ mol^{-1};

2 = ln(A/ mmol h^{-1} g^{-1}cat.).

4.2.2.3 Catalysts prepared by the $VO(O^iBu)_3$ method

A series of VO_x/TiO_2(unwashed) catalyst were prepared by this method as described in Section 3.5.3 of Chapter 3. V_2O_5 contents were between about 0.8 (monolayer catalyst) and 3.6 wt.% V_2O_5.

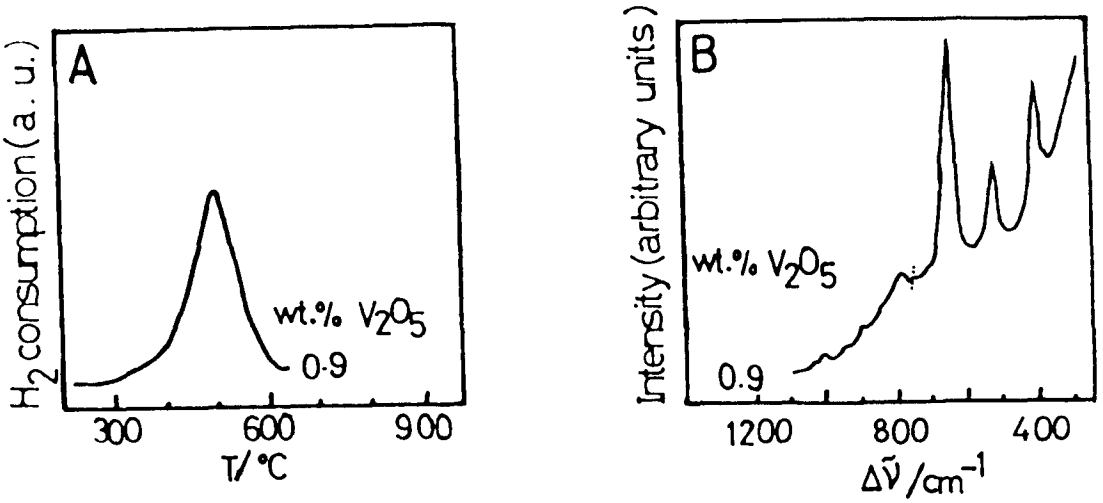

Figure 4.20 TPR profile (A) and laser Raman spectrum (B) for VO_x/TiO_2(unwashed) monolayer catalyst prepared by the $VOCl_3$ method.

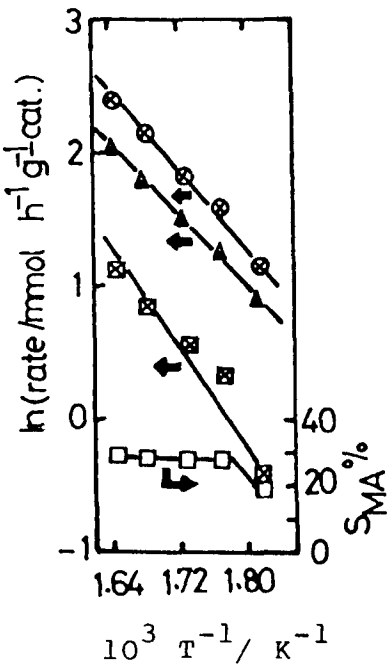

Figure 4.21 Ln(rate/r_B(⊗), r_{MA}(⊠) and r_{CO_x}(△)) and S_{MA}% (□) versus 1/T for VO_x/TiO_2(unwashed) monolayer catalyst, prepared by the $VOCl_3$ method, catalyzed oxidation of 1,3-butadiene.

4.2.2.3.1 Characterisation

The VO_X/TiO_2(unwashed) monolayer catalyst was studied by TPR and laser Raman spectroscopy.

Figure 4.22 shows the TPR profile and Raman spectrum. The results are similar to those for the VO_X/TiO_2(unwashed) monolayer catalyst prepared by the $VOCl_3$ method (see Figure 4.20).

4.2.2.3.2 Oxidation of 1,3-butadiene

The catalytic measurements were carried out within the temperature range of 280 and 370°C. Figure 4.23 shows S_{MA}% as a function of temperature for the monolayer catalyst containing 0.8% V_2O_5. The results are similar to those found with the monolayer catalyst prepared by the $VOCl_3$ method (see Figure 4.21). In Figure 4.24, conversion, S_{MA} and S_{CO_x}% at 320°C, are plotted against the V_2O_5 content. The conversion increases with the V_2O_5 content up to 2.7% V_2O_5, then decreases. The value of S_{MA} is 27% at 0.8% V_2O_5 and increases gradually to 32% at 2.7% V_2O_5. At 3.6% V_2O_5, S_{MA} increases to 44%. Similar shapes of graph were found at 310 and 330°C (the conversion is affected by temperature while the selectivity is not). Figure 4.25 shows r_B, r_{MA} and r_{CO_x} at 320°C plotted as a function of the V_2O_5 content. The values of r_B, r_{MA} and r_{CO_x} increase with V_2O_5, passing through maxima at 2.7% V_2O_5 then decreasing. The values of r_B and r_{CO_x} are higher than r_{MA}.

Figure 4.26 shows the plots of $\ln(r_B$, r_{MA} and $r_{CO_x})$ versus 1/T for the catalyst containing 0.8% V_2O_5, giving E_B, E_{MA} and E_{CO_x}. These parameters were measured at conversions up to 30%. Table 4.7 shows the values of E_B,

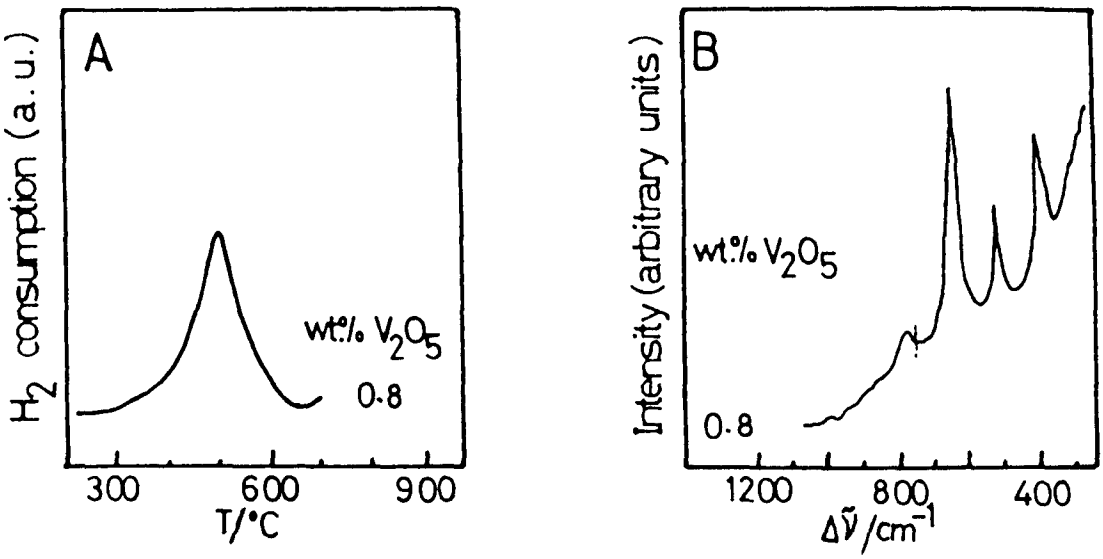

Figure 4.22 TPR profile (A) and laser Raman spectrum (B) for VO_x/TiO_2(unwashed) monolayer catalyst prepared by the $VO(O^iBu)_3$ method.

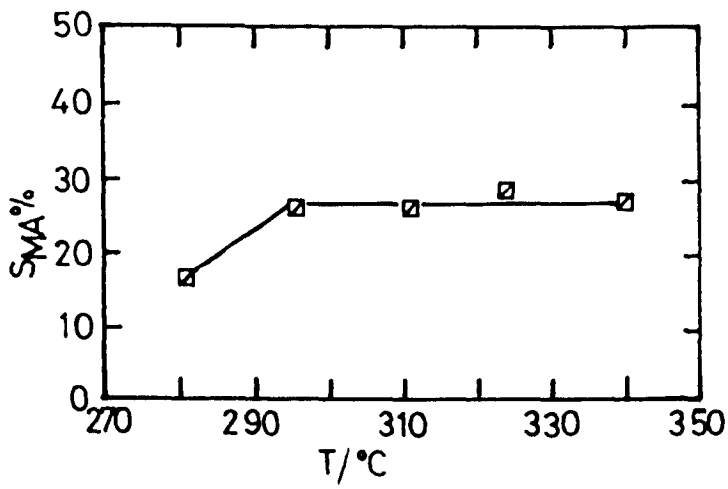

Figure 4.23 Selectivity to maleic anhydride(S_{MA}) as a function of reaction temperature for VO_x/TiO_2(unwashed) monolayer catalyst, prepared by $VO(O^iBu)_3$ method, catalyzed the oxidation of 1,3-butadiene.

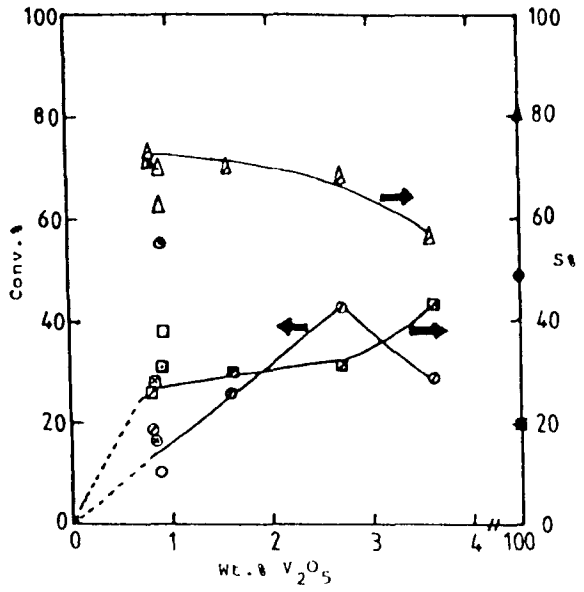

Figure 4.24 Oxidation of 1,3-butadiene on VO_x/TiO_2(unwashed) catalysts prepared by the $VO(O^iBu)_3$ method as a function of V_2O_5 content at 320°C : ⊘, 1,3-butadiene conversion; ⊠, S_{MA}; ▲, S_{CO_x}. Also shown are the results for the VO_x/TiO_2 (unwashed) catalyst prepared by aqueous impregnation method (Figure 4.15)(○,□,△), for the VO_x/TiO_2 (unwashed) catalyst prepared by $VOCl_3$ method (Figure 4.21)(⊘,⊠,▲), for the VO_x/TiO_2 (washed) catalyst prepared by aqueous impregnation method (Figure 4.38)(⊙,⊡,▲) and for unsupported V_2O_5 (Figure 4.2)(●,■,▲).

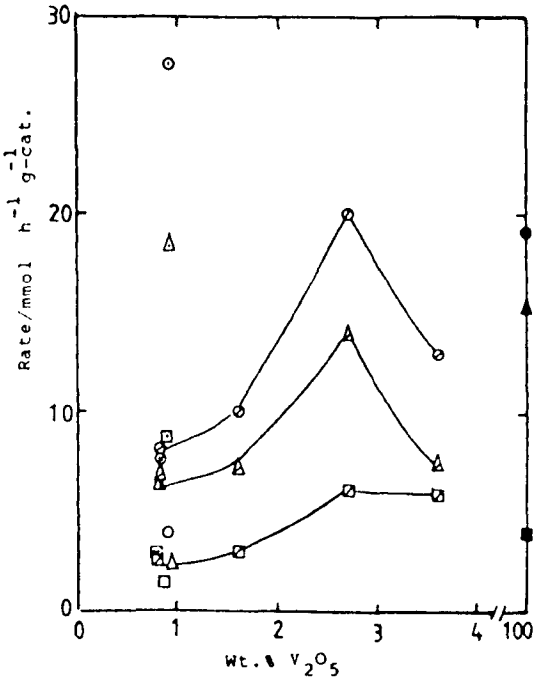

Figure 4.25 The rate of oxidation of 1,3-butadiene for the catalysts shown in Figure 4.24 as a function of the V_2O_5 content at 320°C: ○, r_B; □, r_{MA}; △, r_{CO_x}.

E_{MA} and E_{CO_x} and the corresponding values of lnA for the catalysts which were shown in Figure 4.24. Figure 4.27 shows the values of E_B, E_{MA} and E_{CO_x} (Table 4.7) as a function of the V_2O_5 content. The values of E_B, E_{MA} and E_{CO_x} increase with V_2O_5 content, passing through maxima at 2.7% V_2O_5, then decreasing. The value of E_{MA} is higher than E_B and E_{CO_x}.

Table 4.7

The Arrhenius parameters of VO_x/TiO_2(unwashed) catalysts, prepared by the $VO(O^iBu)_3$ method, catalyzed oxidation of 1,3-butadiene.

Wt.% V_2O_5	E_B[1]	lnA[2]	c.c.	E_{MA}[1]	lnA[2]	c.c.	E_{CO_x}[1]	lnA[2]	c.c.
0.8	60.6	14.5	0.991	82.8	17.5	0.968	54.8	12.9	0.993
1.6	94.1	21.4	0.927	110.0	23.4	0.94	88.7	20.0	0.953
2.7	135.5	30.5	0.983	164.0	35.1	0.994	125.9	28.2	0.978
3.6	62.7	15.2	0.939	90.3	20.0	0.961	49.0	11.7	0.894

1 = E/ kJ mol^{-1};

2 = ln(A/ mmol h^{-1} g^{-1}cat.).

4.2.3 VO_x/TiO_2(CLD 939, anatase, washed, 9.6 m^2g^{-1})

TiO_2(CLD 939,washed) was used as a support; these catalysts contained P_2O_5 and K_2O as impurities but in lower concentrations than in the case of TiO_2 (CLD 939,unwashed) (see Table 3.1, Chapter 3).

4.2.3.1 Catalysts prepared by wet impregnation method

The VO_x/TiO_2 (washed) catalysts were prepared by this method as described in Section 3.5.1 of Chapter 3; They contained 0.4 - 8.8 wt.% V_2O_5.

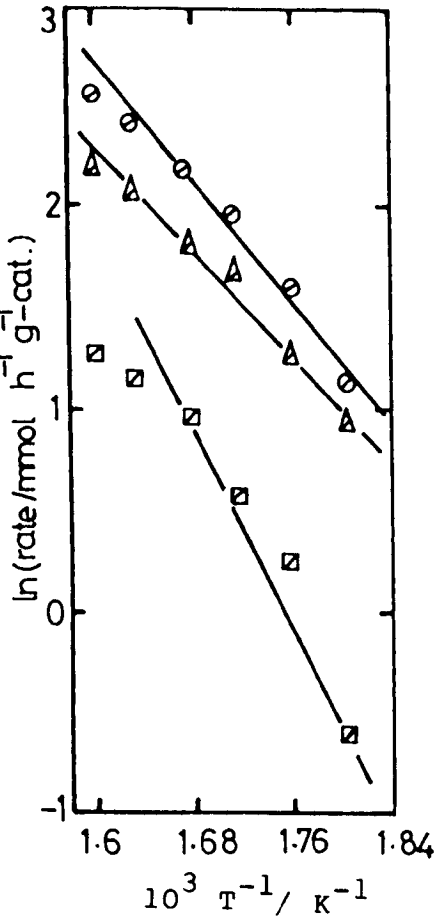

Figure 4.26 Ln(rate/r_B(⊘), r_{MA}(⊠) and r_{CO_x} (⊿) versus 1/T for VO_x/TiO_2(unwashed) monolayer catalyst, prepared by the $VO(O^iBu)_3$ method, catalyzed oxidation of 1,3-butadiene.

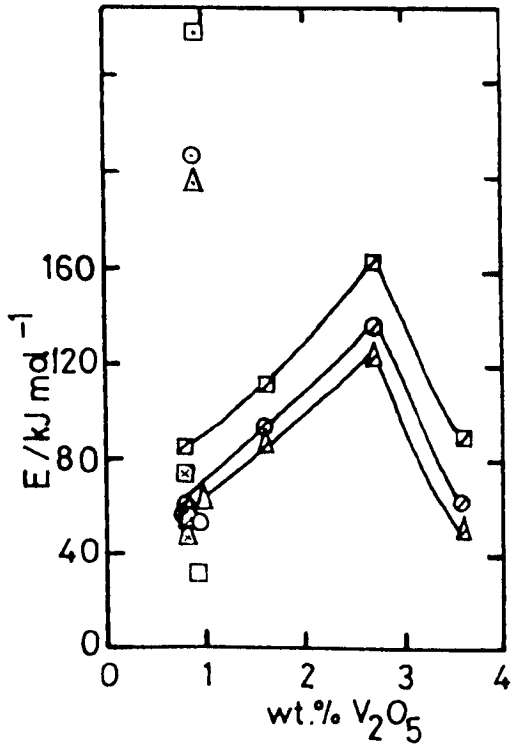

Figure 4.27 E_B(O), E_{MA}(□) and E_{CO_x} (Δ) as a function of V_2O_5 content for samples shown in Figure 4.24.

4.2.3.1.1 Characterisation

The catalysts were studied by TPR, laser Raman spectroscopy and XPS. The results are given below.

TPR

Figure 4.28 shows the TPR profiles for catalysts containing 0.4 - 8.8% V_2O_5. Figure 4.29 shows the dependence of T_{max}, and Figure 4.30 the H_2 consumption per g catalyst, as a function of V_2O_5 content. Figure 4.28 also contains the TPR profiles for the support and for pure V_2O_5 measured under the same conditions.

The TPR profiles for samples containing 0.4 - 5.0% V_2O_5 comprise a single peak, the T_{max} of which increases from about 480°C to 530°C as the V_2O_5 content increases (Figure 4.29). This is well below the T_{max} of the first of the three peaks shown by pure V_2O_5. At and above 5.4% V_2O_5 the peak splits into two, the T_{max} for the first being constant at 530°C, while that for the second continues to increase with V_2O_5 content (Figure 4.29). The quantity of H_2 consumed is accurately proportional to the V_2O_5 content (Figure 4.30) and corresponds to that required for reduction of V(V) to V(III) (i.e. 2 mol H_2/mol V_2O_5). Approximate manual deconvolution of the split peaks (Figure 4.30) appears to show that the first peak attains a constant size after the second starts to appear.

Laser Raman spectroscopy

Laser Raman spectra were obtained for the same series of catalysts, as well as for the support and for the pure V_2O_5 (Figure 4.31). For samples containing up to 5.0% V_2O_5, the

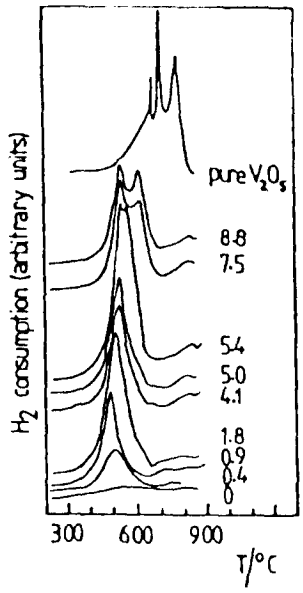

Figure 4.28 TPR profiles for catalysts prepared by aqueous impregnation of TiO_2 anatase(washed), and for the support and for pure V_2O_5. The wt.% V_2O_5 is given for each curve.

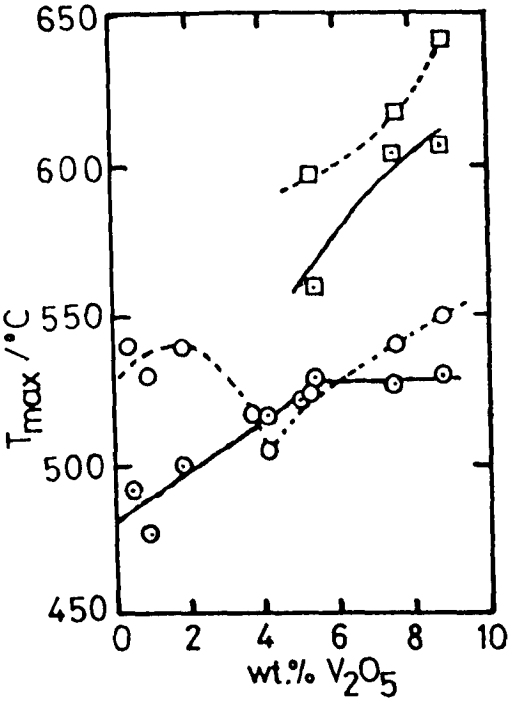

Figure 4.29 Dependence of T_{max} on V_2O_5 content for catalysts shown in Figure 4.28. ⊙, first peak; ⊡, second peak. The data of Figure 4.5 (○, first peak; □, second peak) are shown for comparison.

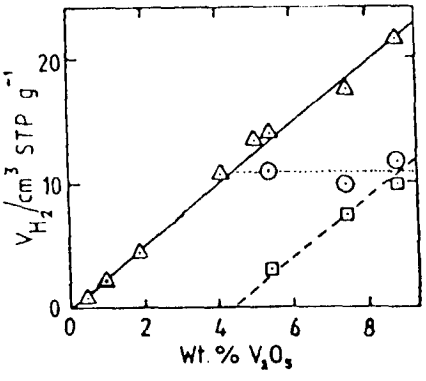

Figure 4.30 Dependence of volume of H_2 consumed in TPR on V_2O_5 content for catalysts shown in Figure 4.28. Symbols as before; triangles represent total H_2 volume.

portion of the spectrum above 850 cm^{-1} was run at a higher sensitivity: some of these results are shown in greater detail in Figure 4.32. The important feature of these spectra is that the 995 cm^{-1} band is not detectable at V_2O_5 loading of less than 1.8% V_2O_5.

The variation of the intensity of the 640 and 995 cm^{-1} bands with V_2O_5 content (Figure 4.33) is similar to the results in the case of the series of VO_x/TiO_2(unwashed) catalysts (see Figure 4.9, Section 4.2.2.1.1).

XPS

Figure 4.34 shows the XP spectra for the V 2p and Ti 2p bands for the same series of catalysts. The spectra of the TiO_2 and pure V_2O_5 are also included in Figure 4.34. The binding energies of the V $2p_{1/2}$ and V $2p_{3/2}$ levels in all samples are 524.5 ± 0.4 and 517.3 ± 0.3 eV respectively. These values are similar to the values of pure V_2O_5 (Table 4.8). They indicate the presence of only V(V) in the calcined samples. The binding energy values of the Ti $2p_{1/2}$ and O 1s satellite levels in the catalysts and in the TiO_2 are the same (Table 4.8).

Figure 4.35 shows the averaged $\bar{R}_{3,4}$ values as a function of the V_2O_5 content. The V/Ti ratio increases rapidly as the first monolayer is formed (0.9% V_2O_5) and remains constant with increasing V_2O_5 content.

XP spectra (figure 4.36) and the averaged $\bar{R}_{3,4}$ values as a function of the V_2O_5 concentration (Figure 4.37) for the dried catalysts are similar to the results for the dried catalysts with unwashed TiO_2 (see Figures 4.13 and 4.14, Section 4.2.2.1.1). The binding energies of the Ti $2p_{1/2}$,

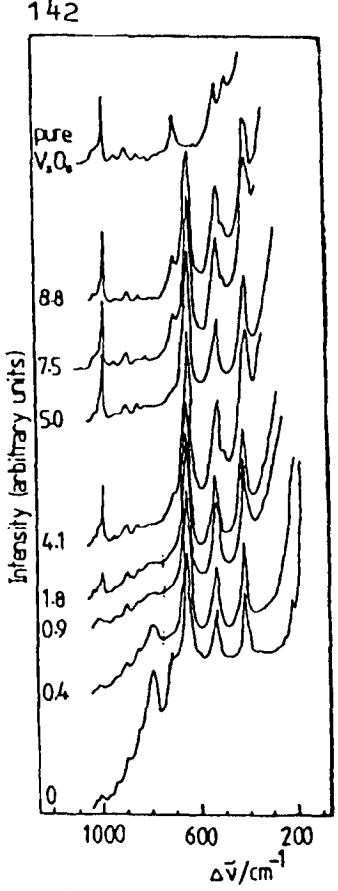

Figure 4.31 Raman spectra of catalysts made by aqueous impregnation of washed anatase: the V_2O_5 content (wt.%) is given by each spectrum. Above 700 cm^{-1}, sensitivities are the same; below 700 cm^{-1} they are varied to bring the 640 cm^{-1} band on scale.

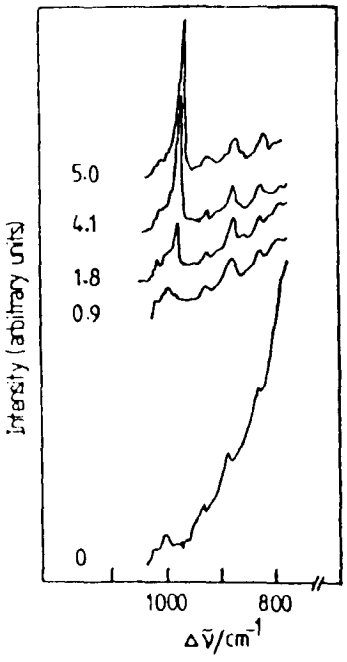

Figure 4.32 Raman spectra of low V_2O_5 content catalysts (as in Figure 4.31) at higher sensitivity.

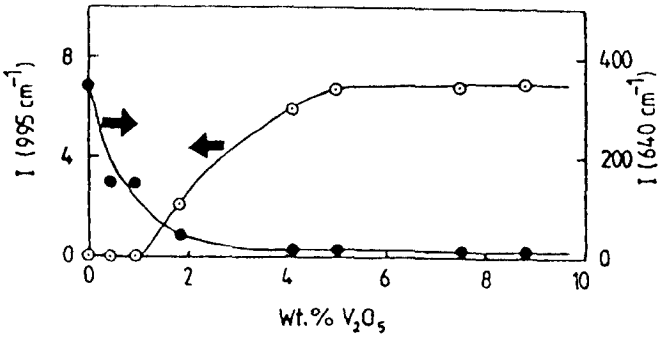

Figure 4.33 Variation in intensities (in cm) of 995 cm^{-1} band (V=O····V) and 640 cm^{-1} (anatase) band with V_2O_5 content for catalysts shown in Figure 4.31.

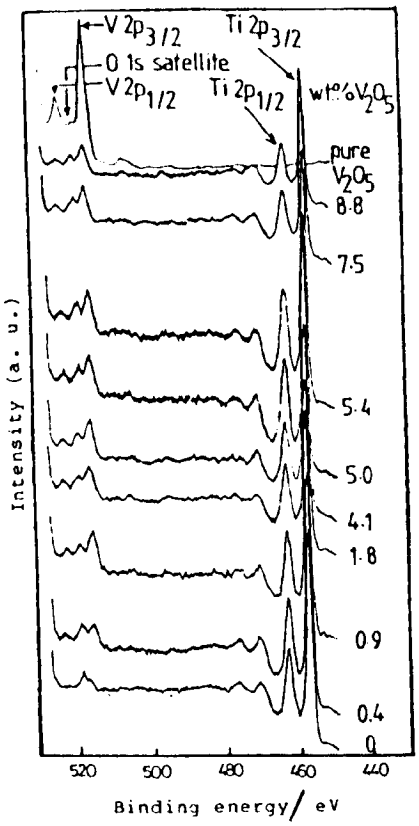

Figure 4.34 XPS spectra of catalysts made by aqueous impregnation of TiO_2 anatase(washed), and for the support and for pure V_2O_5. The wt.% V_2O_5 is given for each curve.

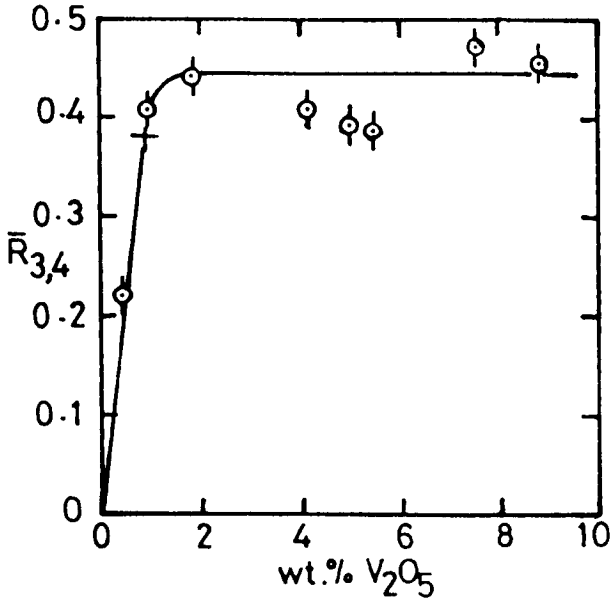

Figure 4.35 Dependence of V/Ti ratio $\bar{R}_{3,4}$(⊙) on %V_2O_5 for the catalysts depicted in Figure 4.34. The curve is that calculated for $f_1 = f_2 = 0.3$, $x = 0.05$; $\bar{R}_{3,4}$ taken as 0.38 at the one monolayer point.

Table 4.8

XPS results of VO_x/TiO_2(anatase, washed, 9.6 m^2g^{-1}) catalysts prepared by wet impregnation, TiO_2, $(NH_4)_2VO(C_2O_4)_2 \cdot 2H_2O$ and unsupported V_2O_5.

wt.% V_2O_5	sample preparation	Binding energy (FWHM) V $2p_{1/2}$	V $2p_{3/2}$	O 1s[a]	Ti $2p_{1/2}$	FWHM(eV)[b] Ti $2p_{3/2}$
0.4	powd.,calcined	524.9(1.2)	517.2(2.4)	520.4(2.2)	464.3(2.6)	1.8
0.9	"	523.9(1.6)	516.8(2.6)	520.3(2.4)	464.1(2.6)	1.7
1.8	"	524.5(1.4)	517.6(3.0)	520.1(--)	464.3(2.6)	1.8
4.1	"	524.6(1.2)	517.2(2.2)	520.5(2.2)	464.2(2.4)	1.9
5.0	"	523.9(1.0)	516.9(2.4)	519.7(2.1)	464.1(2.6)	1.6
5.4	"	524.5(1.6)	517.3(2.2)	520.3(2.4)	464.2(2.5)	1.6
7.5	"	525.1(1.6)	517.7(2.2)	520.5(--)	464.2(2.8)	1.8
8.8	"	524.7(2.5)	517.6(2.2)	520.7(2.2)	464.2(2.6)	1.7
0.4	powd., not calcined		516.1(--)	520.6(--)	464.2(2.7)	1.8
0.9	"		516.3(--)	520.4(--)	464.1(2.3)	1.8
1.8	"		516.1(--)	520.4(--)	464.3(2.3)	1.6
4.1	"		515.7(2.2)	520.4(--)	464.5(2.8)	1.8
5.0	"		515.8(2.8)	520.2(2.8)	464.3(2.8)	2.2
5.4	"		515.7(2.4)	-----	464.4(2.6)	1.6
7.5	"		515.6(2.8)	519.8(2.2)	464.1(2.6)	1.6
8.8	"		515.7(2.8)	519.9(--)	464.3(2.3)	1.8
TiO_2†c				519.9(1.9)	464.3(2.6)	458.4(1.5)
V_2O_5†c		524.5(2.7)	517.2(1.9)	520.2(--)		
$(NH_4)_2VO(C_2O_4)_2 \cdot 2H_2O$†c			515.1(1.8)	520.1(--)		

FWHM = Full width at half of the maximum height;
a = Oxygen satellite;
b = Binding energies of the catalysts were determined by referencing to the Ti $2p_{3/2}$ line at 458.5 eV;
c = Binding energies of the standard compounds were determined by referencing to the C 1s line at 284.6 eV.

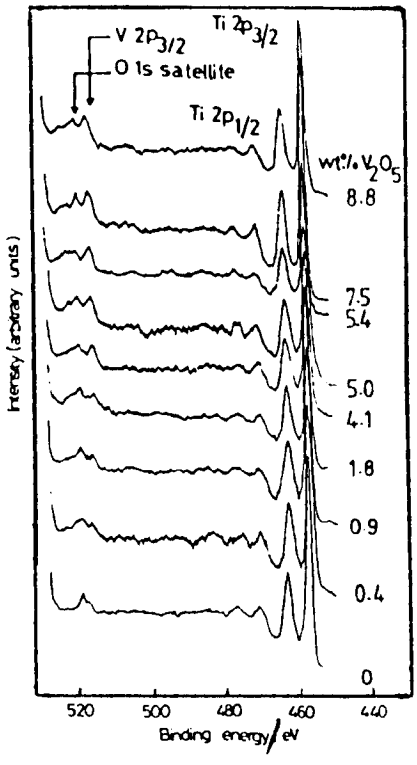

Figure 4.36 XPS spectra for the same catalysts in Figure 4.34, but in the dried stage.

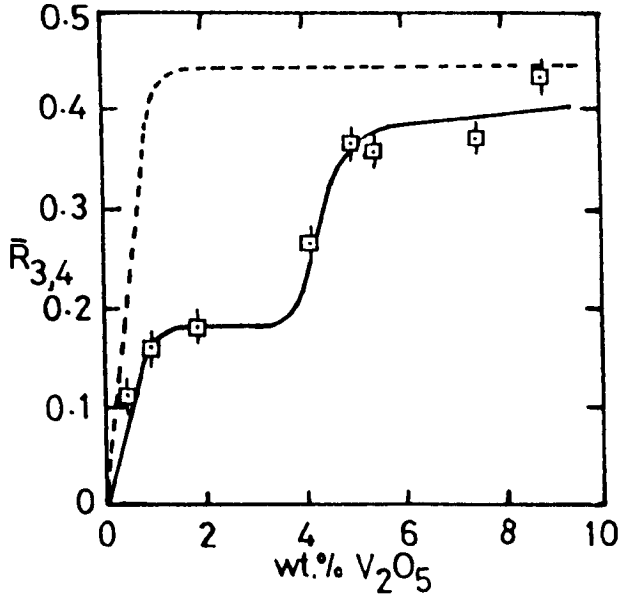

Figure 4.37 Dependence of V/Ti ratio $\bar{R}_{3,4}$(⊡) on $\%V_2O_5$ for the dried catalysts depicted in Figure 4.36. The broken line represents the $\bar{R}_{3,4}$ for the calcined catalysts for same series (see Figure 4.35) are shown for comparison.

V $2p_{3/2}$ and O 1s satellite levels are 464.3 ± 0.1, 515.9 ± 0.25 and 520.2 ± 0.3 eV, respectively (Table 4.8)

4.2.3.1.2 Oxidation of 1,3-butadiene

Only the VO_x/TiO_2(washed) catalyst containing 0.9% V_2O_5 was tested in this reaction (temperature range 283 - 367°C). The value of S_{MA} passed through a maximum (48%) at 350°C and 70% conversion (Figure 4.38 shows the S_{MA}% versus 1/T). Figure 4.38 shows also the plots of ln(r_B, r_{MA} and r_{CO_x}) versus 1/T for the catalyst, giving E_B, E_{MA} and E_{CO_x}. These were measured at conversion up to 30%. Table 4.9 shows the E_B, E_{MA} and E_{CO_x} and the corresponding values of lnA.

Table 4.9

The Arrhenius parameters of VO_x/TiO_2(washed) catalyst, containing 0.9% V_2O_5, catalyzed oxidation of 1,3-butadiene.

E_B[1]	lnA[2]	c.c.	E_{MA}[1]	lnA[2]	c.c.	E_{CO_x}[1]	lnA[2]	c.c.
209.6	45.83	0.917	261.0	55.1	0.94	194.1	42.3	0.903

1 = E/ kJ mol^{-1};

2 = ln(A/ mmol h^{-1} g^{-1}cat.).

4.2.3.1.3 Decomposition of isopropanol

Figure 4.39 shows the results for the decomposition of isopropanol at 220°C. Figure 4.39 shows that no acetone was formed in the case of TiO_2(washed). With VO_x/TiO_2(washed) samples, S_{ac} increases rapidly up to 70% at 0.9% V_2O_5 then gradually decreases with increasing V_2O_5 content. The value

of S_{pr} decreases from 100% to 30% at 0.9% V_2O_5 then increases gradually with V_2O_5 content. The percentage conversion increases to 16% at 0.9% V_2O_5. After this, the percentage conversion remains approximately the same. Similar results were found at 210 and 230°C. Figure 4.40 shows r_t, r_{ac} and r_{pr} at 220°C plotted as a function of the V_2O_5 content. The value of r_t reaches a maximum at about 0.9% V_2O_5 and then decreases, passing through a minimum at 1.8% V_2O_5; it then increases with V_2O_5 content. Results are similar in the case of r_{ac} but the minimum position is in 1.8 - 4.1% V_2O_5 region. Figure 4.40 shows that r_{pr} increases up to 0.9% V_2O_5 and then rises gradually with V_2O_5 content.

Figure 4.41 shows the plots of ln(r_t, r_{ac} and r_{pr}) versus 1/T for the catalyst containing 8.8% V_2O_5, giving E_t, E_{ac} and E_{pr}. Table 4.10 shows the values of E_t, E_{ac} and E_{pr} and the corresponding values of lnA for the catalysts and for TiO_2(washed) which were tested in this reaction. Figure 4.42 shows the values of E_t, E_{ac} and E_{pr} (Table 4.10) as a function of the V_2O_5 content. The value of E_t falls sharply to a minimum at 0.9% V_2O_5 and then increases, passes through a maximum at 1.8% V_2O_5, then decreases up to 4% V_2O_5 and then again increases gradually with V_2O_5 content. The value of E_t for TiO_2 is much higher than for VO_x/TiO_2 catalysts and for unsupported V_2O_5. Figure 4.42 shows that E_{ac} increases up to 1.8% V_2O_5, then decreases up to 4% V_2O_5 and increases gradually with V_2O_5 content. The value of E_{ac} is lower for VO_x/TiO_2 catalysts than for unsupported V_2O_5. The value of E_{pr} falls sharply to a minimum at o.9% V_2O_5 and increases gradually with V_2O_5 content. The value of E_{pr} for

TiO_2 is much higher than for VO_x/TiO_2 catalysts and for unsupported V_2O_5.

Table 4.10

Arrhenius parameters for VO_x/TiO_2(washed) catalysts prepared by wet impregnation, and TiO_2(washed) in the catalytic decomposition of isopropanol.

Wt.% V_2O_5	E_t [1]	lnA [2]	c.c.	E_{ac} [1]	lnA [2]	c.c.	E_{pr} [1]	lnA [2]	c.c.
pure TiO_2	147.2	32.58	0.986	--	--	--	125.9	27.35	0.995
0.9	16.3	5.40	0.949	10.5	3.74	0.975	35.1	8.78	0.894
1.8	29.7	8.58	0.955	25.1	7.12	0.949	39.3	9.87	0.954
4.1	21.7	6.69	0.972	15.0	4.55	0.942	42.7	10.82	0.938
8.8	26.3	8.07	0.956	20.5	6.26	0.957	44.8	11.38	0.944

1 = E/ kJ mol^{-1};

2 = ln(A/ mmol h^{-1} g^{-1}cat.).

4.2.3.2 Catalyst prepared by the $VOCl_3$ method

A VO_x/TiO_2(washed) monolayer catalyst was prepared by the $VOCl_3$ method as described in Section 3.5.2, Chapter 3; it contained 0.8% V_2O_5.

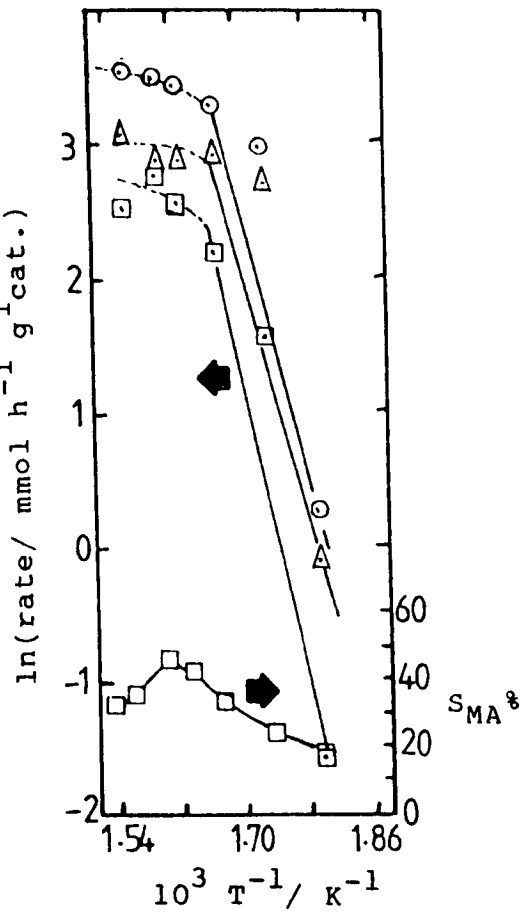

Figure 4.38 Ln(rate/r_B(⊙), r_{MA}(⊡) and r_{CO_x}(△)) and S_{MA}% versus 1/T for VO_x/TiO_2(washed) catalyst, containing 0.9% V_2O_5 prepared by aqueous impregnation, catalyzed oxidation of 1,3-butadiene.

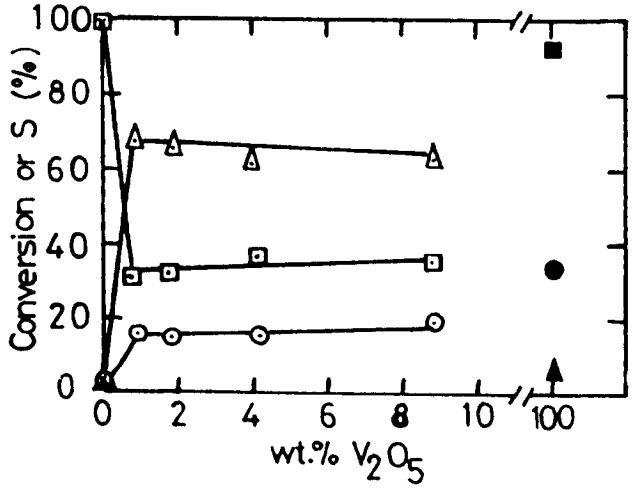

Figure 4.39 Decomposition of isopropanol on VO_x/TiO_2(washed) catalysts, TiO_2(washed) and unsupported V_2O_5 at 220°C: ⊙, isopropanol conversion; ⊡, S_{pr}; △, S_{ac}. Isopropanol conversion(●), S_{pr}(■) and S_{ac}(▲) for unsupported V_2O_5. Isopropanol conversion(⊗), S_{pr}(⊠) and S_{ac}(⊠) for TiO_2(washed).

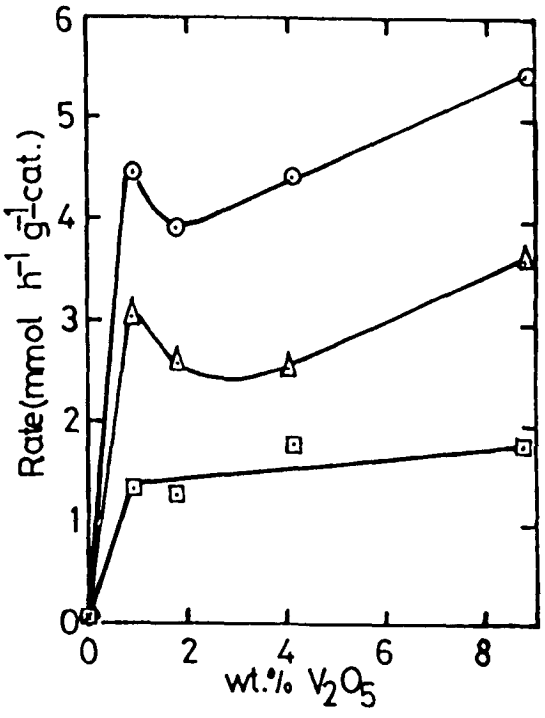

Figure 4.40 The rate for the decomposition of isopropanol(r_t(⊙), r_{ac}(△) and r_{pr}(⊡)) at 220°C as a function of the V_2O_5 content.

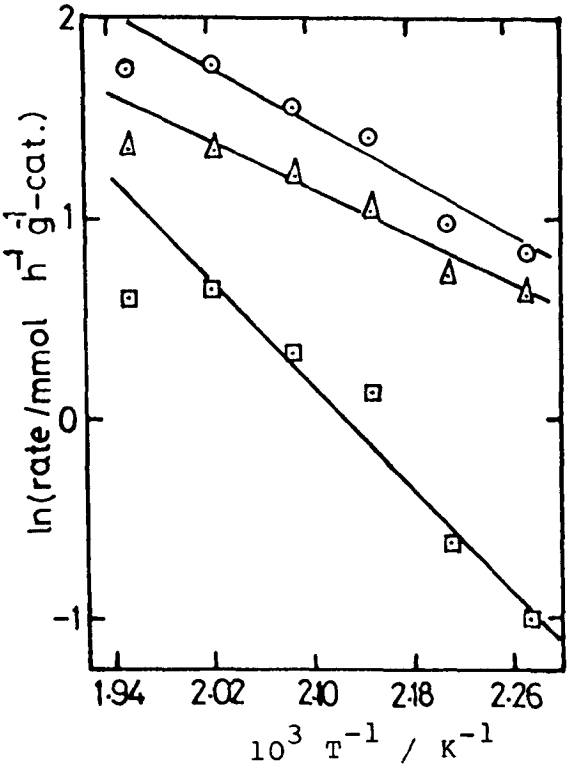

Figure 4.41 Ln(rate/r_t(⊙), r_{ac}(△) and r_{pr}(⊡) versus 1/T for the catalyst containing 8.8% V_2O_5: the decomposition of isopropanol (this catalyst used in Figure 4.39).

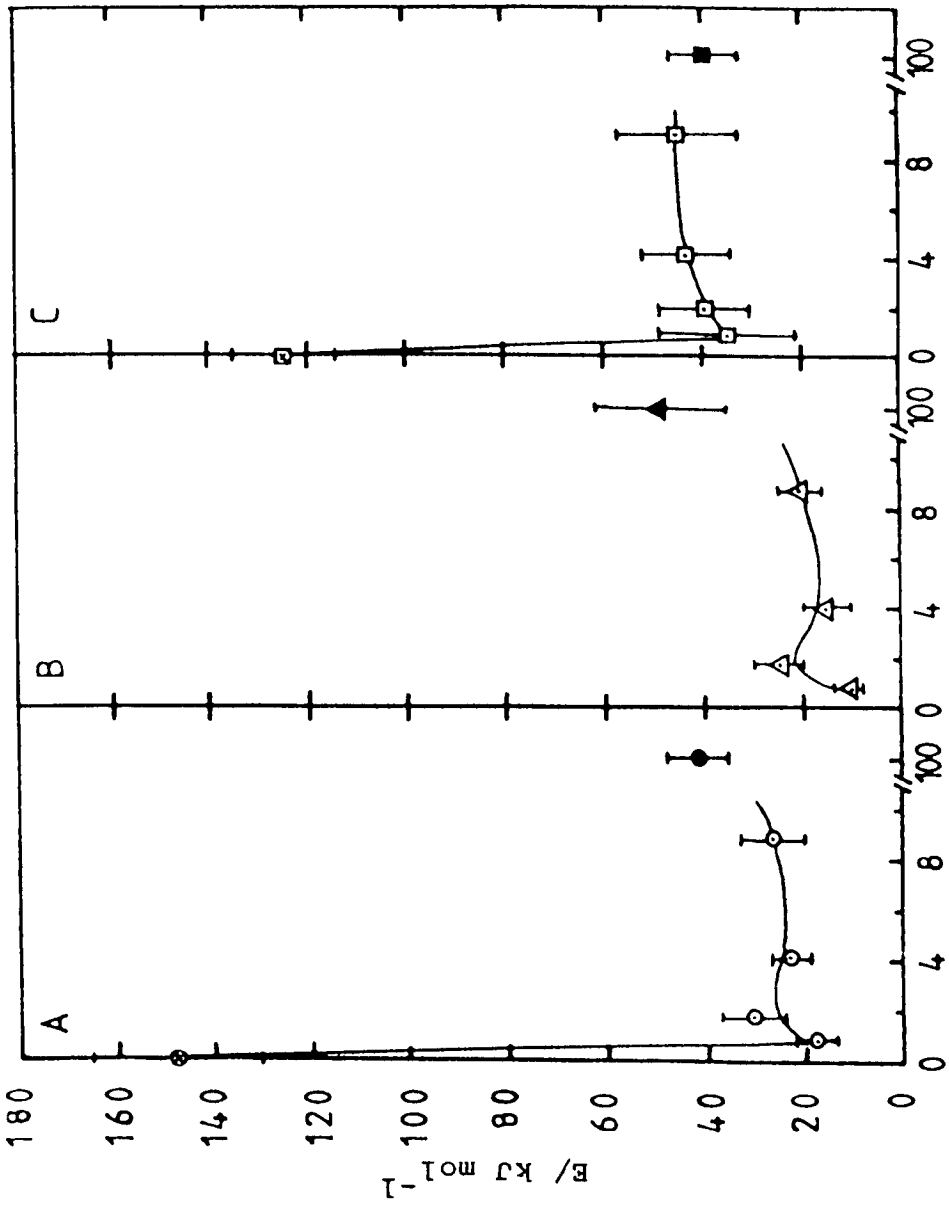

Figure 4.42 E_t(⊙), E_{ac}(△) and E_{pr}(□) as a function of V_2O_5 content for samples shown in Figure 4.39. E_t(●), E_{ac}(▲) and E_{pr}(■) for unsupported V_2O_5. E_t(⊛) and E_{pr}(⊡) for TiO_2(washed).

4.2.3.2.1 Characterisation

The catalyst sample was analysed by TPR and laser Raman spectrocsopy.

TPR

Figure 4.43A shows the TPR profile which has only one peak with T_{max} = 473°C. The quantity of H_2 consumed corresponds to that required for reduction of V(V) to V(III) (i.e. 2 mol H_2/ mol V_2O_5).

Laser Raman spectroscopy

The laser Raman spectrum of this catalyst did not exhibit a band due to crystalline V_2O_5 but rather showed bands due to TiO_2 (Figure 4.43B).

4.2.3.3 Catalyst prepared by the $VO(O^iBu)_3$ method

A VO_x/TiO_2(washed) monolayer catalyst was prepared by the $VO(O^iBu)_3$ method as described in Section 3.5.3 of Chapter 3; it contained 0.8% V_2O_5.

4.2.3.3.1 Characterisation

The catalyst sample was analysed by TPR and laser Raman spectroscopy.

TPR

Figure 4.44A shows the TPR profile for the monolayer catalyst which has only one peak with T_{max} = 475°C. The

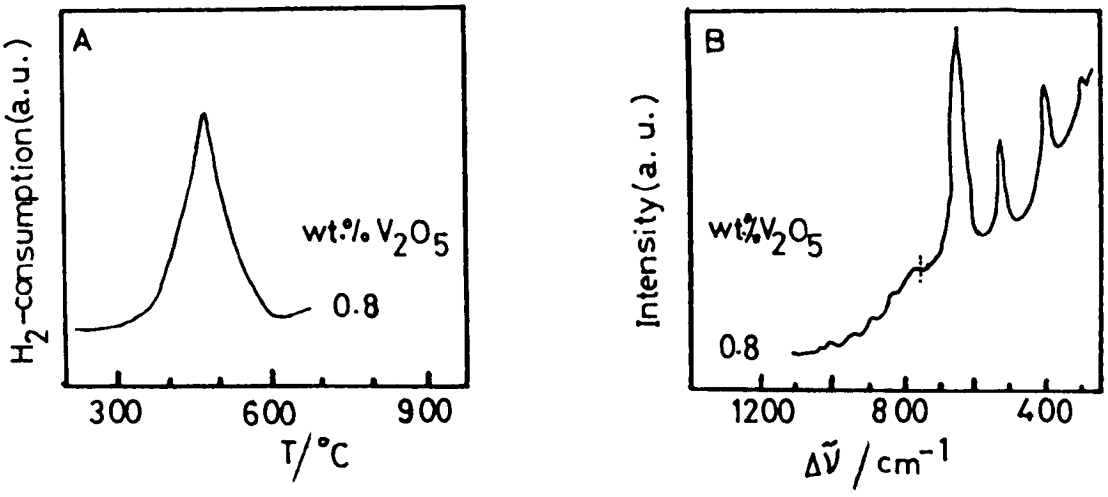

Figure 4.43 TPR profile (A) and Raman spectrum (B) for VO_x/TiO_2(washed) monolayer catalyst prepared by $VOCl_3$ method.

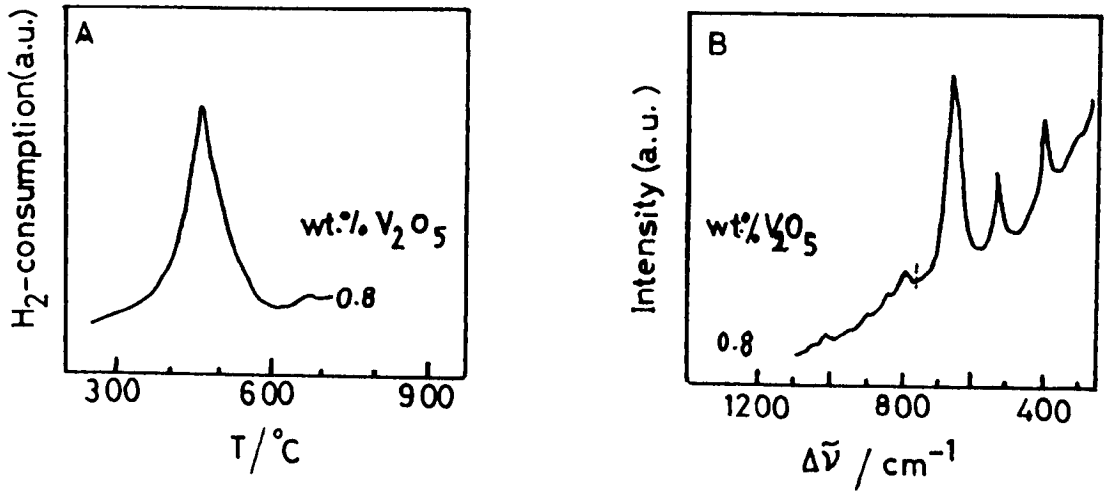

Figure 4.44 TPR profile (A) and Raman spectrum (B) for VO_x/TiO_2(washed) monolayer catalyst prepared by the $VO(O^iBu)_3$ method.

quantity of H_2 consumed corresponds to that required for reduction of V(V) to V(III) (i.e. 2 mol H_2/mol V_2O_5).

Laser Raman spectroscopy

The laser Raman spectroscopy of this monolayer catalyst did not exhibit a band due to crystalline V_2O_5 and just showed the bands due to TiO_2 (Figure 4.44B).

4.2.4 VO_x/TiO_2(P-25) catalysts

TiO_2(P-25) used as a support has 76% anatase and surface area 55 m^2g^{-1} (see Table 3.1, Chapter 3).

4.2.4.1 Catalysts prepared by wet impregnation method

The VO_x/TiO_2(P-25) catalysts were prepared by this method as described in Section 3.5.1, Chapter 3; they contained 2 - 32% V_2O_5.

4.2.4.1.1 Characterisation

The catalysts were studied by TPR, laser Raman spectroscopy and XPS. The results are given below.

TPR

Figure 4.45 shows the TPR profiles for the catalysts containing 2 - 32% V_2O_5 and for the support. Figure 4.46 shows the dependence of T_{max} and Figure 4.47 the H_2 consumption per g catalyst, as a function of V_2O_5 content. The TPR profiles initially exhibited only a single peak and T_{max} increased with V_2O_5 content (Figure 4.46). At very large V_2O_5 contents, equivalent to more than five monolayers, the peak begins to divide (see figures 4.45 and 4.46): this

behaviour is similar to that observed with the low area anatase (figures 4.28 and 4.29) with allowance for the difference in surface area. The corresponding volumes of H_2 consumed per g of catalyst are plotted against V_2O_5 content in Figure 4.47. The values of H_2 consumed are lower than the theoretical values for the reduction of V(V) to V(III) corresponding to the composition of the final oxide of about $V_2O_{3.3}$.

Laser Raman spectroscopy

No satisfactory laser Raman spectra could be obtained with the preparations based on TiO_2(P-25) because of their dark colour.

XPS

Figure 4.48 shows the XP spectra for the same series of catalysts, for the support and for pure V_2O_5. The binding energies of the V $2p_{1/2}$ and V $2p_{3/2}$ levels in all samples are 524.2 $\pm$ 0.3 and 517.0 $\pm$ 0.18 eV; these values are similar to the values of unsupported V_2O_5 (Table 4.11). The binding energies values for the Ti $2p_{1/2}$ and O 1s satellite levels in the catalysts and in the TiO_2(P-25) are the same, viz. 464.2 $\pm$ 0.09 and 464.2 eV, respectively 520.0 $\pm$ 0.24 and 520.2 eV.

Figure 4.49 shows the averaged $\bar{R}_{3,4}$ values as a function of the V_2O_5 content. The V/Ti ratio increases rapidly up to about the monolayer point (4% V_2O_5) and thereafter remains constant.

XP spectra (Figure 4.50) for the dried catalysts are similar to the results for dried catalysts with unwashed and

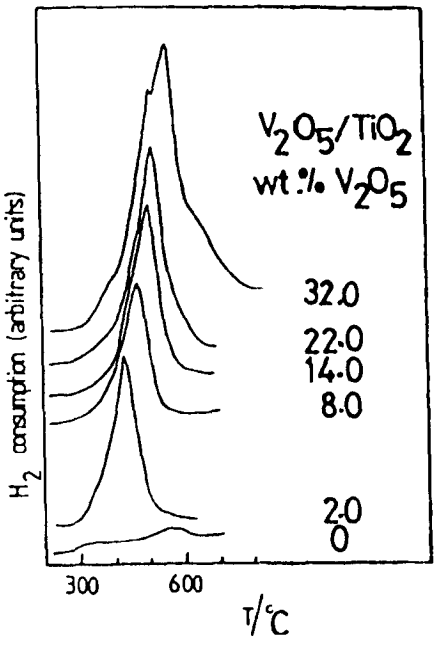

Figure 4.45 TPR profiles for catalysts made by aqueous impregnation of Degussa (P-25) and for the support. The wt.% V_2O_5 is given for each curve.

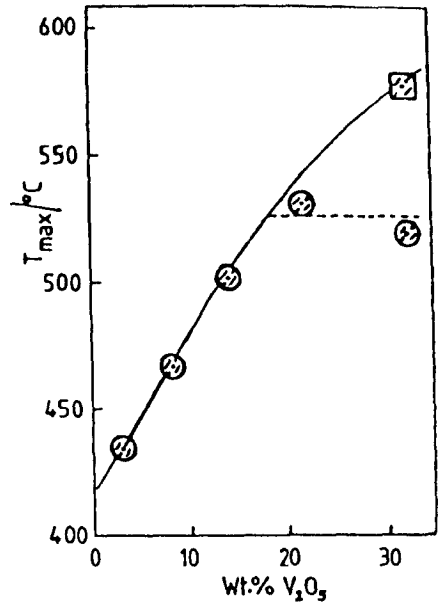

Figure 4.46 Dependence of T_{max} on V_2O_5 content for catalysts shown in Figure 4.45. Circles, first peak; squares, second peak.

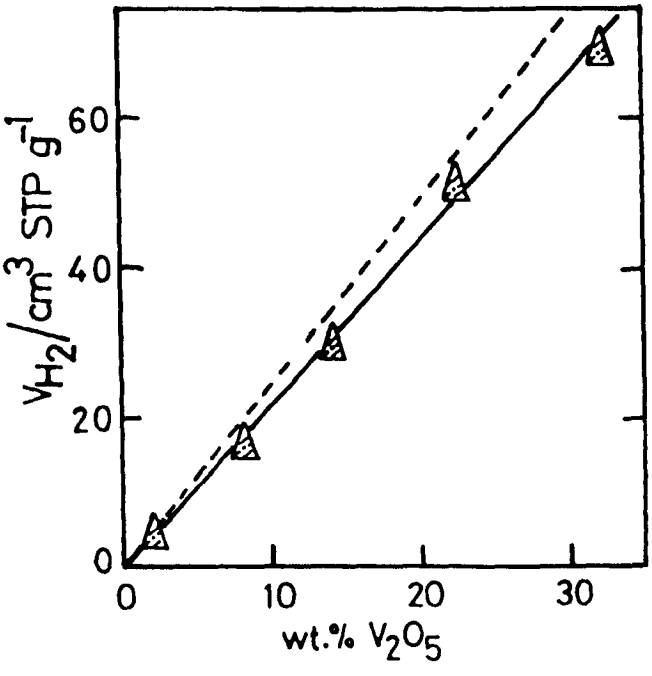

Figure 4.47 Dependence of volume of H_2 consumed in TPR on V_2O_5 content for catalysts shown in Figure 4.45. Triangles represent total H_2 volume. The broken line represents the theoretical volume of H_2 consumed.

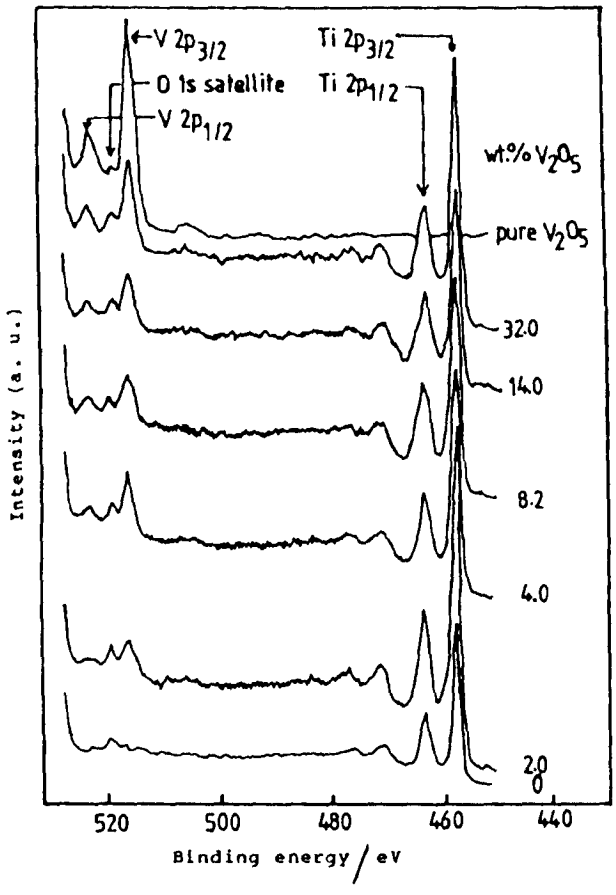

Figure 4.48 XPS spectra of catalysts made by aqueous impregnation of TiO_2(P-25), and for the support and for pure V_2O_5. The wt.% V_2O_5 is given for each curve.

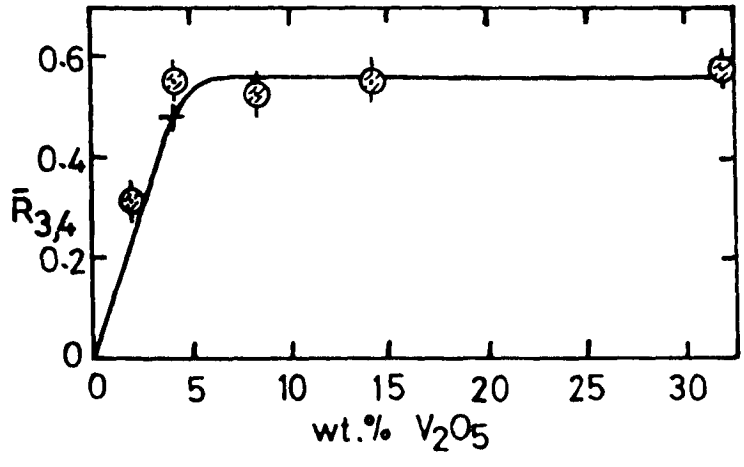

Figure 4.49 Dependence of V/Ti ratio $\bar{R}_{3,4}$(⊛) on %V_2O_5 for the catalysts depicted in Figure 4.48. The curve is that calculated for $f_1 = f_2 = 0.3$, $x = 0.05$; $\bar{R}_{3,4}$ taken as 0.48 at the one monolayer point.

Table 4.11

XPS results of VO_x/TiO_2(P-25) catalysts prepared by wet impregnation, TiO_2, $(NH_4)_2VO(C_2O_4)_2 \cdot 2H_2O$ and unsupported V_2O_5.

wt.% V_2O_5	sample preparation	Binding energy (FWHM) V $2p_{1/2}$	V $2p_{3/2}$	O 1s[a]	Ti $2p_{1/2}$	FWHM(eV)[b] Ti $2p_{3/2}$
2.0	powd.,calcined	524.1(2.4)	516.9(2.4)	520.1(1.6)	464.3(2.4)	1.6
4.0	"	523.9(2.8)	516.8(2.5)	519.8(--)	464.2(2.8)	1.7
8.2	"	524.3(2.6)	517.1(2.8)	520.3(--)	464.3(2.7)	2.0
14.0	"	524.1(2.6)	517.1(2.3)	519.7(--)	464.1(2.6)	1.7
32.0	"	524.7(2.2)	517.1(1.8)	520.1(--)	464.3(2.5)	1.6
2.0	powd., not calcined		515.8(1.6)	519.4(2.2)	464.0(2.4)	1.6
4.0	"		516.1(2.6)	520.1(--)	464.2(2.7)	2.0
8.2	"		516.3(2.2)	519.7(--)	464.1(3.0)	2.0
14.0	"		515.4(2.7)	519.6(--)	464.2(2.6)	2.3
32.0	"		515.7(2.4)	520.3(--)	464.1(2.2)	1.9
TiO_2†c				519.9(1.9)	464.3(2.6)	458.4(1.5)
V_2O_5†c		524.5(2.7)	517.2(1.9)	520.2(--)		
$(NH_4)_2VO(C_2O_4)_2 \cdot 2H_2O$†c			515.1(1.8)	520.1(--)		

FWHM = Full width at half of the maximum height;
a = Oxygen satellite;
b = Binding energies of the catalysts were determined by referencing to the Ti $2p_{3/2}$ line at 458.5 eV;
c = Binding energies of the standard compounds were determined by referencing to the C 1s line at 284.6 eV.

washed TiO_2-low surface area (see Figures 4.13 and 4.36). the binding energies of the Ti $2p_{1/2}$, V $2p_{3/2}$ and O 1s satellite levels are 464.1 ± 0.08, 515.9 ± 0.25 and 519.8 ± 0.37 eV, respectively (Table 4.11). Figure 4.51 shows the averaged $\bar{R}_{3,4}$ values as a function of the V_2O_5 content for the dried catalysts . The V/Ti ratio initially increases in proportion to the V_2O_5 content up to 4% V_2O_5 and then remains constant. Above 8% V_2O_5, the V/Ti ratio increases up to 14% V_2O_5 and increases gradually with V_2O_5 content.

4.2.4.2 Catalysts prepared by the $VOCl_3$ method

A series of VO_x/TiO_2(P-25) catalysts were prepared by this method, as described in Section 3.5.2 of Chapter 3, containing 2.6 - 17% V_2O_5.

4.2.4.2.1 Characterisation

The catalysts were studied by TPR, FTIR, ESR and XPS. The results are given below.

TPR

Figure 4.52 shows that the TPR profiles for these catalysts consist of only a single symmetrical peak. The value of T_{max} increases with V_2O_5 content as in Figure 4.53. The corresponding volumes of H_2 consumed per g catalyst are plotted against V_2O_5 content in Figure 4.54. The volumes of H_2 consumed were as expected for the reduction of V(V) to V(III) except for the catalyst containing 17% V_2O_5 which shows a lower value than expected.

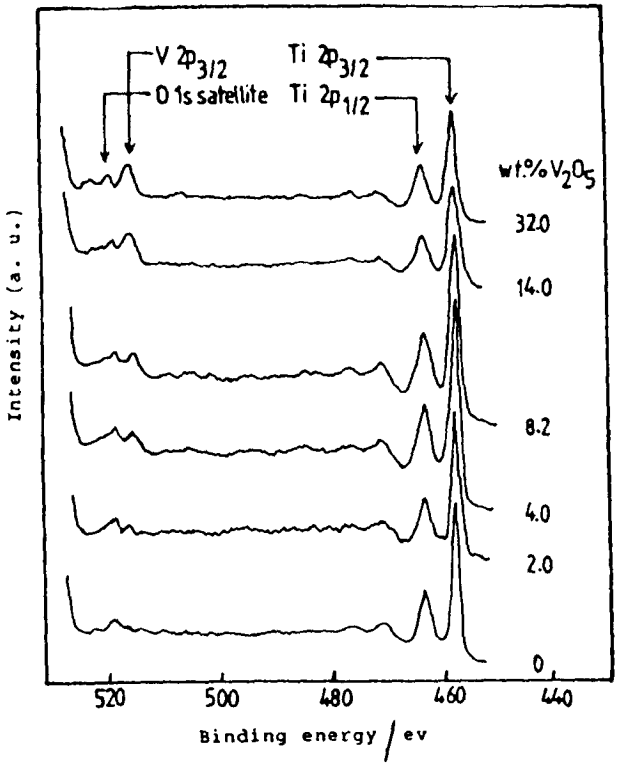

Figure 4.50 XPS spectra for the same catalysts in Figure 4.48, but in the dried stage.

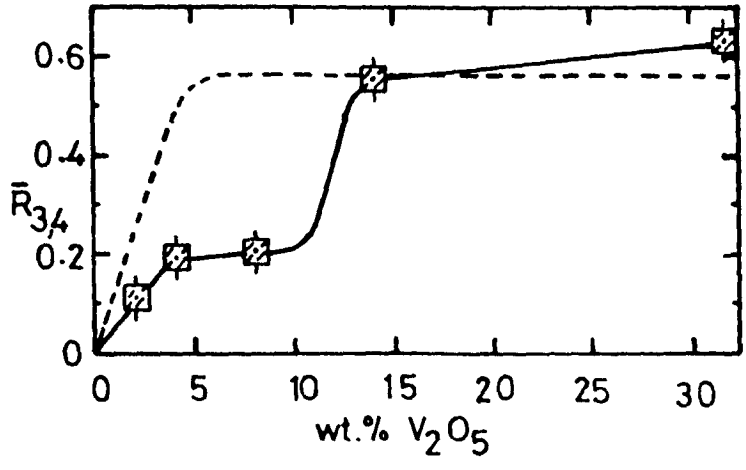

Figure 4.51 Dependence of V/Ti ratio $\bar{R}_{3,4}$(⊠) on $\%V_2O_5$ for the dried catalysts depicted in Figure 4.50. The broken line represents the $\bar{R}_{3,4}$ for the calcined catalysts for same series (see Figure 4.49) are shown for comparison.

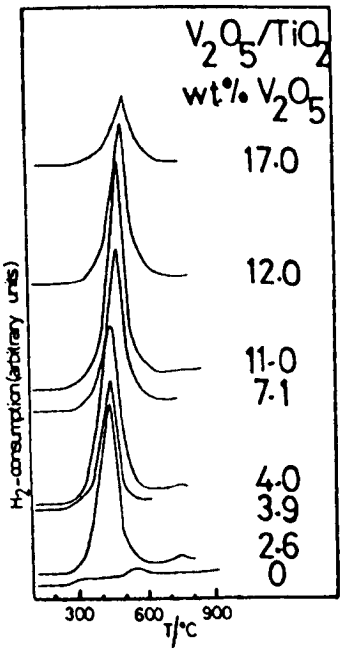

Figure 4.52 TPR profiles for catalysts prepared by treatment of TiO_2(P-25) with $VOCl_3$, and for the support. The wt.% V_2O_5 is given for each curve.

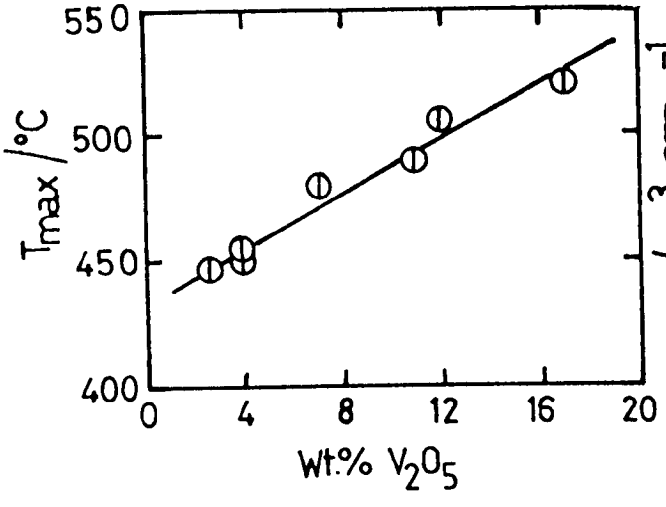

Figure 4.53 Dependence of T_{max} on V_2O_5 content for catalysts shown in Figure 4.52.

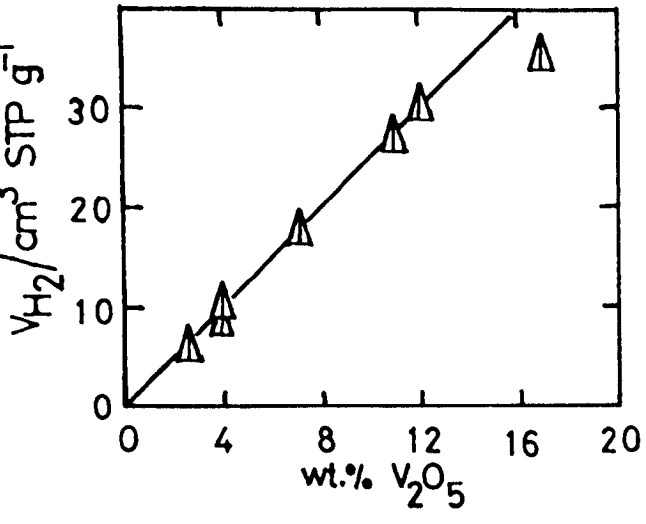

Figure 4.54 Dependence of volume of H_2 consumed in TPR on V_2O_5 content for catalysts shown in Figure 4.52.

FTIR

Figure 4.55 shows FTIR spectra (KBr disk technique) for pure TiO_2(P-25), VO_x/TiO_2(P-25) and unsupported V_2O_5 measured in air.

The TiO_2 spectrum (spectrum a) shows a broad band at 3400 cm^{-1} and a narrow band at 1610 cm^{-1}. The spectra for the VO_x/TiO_2 samples (spectra b, c and d) show the same two bands as in spectrum (a). Two narrow bands appear at 2840 and 2920 cm^{-1} while a shoulder appears at 1020 cm^{-1} for the 7.1% V_2O_5 loading and becomes as a peak at 13% V_2O_5 (spectra c and d). The spectrum of unsupported V_2O_5 (spectrum e) shows bands at 820 and 1020 cm^{-1}, as well as a broad band at 3400 cm^{-1}.

The broad band at 3400 cm^{-1} is due to physically adsorbed water (4). The band at 1610 cm^{-1} is assigned to the OH bending vibration. The bands at 2840 and 2920 cm^{-1} may be related to the symmetric and asymmetric stretching vibration of the CH bond respectively (the CH bond may orginate from the oxidation of residual organic solvent during calcination)(5). The band at 1020 cm^{-1} is thought to be due to the V=O stretching vibration and the band at 820 cm^{-1} in pure V_2O_5 is attributed to a symmetrical V-O-V stretching vibration. Similar spectra were obtained to the spectra in Figure 4.55 when the same samples were evacuated at 100°C for 3h.

ESR

The ESR spectra of pure TiO_2(P-25) and the VO_x/TiO_2(P-25) catalysts are shown in Figure 4.56. The spectrum from TiO_2 (spectrum a), as expected, showed no

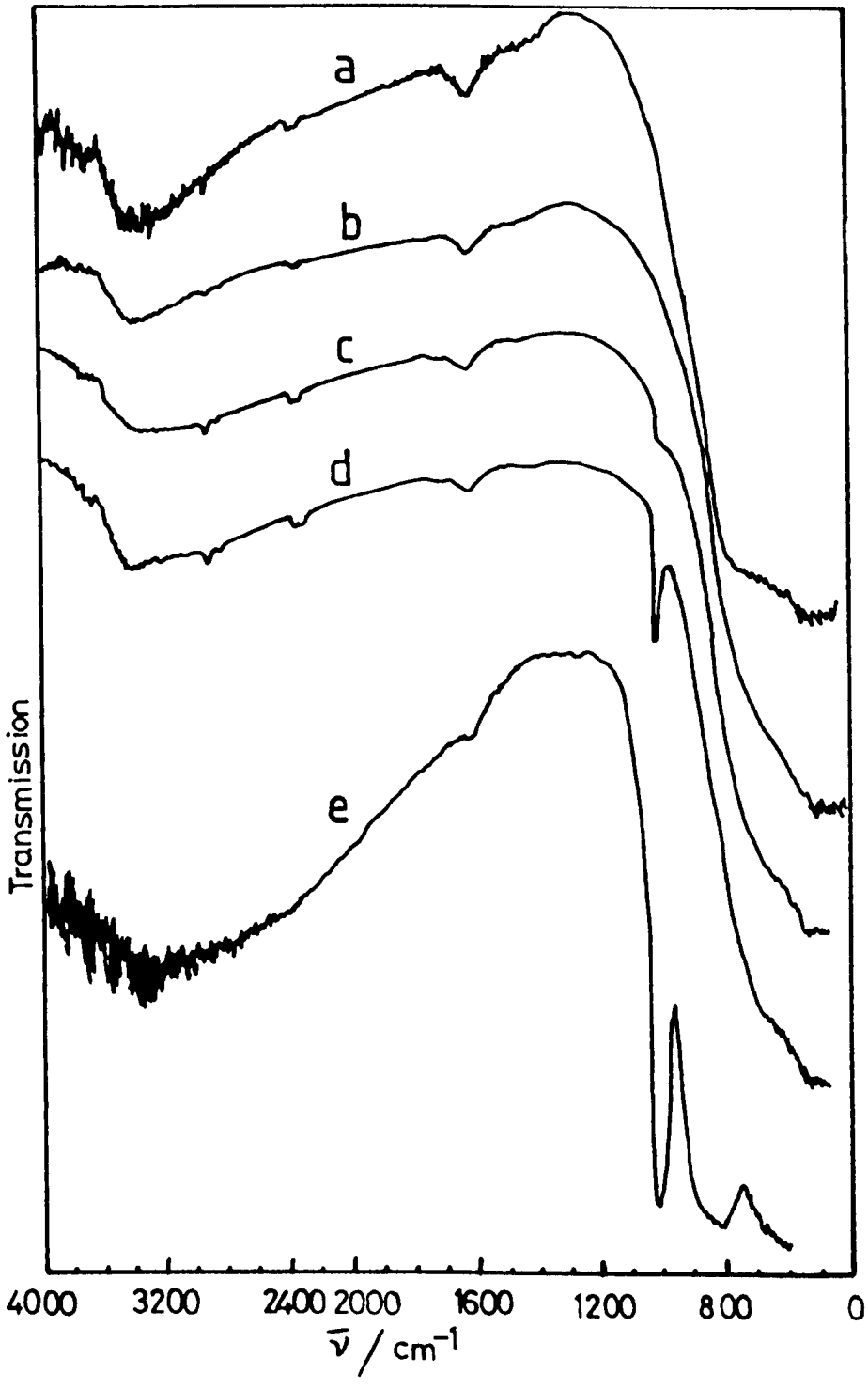

Figure 4.55 FTIR spectra (KBr disc technique) of the VO_x/TiO_2(P-25) catalysts measured at room temperature (in air): a) TiO_2(P-25), b) 4% V_2O_5, c) 7.1% V_2O_5, d) 13% V_2O_5 and e) pure V_2O_5.

signs of resonance whereas the catalysts (spectra b and c) showed strong resonances with hyperfine structure characteristic of the interaction of the unpaired electron with ^{51}V (I = 7/2) in vanadium (IV) ions (6,7).

The spectrum of the VO_x/TiO_2(P-25) monolayer catalyst (spectrum b) is similar to that found for $VOSO_4.5H_2O$ (8), which may be ascribed to vanadyl(IV) VO^{2+} ions. The spectrum c, although less well resolved, was similar in its overall structure.

The g-values of the two observed spectra were centred at 1.98 - 1.99 and estimates of the number of spins by double integration of the signals and comparison with $(NH_4)_2VO(C_2O_4)_2.2H_2O$ suggest that the amount of V(IV) ions supported on the carrier surface is around 5% of the total vanadium present in the case of monolayer catalyst (spectrum b). The VO_x/TiO_2 catalyst with loading 13% V_2O_5 may have more than 5% V(IV) ions (spectrum c).

XPS

Figure 4.57 shows the XP spectra for the same series of catalysts, for the support and for pure V_2O_5. The binding energies of the V $2p_{1/2}$ and V $2p_{3/2}$ levels in all samples are 524.76 $\pm$ 0.2 and 517.6 $\pm$ 0.4 eV (Table 4.12). This indicates the presence of only V(V) in the calcined samples. The binding energy values of the Ti $2p_{1/2}$ and O 1s satellite levels in the catalysts and in TiO_2 are the same, viz. 464.1 $\pm$ 0.1 and 464.2 eV, respectively 520.4 $\pm$ 0.4 and 520.2 eV.

Figure 4.58 shows that the averaged $\bar{R}_{3,4}$ continues to increase significantly above the monolayer point (4% V_2O_5).

Figure 4.59 shows the XP spectra for the same series of

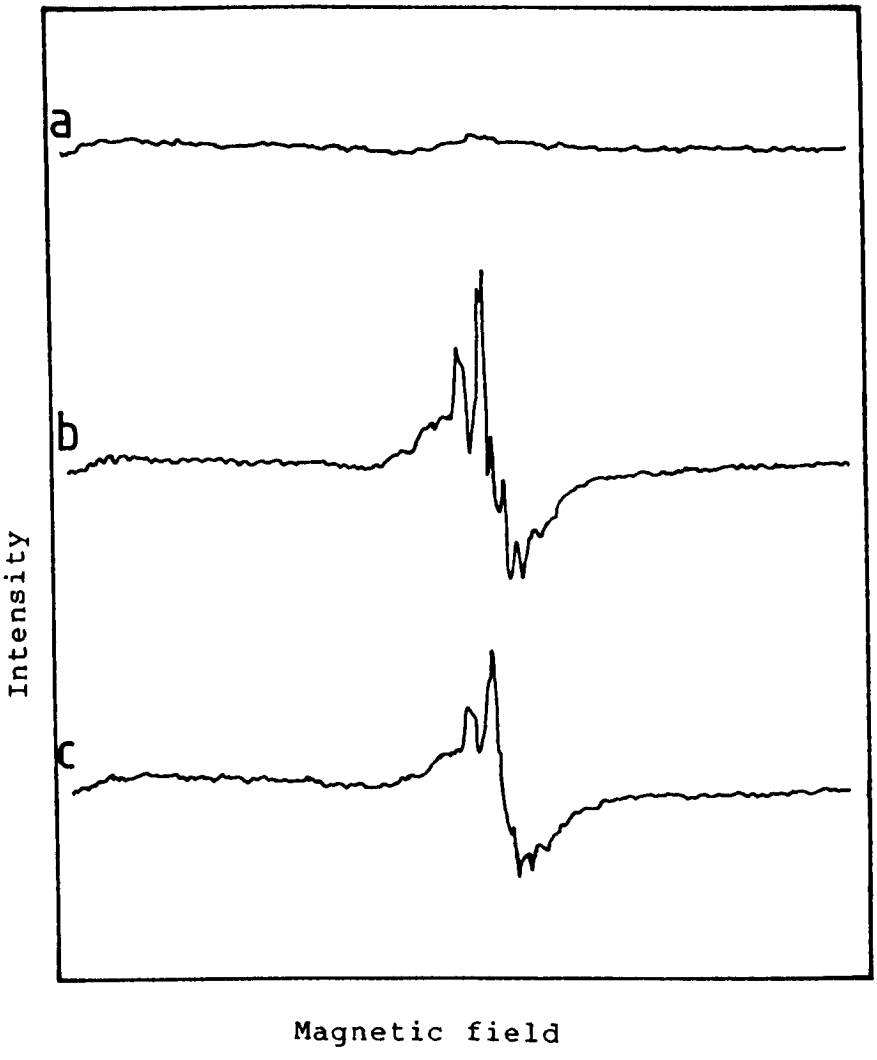

Figure 4.56 ESR spectra of TiO_2(P-25) VO_x/TiO_2(P-25) samples measured at room temperature; a) TiO_2(P-25), b) 4% V_2O_5 and c) 13% V_2O_5.

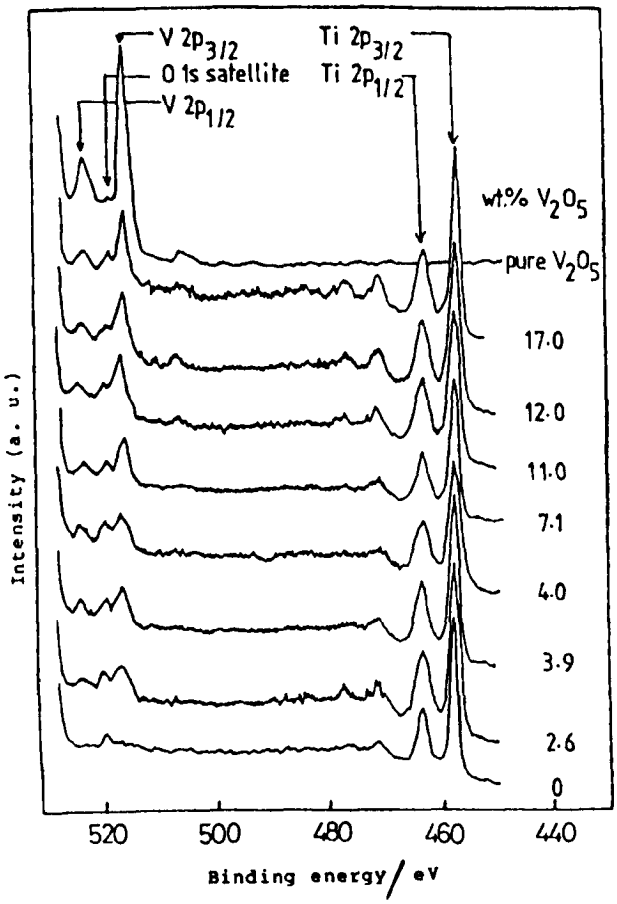

Figure 4.57 XPS spectra of catalysts prepared by treatment TiO_2(P-25) with $VOCl_3$, and for the support. The wt.% V_2O_5 is given for each curve.

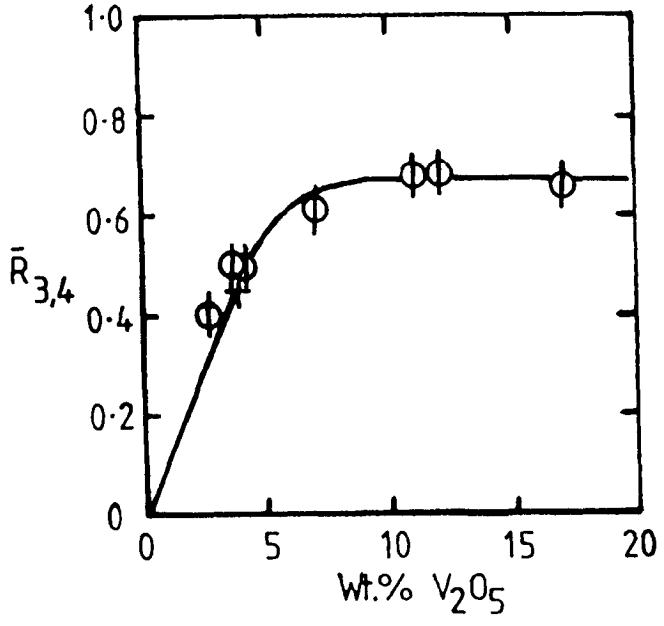

Figure 4.58 Dependence of V/Ti ratio $\bar{R}_{3,4}$(Φ) on $\%V_2O_5$ for the catalysts depicted in Figure 4.57. The curve is that calculated for $f_1 = f_2 = 0.3$, $x = 0.125$; $\bar{R}_{3,4}$ taken as 0.45 at the one monolayer point.

Table 4.12

XPS results of VO_x/TiO_2(P-25) catalysts prepared by the $VOCl_3$ method, TiO_2 and unsupported V_2O_5.

wt.% V_2O_5	sample preparation	Binding energy (FWHM) V $2p_{1/2}$	V $2p_{3/2}$	O $1s^a$	Ti $2p_{1/2}$	FWHM(eV)$_b$ Ti $2p_{3/2}$
2.6	powd.,calcined	524.7(1.4)	517.7(2.8)	520.9(1.8)	464.1(2.9)	1.9
3.9	"	524.9(1.3)	517.8(2.5)	520.6(2.5)	464.2(2.2)	1.8
4.0	"	524.9(1.2)	517.8(2.5)	520.5(2.3)	463.9(2.4)	2.4
7.1	"	525.0(2.4)	517.9(2.4)	520.7(--)	464.1(2.8)	2.0
11.0	"	525.0(1.8)	517.9(2.4)	520.7(--)	464.1(2.8)	1.7
12.0	"	524.7(1.6)	517.4(2.2)	520.1(--)	464.1(2.7)	2.1
17.0	"	524.9(2.0)	517.7(1.7)	520.1(1.8)	464.3(2.5)	1.7
2.6	powd.,not calc.	523.7(1.6)	517.1(2.3)	519.7(1.8)	464.3(2.0)	1.5
3.9	"	523.7(1.6)	517.1(2.3)	519.7(1.8)	464.3(2.0)	1.5
4.0	"	524.2(2.0)	517.0(2.6)	520.2(2.1)	464.3(2.2)	1.5
7.1	"	524.3(2.0)	517.0(2.0)	519.7(--)	464.1(2.4)	1.6
11.0	"	524.7(2.3)	516.9(2.3)	519.9(--)	464.3(2.4)	1.7
12.0	"	524.1(2.6)	517.5(2.5)	520.3(2.0)	464.0(2.9)	1.9
TiO_2↑c				519.9(1.9)	464.3(2.6)	458.4(1.5)
V_2O_5↑c		524.5(2.7)	517.2(1.9)	520.2(--)		

FWHM = Full width at half of the maximum height;
a = Oxygen satellite;
b = Binding energies of the catalysts were determined by referencing to the Ti $2p_{3/2}$ line at 458.5 eV;
c = Binding energies of the standard compounds were determined by referencing to the C 1s line at 284.6 eV.

catalysts at the dried stage. The spectra are similar to those of the calcined catalysts (see Figure 5.57). The binding energies of the V $2p_{1/2}$ and V $2p_{3/2}$ levels in all samples are 524.2 $\pm$ 0.3 and 517.0 $\pm$ 0.2 eV (Table 4.12). These results indicate the presence of V(V) in the dried samples also. Figure 4.60 shows the averaged $\bar{R}_{3,4}$ for the dried catalysts continues to increase significantly above the monolayer point (4% V_2O_5).

4.2.4.2.2 Decomposition of isopropanol

Figure 4.61 shows the results for the decomposition of isopropanol at 220°C. Figure 4.61 shows that on TiO_2(P-25), S_{ac} is 10%. With VO_x/TiO_2 samples, S_{ac} increases to 65% at 2.6% V_2O_5, and remains constant up to 13% V_2O_5. Figure 4.61 also shows the conversion of isopropanol which initially increases with V_2O_5 content. The conversion is 15% at 2.6% V_2O_5 and remains constant up to 13% V_2O_5. Similar results were found at the 210 and 230°C. Figure 4.62 shows r_t, r_{ac} and r_{pr} at 220°C plotted as a function of the V_2O_5 content. The values of r_t, r_{ac} and r_{pr} increase rapidly up to 2.6% V_2O_5, then increase gradually with V_2O_5 content. The value of r_{ac} is always higher than r_{pr}. Figure 4.63 shows the plots of ln(r_t, r_{ac} and r_{pr}) versus 1/T for the catalyst containing 13% V_2O_5, giving E_t, E_{ac} and E_{pr}. Table 4.13 shows their values and the corresponding values of lnA for the catalysts and for TiO_2(P-25) which were tested in this reaction. Figure 4.64 shows the values of E_t, E_{ac} and E_{pr} (Table 4.13) as a function of the V_2O_5 content. The values of E_t and E_{ac} fall sharply with the V_2O_5 content in the V_2O_5 2.6% region. the value of E_t decreases gradually up to 7.1%

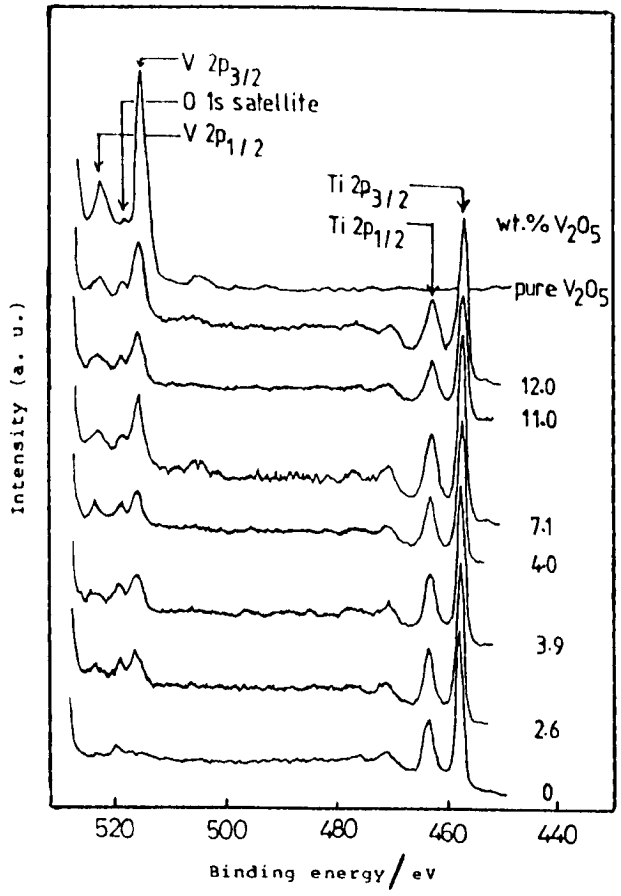

Figure 4.59 XPS spectra of the same catalysts in Figure 4.57, but in the dried stage.

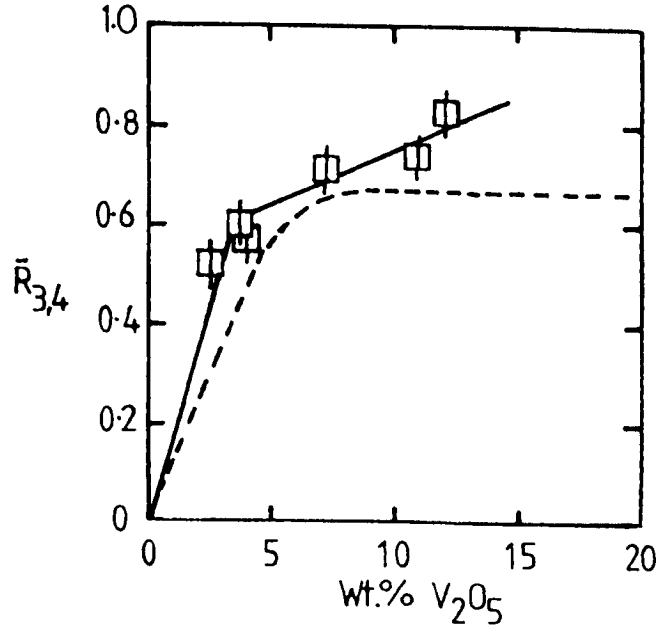

Figure 4.60 Dependence of V/Ti ratio $\bar{R}_{3,4}$ (⊞) on $\%V_2O_5$ for the catalysts depicted in Figure 4.59. The broken line represents the $\bar{R}_{3,4}$ for the calcined catalysts for same series (see Figure 4.58) and are shown for comparison.

V_2O_5 and then increases gradually with V_2O_5 content (up to 13% V_2O_5), while E_{ac} decreases gradually up to 13% V_2O_5. The values of E_t and E_{ac} are lower with VO_x/TiO_2 catalysts than for TiO_2 and unsupported V_2O_5. Figure 4.64 shows that E_{pr} falls with the V_2O_5 content in the V_2O_5 2.6% region, then increases gradually up to 13% V_2O_5. The value of E_{pr} is higher with TiO_2 and VO_x/TiO_2 catalysts than for unsupported V_2O_5.

Table 4.13

Arrhenius parameters for VO_x/TiO_2(P-25) catalysts prepared by the $VOCl_3$ method, and TiO_2(P-25) in the catalytic decomposition of isopropanol.

Wt.% V_2O_5	E_t[1]	lnA[2]	c.c.	E_{ac}[1]	lnA[2]	c.c.	E_{pr}[1]	lnA[2]	c.c.
pure TiO_2	123.0	29.38	0.992	138.0	31.64	0.994	106.2	25.38	0.986
2.6	27.6	8.4	0.969	18.4	5.74	0.913	50.2	12.82	0.996
4.0	29.7	8.69	0.95	18.8	5.63	0.855	54.4	13.66	0.998
7.1	18.0	5.92	0.962	14.6	4.45	0.887	54.0	13.6	0.993
13	25.1	7.75	0.954	11.7	3.96	0.786	59.0	14.93	0.997

1 = E/ kJ mol^{-1};

2 = ln(A/ mmol h^{-1} g^{-1}-cat.).

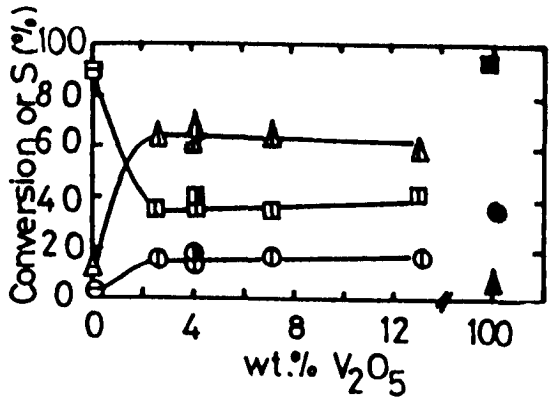

Figure 4.61 Decomposition of isopropanol on VO_x/TiO_2(P-25) catalysts prepared by $VOCl_3$, TiO_2(P-25) and unsupported V_2O_5 at 220°C as a function of V_2O_5 content: ⓘ, isopropanol conversion; ⊡, S_{pr}; ◭, S_{ac}. ◑, isopropanol conversion; ◨, S_{pr}; ◭, S_{ac}: for VO_x/TiO_2(P-25) monolayer catalyst prepared by $VO(O^iBu)_3$ method. ⊖, isopropanol conversion; ⊟, S_{pr}; ⧋, S_{ac}: for TiO_2(P-25). ●, isopropanol conversion; ■, S_{pr}; ▲, S_{ac}: for unsupported V_2O_5.

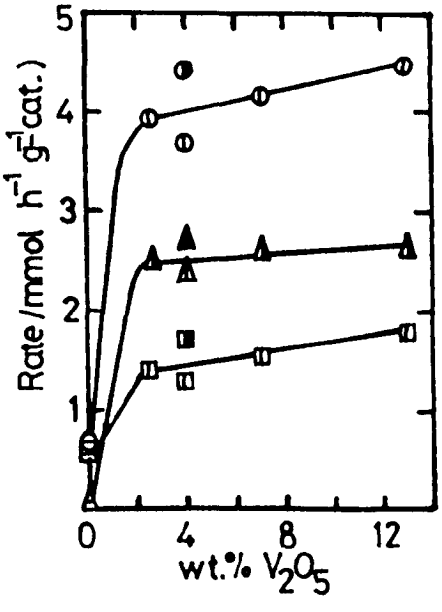

Figure 4.62 The rates for the decomposition of isopropanol (r_t(ⓘ), r_{ac}(◭) and r_{pr}(⊡)) at 220°C as a function of the V_2O_5 content for the samples shown in Figure 4.61.

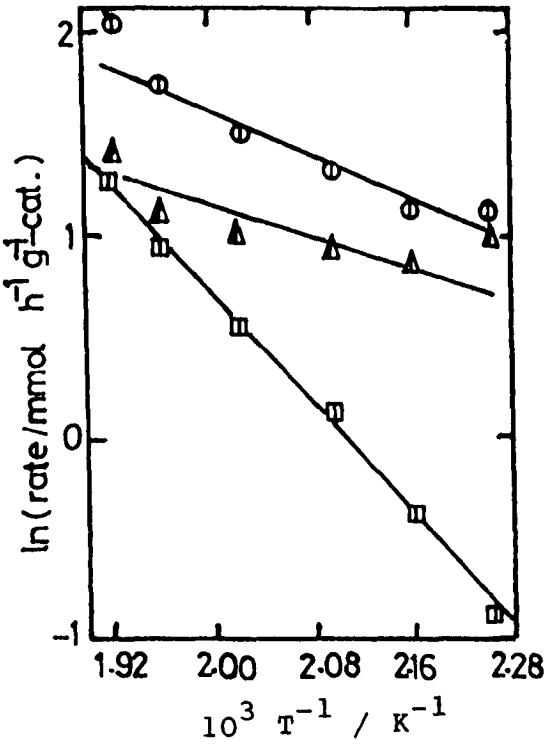

Figure 4.63 Ln(rate/r_t(◐), r_{ac}(◭) and r_{pr}(▥)) versus 1/T for the catalyst containing 13% V_2O_5 catalyzed the decomposition of isopropanol (this catalyst used in Figure 4.61).

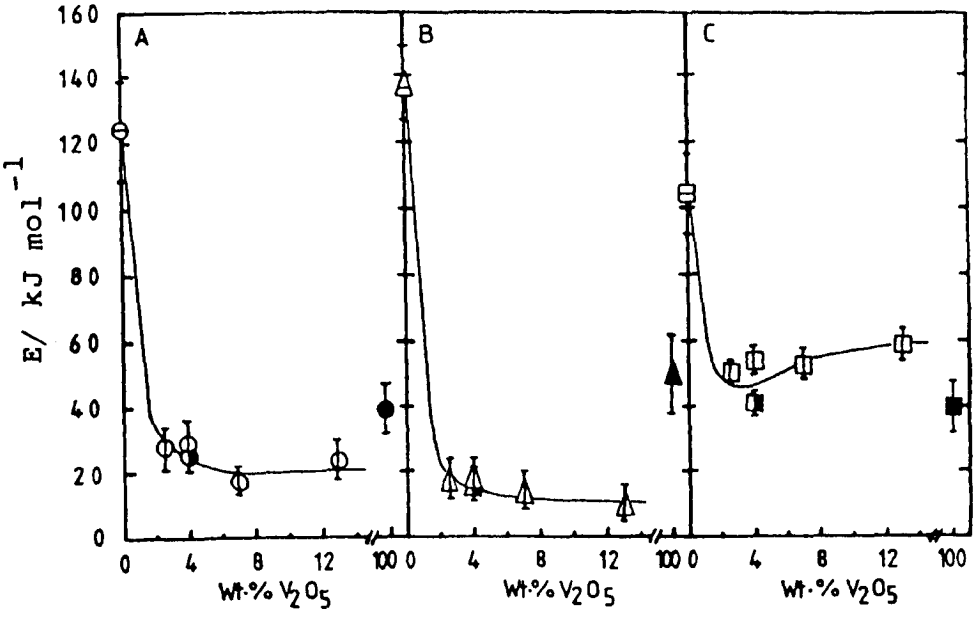

Figure 4.64 E_t(◐), E_{ac}(◭) and E_{pr}(▥) as a function of V_2O_5 content for samples shown in Figure 4.61. E_t(⊖), E_{ac}(△) and E_{Pr}(⊟): for TiO_2(P-25). E_t(◑), E_{ac}(◮) and E_{pr}(◧): for VO_x/TiO_2(P-25) monolayer catalyst prepared by $VO(O^iBu)_3$ method.

4.2.4.3 Catalysts prepared by the $VO(O^iBu)_3$ method

A series of VO_x/TiO_2(P-25) catalysts were prepared by this method, as described in Section 3.5.3 of Chapter 3, containing 3.2 - 12.0 wt.% V_2O_5.

4.2.4.3.1 Characterisation

TPR

Figure 4.65 shows that the TPR profiles for these catalysts consist of only a single peak which is similar to the results for VO_x/TiO_2(P-25) catalysts prepared by the $VOCl_3$ method (see Figure 4.52). The value of T_{max} increases with V_2O_5 content as in Figure 4.66. The corresponding volumes of H_2 consumed per g catalyst are plotted against V_2O_5 content as in Figure 4.67. The volumes of H_2 consumed are lower than expected for the reduction V(V) to V(III), so that the composition of the final oxide is about $V_2O_{3.3}$.

XPS

Figure 4.68 shows the XP spectra for the same series of catalysts and for the support. The binding energies of the V $2p_{1/2}$ and V $2p_{3/2}$ levels in all samples are 524.6 ± 0.2 and 517.2 ± 0.1 eV; these values are similar to the values of pure V_2O_5 (524.5 and 517.2 eV) (Table 4.14). Figure 4.69 shows the averaged $\bar{R}_{3,4}$ continues to increase significantly above the monolayer point (4% V_2O_5).

Figure 4.70 shows the XP spectra for a few catalysts of the same series at the dried stage. The spectra are similar to spectra of the calcined materials. Table 4.14 shows the binding energies which indicate the presence of V(V) in the dried samples also.

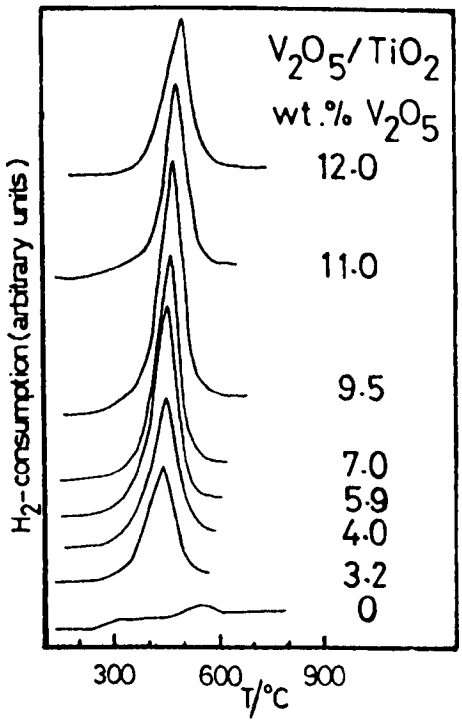

Figure 4.65 TPR profiles for catalysts prepared by treatment of TiO_2(P-25) with $VO(O^iBu)_3$ and for the support. The wt.% V_2O_5 is given for each curve.

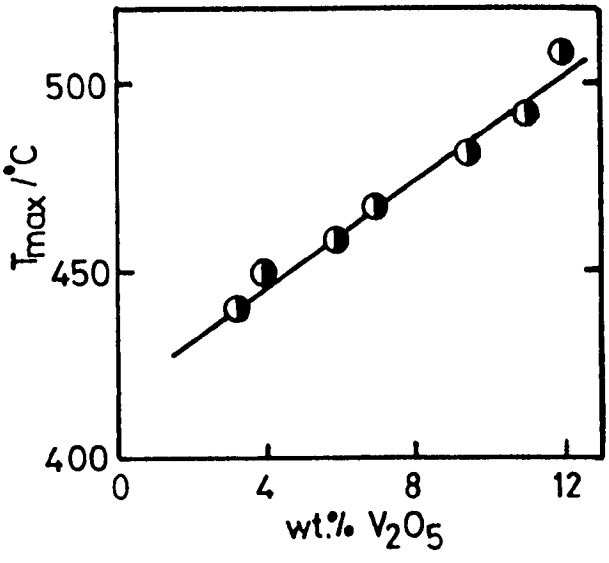

Figure 4.66 Dependence of T_{max} on V_2O_5 content for catalysts shown in Figure 4.65.

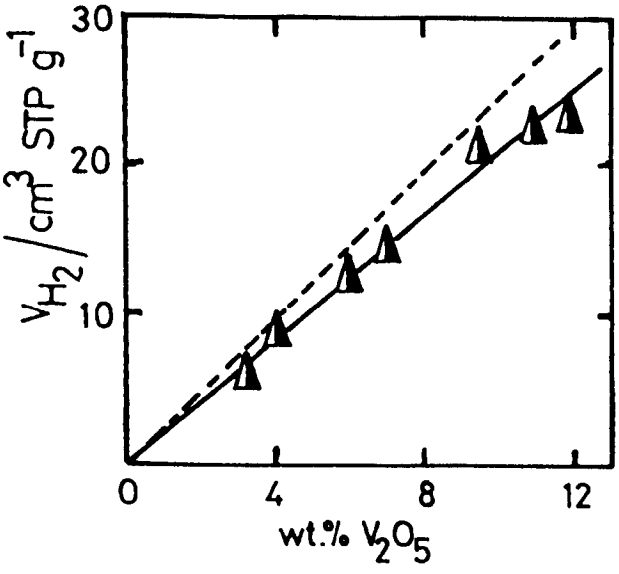

Figure 4.67 Dependence of volume of H_2 consumed in TPR on V_2O_5 content for catalysts shown in Figure 4.65. The broken line represents the theoretical volume of H_2 consumed.

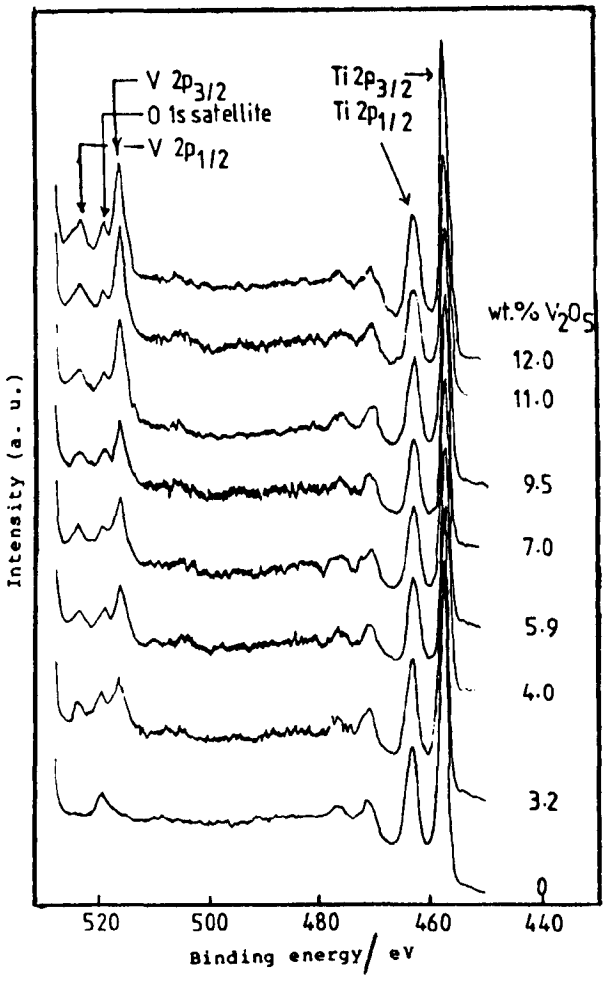

Figure 4.68 XPS spectra of catalysts prepared by treatment TiO_2(P-25) with $VO(O^iBu)_3$, and for the support. The wt.% V_2O_5 is given for each curve.

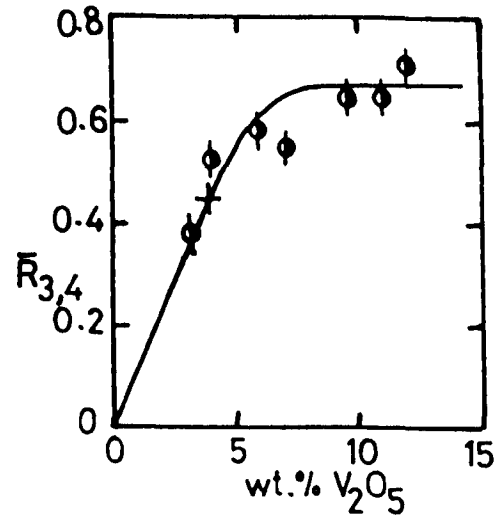

Figure 4.69 Dependence of V/Ti ratio $\bar{R}_{3,4}$(Φ) on %V_2O_5 for the catalysts depicted in Figure 4.68. The curve is that calculated for $f_1 = f_2 = 0.3$, $x = 0.125$; $\bar{R}_{3,4}$ taken as 0.45 at the one monolayer point.

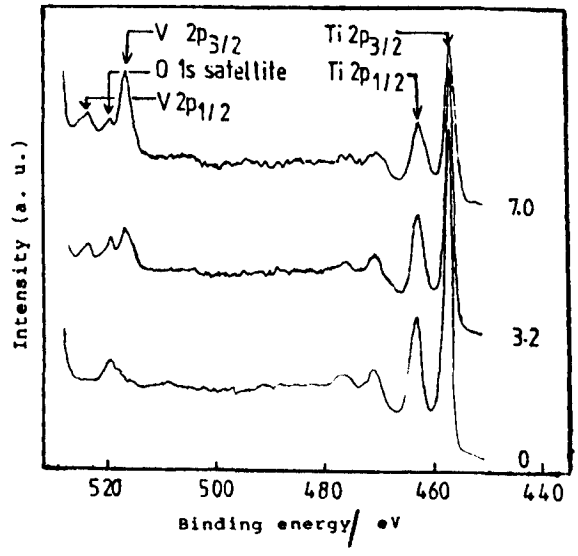

Figure 4.70 XPS spectra for a few catalysts from the Figure 4.68, but in the dried stage. The wt.% V_2O_5 is given for each curve.

Table 4.14

XPS results of VO_x/TiO_2(P-25) catalysts prepared by the $VO(O^iBu)_3$ method, TiO_2 and unsupported V_2O_5.

wt.% V_2O_5	sample preparation	Binding energy (FWHM) V $2p_{1/2}$	V $2p_{3/2}$	O $1s^a$	Ti $2p_{1/2}$	FWHM(eV)$_b$ Ti $2p_{3/2}$
3.2	powd.,calcined	524.3(1.8)	517.1(2.3)	520.1(2.2)	464.1(2.6)	1.7
4.0	"	524.7(2.2)	517.3(2.6)	520.1(2.2)	464.3(2.6)	1.7
5.9	"	524.5(1.9)	517.3(2.4)	520.3(--)	464.3(2.6)	1.8
7.0	"	524.9(2.2)	517.3(2.0)	520.3(2.0)	464.1(2.4)	1.6
9.5	"	524.8(2.4)	517.4(2.2)	520.2(--)	464.2(2.6)	1.8
11.0	"	524.5(2.6)	517.1(1.9)	520.3(--)	464.1(2.9)	1.7
12.0	"	524.3(2.4)	517.3(1.9)	520.1(--)	464.3(2.5)	1.6
3.2	powd.,not calc.	523.9(1.6)	517.5(2.7)	519.9(1.6)	464.1(2.5)	1.6
7.0	"	524.2(2.2)	517.4(2.1)	520.3(2.1)	464.2(3.0)	2.0
TiO_2†c				519.9(1.9)	464.3(2.6)	458.4(1.5)
V_2O_5†c		524.5(2.7)	517.2(1.9)	520.2(--)		

FWHM = Full width at half of the maximum height;
a = Oxygen satellite;
b = Binding energies of the catalysts were determined by referencing to the Ti $2p_{3/2}$ line at 458.5 eV;
c = Binding energies of the standard compounds were determined by referencing to the C 1s line at 284.6 eV.

4.2.4.3.2 Decomposition of isopropanol

Only the VO_x/TiO_2(P-25) monolayer catalyst containing 4% V_2O_5 was tested in this reaction. It shows conversion, S_{ac} and S_{pr}% results at 220°C similar to the results of the VO_x/TiO_2(P-25) monolayer catalyst prepared by the $VOCl_3$ method (see Figure 4.61, Section 4.2.4.2.2). Similar results were found for both monolayer catalysts in the case of r_t, r_{ac} and r_{pr} at 220°C (see Figure 4.62, Section 4.2.4.2.2). Figure 4.71 shows the plots of ln(r_t, r_{ac} and r_{pr}) versus 1/T for the same monolayer catalyst, giving the E_t, E_{ac} and E_{pr}. Table 4.15 shows their values and the corresponding values of lnA. The apparent activation energies (E_t, E_{ac} and E_{pr}) for this catalyst are similar to those of VO_x/TiO_2(P-25) monolayer catalyst prepared by the $VOCl_3$ method (see Figure 4.64, Section 4.2.4.2.2).

Table 4.15

Arrhenius parameters for VO_x/TiO_2(P-25) monolayer catalyst prepared by $VO(O^iBu)_3$ method in the catalytic decomposition of isopropanol.

E_t[1]	lnA[2]	c.c.	E_{ac}[1]	lnA[2]	c.c.	E_{pr}[1]	lnA[2]	c.c.
24.7	7.57	0.993	16.3	5.22	0.987	42.2	10.73	0.997

1 = E/ kJ mol^{-1};

2 = ln(A/mmol h^{-1} $\bar{g}^{-1}$-cat.).

4.2.5 VO_x/TiO_2(Eurotitania) catalysts

The TiO_2(Eurotitania) used as a support has the anatase

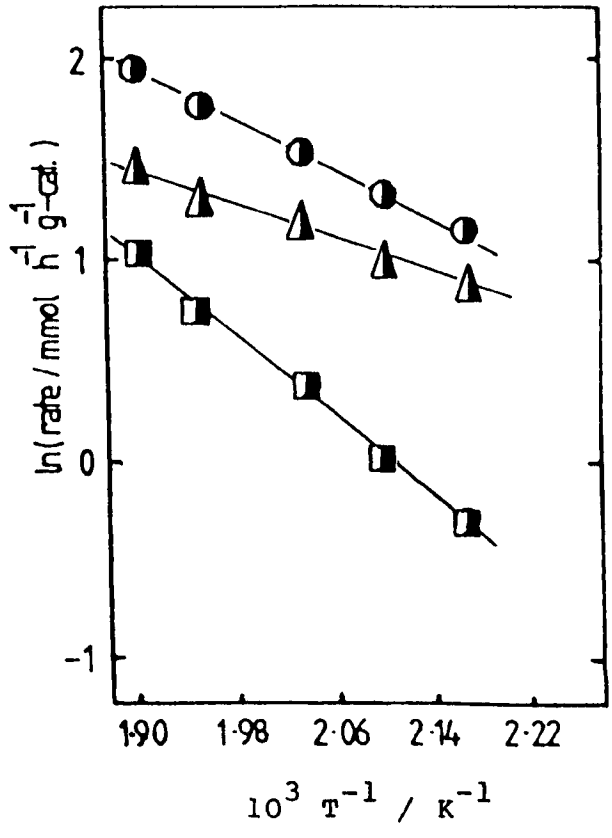

Figure 4.71 Ln(rate/r_t(◑), r_{ac}(◭) and r_{pr}(◧)) versus 1/T for the monolayer catalyst containing 4% V_2O_5 catalyzed the decomposition of isopropanol (this catalyst used in Figure 4.61).

phase, with a surface area of 45.5 m^2g^{-1} (see Table 3.1, Chapter 3).

4.2.5.1 Catalysts prepared by the $VO(O^iBu)_3$ method

The VO_x/TiO_2(Eurotitania) catalysts were prepared by this method as described in Section 3.5.3 of Chapter 3, and contained 2.2 - 19.2 wt.% V_2O_5.

4.2.5.1.1 Characterisation

TPR

Figure 4.72 shows the TPR profiles for these catalysts consist of only one peak. The value of T_{max} increases linearly with V_2O_5 content as shown in Figure 4.73. The values of the quantity of H_2 consumed (Figure 4.74) correspond to that required for reduction of V(V) to V(III).

Laser Raman spectroscopy

No satisfactory laser Raman spectra could be obtained because of their dark colour.

XPS

Figure 4.75 shows the XP spectra for the same series of catalysts, for the TiO_2 and for pure V_2O_5. The binding energies of the V $2p_{1/2}$ and V $2p_{3/2}$ levels in all samples are 524.1 $\pm$ 0.2 and 517.0 $\pm$ 0.25 eV (Table 4.16). These results indicate the presence of V(V) in the calcined samples. Figure 4.76 shows that the average $\bar{R}_{3,4}$ continues to increase significantly after the monolayer point is passed (4.4% V_2O_5).

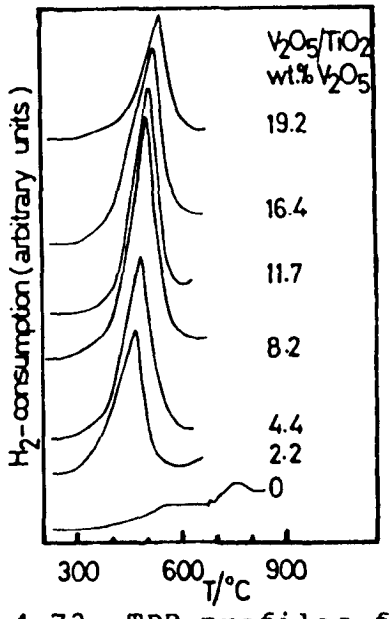

Figure 4.72 TPR profiles for catalysts prepared by treatment of TiO_2(Eurotitania) with $VO(O^iBu)3$, and for the support. The wt.% V_2O_5 is given for each curve.

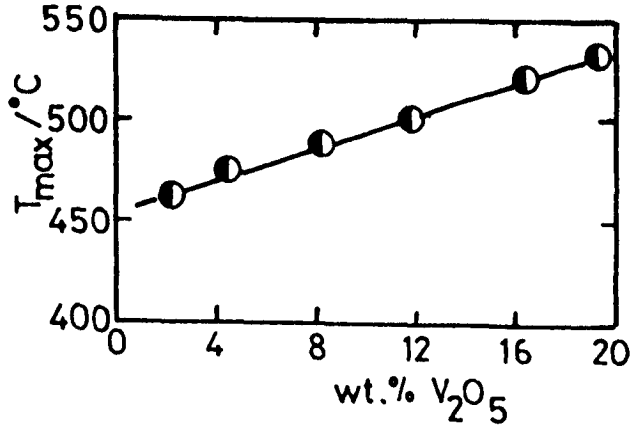

Figure 4.73 Dependence of T_{max} on V_2O_5 content for the catalysts shown in Figure 4.72.

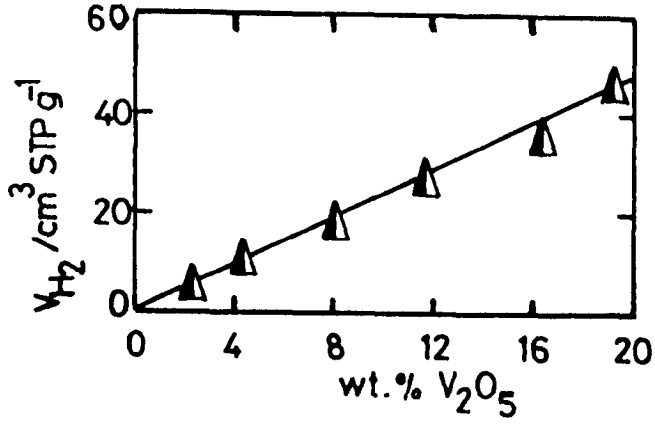

Figure 4.74 Dependence of volume of H_2 consumed in TPR on V_2O_5 content for the catalysts shown in Figure 4.72.

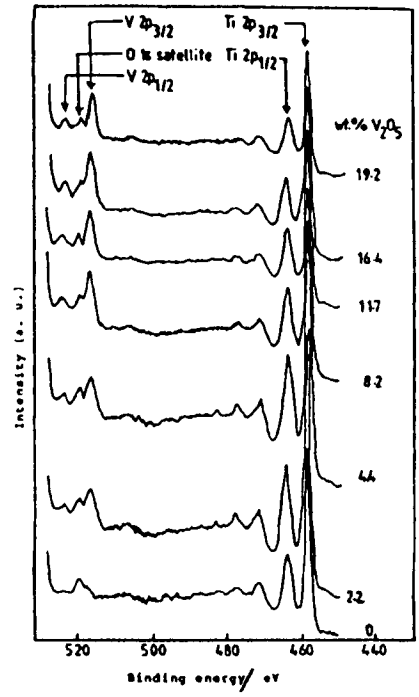

Figure 4.75 XPS spectra of catalysts prepared by treatment TiO_2(Eurotitania) with $VO(O^iBu)_3$, and for the support. The wt.% V_2O_5 is given for each curve.

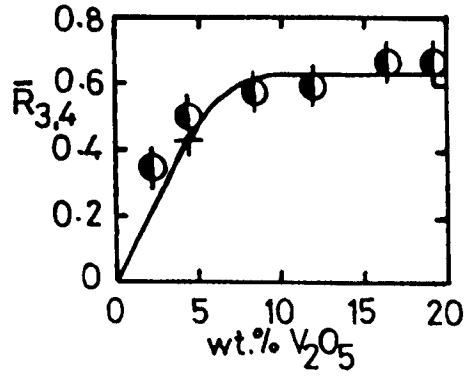

Figure 4.76 Dependence of V/Ti ratio $\bar{R}_{3,4}$(●) on %V_2O_5 for the catalysts depicted in Figure 4.75. The curve is that calculated for $f_1 = f_2 = 0.3$, $x = 0.125$; $\bar{R}_{3,4}$ taken as 0.425 at the one monolayer point.

Table 4.16

XPS results of VO_x/TiO_2(Eurotitania) catalysts prepared by the $VO(O^iBu)_3$ method, TiO_2 and unsupported V_2O_5.

wt.% V_2O_5	sample preparation	Binding energy (FWHM) V $2p_{1/2}$	V $2p_{3/2}$	O 1s[a]	Ti $2p_{1/2}$	FWHM(eV)[b] Ti $2p_{3/2}$
2.2	powd.,calcined	524.0(2.0)	517.3(3.0)	520.1(2.4)	464.3(2.9)	2.0
4.4	"	524.2(1.9)	517.3(2.3)	520.2(1.8)	464.1(2.6)	1.6
8.2	"	524.4(2.0)	517.2(2.6)	520.1(--)	464.2(2.6)	2.0
11.7	"	524.1(2.4)	516.7(2.2)	519.8(1.9)	464.1(2.6)	1.7
16.4	"	523.9(2.0)	516.9(2.2)	519.9(--)	464.1(2.6)	1.8
19.2	"	524.1(2.4)	517.0(1.9)	520.3(--)	464.1(2.6)	1.7
TiO_2↑c				519.9(1.9)	464.3(2.6)	458.4(1.5)
V_2O_5↑c		524.5(2.7)	517.2(1.9)	520.2(--)		

FWHM = Full width at half of the maximum height;
a = Oxygen satellite;
b = Binding energies of the catalysts were determined by referencing to the Ti $2p_{3/2}$ line at 458.5 eV;
c = Binding energies of the standard compounds were determined by referencing to the C 1s line at 284.6 eV.

4.2.5.1.2 Oxidation of 1,3-butadiene

The catalytic measurements for these catalysts were carried out between 241 and 356°C. In Figure 4.77, the conversions, S_{MA} and S_{CO_x}% measured at 290°C, are plotted against the V_2O_5 content. The conversion of 1,3-butadiene falls with V_2O_5 content (up to 12.5% V_2O_5) and remains unchanged with a further increase in content of V_2O_5. The value of S_{MA} is about 35% and remains constant with V_2O_5. The value of S_{CO_x} is higher than S_{MA}. Similar results were found at 280 and 300°C. Figure 4.78 shows r_B, r_{MA} and r_{CO_x} at 290°C plotted as a function of the V_2O_5 content. The values of r_B and r_{CO_x} fall sharply with V_2O_5 content, passing through minima in the 12.5 - 15.0% V_2O_5 region, then increase. The value of r_{MA} falls gradually with V_2O_5 content, passing through a minimum in the 10 - 15% V_2O_5, then increases gradually. The rates at low V_2O_5 content are higher than the rates at high V_2O_5 content.

Figure 4.79 shows the plots of $\ln(r_B, r_{MA}$ and $r_{CO_x})$ versus 1/T for the catalyst containing 4.4% V_2O_5, giving the E_B, E_{MA} and E_{CO_x}. These were measured at conversions up to 30%. Table 4.17 shows the values of the E_B, E_{MA} and E_{CO_x} and the corresponding values of lnA for the catalysts which were shown in Figure 4.77. Figure 4.80 shows the values of E_B, E_{MA} and E_{CO_x} (Table 4.17) as a function of the V_2O_5 content. The values of E_B, E_{MA} and E_{CO_x} increase with V_2O_5 content passing through maxima at 8.2% V_2O_5 then decrease. The value of E_{MA} is higher than E_B and E_{CO_x}.

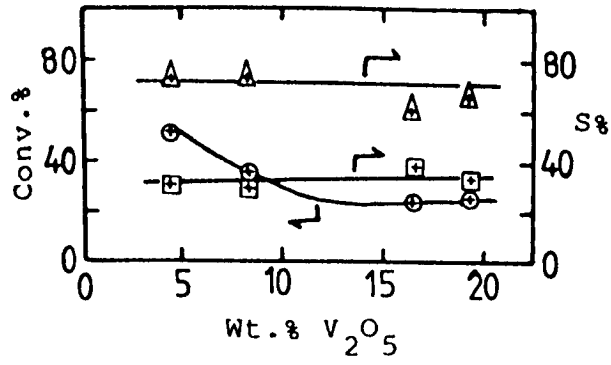

Figure 4.77 Oxidation of 1,3-butadiene on VO_x/TiO_2(Eurotitania) catalysts at 290°C as a function of V_2O_5 content: ⊕, butadiene conversion; ⊞, S_{MA}; ⧋, S_{CO_x}.

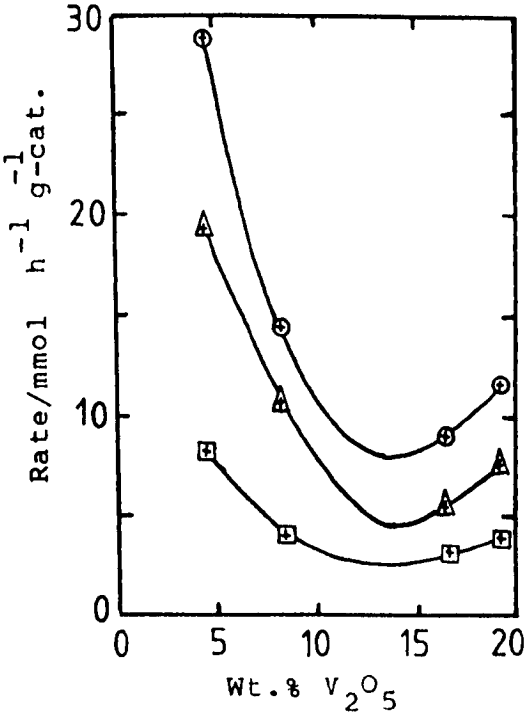

Figure 4.78 The rates for the oxidation of 1,3-butadiene (r_B, r_{MA} and r_{CO_x}) at 290°C as a function of the V_2O_5 content.

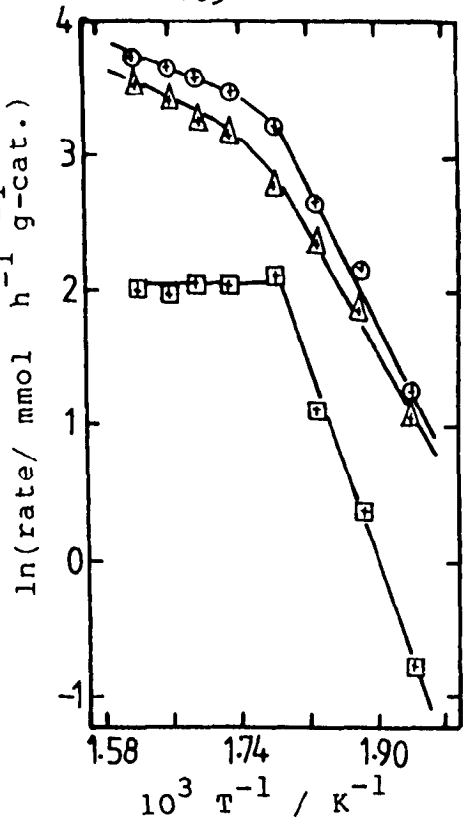

Figure 4.79 Ln(rate) versus 1/T for the catalyst containing 4.4% V_2O_5 catalyzed the oxidation of 1,3-butadiene (this catalyst used in Figure 4.77).

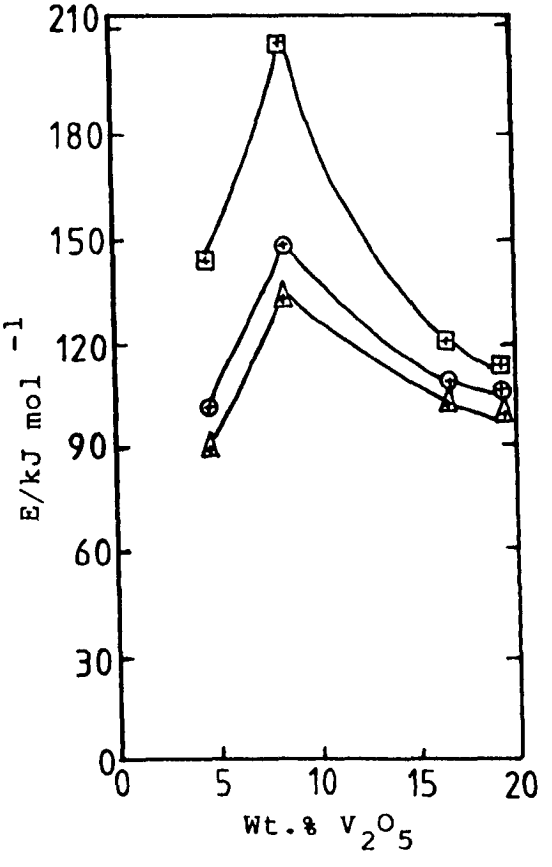

Figure 4.80 E_B(⊕), E_{MA}(⊞) and E_{CO_x} (⧋) as a function of V_2O_5 content for samples shown in Figure 4.77.

Table 4.17

The Arrhenius parameters of VO_x/TiO_2(Eurotitania) catalysts, prepared by the $VO(O^iBu)_3$ method, catalyzed oxidation of 1,3-butadiene.

Wt.% V_2O_5	E_B[1]	$\ln A$[2]	c.c.	E_{MA}[1]	$\ln A$[2]	c.c.	E_{CO_x}[1]	$\ln A$[2]	c.c.
4.4	99.1	24.5	0.994	140.5	32.1	0.997	90.8	22.5	0.992
8.2	144.7	33.6	0.99	201.2	44.3	0.98	120.9	30.4	0.991
16.4	106.7	25.0	0.985	115.9	26.1	0.954	102.5	23.7	0.996
19.2	103.7	24.6	0.979	111.3	25.2	0.917	97.9	22.9	0.989

1 = E/kJ mol^{-1};

2 = ln(A/mmol h^{-1} g^{-1}cat.).

4.2.6 VO_x/TiO_2(CLD 1117/2, anatase, 48.5 m^2g^{-1})

TiO_2(CLD 1117/2,unwashed) was used as a support in these catalysts; it contained P_2O_5, K_2O and SO_3 as impurities (see Table 3.1, Chapter 3). The same support, washed with water as described in Section 3.4.1, Chapter 3, was used as a support in this preparation. The amount of P_2O_5 and K_2O impurities was reduced after washing (Table 3.1, Chapter 3), while the amount of the $SO_4^=$ may decrease slightly.

4.2.6.1 Catalysts prepared by the $VOCl_3$ method

VO_x/TiO_2(unwashed) monolayer catalyst and a series of VO_x/TiO_2(washed) catalysts containing 4.2 - 12.4 wt.% V_2O_5 were prepared as described in Section 3.5.2 of Chapter 3.

4.2.6.1.1 Characterisation

TPR

The TPR profiles for the TiO_2(unwashed) and VO_x/TiO_2(unwashed) monolayer catalyst (5.4% V_2O_5) are shown in Figure 4.81. The TiO_2 profile (Figure 4.81a) shows three peaks at higher temperatures with T_{max} 625, 650 and 670°C; these may be due to reduction of the $SO_4^=$ impurity forming H_2S as a product (by testing the outlet gases from the reactor during the TPR, lead acetate paper changed from white to black(PbS), signifying the presence of S in the TiO_2 sample). The TPR profile (Figure 4.81b) is for TiO_2 after oxidation at 450°C with air (2h) of the sample reduced in Figure 4.81a. It shows no peak which means that all the $SO_4^=$ was reduced in the first TPR(Figure 4.81a). The profile of the VO_x/TiO_2(unwashed) monolayer catalyst (Figure 4.81c) shows just one peak with T_{max} = 480°C. The value of the volume of H_2 consumed is higher than that expected to reduce V(V) to V(III) (i.e. 21.2 cm^3 H_2/g-cat. instead of 13.3 cm^3 H_2/g-cat.). This higher value of H_2 may due to the reduction of V(V) to V(III) and $SO_4^=$ to H_2S together.

Figure 4.82 shows the TPR profile for the fresh monolayer catalyst(Figure 4.82a) (the same catalyst as in Figure 4.81c) and the TPR profile(Figure 4.82b) is for the catalyst after oxidation at 450°C with air (2h) of the catalyst sample reduced in Figure 4.82a. The TPR profiles in Figure 4.82 show just one peak with the same T_{max} = 480°C. The quantity of H_2 consumed in case of (b) is equivalent to that expected to reduce V(V) to V(III) (i.e. 2 mol H_2/mol V_2O_5, which means that the whole $SO_4^=$ may be removed from the catalyst after the first reduction). The reduction of the

VO_x/TiO_2 catalyst may also catalyse the reduction of the $SO_4^=$ impurity in the same range of temperature, and therefore only one peak is shown.

Figure 4.83 shows the TPR profiles for the VO_x/TiO_2(washed) catalysts containing 4.2 - 12.4% V_2O_5 and for the TiO_2(washed). The support profile shows three peaks with T_{max} 495, 563 and 611°C due to the reduction of $SO_4^=$ impurity giving H_2S as product. The TPR profiles for the catalysts give only one peak. The value of T_{max} for the VO_x/TiO_2(washed) monolayer catalyst (4.2% V_2O_5) is similar to that for VO_x/TiO_2(unwashed) monolayer catalyst (see Figure 4.81). The value of T_{max} increases with V_2O_5 content (Figure 4.84). The values of the volume of H_2 consumed are higher than that expected for reduction of V(V) to V(III) (Figure 4.85). This may also be due to the reduction of $V(V)O_x$ and $SO_4^=$ together.

4.2.6.2 Catalysts prepared by the $VO(O^iBu)_3$ method

The VO_x/TiO_2(unwashed) and VO_x/TiO_2(washed) monolayer catalysts were prepared by this method as described in Section 3.5.3 of Chapter 3, and contained 4.8 and 5.1 wt.% V_2O_5 respectively.

4.2.6.2.1 Characterisation

TPR

Figure 4.86 shows the TPR profiles (a) for VO_x/TiO_2(unwashed) and (b) for VO_x/TiO_2(washed) monolayer catalysts. The profiles show only one peak with the same T_{max}, 477°C. The quantity of H_2 consumed was higher than that expected to reduction V(V) to V(III) (i.e. (18.7 -

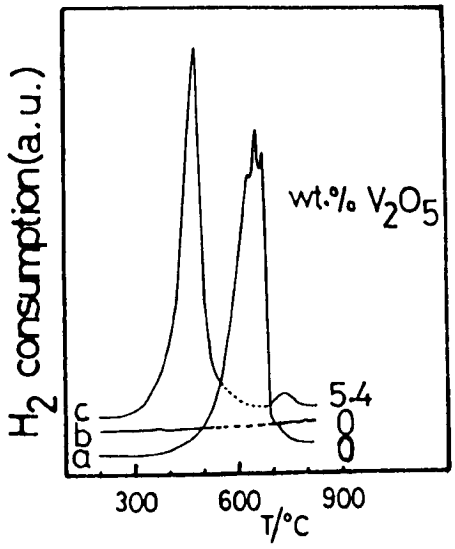

Figure 4.81 TPR profiles for: (a) the fresh TiO_2(unwashed, anatase, 48.5 m^2g^{-1}); (b) the oxidized sample at 450°C with air (2h) of the sample reduced in (a); (c) VO_x/TiO_2 monolayer catalyst.

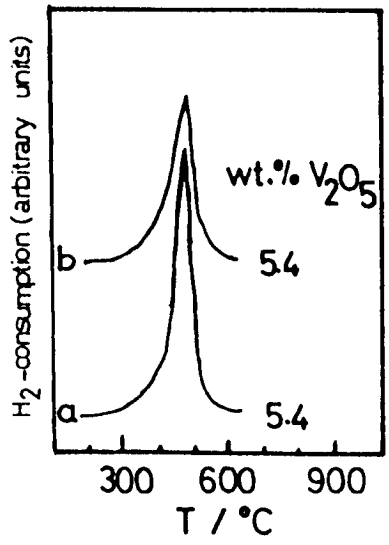

Figure 4.82 TPR profiles for: (a) VO_x/TiO_2 monolayer catalyst which is shown also in Figure 4.81; (b) the oxidized sample at 450°C with air (2h) of the sample reduced in (a).

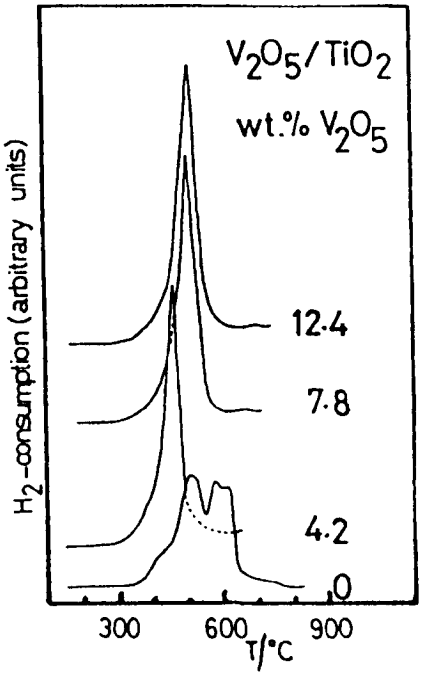

Figure 4.83 TPR profiles for VO_x/TiO_2(washed, anatase, 48.5 m^2g^{-1}) catalysts prepared by the $VOCl_3$ method and for the support. The wt.% V_2O_5 is given for each curve.

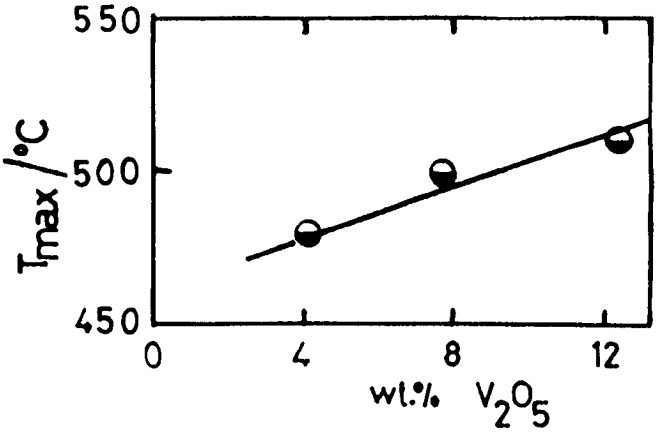

Figure 4.84 Dependence of T_{max} on V_2O_5 content for catalysts shown in Figure 4.83.

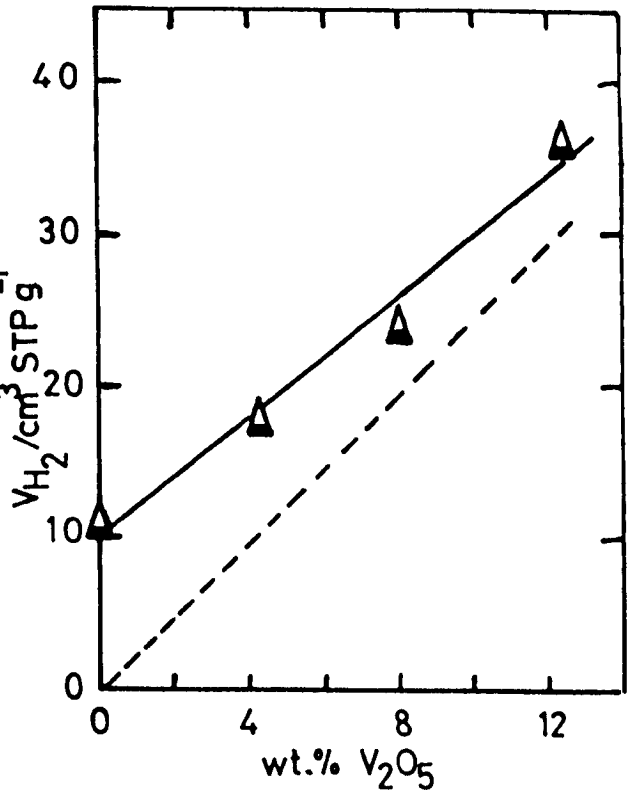

Figure 4.85 Volume of H_2 consumed in TPR as a function of V_2O_5 content for catalysts shown in Figure 4.83. The broken line represents the theoretical value of H_2 consumed.

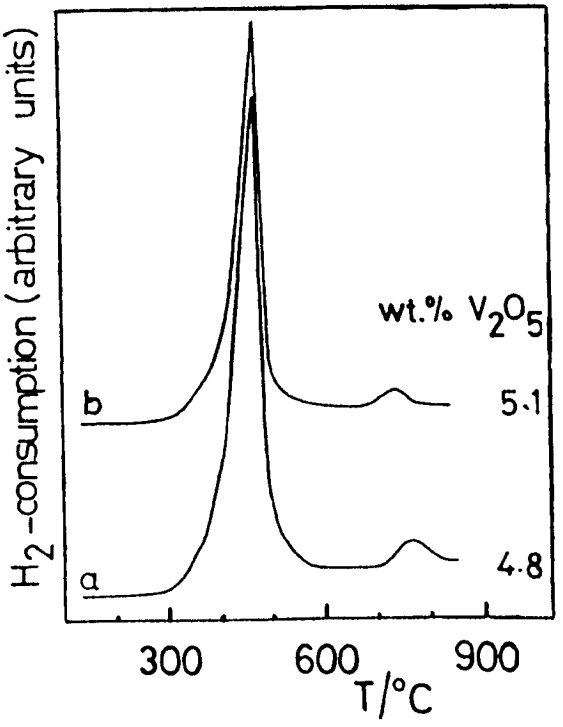

Figure 4.86 TPR profiles for monolayer catalysts made by $VO(O^iBu)_3$ method using TiO2(CLD 1117/2, anatase as a support: (a) VO_x/TiO_2 (unwashed); (b) VO_x/TiO_2(washed). The wt.% V_2O_5 is given for each curve.

19.5) cm^3 H_2/g-cat. instead of (11.8 - 12.5) cm^3 H_2/g-cat.). This may due to the reduction of the $V(V)O_X$ and SO_3 together. Similar results were found for the VO_X/TiO_2 monolayer catalysts which were prepared by the $VOCl_3$ method (Section 4.2.6.1.1).

4.3 Discussion

Effects of modification (P and K impurities and crystal Structure) of the TiO_2 support on the structures of VO_X phases:

On the basis of the above-mentioned results (Section 4.2), different surface structures of VO_X phases are formed at various V_2O_5 contents when different TiO_2 supports are used.

The above results show that P and K impurities and the crystal structure of the TiO_2 have a large influence on the reducibility and the catalytic properties of the VO_X phases.

So, to determine the structures of the VO_X phases, the supports should be divided into two groups (according to the presence or absence of the P and K impurities). The TiO_2(P-25) is included in the group with low impurities. The first group (G1) will consist of the supports with low levels of impurities (P and K) such as anatase (washed,low area), anatase (unwashed,high area), anatase (washed,high area), pure anatase (Eurotitania) and P-25 (see Table 3.1, Chapter 3). The second group (G2) will consist of the supports having relatively high levels of impurities such as anatase (unwashed, low area)(see Table 3.1, Chapter 3). The effect of impurities in (or on) the TiO_2 on the structures and properties of VO_X can now be discussed.

Structures of VO_x/TiO_2 catalysts

The structures of calcined VO_x/TiO_2 catalysts having various V_2O_5 contents and obtained by using the two groups of TiO_2 supports are postulated to be as shown in Figure 4.87. Here, (a) refers to the VO_x monolayer; (b) to the two-four monolayer range and (c) to the range above four monolayers. From the results mentioned above (Section 4.2), the structures of the VO_x phases in (a) and (b) with G1 supports are different from (a) and (b) with G2 supports. This difference may be due to the effect of P and K impurities. The proposed model for VO_x/TiO_2 catalysts agrees with the experimental results and the conclusions are as follows:

(a) VO_x/TiO_2 (up to one VO_x monolayer)

The TPR results for the monolayer catalysts prepared by the three different methods and by using different supports show only a single peak. Similar results were observed for VO_x/TiO_2 monolayer catalysts prepared by the $VO(acac)_2$ method (9). The monolayer catalysts with G1 supports show similar values of T_{max} except for P-25 (see Table 4.18). This difference in T_{max} may find its origin in the detailed structures of the support surfaces. Residual traces of P and K on the surface of washed supports may account for the higher values of T_{max}, in comparsion with the lower values on P-25 where these impurities are absent. In the case of P-25, it is possible that rutile exists as a surface coating over an anatase core. The monolayer catalysts with the G2 supports (unwashed anatase) show higher T_{max} values than those with G1 supports (see Table 4.18). This may be due to

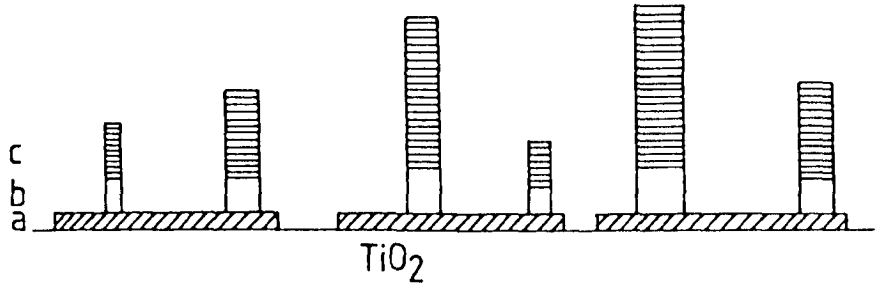

Figure 4.87 Model of V_2O_5 on TiO_2 showing the different phases which are formed as a function of V_2O_5:

a) up to one monolayer (surface VO_x complexes);

b) two - four monolayers (disordered vanadium oxide); and

c) above four monolayers (paracrystalline V_2O_5).

the effect of impurities, especially K, which may form a potassium salt with part of the VO_x phase. It is concluded from these results (Table 4.18) that the monolayer catalysts prepared by different methods using the same support give similar T_{max} values. This shows that the reducibility of VO_x species is more determined by the support than by the preparation method.

Table 4.18

T_{max} values for the monolayer catalysts prepared by different methods and by using different supports.

support	method	wt.% V_2O_5	T_{max}/°C
Anatase (washed, low area)	Impregn.	0.9*	476
"	$VOCl_3$	0.8	473
"	$VO(O^iBu)_3$	0.8	475
Anatase (unwashed,low area)	Impregn.	0.9*	530
"	$VOCl_3$	0.9	503
"	$VO(O^iBu)_3$	0.8	505
Anatase (unwashed,high area)	$VOCl_3$	5.4	480
"	$VO(O^iBu)_3$	5.1	477
Anatase (washed, high area)	$VOCl_3$	4.2	478
"	$VO(O^iBu)_3$	4.8	477
Pure anatase (Eurotitania)	$VO(O^iBu)_3$	4.4	465
Degussa P-25	Impregn.	4.0*	455
"	$VOCl_3$	4.0	450
"	$VO(O^iBu)_3$	4.0	450

* The catalysts prepared by the impregnation method contain wt.% V_2O_5 equivalent to monolayer loading.

For all catalysts on G1 supports, except anatase high area washed and unwashed, and on the G2 support, the total H_2 consumption conforms closely to that expected for the reduction of V(V) to V(III) (9,10). With the high area unwashed and washed supports, the situation is a little more complicated (Figure 4.81): due to the presence of the $SO_4^=$ impurity, the V_{H_2} consumed is due to reduction of the $SO_4^=$ as well as the VO_X species. The latter catalyse the reduction of $SO_4^=$ and the peaks of the two reduction processes overlap. The V_{H_2} consumed for the catalyst after reoxidizing the reduced catalyst corresponds to that for the reduction V(V) to V(III) (Figure 4.82).

Concerning the species present in the monolayer, a detailed EXAFS study (11) has concluded that they are dioxovanadium species linked to the surface by two bridging oxygens (structure A), and arranged in a disordered fashion. Haber (12) also has suggested the same structure (A) on the (010) surface:

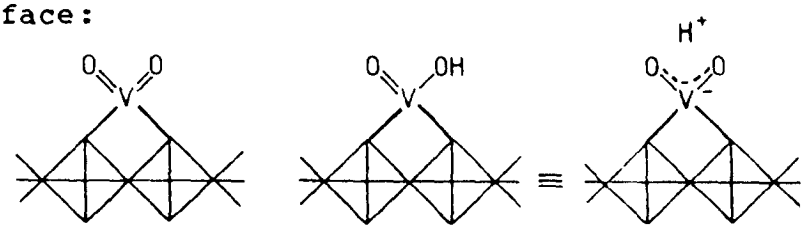

This representation is however inadequate on several grounds. The V=O bond order cannot be as high as two, and is more probably about 1.5 (11); the structure does not have the facility to react with further V precursor to form a second layer, nor does it explain the observation of increased Lewis acidity (13). For these reasons the oxohydroxy formulation (B) is more realistic or a structure (C) in which the electrons are delocalised. This may also

explain the absence of the 995 cm^{-1} band below the monolayer point (Figures 4.31 and 4.33). Recently Kijenski et al. (14) concluded that the surface vanadia species which were obtained by reaction of an organic solution of $VO(O^{i}Bu)_3$ with the surface hydroxyl groups have a structure similar to structure (B).

The EXAFS measurements were performed with a very high area ($\sim$180 m^2g^{-1}) anatase, and from the calculation for monolayer loading, the materials used had coverages of 0.33 and 0.66 monolayer. It is therefore plausible that the VO_X groups were in the main isolated and randomly disposed on the surface.

FTIR spectra for VO_X/TiO_2(P-25) catalysts (Figure 4.55) show a band at 3400 cm^{-1}, due to physically adsorbed water because the experiments were done in air. As mentioned by Nakagawa et al. (15), the stretching frequency of V=O in the VO_X monolayer falls to 980 cm^{-1}. When crystalline V_2O_5 is present, a further band appears centred at 1020 cm^{-1}. According to these authors, the spectrum for the VO_X/TiO_2(P-25) monolayer sample (spectrum b, 4.0% V_2O_5 loading) did not show a band at 1020 cm^{-1}. This may be because the band due to V=O shifts to the lower position and is not observed due to strong TiO_2 lattice vibrations.

The band due to the first overtone of the V=O stretching vibration is missing in the monolayer spectrum (Figure 4.55b): this may help in considering the results found by Busca et al. (16,17). More work needs to be done in this field to get more information about the structure of the VO_X species especially under vacuum and high temperature conditions (e.g., up to 400°C) and to detect the position of

V-OH groups. The literature states that the position of the V-OH vibration frequency is at 3650 cm^{-1} (16,18,19).

The ESR spectrum of the VO_X/TiO_2(P-25) monolayer catalyst (Figure 4.56b) suggests that the V species on the TiO_2 support surface is V(V) with only about 5% being in the reduced form, V(IV). The V(IV) ions may be in the form of VO^{2+}. In recent ESR studies of V_2O_5/TiO_2 catalysts calcined at 500°C, Inomata et al. (13) concluded that the amounts of V(IV) formed were negligible. The structure of VO_X monolayer species supported on the G2 support (unwashed, low area) may be different from that on G1 supports. P and K impurities present in the TiO_2 surface prevent the formation of ideal monolayer structures.

K may react with part of VO_X species and form potassium-containing vanadium oxide and the structure can be represented as in D

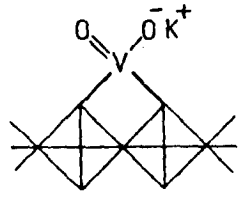

(D)

Andersson (20) studied the structures of supported V_2O_5 catalysts by using different types of TiO_2. His TiO_2 contained P and K as impurities which were mainly confined to the surface. He concluded that the K reacts with vanadia forming potassium vanadate crystallites.

In the case of P, the TiO_2 with a high surface concentration of P may show that part of it is present as a surface-bonded phosphate. The possibility then occurs that some VO_X species will be bonded on top of the phosphate species. The other possibility is that some of the PO_X may

be incorporated in the VO_X monolayer forming the structure represented in E. The formation of this type of mixed monolayer (E) is to be expected from the fact that the chemistries of V and P are very similar (8).

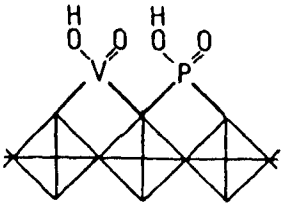

(E)

Andersson (20) suggested in the case of P, that VO_X on such a surface is bonded by V-O-Ti as well as by V-O-P bonds to extents dependent on the free TiO_2 and the phosphate covered surface, respectively. XPS results for the VO_X/TiO_2 samples revealed that the VO_X monolayer species are present as V(V) in the calcined samples (Tables 4.3,4.8,4.11,4.12,4.14 and 4.16). The results show that the V/Ti ratio increases with V_2O_5 content up to the monolayer. More discussion on XPS will be considered further below in this Section.

(b) VO_X/TiO_2 (two-four monolayers)

In this region, the VO_X catalysts supported on G1 supports show only a single peak in TPR, the value of T_{max} increasing with V_2O_5 content (Figures 4.29,4.46,4.53,4.66, 4.73 and 4.84): on the high area supports, the rates of increase are similar for all preparative methods.

With VO_X catalysts supported on the G2 support (unwashed, low area), T_{max} shows a complex dependence on V_2O_5 content in the two to four momolayer region compared to the washed support (see Figure 4.29) and all values exceed 505°C. For

all catalysts on low area anatase, the total V_{H_2} conforms closely to that expected for the reduction of V(V) to V(III). With high area supports, the situation is a little more complicated (see next Section).

On selected parts of the monolayer surface, structures such as (B) react with further vanadium precursor to form this second phase growing away from the surface.

In the case of G1 supports, the VO_X phase formed is described as "disordered vanadium oxide". This phase has the same reducibility as the monolayer species but is characterised by the appearance of the 995 cm^{-1} Raman band due to the V=O····V vibration. This suggests that the general class of structure present in the first monolayer continues to be found as the V_2O_5 content increases up to the equivalent of about four monolayers, and that this contains V=O····V.

FTIR results for VO_X/TiO_2(P-25) in the same region also show the band at 1020 cm^{-1} due to the V=O····V stretching vibration starting at the second monolayer and increasing with V_2O_5 content (Figure 4.55). The ESR spectrum (Figure 4.56c) shows that the amount of V(IV) in the VO_X/TiO_2(P-25) catalyst containing 13% V_2O_5 may be more than 5% because the spectrum is broad compared to that of the monolayer catalyst (Figure 4.56b).

In the case of the G2 support (unwashed, low area), the vanadium oxide constituting the two - four monolayer range does not form the same "disordered vanadium oxide" as is observed for catalysts made with G1 supports. It reacts with selected parts of the monolayer surface forming another type of potassium-containing vanadium oxide with high

reducibility and not detectable with laser Raman spectroscopy (Figures 4.5 and 4.7).

XPS results for the catalysts supported on both supports are similar and show that the V in this region is present as V(V) (Table 4.3,4.8,4.11,4.12,4.14 and 4.16). The XPS results show that the V/Ti ratio does not continue to increase as the V_2O_5 content is increased beyond the monolayer point. This suggests that, after completion of the first monolayer, the second phase (in the case of both groups of supports) forms blocks which grow into towers covering only a limited part of the monolayer surface. Further quantitative discussion on the XPS results will given below, and this will provide further support for the proposed model (Figure 4.87).

(c) VO_X/TiO_2 (above four monolayer)

TPR results show with unwashed and washed (anatase, low area) and P-25 supports, a second higher temperature peak which is apparent when more than the equivalent of about four monolayers of VO_X are present (Figure 4.5,4.29 and 4.45) on catalysts prepared by wet impregnation. Above the four monolayers point, T_{max} for the first peak ceases to increase (Figures 4.5 and 4.29) and its size remains about constant (Figures 4.6 and 4.30); T_{max} for the second peak however continues to increase. The values of T_{max} for both peaks in case of unwashed (anatase, low area) are higher than those for the washed support above four monolayers loading (Figure 4.29). This may also show the influence of P and K impurities on the reducibility even at high V_2O_5 content. Raman results still show the 995 cm^{-1} band for

catalysts made with washed supports (Figure 4.31). Raman results for catalysts made with the unwashed support show the 995 cm^{-1} band above four monolayers and its intensity increases with V_2O_5 content (Figure 4.7 and 4.9). The total V_{H_2} conforms closely to that expected for reduction of V(V) to V(III) (Figures 4.6 and 4.30). With the high area supports, the situation is a little more complicated (Figures 4.47 and 4.67): catalysts made by aqueous impregnation or by the $VO(O^iBu)_3$ method on P-25 show consistently low values of V_{H_2}, corresponding to a final oxidation of about $V_2O_{3.3}$. VO_X catalysts on high area washed anatase prepared by the $VOCl_3$ method show that due to the presence of the $SO_4^=$ impurity, V_{H_2} consumed is due to the reduction of the $SO_4^=$ as well as the VO_X species (Figure 4.85).

The TPR and Raman spectroscopy results show that above four monolayers, the amount of the "second phase" ceases to increase and is replaced by a third phase (c) described as "paracrystalline V_2O_5". It is clearly not the same as normal bulk V_2O_5 in that it is more easily reduced (Figures 4.5 and 4.29). This phase is formed by extension of the columns of the second phase (see Figure 4.87b), and it ultimately leads to the very thin acicular crystals observed (21,22) by electron microscopy growing away from the TiO_2 surface. These crystals will expose chiefly the ac and bc planes, growth occuring in the c direction. Their greater reducibility may be explained by the ease of extraction of O atoms through the a and b planes, with the formation of shear structures (12,23). Wachs et al. (3) concluded that in the V_2O_5/TiO_2(anatase) system, above the monolayer loading ,

both surface vanadia species and crystalline V_2O_5 are formed. Both states of vanadia reduce more readily than unsupported V_2O_5. Similar observations were also made by Roozeboom et al. (1) for vanadia supported on other oxides (Al_2O_3 and SiO_2).

This model is an advance upon that proposed recently by Wachs et al. (3,24), giving a more precise description of possible surface structures. It differs considerably from that of Inomata et al. (13) who clearly believe that it is possible to form a large number of V_2O_5 lamella parallel to the surface, with some minor variation in thickness.

XPS results show that the V/Ti intensity ratio for catalysts containing the more than four monolayers "third phase" is similar to that range between the two and four monolayers "second phase". This observation supports the suggested model which proposes that, after completion of the first monolayer, some kind of VO_x phase (or potassium-containing vanadium oxide, in the case of unwashed anatase, low area) forms blocks which grow into "disordered vanadium oxide" towers covering only a limited part of the monolayer surface (see Figure 4.87b). It is not expected that the XPS intensity measurements will discrimate between the second and the third phases.

Previous work on the MoO_3/Al_2O_3 system (25), as well as on the V_2O_5/TiO_2 system (26,27,28), has shown that the slope of the M/S versus (M) plot (M representing the element of the supported oxide and S that of the supporting oxide) often decreases at about the point at which a first complete monolayer might be formed, but little or detailed

consideration has been given to the implications. Reference is made to the formation of a less well-dispersed phase above the monolayer, e.g., " the appearance of multilayered V structures" (26) or " the partial occurence of vanadium oxides of low dispersion" (27). None of the published papers attempts the construction of a quantitative model to account for the observed results. In this work, a model in which, after completion of the first monolayer, some kind of vanadium oxide phase (or potassium-containing vanadium oxide in the case of unwashed anatase) forming blocks which grow into microcrystalline towers covering only a limited part of the monolayer appears to be a suitable basis for a quantitative interpretation of the results (see Figures 4.87 and 4.88). The inter-related variables of this model are the fraction of the surface covered by the "towers", the height of the towers (assuming that all the "towers" are of uniform height) and the number of monolayer equivalents to which the V_2O_5 concentration corresponds (see Appendix IV). The fundamental expression for the dependence of signal intensity I upon the depth at which the electron originates is

$$I = I_o \exp(-nd/\lambda)$$

for electrons emitted in a direction normal to the surface, λ being termed the escape depth (29) and d the thickness of a single layer of the oxide. Since this calculation is only concerned with the relative intensities,the value of I_o is

irrelevant, and so I(Ti) and I(V) are defined as the fractional intensities for each element, i.e., I/I_o (see Appendix IV).

Figure 4.89 shows how the calculated V/Ti intensity ratio varies with the number of monolayer equivalents as x is varied, taking f_1 and f_2 as both equal to $0.\dot{3}$. Clearly as x tends towards unity, the slope of the curve above the monolayer point increases until ultimately, when x is exactly unity, one has a uniform second and subsequent layers. As x tends to zero, the slope of the curve becomes less. It is a feature of the calculations that even for quite low values of x the intensity ratio continues to rise above the monolayer point, to an extent depending upon the value of x, before reaching a limited value. The extent to which the calculated intensity ratio increases between the one monolayer point and the limiting value is a useful parameter to assist with fitting the calculated curves to the experimental points. The fitting was done in the following way. The weight percentages equivalent to one monolayer have been taken as 0.9 for anatase (washed and unwashed, low area); 4.0 for P-25; and 4.4 for Eurotitania (see Chapter 3). Accepting these values, the calculated curve is adjusted to a value of $\bar{R}_{3,4}$ at the monolayer point giving the best fit through out the whole V_2O_5 concentration range. Figures 4.12,4.35,4.49,4.58,4.69 and 4.76 show curves calculated and fitted as described in the legends. With the catalysts prepared by wet impregnation (Figures 4.12,4.35 and 4.49), acceptable fits are obtained with x = 0.05, i.e., only 1/20th of the monolayer is covered by "towers". With

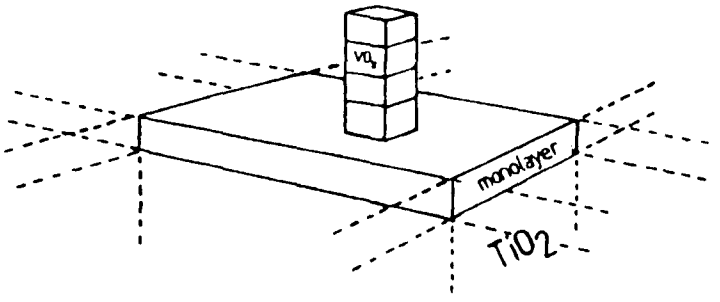

Figure 4.88 Illustration of a "tower" on top of the monolayer.

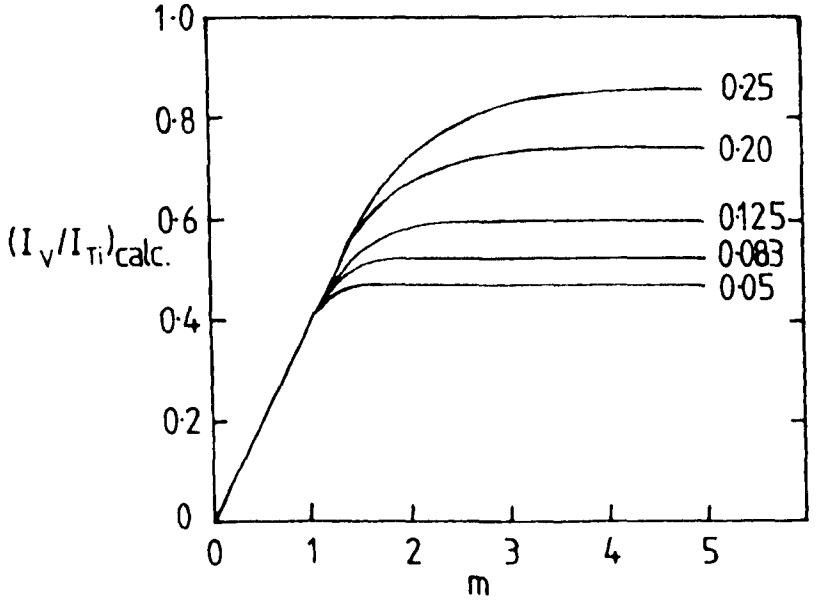

Figure 4.89 Dependence of the calculated intensity ratio on number of monolayer equivalents for $f_1 = f_2 = 0.\dot{3}$ and various values of x as shown.

those prepared by reaction of the support with the $VOCl_3$ or $VO(O^iBu)_3$, a value of x of 0.125 gives good fits (Figures 4.58,4.69 and 4.76). It would appear that the different preparative methods afford different dimensions of "towers" above the monolayer point.

Although the value for the f parameter was selected on the basis of reasonable estimates for d and λ as described above, the sensitivity of the calculated curves to the values of f_1 and f_2 used has also been examined also. Changing $f_{1,2}$ from 0.27 to 0.39 only alters the ratio of I_∞/I_m (i.e. the factor by which the intensity ratio increases from its value at one monolayer to the limiting value) from 1.60 to 1.44; it is 1.50 when $f_{1,2}$ is $0.\dot{3}$. This change corresponds to decreasing the escape depth λ from 1.85 to 1.28 nm. Similarly, altering f_1 and f_2 independently between 0.27 and 0.39 affords values of I_∞/I_m in the same range. The calculated curves are not therefore highly responsive to the values of f_1 and f_2 employed.

Two of the other assumptions have also been investigated. It is improbable that all of the "towers" will have the same height. The intensity ratio for m = 2 (x = 0.1, $f_{1,2} = 0.\dot{3}$) calculated assuming equal numbers of "towers" whose heights are in the ratio 1:2:3; the value obtained (0.538) is very close to that found (0.545) when all "towers" were taken as of equal height. Finally, the projected dimensions of the "towers" are unlikely to be uniform. A trial calculation assuming one-half the surface has "large towers" (x = 0.2) and the other half has "small towers" (x = 0.1), the heights of which are such that the masses of V_2O_5 in the two parts

are the same, produced a curve of intermediate shape. However the introduction of too many disposable parameters having no experimental justification into such a simply-conceived calculation is unprofitable. The quality of the fits obtained with the experimental results suggests that the "towers" are of fairly similar cross cross-sectional area.

XPS results for the dried catalyst samples prepared by wet impregnation revealed that the vanadia is present as V(IV) (see Tables 4.3, 4.8 and 4.11). The V $2p_{3/2}$, O 1s satellite and Ti $2p_{1/2}$ binding energies for the dried VO_x/TiO_2 samples are presented in Tables 4.3, 4.8 and 4.11.

The V/Ti intensity ratios for the dried catalysts versus the V_2O_5 loading are reported in Figures 4.14, 4.37 and 4.51. The above Figures also include the results for calcined catalysts for comparison. A model which suggests for the dried catalyst depending on the V_2O_5 loading is shown in Figure 4.90 and can postulate a change in the structure of the catalyst upon calcination.

At low vanadyl oxalate concentrations (i.e., V_2O_5 contents up to 1 monolayer), two layers of vanadyl oxalate may be formed on the surface of the support as shown in Figure 4.90a. At intermediate vanadyl oxalate concentrations (i.e., V_2O_5 contents in the range of two to four monolayers), the V/Ti intensity ratio remains constant which suggests the formation of towers of vanadyl oxalate which cover only a limited number of vanadyl oxalate patches (Figure 4.90b). These towers have no effect on the V/Ti intensity ratio (see Figures 4.14, 4.37 and 4.51). At higher

vanadyl oxalate concentrations (i.e., at a V_2O_5 content of about five monolayers), the vanadyl oxalate may form on top of the oxalate groups which already cover the titania surface in the monolayer region. This may explain why the V/Ti intensity ratio finally increases, and show that the monolayer has been achieved. Above five monolayers V_2O_5 (above 3 monolayers in the case of P-25), the V/Ti intensity ratio remains constant, which may suggest that more towers grow (It may also be that some of the vanadyl oxalate increases the height of the previous towers which was already formed in the range of two to four monolayers) (Figure 4.90c). Saleh et al. (30) studied a 7 wt.% V_2O_5/TiO_2(anatase) by XPS over a range of temperatures. The initially high V/Ti ratio suggested that at 110-200°C several layers of vanadyl oxalate were present on the TiO_2(anatase) support. They also found that at 350°C the V/Ti ratio was significantly reduced because of the decomposition of vanadyl oxalate to form a vanadia phase which began to agglomerate and crystallize.

After calcination of the dried catalysts, the V/Ti intensity ratio increases by a factor of two in the region of two to five monolayers. At even higher loading, the V/Ti intensity ratio becomes constant nearly at the same level as in the case of the dried catalysts above five monolayers. These changes in the structure can be explained on the basis of the model suggested above (Figure 4.90)

In the case of the vanadyl oxalate loading which is equivalent to the monolayer coverage (Figure 4.90a), the

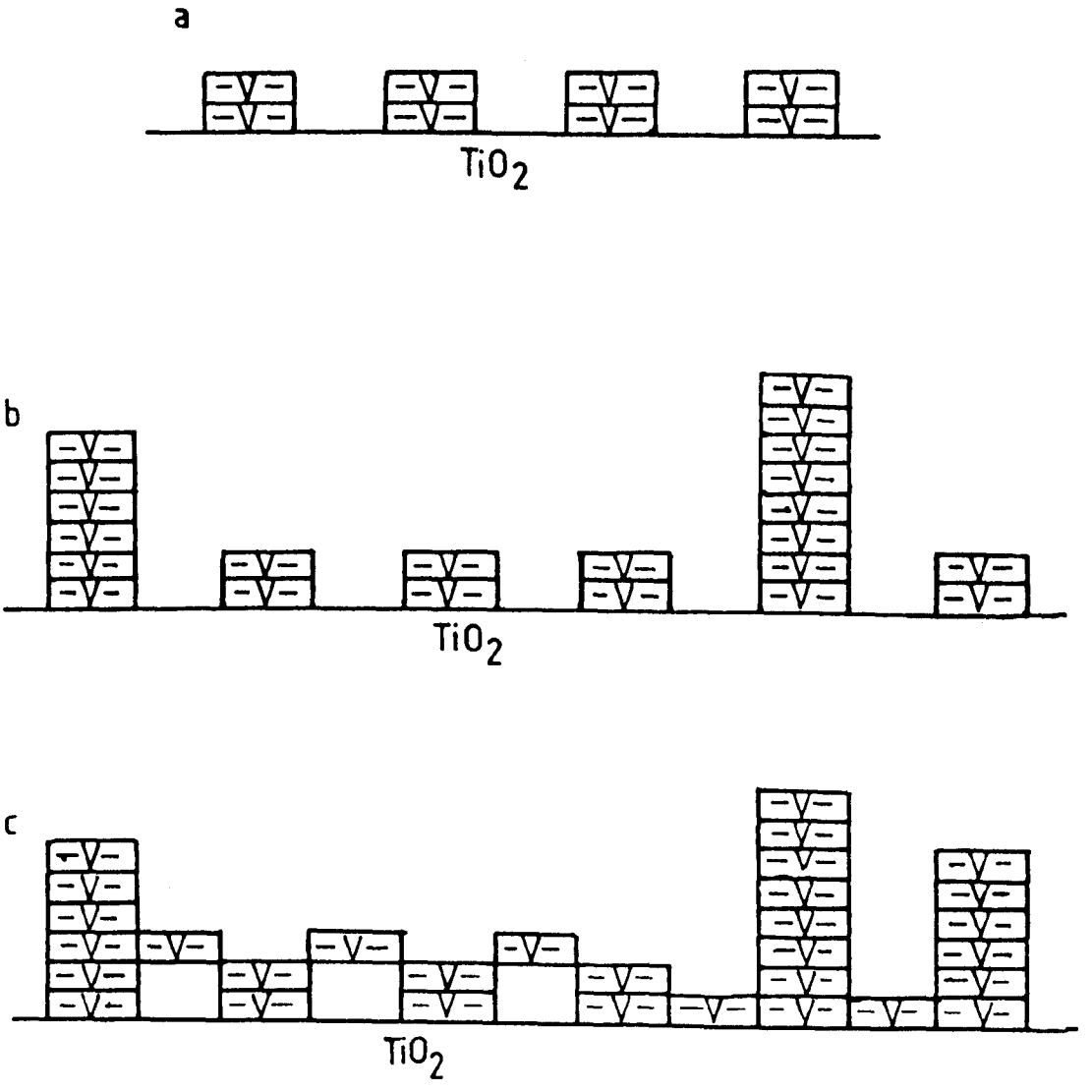

Figure 4.90 Models for surface structures for the catalysts prepared by wet impregnation at the dried stage: a) at about the monolayer point (i.e., VO_x monolayer loading; b) at about the four monolayer point; c) above four monolayer point. [-V-] : represents the vanadyl oxalate.

V/Ti intensity ratio increases after calcination as a consequence of modification of the dispersion after the decomposition of vanadyl oxalate. This suggests the formation of VO_X species in a good state of dispersion (monolayer). In the case of the VO_X loadings corresponding to one to four monolayers (Figure 4.90b), on calcination, the monolayer is achieved by migration of VO_X species from the second layer and excess VO_X forms the second phase (b) which is represented as towers. Kasztelan et al. (31) have already suggested a similar migration of Mo species from a multilayer at the dried stage to a monolayer dispersion at the calcined stage.

In the case of VO_X loading above four monolayers, on calcination, VO_X species formed the third phase (see Figure 4.87).

The V/Ti intensity ratio versus the V_2O_5 content for the dried catalysts prepared by the $VOCl_3$ method (Figure 4.60) is similar to that of the calcined catalysts. These results suggest that there is no significant change in the structure of the VO_X phases as a result of calcination. These results also support the model which has been suggested in Figure 4.87.

Decomposition of isopropanol

Results for unsupported V_2O_5 show the high activity of V_2O_5, and a high propylene selectivity. At about 202°C, the propylene selectivity is 0.93 which is in good agreement

with literature values (Table 4.19)(32,33). In the case of the TiO_2 samples, at 220°C, they show low activities (Figures 4.16, 4.39 and 4.61) and the order of propylene selectivity was shown to be:

washed anatase (100%) > P-25 (90%) > unwashed anatase (38%)

The lower propylene selectivity in the case of unwashed anatase may be due to the effect of impurities such as P and K on the surface of the anatase support. Table 4.19 shows the propylene selectivity at 202°C for the same TiO_2 samples. Cunningham's values for a very pure anatase and for Degussa P-25 are respectively 73 and 4% at 202°C (Table 4.19)(33). Table 4.19 shows also the rates and activation energies for the various TiO_2 samples and for V_2O_5 found in this work and compares then with literature values (33).

In the case of catalysts supported on the low area washed anatase, the form of the results in Figures 4.39 and 4.40 strongly suggests that the activity is principally due to the vanadate monolayer species, and that little contribution is made by the disordered or paracrystalline particles of V_2O_5 thought to be formed above the monolayer point. This conclusion is derived more clearly when the total rate(r_t) per g-V_2O_5 is plotted against V_2O_5 content, as shown in Figure 4.91. The monolayer catalyst (0.9% V_2O_5) is some 74 times more active than unsupported V_2O_5 on this basis. The initial increase in rates (Figure 4.40) is accompanied by a marked fall in the activation energies (Figure 4.42), which then show little significant change with increasing amount of V_2O_5 (e.g., a marked decrease in activation energy for

Table 4.19

Kinetic parameters for decomposition of isopropanol on TiO_2 and V_2O_5

Catalyst	S.A./m^2g^{-1}	r_{pr} [1]	r_{ac} [1]	S_{pr} [2]	log R_{pr} [3]	log R_{ac} [3]	E_t [4]	E_{pr} [4]	E_{ac} [4]	Ref.
TiO_2 (CLD 939) washed	9.6	0.01	0	1.0	14.24	--	147	126	--	this work
TiO_2 (anatase)	170	--	--	0.73	14.04	13.60	--	149	109	33
TiO_2 (CLD 939) unwashed	9.6	0.10	0.19	0.34	15.26	15.51	89.5	100	84.1	this work
TiO_2 (P-25)	55	0.17	0	1.0	14.72	--	123	106	138*	this work
TiO_2 (P-25)	50	--	--	0.04	14.08	15.53	--	143	63	33
V_2O_5	8.5	6.2	0.46	0.93	17.08	15.96	41.0	40.1	49.0	this work
V_2O_5	2.6	--	--	0.96	18.08	16.71	--	84	59	33
V_2O_5	--	--	--	0.8-0.9	--	--	--	--	--	32

1 Rate in mmol h^{-1} g^{-1} at 202°C;

2 propylene selectivity at 202°C;

3 Rate in molecule $m^{-2}s^{-1}$ at 202°C;

4 Activation energy in kJ mol^{-1};

* in range 227-257°C.

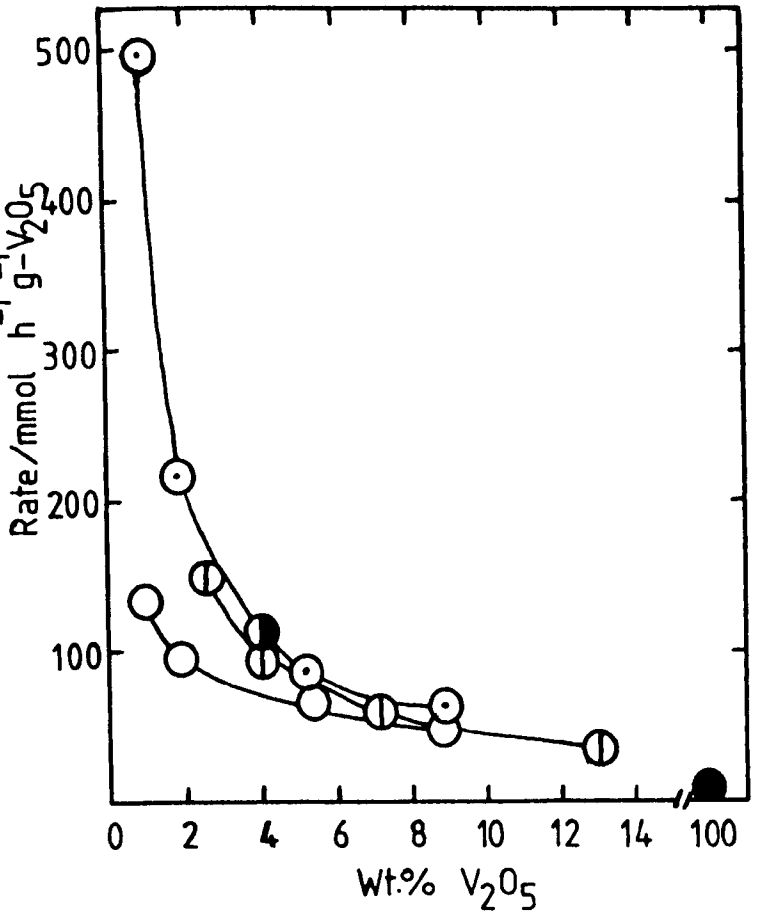

Figure 4.91 The rate of isopropanol removal per g-V_2O_5 for the catalysts shown in Figures 4.17, 4.40 and 4.62 and for unsupported V_2O_5 as a function of V_2O_5 content at 220°C. Symbols as in Figures 4.17, 4.40 and 4.62.

isopropanol removal from 147 to 17 kJ mol^{-1} thereafter it remains between 17 and 30 kJ mol^{-1}). This suggests the superior activity of the monolayer species. For all supported VO_x catalysts, the activation energies for propylene formation are higher than those for acetone formation (Figure 4.42), so that highest acetone selectivities are observed at the lowest temperatures. Similar results were published by Gasior et al. (32,34) concerning this reaction on VO_x/TiO_2(anatase) catalysts, in that acetone becomes a major product at low V_2O_5 concentration (monolayer catalyst). The results for the VO_x/TiO_2(P-25) catalysts prepared by the $VOCl_3$ and $VO(O^iBu)_3$ methods are discussed below.

The results in Figures 4.61 and 4.62 show that the catalyst containing the smallest concentration of V_2O_5 (2.6%, equivalent to about 0.6 of a monolayer) is substantially more active than the support but Figure 4.61 shows that the propylene selectivity is very much lower (35% compared to 90% for the support alone). Further increase in the V_2O_5 content produces little additional change in either rates (r_t, r_{ac} and r_{pr}) or propylene selectivity (Figures 4.61 and 4.62). Figure 4.91 shows also that the 0.6 monolayer catalyst is some 22 times more active than V_2O_5 on the basis of the total rate(r_t) per g-V_2O_5. The catalyst made by using the $VO(O^iBu)_3$ method (Section 4.2.5.3.3) is almost identical to the catalyst made by the $VOCl_3$ method having the same V_2O_5 loading (see Figures 4.61 and 4.62). Once again the initial increase in rates (r_t, r_{ac} and r_{pr})(Figure 4.62) is accompanied by a marked fall in the activation energies (E_t, E_{ac} and E_{pr})(Figure 4.64), which then show little significant change with increasing amount

of V_2O_5. This once again suggests the superior activity of the monolayer species, and it is interesting that the catalyst having only about 0.6 of a vanadate monolayer shows the full characteristics of a monolayer catalyst. Similarly to the VO_x catalysts prepared by impregnation, the catalysts prepared by the $VOCl_3$ and the $VO(O^iBu)_3$ methods show activation energies for propylene formation higher than those for acetone formation, so that that highest acetone selectivities are observed at the lowest temperatures.

In the paragraph below, the results of VO_x/TiO_2(anatase, unwashed) catalysts which were prepared by the wet impregnation will be discussed.

Figures 4.16 and 4.17 show that the catalyst containing 0.9% V_2O_5 is more active than the support alone but less selective for propylene formation (22% compared to 38% for the support alone). Above 0.9% V_2O_5, the rates (r_t, r_{ac} and r_{pr}) and propylene selectivity increase with V_2O_5 content (Figures 4.16 and 4.17).

The results show that the monolayer catalyst (0.9% V_2O_5) is less active and less selective for propylene formation compared to the second phase (potassium-containing vanadium oxide) or paracrystalline particles of V_2O_5 (Figure 4.16). The low activity and low propene selectivity for the monolayer species may be due to the effect of impurities especially K which is forming potassium-containing vanadium oxide (see structure D). With increasing V_2O_5 content, the effect of impurities decreases. For the catalyst containing 8.8% V_2O_5, the activity and selectivities (S_{ac} and S_{pr}) (Figure 4.16 and 4.17) are similar to those for the washed anatase catalyst with the same loading (see Figures

4.39 and 4.40). Figure 4.91 shows that the monolayer catalyst (0.9% V_2O_5) is some 19 times more active than V_2O_5 on the basis of the rate(r_t) per g-V_2O_5. The increase in the rates (r_t, r_{ac} and r_{pr}) with V_2O_5 content (Figure 4.17) is accompanied by a decrease in the activation energies for E_t, E_{ac} and E_{pr}, (up to 4-5% V_2O_5) which then show little increase up to 8.8% V_2O_5 (Figure 4.19). The monolayer species did not show a higher activity compared to the monolayer catalyst for which washed anatase was used as a support, perhaps because of the negative effect of the P and K on the VO_x species. As with all VO_x catalysts supported on washed anatase and P-25, the activation energies for propylene formation are higher than those for acetone formation (Figure 4.19).

The VO_x/TiO_2(unwashed,anatase) catalysts show different results from the VO_x/TiO_2(washed,anatase) and the VO_x/TiO_2(P-25) catalysts. It is again concluded that the activity is chiefly associated with the monolayer vanadate species while the VO_x/TiO_2(unwashed,anatase) monolayer catalyst shows lower activity due to the negative effect of impurities especially K which may form potassium-containing vanadium oxide with VO_x species (structure D). The impregnation and grafting methods seem to produce structures having closely similar catalytic properties.

Compensation effect

Figure 4.92 shows the compensation effect plot of Arrhenius parameters for the supports and the VO_x catalysts which are shown in Tables 4.2, 4.5, 4.10, 4.13 and 4.15 and which relate to the formation of products. Values of A are

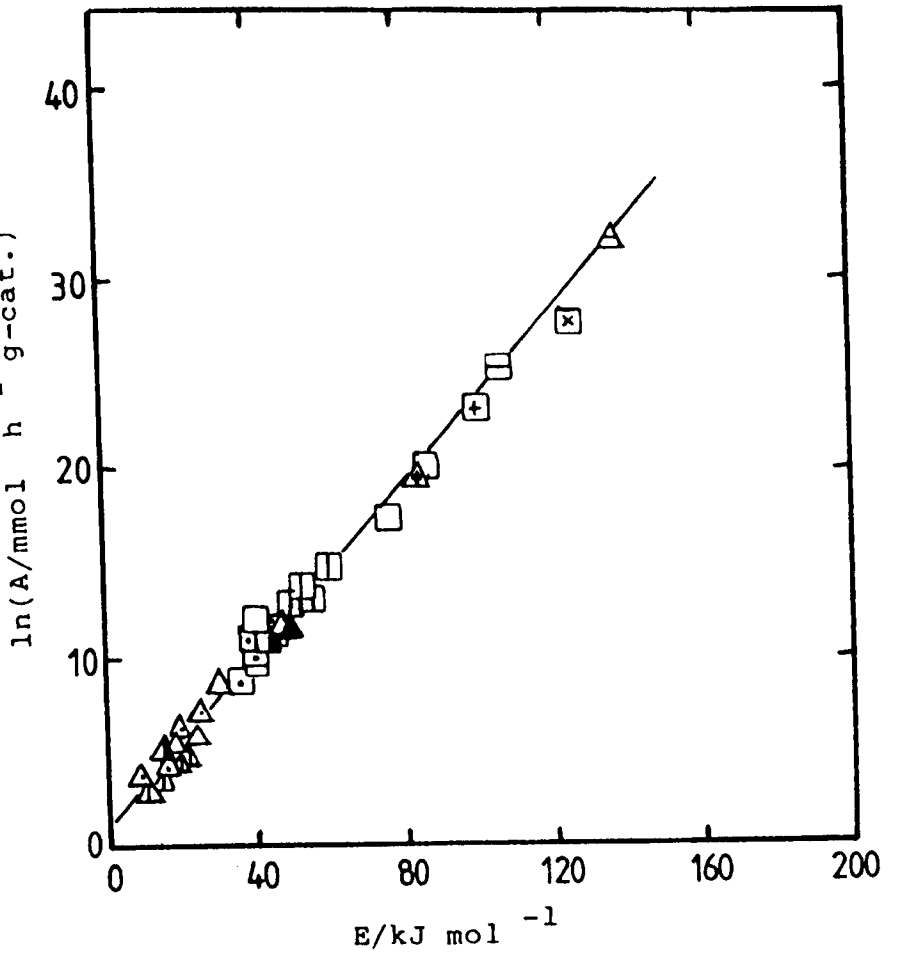

Figure 4.92 Compensation effect for the decomposition of isopropanol catalyzed by the catalysts shown in Figures 4.19, 4.42 and 4.64 and supports and unsupported V_2O_5 (■ , ▲). The plot shows the Arrhenius parameters for the formation of acetone (triangles) and of propylene (squares).

expressed as mmol h^{-1} g^{-1}-cat. to permit inclusion of the results for the TiO_2 supports. Points for both reactions, i.e., dehydration and dehydrogenation, lie approximately on the same line, the slope of which corresponds to an isokinetic temperature of 561 K. This suggests the identity of the active centres for the two reactions and highlights the probable role of V-OH groups in their mechanisms (see next Section).

Reaction mechanisms

The VO_x monolayer species, which it is argued are more reactive than the V_2O_5 microcrystals formed at higher V_2O_5 contents, are comparably active for both dehydrogenation and dehydration. At 220°C the former is faster, but the higher activation energies for the latter mean that, towards the upper end of the temperature range used, the rates become more nearly equal. It therefore appears that there is no common intermediate for the two reactions, and that the different paths followed are consequences of different modes of interaction of the isopropanol molecule with the vanadate groups constituting the monolayer. It is suggested from the results in this work that the structure of the monolayer species (oxohydroxy species) can be represented as:

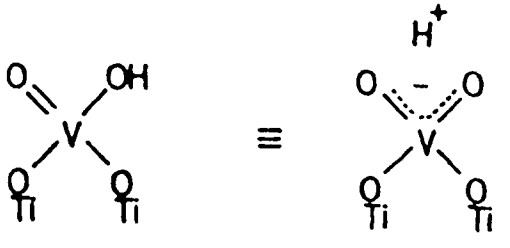

It is therefore logical to associate dehydrogenation with the V=O bond (15) and dehydration with the V-OH group, which

is presumably sufficiently acidic to cause the breaking of the C-O bond in isopropanol, with the formation of water and a carbonium ion.

It is clear from the rates and activation energies that dehydration is not simply caused by Ti-OH groups as compared with V-OH. Unwashed anatase which contains P and K as impurities shows different results from washed anatase and P-25 (see Figures 4.16, 4.39 and 4.61 and Table 4.19). This may be due to a modification of the TiO_2 surface, i.e., a decrease in the acidity of Ti-OH groups, which causes low dehydration selectivity at 220°C and at the same time increases the dehydrogenation selectivity (Figure 4.16).

It may be supposed that dehydrogenation occurs through oxidative addition of isopropanol across the V=O bond: this and the suggested subsequent progress of the reaction are illustrated below:

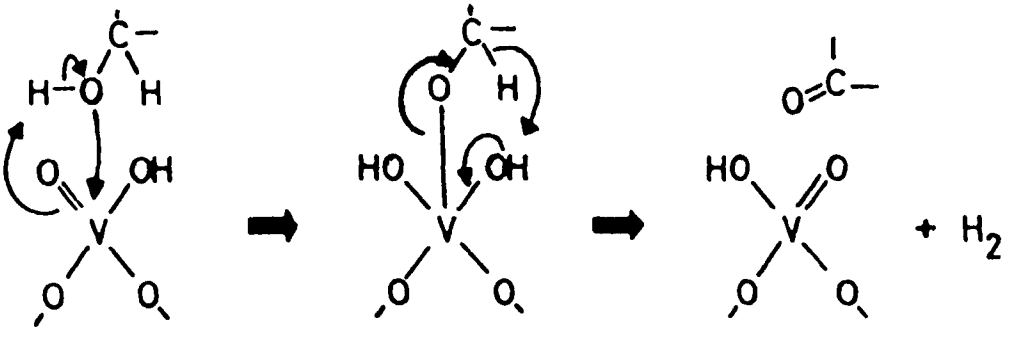

In the case of VO_x/TiO_2(unwashed,anatase) catalysts, the P and K impurities have a negative effect on the dehydration reaction while increasing the dehydrogenation reaction. These results may support the proposition that K^+ is exchangeable with H^+ in some of V-OH groups (structure D). Phosphorus may have a little effect on the monolayer species and on both reactions because P and vanadium have similar chemistry. With increasing V_2O_5 content (above 4 monolayers) the effect of P and K decreases and the activity and

propylene selectivity become similar to those for VO_x/TiO_2(washed,anatase). Alkali metals, often used as promoters in industrial catalysts (35), can also reduce the surface acidity of a catalyst (36,37). Ai et al. (38) found that the activity of V_2O_5-P_2O_5 catalysts for the dehydration of isopropanol, sharply decreased with increasing P_2O_5 up to 20 mol% P_2O_5.

The necessary combination of surface groups is not to be found on the basal plane of the V_2O_5 surface, which explains the low selectivity of bulk V_2O_5 for dehydrogenation. They may however be located at steps and edges, thus accounting for the existence of some dehydrogenation capability. Dehydration on the other hand requires only acidic OH groups, which may be present on the basal surface in consequence of the hydration of V=O and V-O-V bonds.

Selective Oxidation of 1,3-butadiene

VO_x/TiO_2(anatase, low area)

TiO_2(unwashed) alone had a negligible activity for butadiene oxidation. The form of the results shown in Figure 4.24 suggests that the activity of the monolayer catalysts prepared by the different methods using anatase (unwashed, low area) as the support at 320°C are similar. The one which was prepared by the impregnation method using anatase (washed, low area) shows higher activity than monolayer catalysts on unwashed supports (Figure4.24). The selectivities for maleic anhydride are similar for both sets of monolayer catalysts (Figure 4.24). These results show that the monolayer catalyst with only minor amounts of impurities (P and K) is more active than the unwashed

monolayer catalyst which contains significant quantities of P and K as impurities. This negative effect of impurities on the catalytic behaviour of the VO_x/TiO_2(anatase, unwashed, low area) in the selective oxidation of toluene was also found by van Hengstum et al. (40). Bond et al. (6) suggested this negative effect in their study of oxidation of butadiene. It may be due to that part of the VO_x monolayer phase which is deactivated by the formation of a potassium-vanadium bronze compound which has low activity.

Removing the impurities (P and K) from the TiO_2 by washing affects the surface acidity of the catalyst. By washing, the surface acidity may be increased compared to the unwashed one. This may explain why a lower S_{MA} is observed at low conversion (Figure 4.38). At higher conversions, the desorption of the product maleic anhydride will be enhanced when the surface acidity of the catalyst is increased, resulting in a higher selectivity. Unsupported V_2O_5 is more active than monolayer catalysts on the unwashed support but less selective towards maleic anhydride.

Figure 4.24 also shows that increasing the V_2O_5 content leads to a continuous increase of the activity and of S_{MA}, but the activity decreases above 2.7% V_2O_5. This may explain why more VO_x is needed to obtain the most effective catalyst as is shown in Figure 4.24. The VO_x phase is formed on the surface of the monolayer as towers with different composition (i.e., structures B and E may form towers of VO_x while structure D may react with VO_x forming another type of potassium-containing vanadium oxide which may have a low concentration of K). These towers may explain the improvement in the catalytic behaviour of the catalysts.

Bond et al. (6) have studied the oxidation of butadiene using the same type of support. They observed that the activity as well as S_{MA} increases with increasing V_2O_5 content up to ..10% V_2O_5. van Hengstum et al. (40) observed in the oxidation of toluene to benzoic acid, using the same type of support (unwashed), that the activity and maximum yield of benzoic acid increased with V_2O_5 content up to 3.3% V_2O_5. The same authors (40) observed, when P and K impurities were both largely removed, that optimum catalytic behaviour was achieved at much lower vanadium contents.

Figure 4.25 shows the variation of the rates per g-cat. as a function of V_2O_5. It shows that the total rate in the monolayer region for the catalyst on the washed support is higher than that obtained with the unwashed catalyst. It seems that the rate of formation of CO_x is higher (low activation energies) than the rate of formation of maleic anhydride (high activation energies) (see Figures 4.25 and 4.26. This may be due to the fact that the major amount of CO_x is formed from the decomposition of butadiene and not from the decomposition of maleic anhydride.

VO_x/TiO_2(Eurotitania)

TiO_2(Eurotitania) itself is not active for the oxidation of butadiene. Figure 4.77 shows that the activity decreases with V_2O_5 content up to 12% V_2O_5, and then remains constant; S_{MA} does not vary. The most effective catalyst will therefore be obtained when the TiO_2 support is completely covered with a monomolecular layer of VO_x species. The decreasing trend in the activity may be due to the low reducibility of VO_x with increasing V_2O_5 content (Figure

4.73). It can furthermore be concluded that disordered vanadium oxide formed above the monolayer is less active. These results strongly suggest that the activity is principally due to the monolayer species. van Hengstum et al. (40) used VO_x/TiO_2(P-25) catalysts for the oxidation of toluene. They found that both activity and maximum yield to benzoic acid were constant above 3.9% V_2O_5 which indicated complete monolayer coverage of the support at this value.

Figure 4.78 shows the rates decrease with V_2O_5 content. The rate of formation of CO_x is higher (low activation energies) than the rate of formation of maleic anhydride (high activation energies) with V_2O_5 content (Figures 4.78 and 4.80). This means that the majority of the CO_x is formed from the oxidation of butadiene and not from the oxidation of maleic anhydride.

As described in the literature, selective oxidation of 1,3-butadiene proceeds by a reduction-oxidation mechanism and the surface V=O species has the active role. It has been suggested that the butadiene molecule is adsorbed and activated on a Bronsted acid site and that the reaction is initiated by the nucleophilic attack of the oxygen atom of a surface V=O species on the adsorbed butadiene molecule to form an intermediate (41). Since the reaction proceeds by a reduction-oxidation mechanism, these oxygen atoms are not directly supplied from gaseous O_2, but supplied by the oxygen of the catalyst (41). According to Ai (42,43), furan is an intermediate compound in the formation of maleic anhydride.

Compensation effect

Figure 4.93 shows the compensation effect plot for the

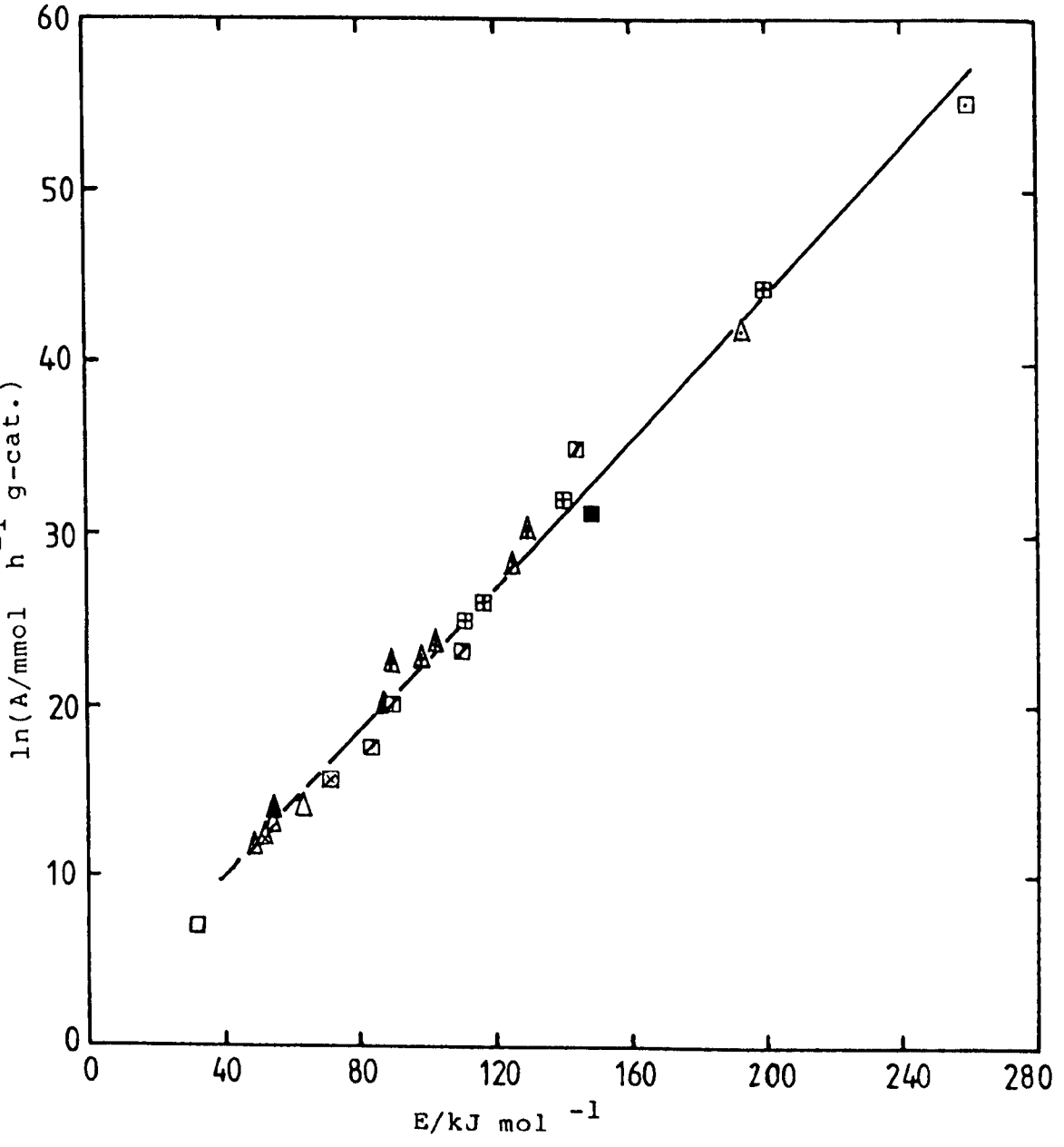

Figure 4.93 Compensation effect for oxidation of 1,3-butadiene catalyzed by catalysts shown in Figures 4.15, 4.21, 4.27, 4.38 and 4.80 and unsupported V_2O_5 (■, ▲). The plot shows the Arrhenius parameters for the formation of maleic anhydride (squares) and of carbon oxides (triangles).

Arrhenius parameters for the VO_x catalysts which are shown in Tables 4.1, 4.4, 4.6, 4.7, 4.9 and 4.17 and which relate to the formation of MA and CO_x. Points for both reactions lie about the same line, the slope of which corresponds to an isokinetic temperature of 572 K. This suggests the identity of the active centres for the two reactions (44) and may indicate that the partially oxidized product (MA) is formed by the use of lattice oxygen while the nonselective reaction (CO_x product) involves adsorbed oxygen species (45,46).

4.4 Conclusions

Vanadium oxide catalysts were prepared on two groups of TiO_2 supports: the first group of TiO_2 samples contained very small amounts of additives, especially P and potassium, while the other group contained more P and K impurities (four times in the case of P and five times in the case of K, compared to the first group).

With the first group of supports, TPR and Raman spectroscopy showed the formation above the monolayer of a compound (disordered vanadium oxide) which has the same reducibility as the monolayer but which has a band at 995 cm^{-1}. Above four monolayers, paracrystalline V_2O_5 was formed. With the second group of supports, TPR and Raman spectroscopy showed that above the monolayer a potassium-containing vanadium oxide may form, which has a high reducibility and no band at 995 cm^{-1}. Crystalline V_2O_5 is formed above four monolayers. XPS results confirm the dispersion of VO_x species on the surface of the support in the monolayer region. The XPS results also show that the

second and third phases occupy a limited area of the monolayer surface, but could not distinguish between the second and the third phases. The XPS results for dried catalysts prepared by wet impregnation in the monolayer region show two layers of vanadyl oxalate. Above the monolayer, many towers form. ESR results show that 5% of V in the monolayer coverage is V(IV). In the case of catalysts made from the first group of supports, activities in butadiene oxidation and isopropanol decompostion are principally due to the monolayer species and little contribution is made by the disordered or paracrystalline V_2O_5. In the case of catalysts employing the second group of supports, the activity in both reactions increases with V_2O_5 content in the region of one to four monolayers.

4.5 References

1. F. Roozeboom, M.C. Mittelneijer-Hazeleger, J.A. Moulijn, J. Medema, V.H.J. de Beer and P.J. Gellings, J. Phys. Chem., 84, 2783 (1980).
2. I.R. Beattie and T.R. Gilson, J. Chem. Soc. (A), 2322 (1969); Proc. Roy. Soc. A, 307, 407 (1968).
3. I.E. Wachs, R.Y. Saleh, S.S. Chan and C.C. Chersich, Appl. Catal., 15, 339 (1985).
4. P. Jackson and G.D. Parfitt, Trans. Faraday Soc., 67, 2669 (1971).
5. A. Ueno, T. Onishi and K. Tamaru, Trans. Faraday Soc., 67, 3585 (1971).
6. G.C. Bond, A.J. Sarkany and G.D. Parfitt, J. Catal., 57, 476 (1979).
7. M. Akimoto, M. Usami and E. Echigoya, Bull. Chem. Soc. Jpn., 51, 2195 (1978).
8. M.J. Perez Zurita, Ph.D. Thesis, Brunel University, Uxbridge, United Kingdom (1984).
9. A.J. van Hengstum, J.G. van Ommen, H. Bosch and P.J. Gellings, Proc. 8th Internat. Congr. Catalysis, Dechema, Frankfurt-am-Main, I 297 (1984).
10. J. Haber, A. Kozlowska and R. Kozlowski, J. Catal., 102, 52 (1986).
11. R. Kozlowski, R.F. Pettifer and J.M. Thomas, J. Phys. Chem., 87, 5176 (1983).
12. J. Haber, Proc. 8th Internat. Congr. Catalysis, Dechema, Frankfurt-am-Main, I 85 (1984).
13. M. Inomata, K. Mori, A. Miyamoto, T. Ui and Y. Murakami, J. Phys. Chem., 87, 754 (1983).
14. J. Kijenski. A. Baiker, M. Glinski, P. Dollenmeier and A. Wokaun, J. Catal., 101, 1 (1986).

15. Y. Nakagawa, T. Ono, H. Miyata and Y. Kubokawa, J. Chem. Soc., Faraday Trans. 1, 79, 2929 (1983).

16. G. Busca, G. Centi, L. Marchetti and F. Trifiro, Langmuir, 2, 568 (1986).

17. G. Busca and J.C. Lavelley, Spectrochimica Acta, 42A, 443 (1986).

18. G. Busca and Marchetti, G. Centi and F. Trifiro, J. Chem. Soc., Faraday Trans. 1, 81, 1003 (1985).

19. G. Busca, Langmuir, 2, 577 (1986).

20. S.L.T. Andersson, J. Chem. Soc., Faraday Trans. 1, 82, 1537 (1986).

21. G.C. Bond and N. Furlong, Unpublished work.

22. A.J. van Hengstum, J.G. van Ommen, H. Bosch and P.J. Gellings, Appl. Catal., 8, 369 (1983).

23. M. Gasior and T. Machej, J. Catal., 83, 472 (1983).

24. R.Y. Saleh and I.E. Wachs, U.S. Patent, 4,582,912 (1986).

25. P. Dufresne, E. Payen, J. Grimblot and J.P. Bonnelle, J. Phys. Chem., 85, 2344 (1981).

26. F.J. Gil-Llambías, A.M. Escudey, J.L.G. Fierro and A. Lopez Agudo, J. Catal., 95, 520 (1986).

27. B. Jonson, B. Rebenstorf, R. Larsson, S.L.T. Andersson and S.T. Lundin, J. Chem. Soc., Faraday Trans. 1, 82, 767 (1986).

28. G. Meunier, B. Mocacr, S. Kasztelan, L.R. Le Coustumer, J. Grimblot and J.P. Bonnelle, Appl. Catal., 21, 329 (1986).

29. J.C. Védrine in "Surface Properties and Catalysis by Non-Metals", eds., J.P. Bonnelle, B. Delmon and E. Derouane, Reidel, Dordrecht,p. 159 (1983).

30. R.Y. Saleh, I.E. Wachs, S.S. Chan and C.C. Chersich, J. Catal., 98, 102 (1986).

31. S. Kasztelan, J. Grimblot, J.P. Bonnelle, E. Payen, H. Toulhoat and J. Jacquin, Appl. Catal., 7, 91 (1983).

32. M. Gąsior, I. Gąsior and B. Grzybowska, Appl. Catal., 10, 87 (1986).

33. J. Cunningham, B.K. Hodnett, M. Ilyas, J. Tobin, E.L. Leahy and J.L.G. Fierro, Faraday Disc. Chem. Soc., 72, 283 (1981).

34. B. Grzybowska-Swierkosz, in "Catalysis by Acids and Bases", Eds., B. Imelik, C. Naccache, G. Coudurier, Y.B. Taarit and J.C. Vedrine, Elsevier, Amsterdam, 45 (1985).

35. J.M. Maselli and G. Kin, Canadian Patent No. 873,904 (1921), to W.R. Grace and Co.

36. V.M. Bondareva, T.V. Andrushkevich, T.P. Gorshkova, G.Ya. Popova and A.A Davydov, React. Kinet. Catal. Lett., 12, 25 (1979).

37. G.K. Boreskov, A.A. Ivanov, O.M. Ilyinich and V.G. Ponomareva, React. Kinet. Catal. Lett., 3, 1 (1975).

38. M. Ai and S. Suzuki, Bull. Chem. Soc. Jpn., 47, 3074 (1974).

39. A.J. van Hengstum, J.G. van Ommen, H. Bosch and P.J. Gellings, Appl. Catal., 8, 369 (1983).

40. A.J. van Hengstum, J. Pranger, J.G. van Ommen and P.J. Gellings, Appl. Catal., 11, 317 (1984).

41. K. Mori, A. Miyamoto and Y. Murakami, J. Chem. Soc., Faraday Trans. 1, 82, 13 (1986).

42. M. Ai, J. Catal., 67,110 (1981).

43. M. Ai, Bull. Chem. Soc. Jpn., 50, 355 (1977).

44. G.C. Bond, Z. Phys. Chem., N. F., 144, 21 (1985).

45. N.S. Butt, A. Fish and F.Z. Saleeb, J. Catal., 5, 508 (1966).

46. J.A. Juusola, R.F. Mann and J. Downie, J. Catal., 17,

CHAPTER 5

INFLUENCE OF PHOSPHORUS AND POTASSIUM IMPURITIES ON THE PROPERTIES OF VANADIUM OXIDE CATALYSTS SUPPORTED ON TITANIA

5.1 Introduction

The purpose of this Chapter is to study the effects of the phosphorus and potassium impurities on the properties of VO_x/TiO_2 catalysts prepared by the wet impregnation method. The amount of VO_x species in these catalysts is equivalent to a single monolayer. The pretreatment of the TiO_2 washed and unwashed (CLD 939, anatase, 9.6 m^2g^{-1}) supports and the preparation of the catalysts were described in Sections 3.4.2 and 3.5.1 of Chapter 3 respectively.

In this Chapter two techniques were used, namely, temperature programmed reduction (TPR) and laser Raman spectroscopy, to characterise the VO_x species which were formed in the presence of phosphorus and potassium as impurities in or on the support. The catalytic oxidation of 1,3-butadiene has been studied with these catalysts.

5.2 Results

5.2.1 Effect of phosphorus

Four VO_x/TiO_2 catalysts with different amounts of P_2O_5 were prepared, see Table 5.1. In preparing the P_1 catalysts, the support employed was TiO_2(CLD 939, washed) (see Table 3.1, Chapter 3) doped with 0.15% K_2O. TiO_2(CLD 939, unwashed) was employed in the preparation of the P_2 catalyst while in P_3 and P_4 catalysts, the support employed was TiO_2(CLD 939, unwashed) doped with 0.25% and 0.75% P_2O_5. The

amount of VO_x species on the supports in these catalysts is equivalent to the monolayer loading.

Table 5.1

Composition (wt.% P_2O_5 and wt.% K_2O) of catalysts supported on TiO_2(CLD 939, unwashed)

Catalyst	Wt.% V_2O_5	Wt.% P_2O_5	Wt.% K_2O
P_1*	1.0	0.15	0.20
P_2	0.9	0.45	0.28
P_3	1.0	0.70	0.28
P_4	1.1	1.20	0.28

* The support employed for this catalyst was the TiO_2(CLD 939, washed) doped with 0.15 wt.% K_2O.

5.2.1.1 Characterisation

The catalyst samples were studied by TPR and laser Raman spectroscopy. The results are given below.

TPR

Figure 5.1 shows that the TPR profiles for these catalysts consist of only a single peak. The value of T_{max} remains nearly constant in the range 520 - 530°C with the P_2O_5 content as in Figure 5.2. The quantities of H_2 consumed show that V(V) was reduced to V(III) (i.e. 2 mol H_2/mol V_2O_5).

Laser Raman spectroscopy

Figure 5.3 shows the laser Raman spectra of these catalysts over the frequency range from 750 - 1050 cm^{-1}. The TiO_2 gives a number of relatively intense bands (anatase: 636, 515 and 395 cm^{-1}). The spectra did not exhibit a band due to crystalline V_2O_5.

5.2.1.2 Oxidation of 1,3-butadiene

Catalytic measurements were carried out between 255 and 399°C. In Figure 5.4 conversion, S_{MA} and S_{CO_x} % measured at 320°C are plotted against the P_2O_5 content. The percentage conversion remains constant with P_2O_5 content.

The value of S_{MA} increases up to 40% at 0.7% P_2O_5, and then remains constant at 1.2% P_2O_5. Similar results were found at 310 and 330°C. Figure 5.5 shows r_B, r_{MA} and r_{CO_x} at 320°C plotted as a function of the P_2O_5 content. The r_B and r_{CO_x} remain constant with P_2O_5 content. The value of r_{MA} increases very slowly with P_2O_5 content. Figure 5.6 shows the plots of $\ln(r_B, r_{MA}$ and $r_{CO_x})$ versus 1/T for the catalyst containing 0.45% P_2O_5, giving E_B, E_{MA} and E_{CO_x}. Table 5.2 shows the values of E_B, E_{MA} and E_{CO_x} and the corresponding values of lnA for the catalysts which were tested in this reaction. Figure 5.7 shows the values of E_B, E_{MA} and E_{CO_x} (Table 5.2) as a function of the P_2O_5 content. The value of E_B reaches a maximum at 0.7% P_2O_5 and then decreases. The value of E_{MA} increases rapidly, passing through a maximum at 0.7% P_2O_5, then decreases, while E_{CO_x} reaches a maximum at 0.45% P_2O_5 and then decreases.

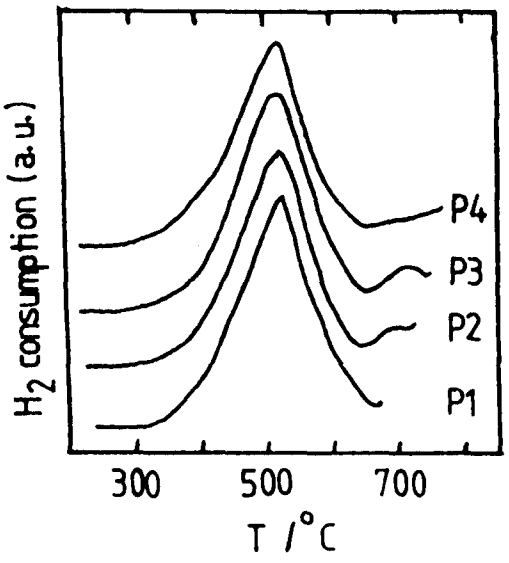

Figure 5.1 TPR profiles of VO_x/TiO_2 catalysts. The TiO_2 is doped with various amounts of P_2O_5 impurity (P_1 = 0.15% P_2O_5; P_2 = 0.45% P_2O_5; P_3 = 0.70% and P_4 = 1.2% P_2O_5).

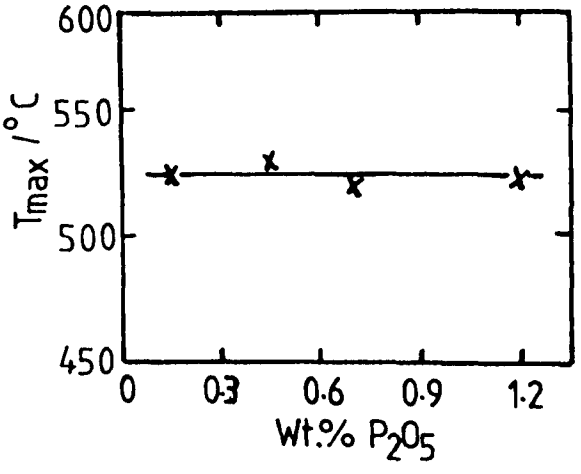

Figure 5.2 T_{max} of profiles shown in Figure 5.1 as a function of the wt.% P_2O_5.

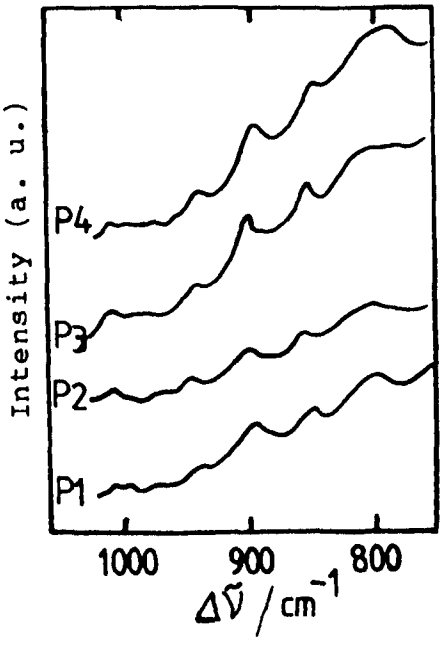

Figure 5.3 Raman spectra of VO_x/TiO_2 catalysts. The TiO_2 is doped with various amounts of P_2O_5 impurity (P_1 = 0.15% P_2O_5; P_2 = 0.45% P_2O_5; P_3 = 0.70% P_2O_5 and P_4 = 1.2% P_2O_5).

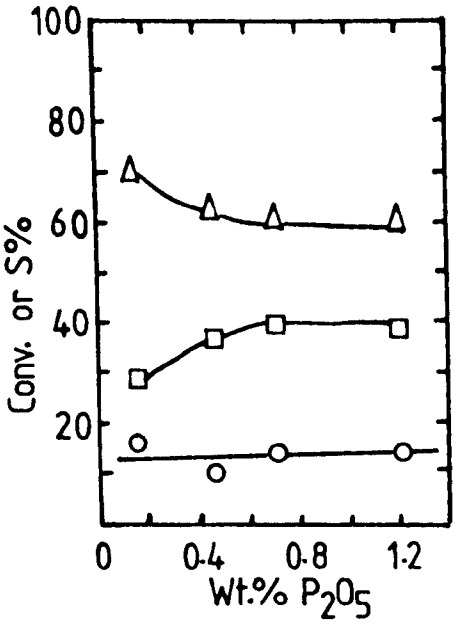

Figure 5.4 Effect of P_2O_5 on the catalytic properties of VO_x/TiO_2 catalysts in the oxidation of 1,3-butadiene at 320°C: O,1,3-butadiene conversion; □, S_{MA}; Δ, S_{CO_x}.

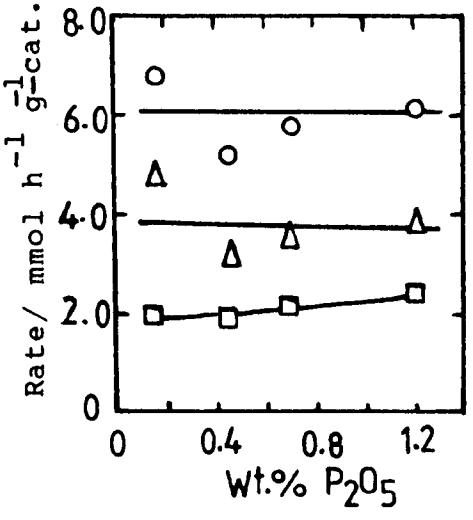

Figure 5.5 Effect of P_2O_5 impurity on the rate of 1,3-butadiene oxidation (r_B, r_{MA} and r_{CO_x}) on the VO_x/TiO_2 catalysts at 320°C: O, r_B; □, r_{MA}; Δ, r_{CO_x}.

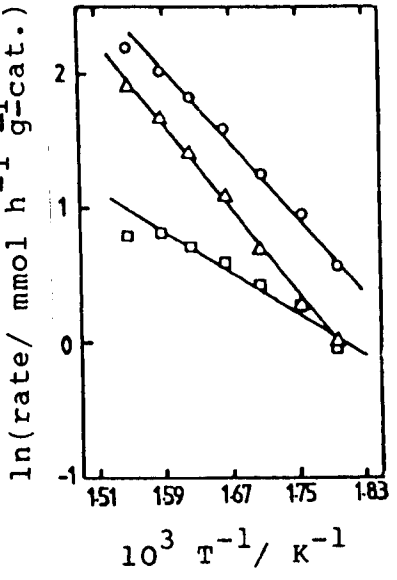

Figure 5.6 Ln(rate) versus 1/T for VO_x/TiO_2 catalyst (P_2 catalyst = 0.45 wt.% P_2O_5).

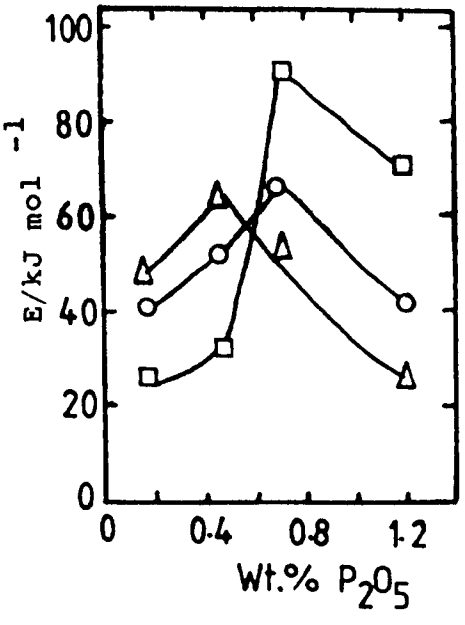

Figure 5.7 E_B(O), E_{MA}(□) and E_{CO_x}(Δ) as a function of P_2O_5 content for samples shown in Figure 5.5.

Table 5.2

The Arrhenius parameters of VO_x/TiO_2 catalysts (the TiO_2 is doped with various amounts of P_2O_5 impurity as shown in Table 5.1) catalyzed oxidation of 1,3-butadiene.

Cat.	E_B [1]	lnA [2]	c.c.	E_{MA} [1]	lnA [2]	c.c.	E_{CO_x} [1]	lnA [2]	c.c.
P_1	41.0	10.2	0.965	26.3	6.1	0.898	48.1	11.3	0.973
P_2^1	52.7	12.0	0.994	32.2	7.0	0.920	64.4	13.9	0.997
P_3^2	66.9	15.2	0.960	91.2	19.1	0.940	53.5	12.1	0.951
P_4^3	41.8	10.3	0.999	71.5	15.1	0.995	25.5	6.6	0.991

1 = E/kJ mol^{-1};

2 = ln(A/mmol h^{-1} $g\text{-}cat.^{-1}$);

c.c. = correlation coefficient.

5.2.2 Effect of potassium

Three VO_x/TiO_2 catalysts with different amounts of K_2O were prepared, see Table 5.3. In preparing the K_1 catalyst, the support employed was TiO_2(CLD 939, washed) while in K_2 and K_3 catalysts, the support employed was TiO_2(CLD 939, washed) doped with 0.15% and 0.35% K_2O. The amount of VO_x species on the supports in these catalysts is equivalent to the monolayer loading.

Table 5.3

Composition (wt.% K_2O and wt.% P_2O_5) of catalysts supported on TiO_2(CLD 939, washed)

Catalyst	Wt.% V_2O_5	Wt.% K_2O	Wt.% P_2O_5
K_1	0.9	0.05	0.15
K_2^1	1.0	0.20	0.15
K_3^2	0.9	0.40	0.15

5.2.2.1 Characterisation

The catalyst samples were studied by TPR and laser Raman spectroscopy. The results are given below.

TPR

Figure 5.8 shows that the TPR profiles for these catalysts consist of only a single peak, T_{max} of which increases from about 478°C to 590°C as the K_2O content increases (see Figure 5.9). In the K_3 catalyst, a small additional peak appears on the low temperature side of the peak; this occurs at about the same T_{max} for K_2 catalyst. The quantities of H_2 consumed show that V(V) was reduced to V(III) (i.e. 2 mol H_2/mol V_2O_5).

Laser Raman spectroscopy

Figure 5.10 shows the laser Raman spectra of these catalysts over the frequency range from 750 - 1050 cm^{-1}. TiO_2 gives a number of relatively intense bands (anatase: 636, 515 and 395 cm^{-1}). The spectra did not exhibit a band due to crystalline V_2O_5.

5.2.2.2 Oxidation of 1,3-butadiene

Catalytic measurements were carried out between 255 and 470°C. In Figure 5.11 conversion, S_{MA} and S_{CO_x} %, measured at 350°C, are plotted against the K_2O content. The percentage conversion falls sharply with K_2O content; S_{MA} decreases with K_2O content. Similar results were found at 340 and 360°C. Figure 5.12 shows r_B, r_{MA} and r_{CO_x} at 350°C plotted as a function of the P_2O_5 content. In general, r_B, r_{MA} and

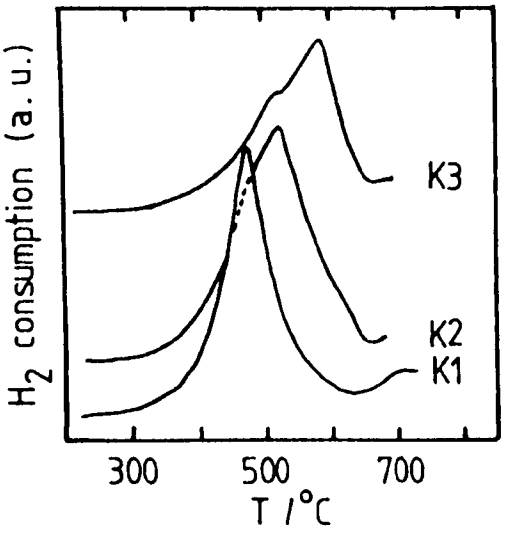

Figure 5.8 TPR profiles of VO_x/TiO_2 catalysts. The TiO_2 is doped with various amounts of K_2O impurity (K_1 = 0.05% K_2O; K_2 = 0.2% K_2O and K_3 = 0.4% K_2O).

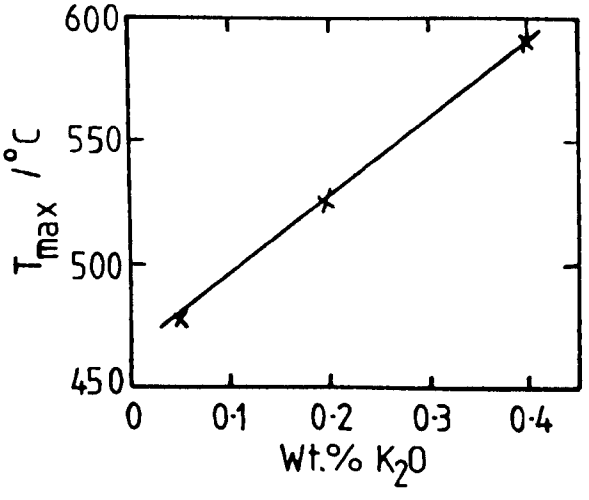

Figure 5.9 T_{max} of profiles shown in Figure 5.8 as a function of the wt.% K_2O.

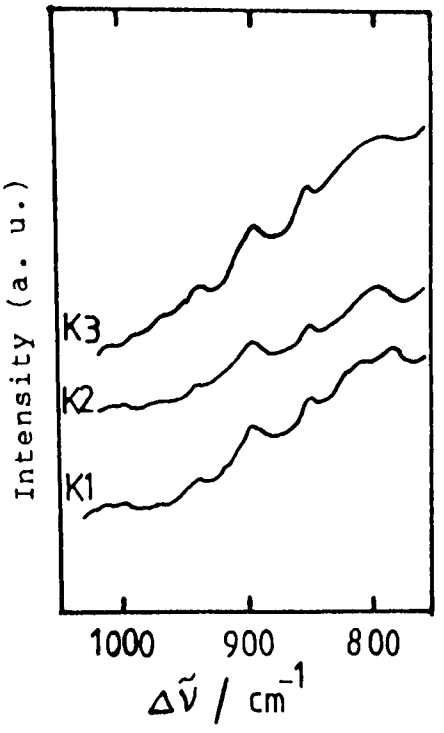

Figure 5.10 Raman spectra of VO_x/TiO_2 catalysts. The TiO_2 is doped with various amounts of K_2O impurity (K_1 = 0.05% K_2O; K_2 = 0.20% K_2O and K_3 = 0.40% K_2O).

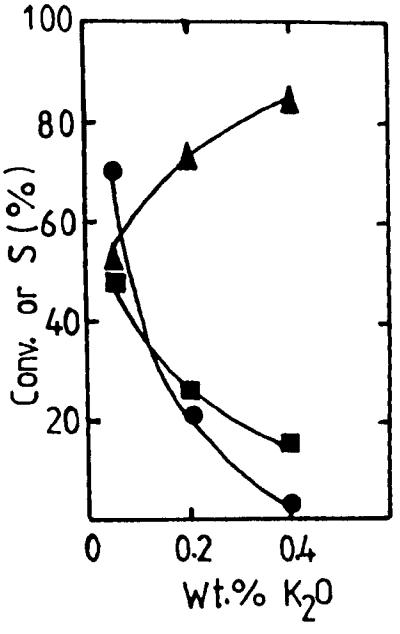

Figure 5.11 Effect of K_2O impurity on the catalytic properties of VO_x/TiO_2 catalysts in the oxidation of 1,3-butadiene at 350°C: ●, 1,3-butadiene; ■, S_{MA}; ▲, S_{CO_x}.

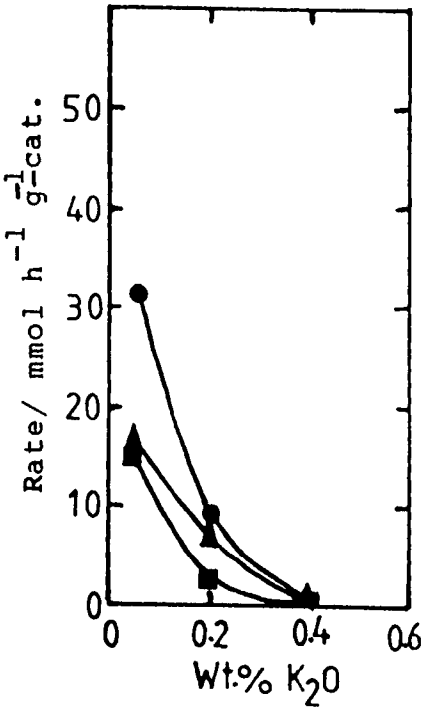

Figure 5.12 Effect of K_2O impurity on the rate of 1,3-butadiene oxidation (r_B, r_{MA} and r_{CO_x}) on the VO_x/TiO_2 catalysts at 350°C: ●, r_B; ■, r_{MA} and ▲, r_{CO_x}.

r_{CO_x} decrease with K_2O content. Figure 5.13 shows the plots of ln(r_B, r_{MA} and r_{CO_x}) versus 1/T for the catalyst containing 0.2% K_2O, giving E_B, E_{MA} and E_{CO_x}. Table 5.4 shows the values of E_B, E_{MA} and E_{CO_x} and the corresponding values of lnA for the catalysts which were tested in this reaction. Figure 5.14 shows the values of E_B, E_{MA} and E_{CO_x} (Table 5.4) as a function of the P_2O_5 content. The values of E_B, E_{MA} and E_{CO_x} fall sharply, passing through minima at 0.20% K_2O, then inrease.

Table 5.4

The Arrhenius parameters of VO_x/TiO_2 catalysts (the TiO_2 is doped with various amounts of K_2O impurity as shown in Table 5.3) catalyzed oxidation of 1,3-butadiene.

Cat.	E_B[1]	lnA[2]	c.c.	E_{MA}[1]	lnA[2]	c.c.	E_{CO_x}[1]	lnA[2]	c.c.
K_1	209.6	45.8	0.917	261.0	55.1	0.940	194.1	42.3	0.903
K_2	41.0	10.2	0.965	26.3	6.1	0.898	48.1	11.3	0.973
K_3	61.1	12.4	0.991	38.2	6.4	0.964	64.8	12.9	0.990

1 = E/kJ mol^{-1};

2 = ln(A/mmol h^{-1} g^{-1}-cat.);

c.c. = correlation coefficient.

5.3 Discussion

From the results presented in this Chapter, it can be concluded that phosphorus and potassium impurities in (or on) the TiO_2 support influence the properties of the VO_x

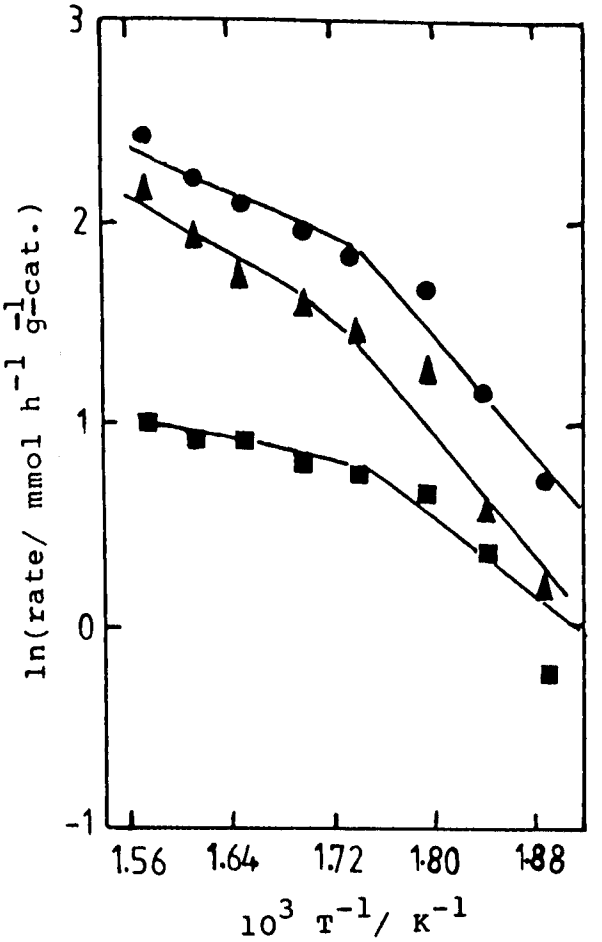

Figure 5.13 Ln(rate) versus 1/T for VO_x/TiO_2 catalyst(K_2 catalyst = 0.20 wt.% K_2O).

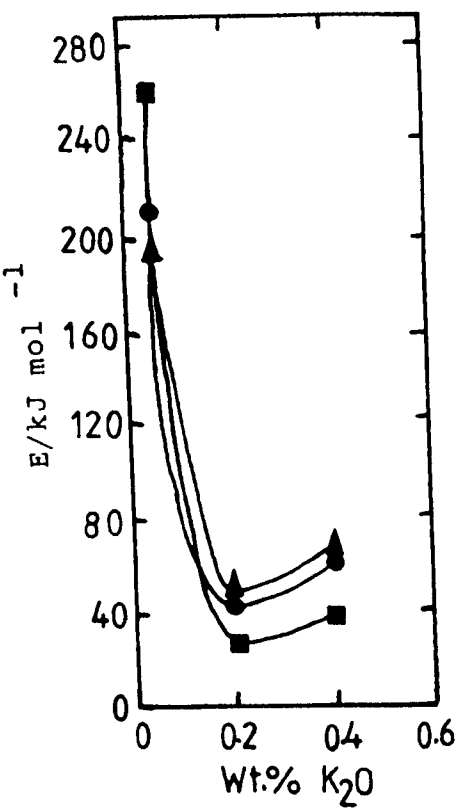

Figure 5.14 E_B(●), E_{MA}(■) and E_{CO_x}(▲) as a function of K_2O content for samples shown in Figure 5.11.

monolayer phase. The properties of the VO_x phase change with the removal of the impurities from the TiO_2 support (Section 4.2.3, Chapter 4). From the results of experiments in which the influences of phosphorus and potassium have been studied separately, it is clear that potassium has a larger effect than phosphorus (Figures 5.4 and 5.11).

Figure 5.8 shows that when potassium is added to the VO_x/TiO_2 monolayer catalysts, the reducibility is decreased. Figure 5.9 shows the T_{max} value increases with K_2O wt.% content. No crystalline VO_x could be detected by laser Raman spectroscopy (Figure 5.10) From the results presented in Figure 5.11, it can be seen that potassium has a negative influence on the value of S_{MA}. At low potassium content, the effect on the activity is relatively small. At higher contents, the activity is strongly reduced. The value of S_{MA} decreases with K_2O content. Potassium is often used as a promoter in commercial oxidation catalysts (1). According to Boreskov et al. (2), the surface acidity of the catalyst is reduced by adding potassium or other alkali metals and this will result in a reduction of the extent of the destructive oxidation of the basic molecule. Other authors (3) assign the effect of potassium to a weakening of the M=O bonds, which are considered to play an important part in selective oxidation. The promoting effect of potassium is however only observed at a relatively low ratio of potassium to the active component. At high potassium contents, bronzes are formed, as was observed by Balandin et al. (4). Bond et al. (5) suggested that part of the active phase (VO_x) might be deactivated because of the formation of bronze compounds.

Andersson (6) also found that unselective potassium vanadate crystallites are formed by the reaction of the VO_x phase with the high potassium surface concentration on the TiO_2 support. The potassium contents for some of the catalysts in this work are relatively high. It is therefore to be expected that the major part of the VO_x phase applied will have reacted with the potassium present to form potassium - containing vanadium oxide (structure D, Chapter 4) and this structure increases with potassium content. Figure 5.12 shows that the rates decrease with potassium content (perhaps due to formation of the potassium - containing vanadium oxide (structure D, Chapter 4) which may be inactive. van Hengstum et al. (7) obtained similar results in the oxidation of toluene by using VO_x/TiO_2 monolayer catalysts with different amount of potassium. They found that potassium has a negative influence on the activity and maximum yield of benzoic acid especially at high potassium content. They concluded that potassium has a major effect on the nature of the reactive site, possibly because of the formation of amorphous bronzes.

The rate of formation of CO_x is higher than the rate of formation of maleic anhydride (Figure 5.12). The activation energies and pre-exponential factors for CO_x formation are higher than those for maleic anhydride formation (Figure 5.14). This may show that CO_x is formed from the oxidation of butadiene by using adsorbed O_2 for oxidation.

Figure 5.2 shows that the reducibility of the VO_x monolayer species is not, or only slightly, affected by increasing the phosphorus content. In none of the catalysts

could crystalline V_2O_5 be detected with laser Raman spectroscopy (Figure 5.3).

Figure 5.4 shows that the addition of phosphorus to the VO_x/TiO_2 monolayer catalysts has no effect on the activity, which seems to run parallel with the reducibility of the catalysts (see Figure 5.2). The value of S_{MA} increases with phosphorus content up to 0.7% P_2O_5 and then remains constant. van Hengstum et al. (7) studied the effect of addition of phosphorus on the oxidation of toluene to benzoic acid by using VO_x/TiO_2 monolayer catalysts. The support is similar to the one used in this work but contains a lower level of K_2O ($\sim$0.07%). They found that addition of phosphorus has a slight effect on the activity which also parallels reducibility. They also found that the addition of phosphorus leads to an increase of the maximum yield of benzoic acid.

According to Ai et al. (8) and Bondareva et al. (9), phosphorus affects the surface acidity of catalysts. A change in surface acidity will definitely influence the adsorption/desorption of reactants and products. van Hengstum et al. (7), concluded that addition of phosphorus resulted in an increase in the surface acidity of VO_x/TiO_2 catalysts.

The results for the phosphorus - containing catalysts in the oxidation of butadiene show that the complete oxidation of the acidic product maleic anhydride may be suppressed (Figure 5.4), suggesting that the acidity has been increased by the addition of phosphorus. An increase of acidity also leads to a stronger adsorption of the butadiene reactant and

hence to an increase in destructive oxidation (2). In general, lower S_{MA} was observed for these catalysts. For VO_X/TiO_2 monolayer catalyst with 1.2% P_2O_5, a lower S_{MA} is observed at low conversion. At high conversion, the desorption of the maleic anhydride will be enhanced when the surface acidity of the catalyst is increased, resulting in a higher selectivity. This is in agreement with the catalytic results for oxidation of toluene reported by van Hengstum et al. (7).

The rate of formation of CO_x is higher than the rate of formation of maleic anhydride (Figure 5.5). At high phosphorus contents, the activation energies of CO_x formation are lower than those for maleic anhydride formation (Figure 5.7). This is explained by the main CO_x formation arising from oxidation of butadiene.

A model which can be suggested for these catalysts is as follows: in the case of catalysts with low $\%P_2O_5$, the structure of the surface of VO_X/TiO_2 catalysts is similar to that suggested in Chapter 4 (Discussion Section, structure E). Above 0.7% P_2O_5 loadings, the surface of the TiO_2 may be covered by a layer of PO_X or two layers of PO_X in case of 1.2% P_2O_5. So, PO_X is suggested to be present as surface-bonded phosphate ions (6). The VO_X monolayer species on such a surface is bonded by V-O-P bonds. The VO_X monolayer may contain some PO_X species or the PO_X layer perhaps contains some VO_X species.

5.4 Conclusions

The results presented in this Chapter show that

phosphorus and potassium impurities in (or on) the TiO_2 support have an influence on the structure and catalytic properties of the VO_x monolayer phase. Addition of phosphorus increases the acidity of the catalyst which suppresses the oxidation of maleic anhydride. Addition of potassium decreases the activity and S_{MA} because of the formation of potassium - containing vanadium oxide which has low reducibility.

5.5 References

1. J.M. Maselli and G. Kin, Canadian Patent No. 873.904 (1921).
2. G.K. Boreskov, A.A. Ivanov, O.M. Ilyinich and V.G. Ponomareva, React. Kinet. Catal. Lett., 3, 1 (1975).
3. K. Tamara, S. Teranishi, S. Yoshida and N. Tamura, Proc. 3rd Internat. Congr. Catalysis, Amsterdam, p. 282 (1965).
4. A.A. Balandin and N.P. Sokolova, Probl. Kinet. Katal., 363 (1960).
5. G.C. Bond, A.J. Sarkany and G.D. Parfitt, J. Catal., 57, 476 (1979).
6. S.L.T. Andersson, J. Chem. Soc., Faraday Trans. 1, 82, 1537 (1986).
7. J.A. van Hengstum, J. Pranger, J.G. van Ommen and P.J. Gellings, Appl. Catal., 11, 317 (1984).
8. M. Ai, Bull. Chem. Soc. Jap., 50, 355 (1977).
9. V.M. Bondareva, T.V. Andrushkevich, T.P. Gorshkova, G.Ya. Popova and A.A. Davydov, React. Kinet. Catal. Lett., 12, 25 (1979).

CHAPTER 6

TITANIA-SUPPORTED MOLYBDENUM OXIDE CATALYSTS

6.1 Introduction

The catalysts studied in this Chapter were prepared as described in Chapter 3. The purpose of this study is to characterise the surface species resulting from the impregnation of the support with an aqueous solution obtained by dissolving $(NH_4)_6Mo_7O_{24}.4H_2O$ in water with oxalic acid, and those obtained with the grafting method ($MoOCl_4$ method). Various techniques were used (temperature programmed reduction (TPR), Laser Raman spectroscopy and X-ray photoelectron spectroscopy (XPS)) to characterise the MoO_x species formed by the two methods. Two types of TiO_2 have been used as support(TiO_2(CLD 782 anatase,unwashed and TiO_2(P-25)). The catalytic oxidation of 1,3-butadiene has been studied for some of these catalysts. The Arrhenius parameters for the oxidation of 1,3-butadiene show a compensation effect (see Discussion Section, Figure 6.17).

6.2 Results

6.2.1 MoO_x/TiO_2(CLD 782, anatase, 9.6 m^2g^{-1})

MoO_x/TiO_2 catalysts were prepared by using TiO_2 CLD 782 (anatase) as the support. The support contained P_2O_5 and K_2O as impurities (see Table 3.1, Chapter 3).

6.2.1.1 Catalysts prepared by wet impregnation method

The MoO_x/TiO_2 catalysts, prepared as described in Section 3.5.1, Chapter 3, contained 0.25-9.5 wt.% MoO_3.

6.2.1.1.1 Characterization

MoO_X/TiO_2 catalysts were studied by TPR, Laser Raman spectroscopy and XPS.

TPR

The TPR profiles for the TiO_2, for MoO_3 and MoO_X/TiO_2 catalysts are shown in Figure 6.1; they show two well-separated peaks. Figure 6.2 shows the dependence of T_{max}, and Figure 6.3 the H_2 consumption per g catalyst for both peaks, as a function of MoO_3 content. In Figure 6.2, the TPR profile for the low Mo content sample (0.25% MoO_3) shows T_{max} for the first peak at 480°C, the T_{max} for the second peak at 780°C, with a shoulder on the high-temperature side at 870°C, due to partial reduction of the support. The TPR profile for the 0.4% MoO_3 sample shows a shift in T_{max} for the first peak to 540°C with a shoulder on the low-temperature side at 430°C, while T_{max} for the second peak shifts to 753°C. Up to 1.3% MoO_3, the T_{max} values for the first reduction peak shift first to lower temperature (510°C), then start to increase to 570°C and become constant above 5.1% MoO_3. The T_{max} values for the second peak above 0.4% MoO_3 shift to higher temperature (830°C) and become constant above 3.3% MoO_3 (Figure 6.2). The TPR profile for 9.5% MoO_3 sample shows an additional peak on the high-temperature side of the first reduction peak; this occurs at about the same temperature as the shoulder on the low-temperature side of the first reduction peak in pure MoO_3 (Figure 6.1). It is clear that the first reduction step

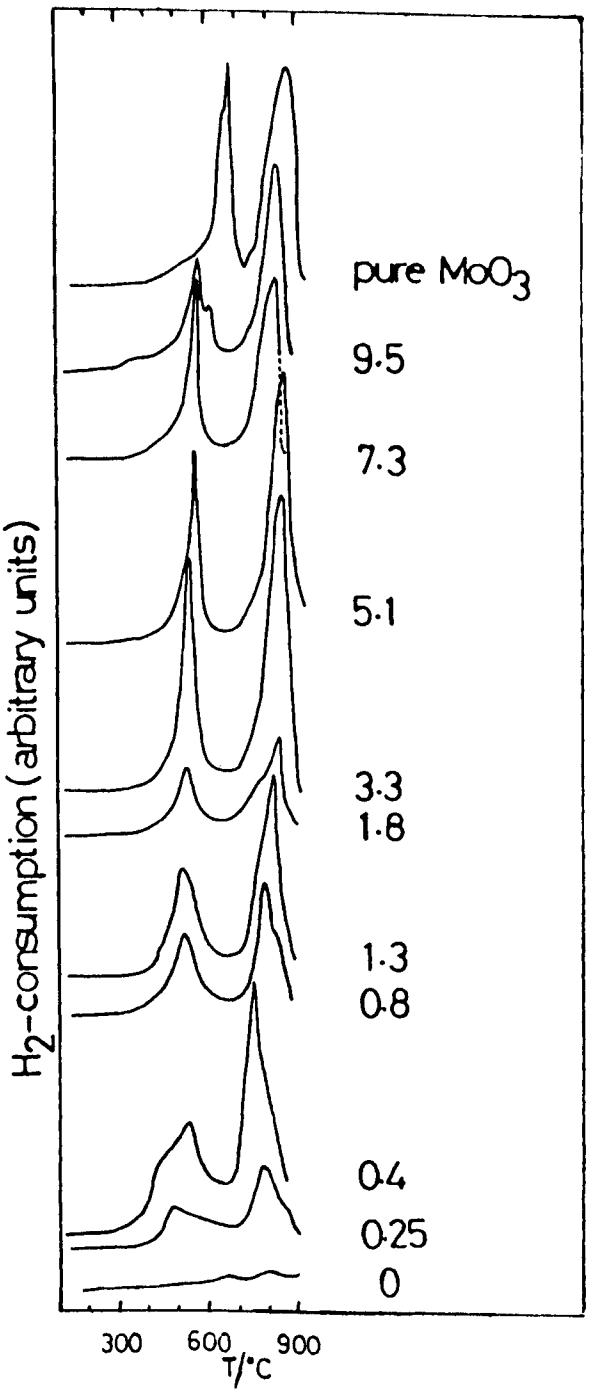

Figure 6.1 TPR profiles for catalysts prepared by aqueous impregnation of anatase CLD 782, and for the support and for pure MoO_3. The wt.% MoO_3 is given for each curve.

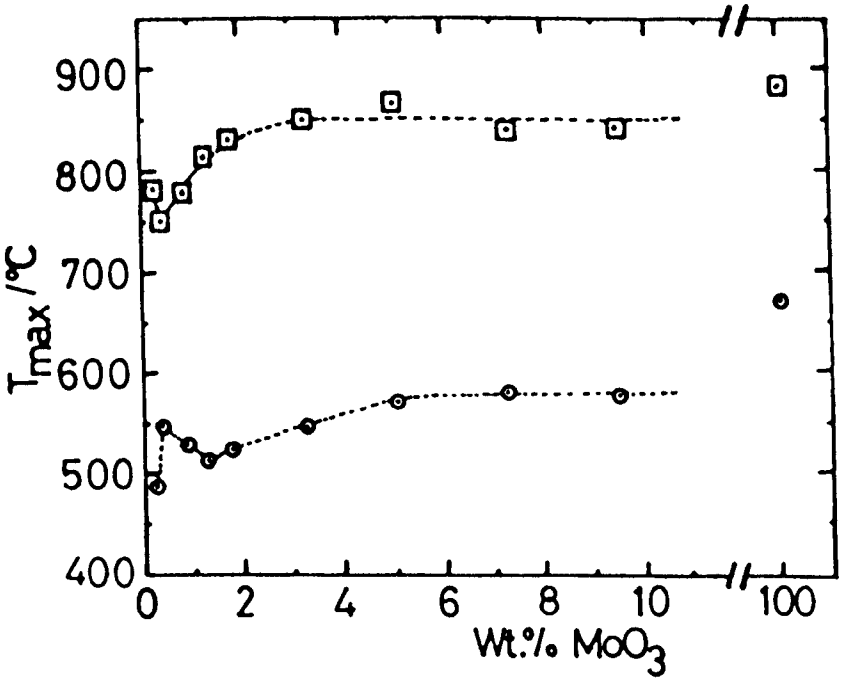

Figure 6.2 Dependence of T_{max} on MoO_3 content for catalysts prepared by aqueous impregnation of anatase CLD 782 and for pure MoO_3. Circles, first peak; squares, second peak.

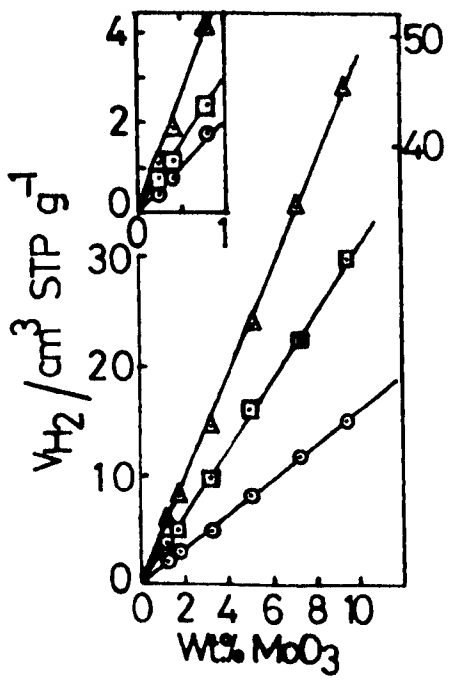

Figure 6.3 Dependence of volume of H_2 consumed in TPR on MoO_3 content for catalysts shown in Fig. 6.1. Symbols as before; triangle represent total H_2 volume.

for MoO_x species on the support occurs at a lower temperature than for pure MoO_3, although the second stage takes place at about the same temperature in each case (Figures 6.1 and 6.2). The quantity of H_2 consumed is accurately proportional to the MoO_3 content (Figure 6.3) and corresponds to that required for the reduction of Mo(VI) to Mo(0) in two steps with the ratio being almost exactly 1:2, i.e. $MoO_3 \rightarrow MoO_2$ and $MoO_2 \rightarrow Mo$.

Laser Raman spectroscopy

Figure 6.4 shows the Raman spectra for MoO_x/TiO_2 catalysts as well as for the support and for pure MoO_3. The TiO_2 gives a number of relatively intense bands (anatase: 640, 515 and 395 cm^{-1}). Bands at 998, 821 and 668 cm^{-1} in pure MoO_3 were readily detectable (1).

With the supported MoO_x catalysts, however, no significant bands were observed due to MoO_x species at MoO_3 contents of 0.8% or below. The anatase phase of the TiO_2 support has a weak second-order feature at 795 cm^{-1} (1).

At 1.3% MoO_3 catalyst, there is a small band at 982 cm^{-1} and a shoulder on the low-frequency side at 972 cm^{-1}. At 1.8% MoO_3, the intensity of the band at 982 cm^{-1} increases and the shoulder at 972 cm^{-1} remains constant while a band at 821 cm^{-1} and a shoulder at 996 cm^{-1} appear (due to crystalline MoO_3). Above 1.8 wt.% MoO_3, the intensity of the bands at 821, 982 and 996 cm^{-1} increase, while at 5.1% MoO_3 the band at 996 cm^{-1} increases at the expense of the band at 982 cm^{-1} (Figure 6.4). This latter band becomes a shoulder at 9.5% MoO_3 and the shoulder at 972 cm^{-1} disappears at 7.3%

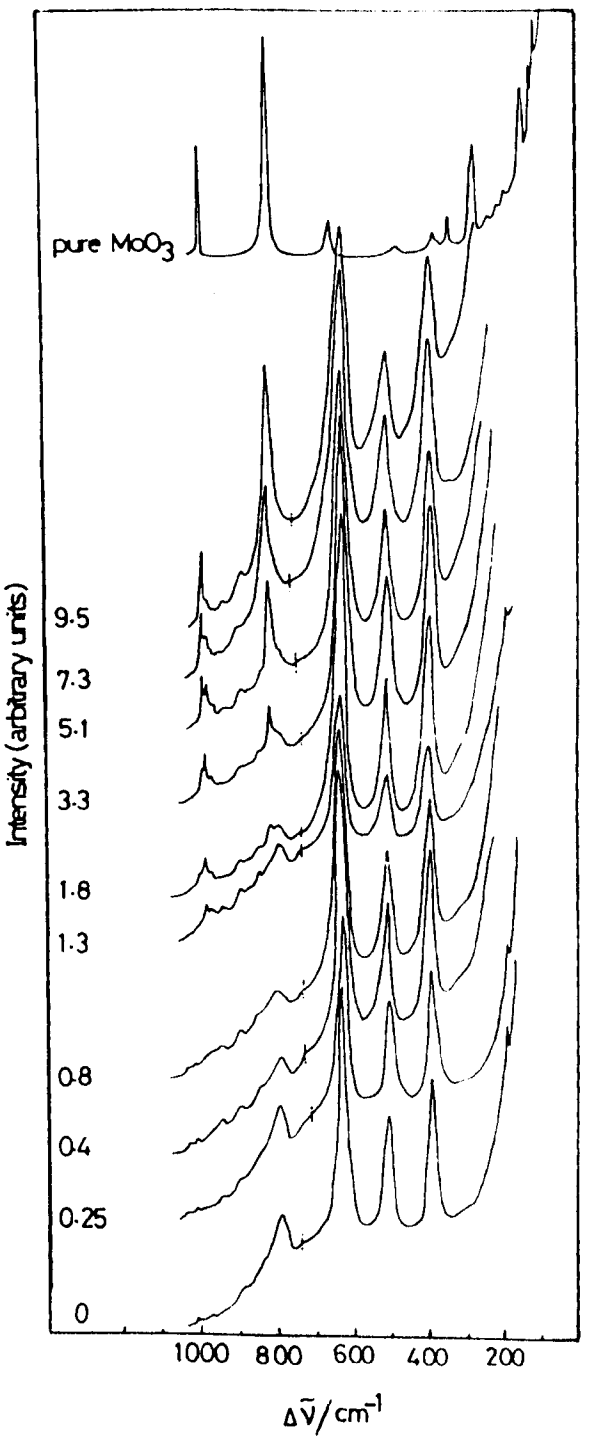

Figure 6.4 Raman spectra of MoO_x/TiO_2(CLD 782) catalysts made by aqueous impregnation of anatase CLD 782, and for the support and for pure MoO_3. The wt.% MoO_3 is given for each spectrum.

MoO_3. The intensity of the band of the support at 640 cm^{-1} decreases with increasing Mo content due to the change in the colour of the catalyst. Figure 6.5 shows the variation of the intensity of the bands 640, 821, 972, 982 and 996 cm^{-1} with MoO_3 content.

XPS

Figure 6.6 shows the XP spectra corresponding to Mo 3d levels of Mo and Ti 2p levels of Ti for the same series of cataysts. The XP spectra of the support and pure MoO_3 are also included in Figure 6.6 for comparison. In general, the binding energies of the Mo $3d_{3/2}$ and Mo $3d_{5/2}$ levels in all samples are observed at 235.0 $\pm$ 0.2 and 231.8 $\pm$ 0.3 eV, respectively; these values are similar to the values of pure MoO_3 (235.1 and 232.2 eV) (Table 6.1) (2). This indicates the presence of only Mo(VI) in the calcined samples. The binding energy values of C 1s electrons in the catalysts and in TiO_2 are 283.9 $\pm$ 0.3 and 284.4 eV, respectively (Table 6.1). Figure 6.7 shows the Mo/Ti intensity ratio for the catalysts in Figure 6.6 (see the calculation in Section 2.2.5, Chapter 2) as a function of the MoO_3 content. The ratio initially increases in proportion to the MoO_3 content, but the curve deviates above 1.0 wt.% MoO_3. This value is similar to the experimental monolayer capacity which was given by the $MoOCl_4$ method (Section 3.6.2 of Chapter 3). This change in the slope may signal the end of the monolayer region.

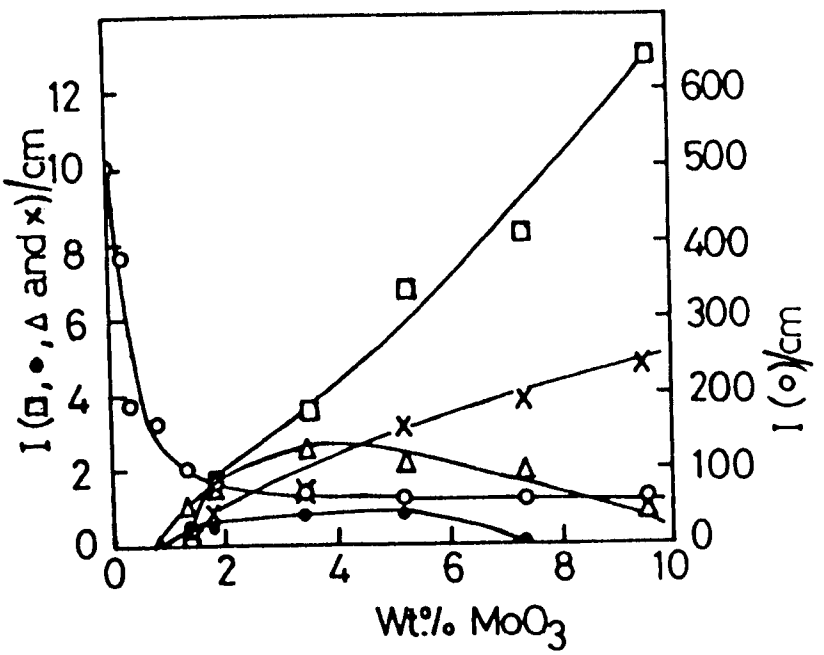

Figure 6.5 Variation in Raman intensities of MoO_x/TiO_2(CLD 782) catalysts with Mo content. Band frequencies are 821(□), 972(●), 982(Δ), 996(X) and 640(○) cm^{-1}.

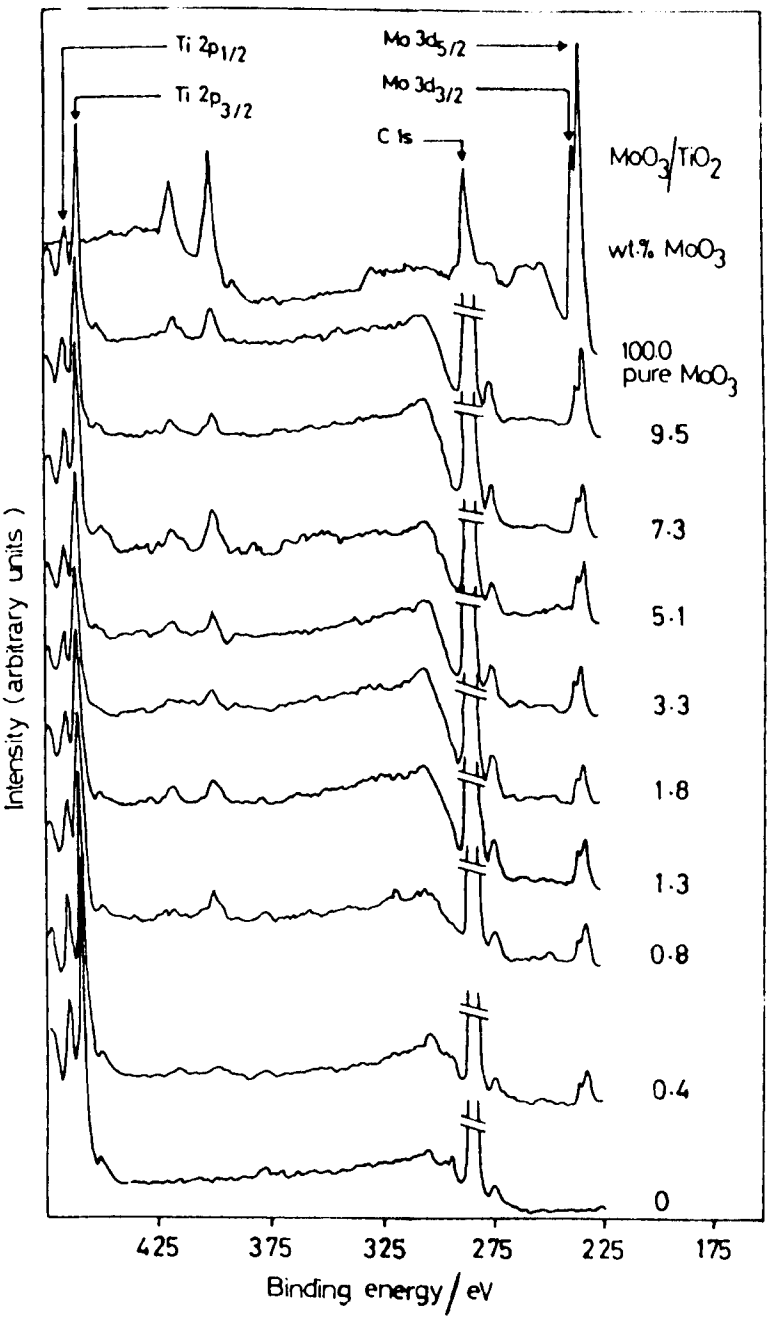

Figure 6.6 XP spectra of MoO_x/TiO_2(CLD 782) catalysts made by aqueous impregnation of anatase CLD 782, and for the support and for pure MoO_3. The wt.% MoO_3 is given for each spectrum.

Table 6.1

XPS results of MoO_x/TiO_2(CLD 782) catalysts prepared by wet impregnation , TiO_2 and unsupported MoO_3.

wt.% MoO_3	sample preparation	Binding energy(FWHM) Mo $3d_{3/2}$	Mo $3d_{5/2}$	C 1s	Ti $2p_{1/2}$	FWHM(eV)[a] Ti $2p_{3/2}$
0.4	powd.,calc.	234.9(1.6)	231.4(1.9)	284.0(--)	464.1(2.4)	1.6
0.8	"	234.9(2.3)	231.7(1.9)	284.5(--)	464.1(2.4)	1.6
1.3	"	234.6(2.6)	231.3(2.4)	283.9(--)	463.9(2.7)	1.9
1.8	"	235.3(2.6)	231.6(2.4)	284.0(--)	464.1(2.4)	1.6
3.3	"	235.1(2.4)	231.7(2.6)	283.7(--)	464.1(2.4)	1.9
5.1	"	234.8(2.3)	232.1(2.0)	283.7(--)	464.1(2.6)	1.7
7.3	"	235.0(2.4)	231.9(2.4)	283.7(--)	464.0(2.6)	1.8
9.5	"	235.1(2.0)	232.1(2.2)	284.0(--)	464.1(2.6)	1.6
MoO_3[b]	powd.	235.1(1.8)	232.2(1.8)			
TiO_2[b]	"				464.1(2.6)	458.2(1.6)

FWHM = full width at half of the maximum height;

a = Binding energies of the catalysts were determined by referencing to the Ti $2p_{3/2}$ line at 458.5 eV;

b = Binding energies of the standard compounds were determined by referencing to the C 1s line at 284.6 eV.

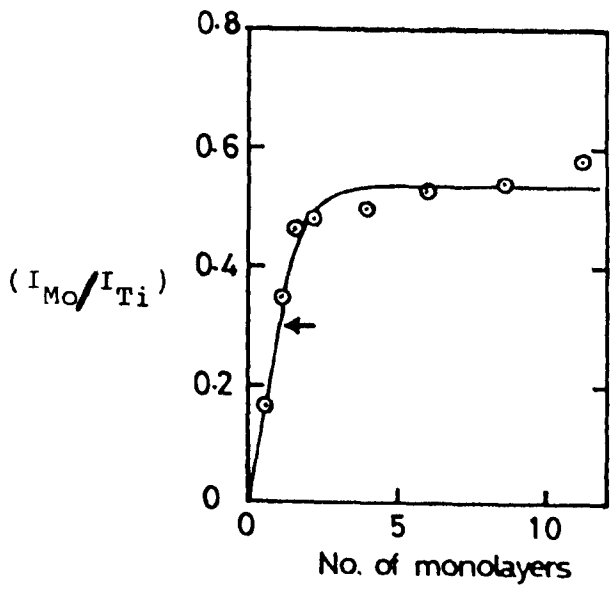

Figure 6.7 XPS intensity ratio (I_{Mo} / I_{Ti}) as a function of the number of monolayers for MoO_X/TiO_2 catalysts prepared by aqueous impregnation on anatase(CLD 782,unwashed). The curve is calculated as described in the Discussion, taking the fractions of surface covered by "towers" as 2.5%. $\bar{R}_{3,4}$ taken as 0.3 at the one monolayer point.

6.2.1.1.2 Oxidation of 1,3-butadiene

The MoO_x/TiO_2 catalysts were tested using this reaction at 285 - 385°C. Figure 6.8 shows the percentage conversion of butadiene (Conv.%), selectivity to maleic anhydride (S_{MA}%) and selectivity to carbon oxides (S_{CO_x}%) as a function of temperature for the catalyst containing 9.5% MoO_3. The value of S_{MA}% increases gradually with temperature up to a maximum (20%) at 335°C, thereafter remaining constant. Conversion increases with temperature. Figure 6.9 shows Conv.%, S_{MA}% and S_{CO_x}% as a function of the MoO_3 content at 350°C. S_{MA}% increases gradually with MoO_3 content up to a maximum (20%) at 5.0% MoO_3. After this, the S_{MA}% remains approximately the same. Conversion increases gradually with the MoO_3 content. The same phenomena were found at 340 and 360°C. Figure 6.10 shows the rate of butadiene removal (r_B), the rate of formation of maleic anhydride (r_{MA}) and the rate of formation of carbon oxides (r_{CO_x}) as a function of MoO_3 content. The values of r_B and r_{CO_x} are almost constant up to 5.3% MoO_3 (5 monolayers), then increase with MoO_3 content. The value of r_{MA} increases gradually with MoO_3 content. Figure 6.11 shows the plots of $\ln(r_B, r_{MA}$ and $r_{CO_x})$ versus 1/T for the catalyst containing 9.5% MoO_3 from which the activation energies (E_B, E_{MA} and E_{CO_x}) are derived. Table 6.2 shows E_B, E_{MA} and E_{CO_x} and the corresponding values of lnA for the same catalysts that are shown in Figure 6.9. Figure 6.12 shows E_B, E_{MA} and E_{CO_x} (Table 6.2) as a function of the MoO_3 content. There is little change in E_B as the MoO_3 concentration is increased. E_{CO_x} mimics the curve for E_B. The value of E_{MA} initially

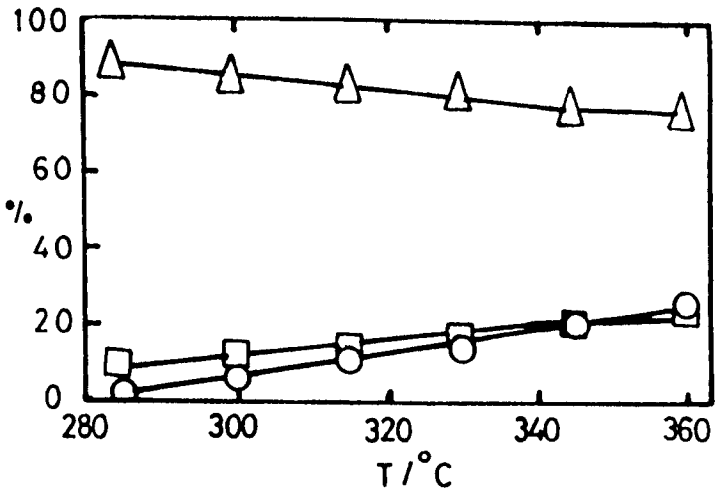

Figure 6.8 Oxidation of 1,3-butadiene on MoO_x/TiO_2(CLD 782,unwashed) catalyst containing 9.5% MoO_3 as a function of temperature: ○, 1,3-butadiene conv.; □, S_{MA}; △, S_{CO_x}.

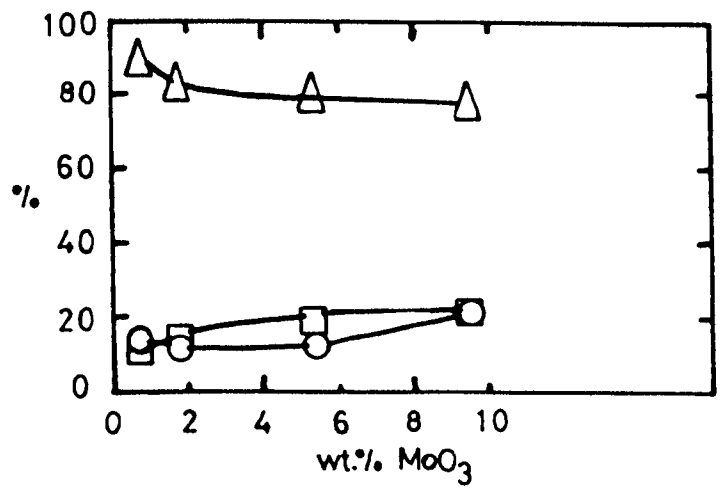

Figure 6.9 Oxidation of 1,3-butadiene on MoO_x/TiO_2(CLD 782,unwashed) catalysts at 350°C as a function of MoO_3 content: ○, 1,3-butadiene conv.; □, S_{MA}; △, S_{CO_x}.

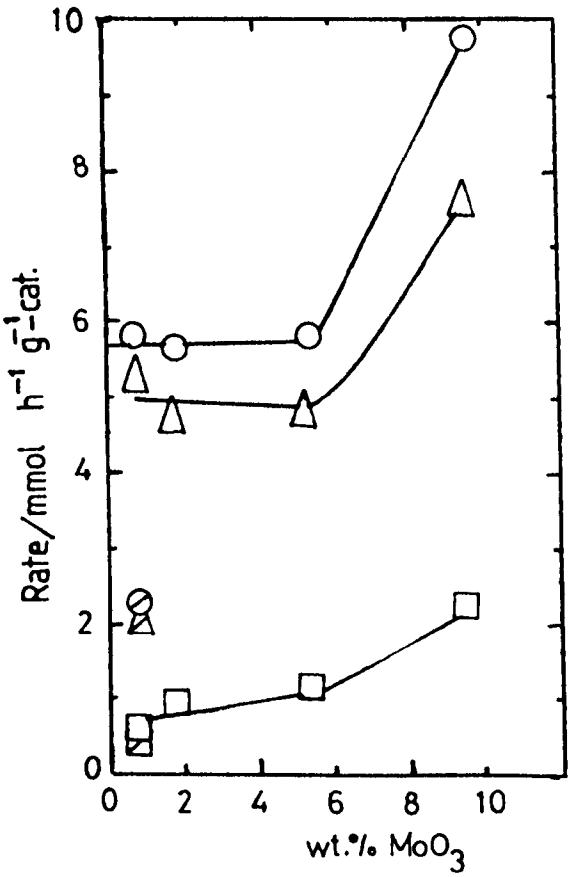

Figure 6.10 The rate for oxidation of 1,3-butadiene (r_B, r_{MA} and R_{CO_x}) at 350°C as a function of the MoO_3 content: ○, r_B; □, r_{MA}; △, r_{CO_x}. ⊘, r_B; ⊠, r_{MA}; ⊿, r_{CO_x}: for MoO_x/TiO_2(CLD 782,unwashed) monolayer catalyst prepared by $MoOCl_4$ method.

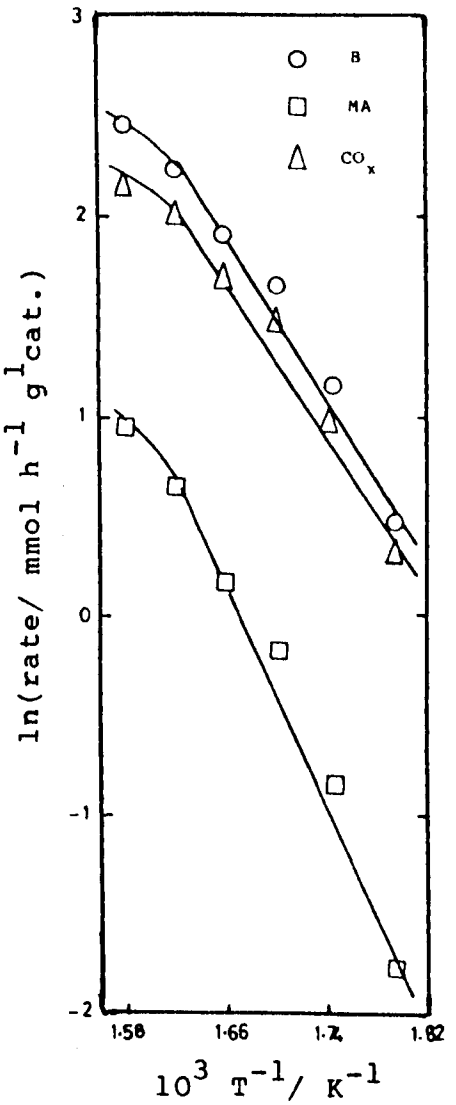

Figure 6.11 ln(rate) versus 1/T for MoO_x/TiO_2(CLD 782,unwashed) catalyst containing 9.5% MoO_3 prepared by the wet impregnation method, catalyzed oxidation of 1,3-butadiene.

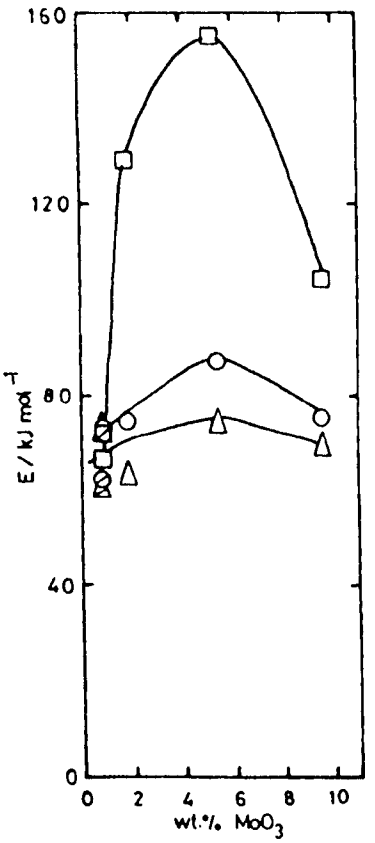

Figure 6.12 E_B(○), E_{MA}(□) and E_{CO_x}(△) as a function of MoO_3 content for samples showing in Figure 6.9. E_B(⊖), E_{MA}(▨) and E_{CO_x}(▲) for MoO_x/TiO_2(CLD 782,unwashed) monolayer catalyst.

increases sharply with MoO_3 content, passing through a maximum at 5.0% MoO_3, then falls sharply with MoO_3 content.

Table 6.2

The Arrhenius parameters of MoO_x/TiO_2 (CLD 782) catalysts, prepared by wet impregnation method, in the catalyzed oxidation of 1,3-butadiene.

wt.% MoO_3	E_B[1]	lnA[2]	c.c.	E_{MA}[1]	lnA[2]	c.c.	E_{CO_x}[1]	lnA[2]	c.c.
0.8	73.6	16.0	0.917	67.3	12.4	0.972	74.0	16.0	0.911
1.8	74.5	16.1	0.989	130.1	25.0	0.987	63.2	13.7	0.986
5.3	87.4	18.5	0.987	154.3	29.8	0.991	75.3	15.9	0.979
9.5	76.1	17.0	0.981	104.1	20.9	0.986	70.7	15.7	0.978

1 = E/kJ mol^{-1};

2 = ln(A/mmol h^{-1} g^{-1}-cat.).

6.2.1.2 MoO_x/TiO_2 catalyst prepared by the $MoOCl_4$ method

The MoO_x/TiO_2 monolayer catalyst was prepared as described in Section 3.6.2, Chapter 3 and contained 0.8% MoO_3.

6.2.1.2.1 Characterization

The MoO_x/TiO_2 monolayer catalyst was characterized with TPR and Laser Raman spectroscopy.

Figure 6.13A shows the TPR profile of MoO_x/TiO_2 monolayer catalyst. In Table 6.3 are shown the values of T_{max} and of V_{H_2} consumed during the reduction of the catalyst.

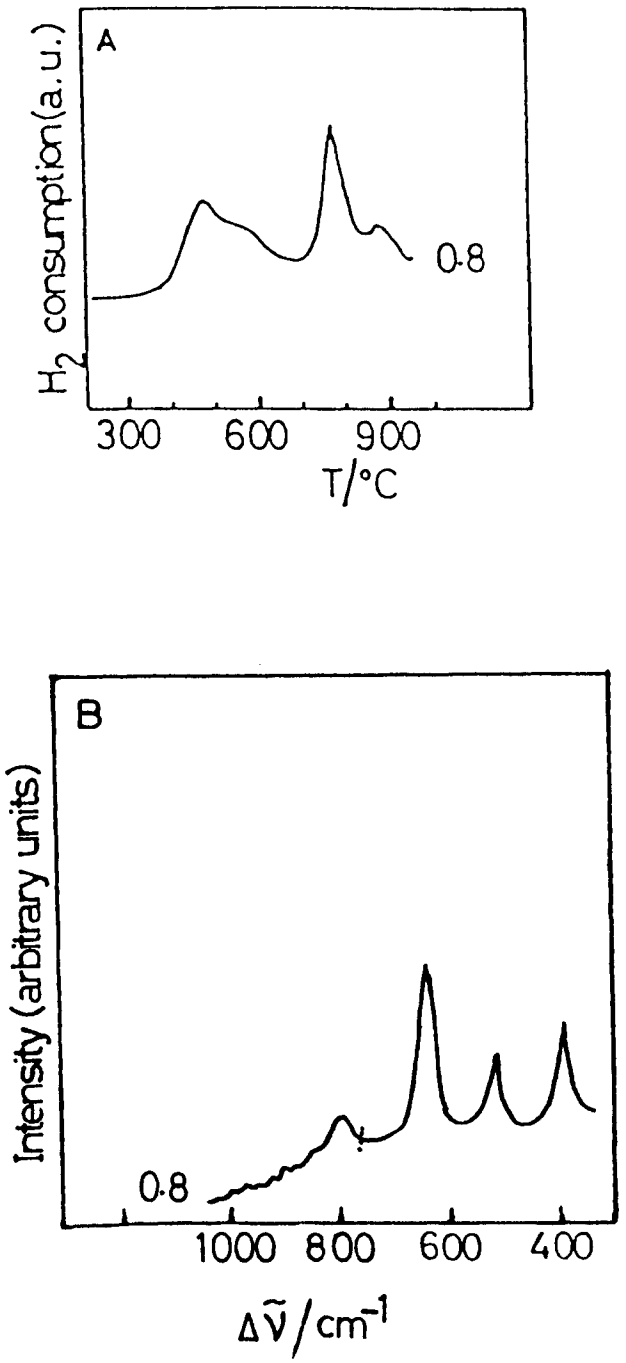

Figure 6.13 TPR profile (A) and Raman spectrum (B) for the MoO_x/TiO_2(CLD 782,unwashed) monolayer catalyst prepared by the grafting method ($MoOCl_4$ method).

Table 6.3

TPR parameters of MoO_x/TiO_2 monolayer catalyst (0.8% MoO_3).

$T_{max}1/^oC$	$T_{max}2/^oC$	$T_{max}3/^oC$	V_{H2} cm^3 STP.g^{-1}cat.
473	broad shoulder 586	770	3.75

The peak at 880°C is due to partial reduction of the support. The quantity of H_2 consumed corresponds to that required for reduction of Mo(VI) to Mo(0). Figure 6.13B shows the Raman spectrum for MoO_x/TiO_2 monolayer catalyst and exhibits only bands due to the support.

6.2.1.2.2 Oxidation of 1,3-butadiene

The catalyst was tested in the temperature range 335 - 439 °C. The value of S_{MA}% passed through a maximum (25%) at 410°C and 17% conversion. The values of r_B, r_{MA} and r_{CO_x} for this catalyst are shown in Figure 6.10, Section 6.2.1.1.2. Values of r_B and r_{CO_x} are lower than for the 0.8% MoO_3 catalyst prepared by wet impregnation, while values of r_{MA} are nearly the same. Figure 6.14 shows the plots of ln(r_B, r_{MA} and r_{CO_x}) versus 1/T which afford E_B, E_{MA} and E_{CO_x}. Table 6.4 shows E_B, E_{MA} and E_{CO_x} and the corresponding values of ln A. The values of E_B, E_{MA} and E_{CO_x} are shown in Figure 6.12. Figure 6.12 shows that E_B, E_{MA} and E_{CO_x} values are nearly the same for the monolayer catalyst and the 0.8% MoO_3 catalyst prepared by the impregnation method.

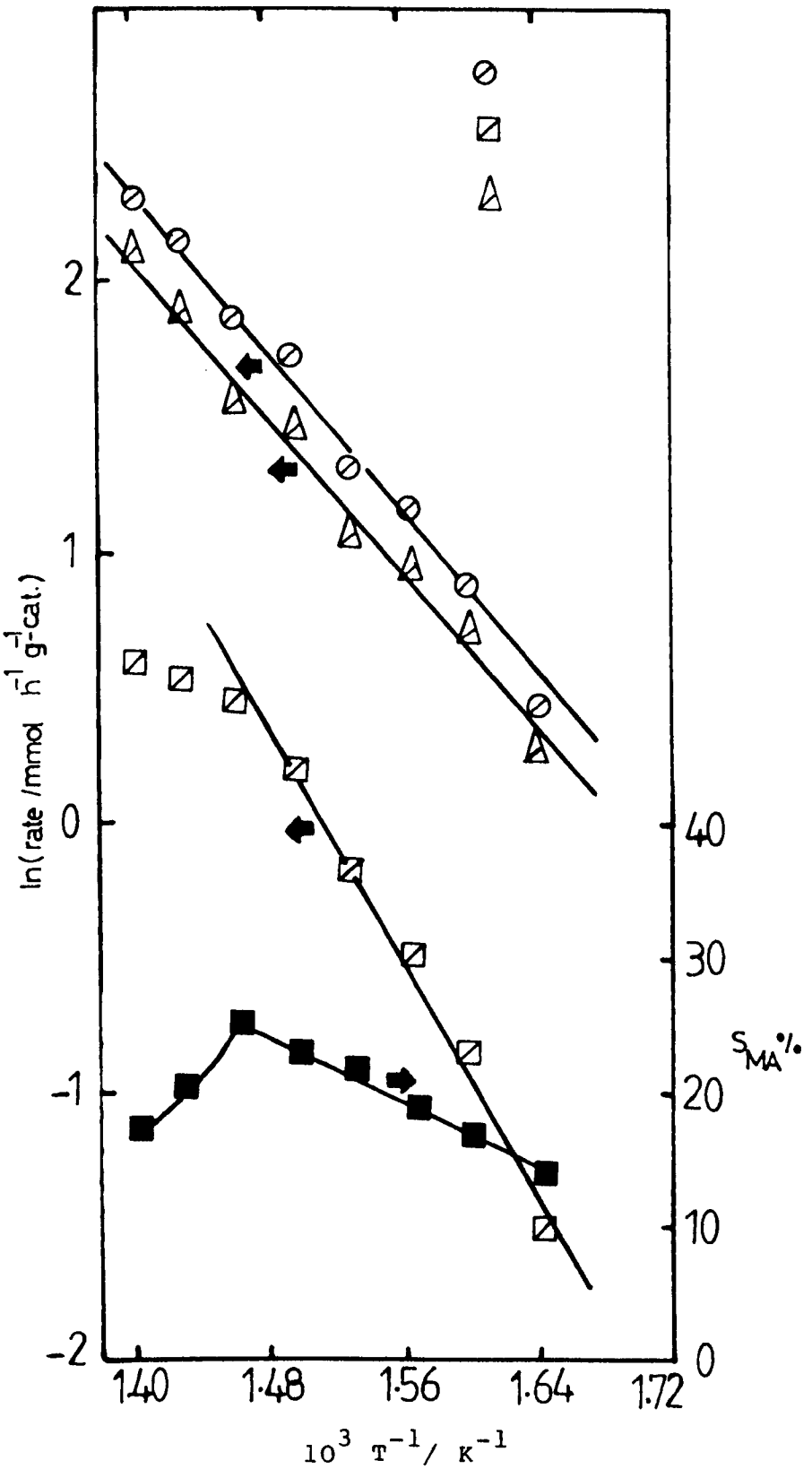

Figure 6.14 ln(rate) versus 1/T for MoO_x/TiO_2(CLD 782,unwashed) monolayer catalyst, prepared by the grafting method ($MoOCl_4$ method), catalyzed oxidation of 1,3-butadiene. Also shown S_{MA}%(■) versus 1/T.

Table 6.4

The Arrhenius parameters of MoO_X/TiO_2(CLD 782) monolayer catalyst prepared by the grafting method ($MoOCl_4$ method) catalyzed oxidation of 1,3-butadiene.

E_B[1]	lnA[2]	c.c.	E_{MA}[1]	lnA[2]	c.c.	E_{CO_X}[1]	lnA[2]	c.c.
62.7	13.0	0.996	72.4	13.1	0.972	60.6	12.4	0.995

1 = E/kJ mol^{-1};

2 = ln(A/mmol h^{-1} $g\text{-cat.}^{-1}$).

6.2.2 MoO_X/TiO_2(P-25) catalyst

A MoO_X/TiO_2(P-25) monolayer catalyst was prepared using TiO_2(P-25), 76% anatase, as the support. The support contains Al_2O_3 and SiO_2 as impurities (see Table 3.1, Chapter 3).

6.2.2.1 MoO_X/TiO_2(P-25) catalyst prepared by the $MoOCl_4$ method

The MoO_X/TiO_2(P-25) monolayer catalyst was prepared as described in Section 3.6.2, Chapter 3, and contained 4.1% MoO_3.

6.2.2.1.1 Characterization

The MoO_X/TiO_2(P-25) monolayer catalyst was characterized with TPR and Laser Raman spectroscopy.

Figure 6.15A shows the TPR profile of the catalyst. In Table 6.5 are shown the values of T_{max} and of V_{H_2} consumed during reduction of the catalyst.

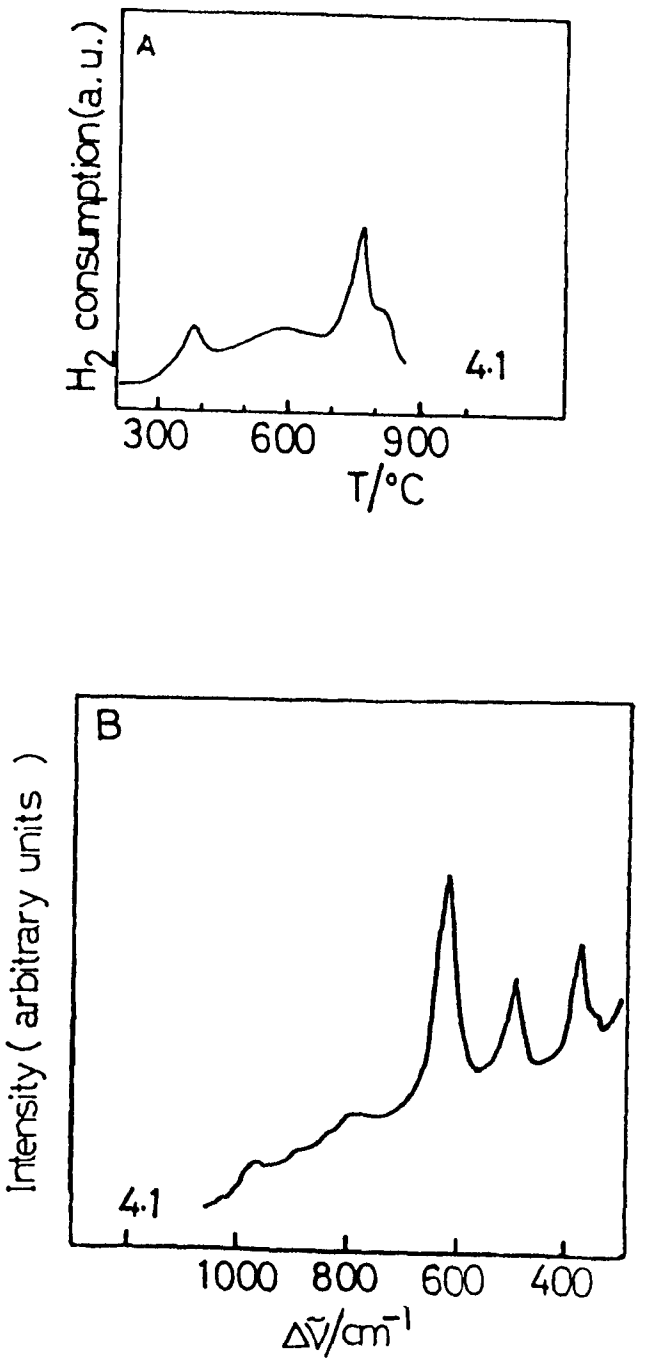

Figure 6.15 TPR profile (A) and Raman spectrum (B) for the MoO_x/TiO_2(P-25) monolayer catalyst prepared by the grafting method ($MoOCl_4$ method).

Table 6.5

TPR parameters of MoO_x/TiO_2(P-25) monolayer catalyst (4.1% MoO_3).

$T_{max}1/^oC$	$T_{max}2/^oC$	$T_{max}/^oC$	V_{H_2} cm^3 STP.g^{-1}-cat.
389	broad peak 470 - 650	763	18.58

The shoulder at 818°C is due to partial reduction of the support. The quantity of H_2 consumed corresponds to that required for reduction of Mo(VI) to Mo(0). Figure 6.15B shows the Raman spectrum of the catalyst and exhibits only bands due to the support.

6.3 Discussion

Characteristics of the oxide monolayer

The structure of the MoO_x monolayer catalyst has been shown in Section 3.6.2, Chapter 3. The structure suggested depends on theoretical and experimental calculations (see Section 3.6.2, Chapter 3). For the purpose of the following discussion, the structure of MoO_x monolayer species is reproduced below:

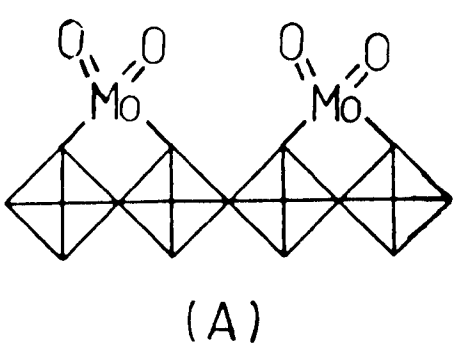

(A)

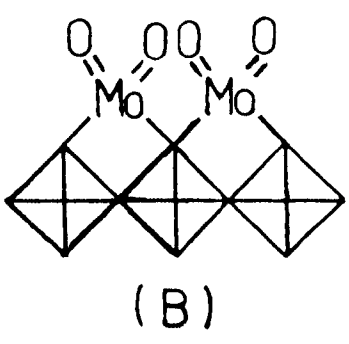

(B)

Reduction of the MoO_x monolayer species on low-area anatase proceeds in two well-defined steps, through Mo(IV) to Mo(0) (Figures 6.1 and 6.3). The broad peak shapes and the variability of T_{max} in this region (Figure 6.2) are probably caused by the P and K impurities (3). Similar effects have also been seen in the VO_x/TiO_2 system but are eliminated by washing the support before use (see Chapter 4)(4,5). The monolayer Mo catalyst made by the $MoOCl_4$ method on the same low area anatase support (Figure 6.13A) shows a similar TPR profile to that of the materials made by impregnation at an MoO_3 content of 0.25% (Figure 6.1). The MoO_x/TiO_2(P-25) monolyer catalyst however also exhibits a similar TPR profile (Figure 6.15A), with a first reduction step at only 390°C. No significant Raman bands due to MoO_3 were detected in this region (i.e. monolayer region)(see Figures 6.4, 6.13B and 6.15B). van Hengstum (6) investigated by Raman spectroscopy and thermogravimetric analysis (TGA) an MoO_x/TiO_2(P-25) monolayer catalyst which was prepared by adsorption of ammonium molybdate from an acidic solution. He reported that the TGA results showed MoO_x/TiO_2 to be reduced in two steps to Mo(0) while the Raman spectrum showed a relatively broad, weak Raman band between 970 and 980 cm^{-1}, which indicated that the supported species is not isostructural with the species present in the bulk oxide. The broadening of the band was attributed to the presence of a crystallographically ill-defined Mo oxide complex on the surface of the TiO_2 support.

The Mo/Ti XPS ratio increases linearly with Mo content below the monolayer point (Figure 6.7). Similar results have been reported with the MoO_3/Al_2O_3 (7), WO_x/TiO_2 (8), VO_x/TiO_2 (Chapter 4)(9), and VO_x/Al_2O_3 systems (9).

The supramonolayer region

In the MoO_x/TiO_2(low area anatase) system, with increasing Mo content, the two stages of the reduction continue to be well-defined, showing that MoO_2 is a stable intermediate in the supramonolayer region, although T_{max} values for both stages increase in the one to four monolayer region (Figures 6.1 and 6.2) and then remain constant, although T_{max} for the first stage is always significantly lower than in pure MoO_3. The Raman intensity results (Figure 6.5) provide additional evidence for two distinguishable phases above the monolayer point. The Raman intensity measurements (Figure 6.5) however give clear evidence for an intermediate phase with which are associated the bands at 972 and 982 cm^{-1}, and probably due to octahedral species (10). The intensities of these bands change similarly and pass through a maximum at about 4% MoO_3. The advent of this intermediate phase of "disordered MoO_3" is rapidly succeeded by the formation of a "paracrystalline MoO_3" that gives rise to Raman bands at 821 and 996 cm^{-1} (Figure 6.5) and thus strongly resembles bulk MoO_3.

The variation in the XPS intensity ratio for this system (Figure 6.7) strongly suggests a change in structure above the monolayer point. The TPR, Raman spectroscopy and XPS results have led to the model which is suggested in Figure 6.16. A similar model has been proposed for the VO_x/TiO_2 system (Figure 4.87 , Chapter 4). The disordered MoO_3 and paracrystalline MoO_3 exist as patches on a limited part of the monolayer-coated surface, growing finally into "towers" (Figure 6.16). The same simple theoretical model which was used in the VO_x/TiO_2 system (Chapter 4) is used here, based

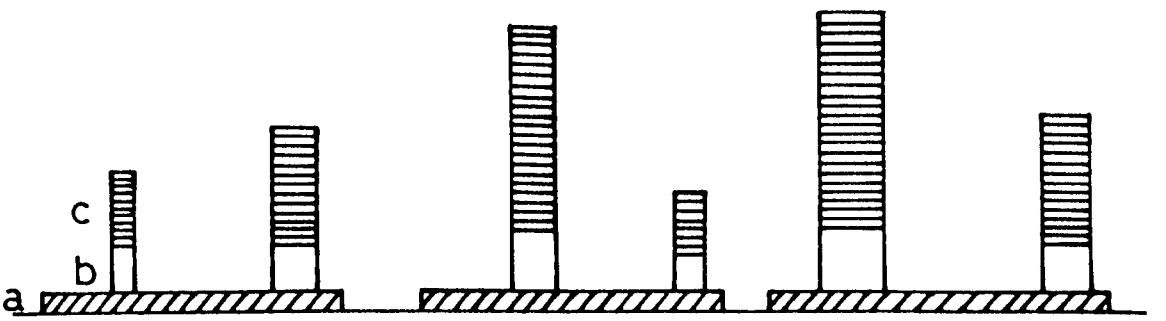

Figure 6.16 Model of MoO_3 on TiO_2 showing the different phases which are formed as a function of MoO_3:

a) up to one monolayer (surface MoO_x complexes);

b) two-four monolayers (disordered MoO_3); and

c) above four monolayers (paracrystalline MoO_3).

on the model shown in Figure 6.16, to calculate the surface coverage by "towers". The escape depths of the Ti 2p and Mo 3d electrons, and the fraction of surface covered by the "towers", are the only adjustable parameters. The escape depths of the Ti2p and Mo 3d electrons are taken as respectively 15 and 27 ^{o}A: the curve shown in Figure 6.7 is that calculated for a surface coverage by "towers" of 2.5%. This fits the experimental points well up to about the ten monolayer point, but deviation is observed at higher MoO_3 contents, probably because more of the surface is covered by MoO_3 microcrystals in this region. The same theoretical model has been used for both the MoO_x/TiO_2 and WO_x/TiO_2 systems (8), and fitted well with the experimental results.

Comparison with MoO_x/Al_2O_3

There have been a number of studies of this system. No attempt is made here to review the estimate of monolayer capacity, but it is worth noting that several TPR studies have been published, most of which show that the monolayer MoO_x surface species are reduced in one step to Mo metal (at 610 - 880^{o}C) and that the other phase (bilayer/multilayer) formed at higher MoO_3 contents is reduced in one step to Mo metal at lower temperatures (between 380 and 460^{o}C)(11,12,13). Caceres et al.(14) found that supported MoO_3 is reduced first to MoO_2 (at 415-590^{o}C) and then to Mo metal (between 740-770^{o}C). TPR profiles for MoO_3/Al_2O_3 catalysts heated to 730^{o}C show just one peak at 500-520^{o}C which is due to the reduction of Mo(VI) to Mo(IV) (15). The first step on MoO_3/Al_2O_3 seems somewhat similar to MoO_3/TiO_2.

Oxidation of 1,3-butadiene

The analysis system was capable of detecting unreacted butadiene and the main selective oxidation product maleic anhydride(MA), but was unable to detect other oxidation products. In calculating the selectivities it was assumed that only CO and CO_2 were the other oxidation products.

TiO_2 alone had a negligible activity for the butadiene oxidation. The results in Figures 6.9 and 6.10 may suggest that the activity is principally due to MoO_x monolayer species and that little contribution is made by the disordered or paracrystalline particales of MoO_3.

The MoO_x monolayer catalyst which was made by the $MoOCl_4$ method shows low activity but higher selectivity at 350^oC than the catalyst with the same loading prepared by wet impregnation (see Figures 6.9 and 6.14). In general, the low activities and low selectivities for these catalysts are strongly supported by the TPR results (Figure 6.2) which show the reduction of MoO_x species occurs at higher temperatures (lower reducibility)

According to the oxidation-reduction mechanism generally applied in oxidation catalysis, lattice oxygen is used in oxidation reactions. It has already been shown that the selectivity to MA formation is strongly affected by the kind of oxygen species formed on the molybdenum ion and that double bond type lattice oxygen $Mo^{6+}{=}O$ plays an important role as a selective oxygen species. Mo^{5+} was also found to be an active site for the oxidation (16). Due to the importance of this type of oxygen , it can be expected that the activity 'and/or' selectivity of a catalyst in an oxidation reaction is related to the energy of oxygen

bonding or the reducibility (i.e. the ease of the oxygen removal) of the catalyst. This kind of relationship has indeed been established for the oxidation of CO (17) and methanol (18,19).

VO_X catalysts have been prepared by different methods and by using a similar type of TiO_2 support (Chapter 4). These catalysts showed high activities and selectivities in the oxidation of butadiene, and easier reducibility (Section 4.2.2, Chapter 4) than MoO_X/TiO_2 catalysts. van Hengstum (6) reported that a VO_X monolayer catalyst supported on TiO_2(P-25) is more active and selective than MoO_X monolayer catalyst in the oxidation of toluene and o-xylene to benzoic acid and phthalic anhydride respectively. However, he found that the MoO_X catalyst was reduced more easily than the VO_X monolayer catalyst. Several other quite similar selectivities (40-50%) have been found when butadiene is oxidized to MA at 40-60% conversion by using Mo-Ti-O catalysts. These catalysts were prepared from $Ti(OH)_4$ and an aqueous solution of ammonium molybdate (16,20), while the others were prepared by mixing anatase with an aqueous solution containing molybdic acid and oxalic acid (21).

The TiO_2 support used in this work contained K and P as impurities. They may form some compounds with MoO_X species which may explain the low selectivities with these catalysts. For Mo catalysts, the formation of the bronzes decreased the effectiveness of the catalysts as was demonstrated for several alkali metals (22).

Figure 6.10 shows r_B and r_{CO_x} values are almost constant in the 1 to 5 monolayers range while r_{MA} is gradually

increased. Above 5 monolayers, the rates increase. Figure 7.12 shows that E_B and E_{CO_x} are nearly constant with MoO_3 content, while there is a larger change with E_{MA}, passing through maximum at 5.3% MoO_3.

Figure 6.17 shows the compensation effect plot for the Arrhenius parameters observed in this work relating to the butadiene removal and to the formation of products. Points for MA formation lie on one line as shown (line A), with the point for 9.5% MoO_3 above the line; this means its rate is greater than for others. Points for both butadiene removal and CO_x formation lie on another (higher activity) line (line B), but rather scattered. The MoO_x monolayer catalyst which was prepared by the $MoOCl_4$ method, shows activation energies similar to those for the impregnation catalyst (0.8% MoO_3) although the rates are lower (the ln A terms lower, but not for MA). This confirms the low activity of this catalyst. The slopes of the lines A and B correspond to isokinetic temperatures of 594.2 and 650.0 K respectively.

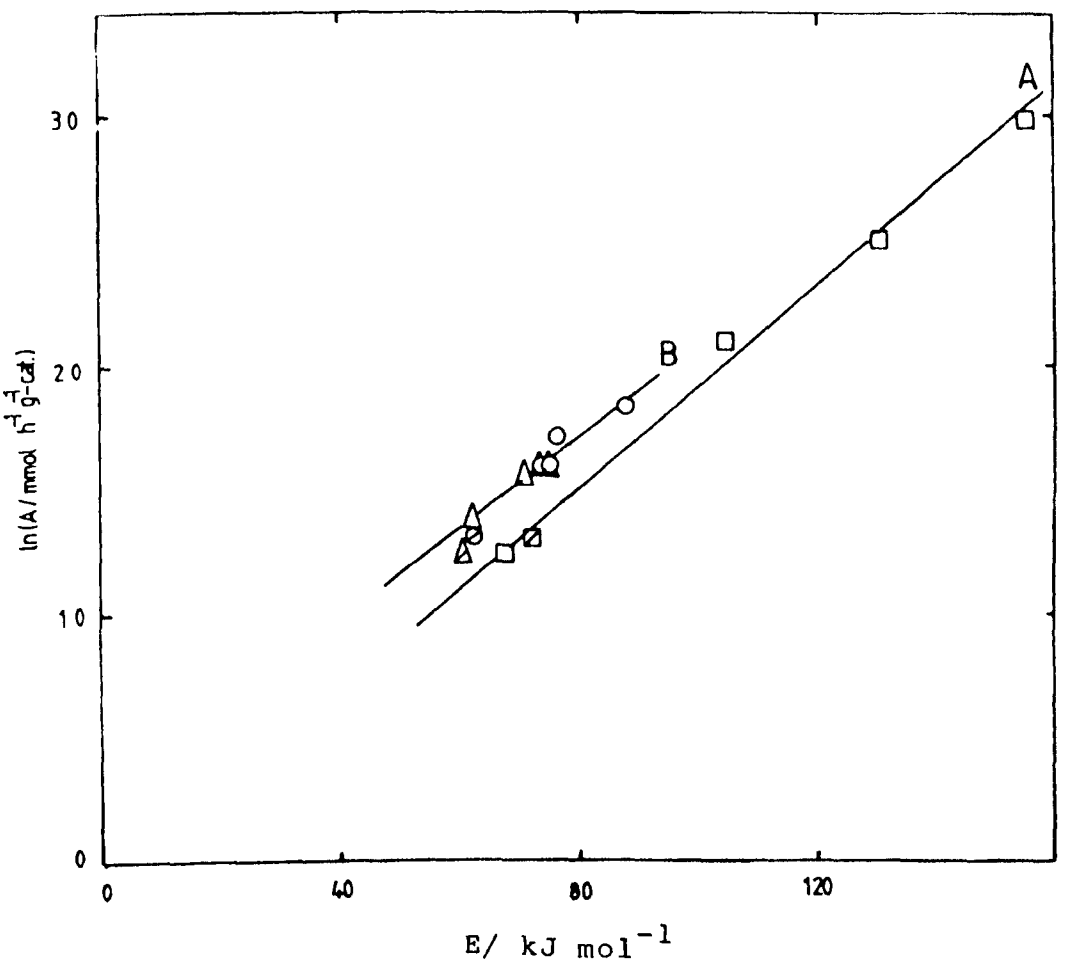

Figure 6.17 Compensation effect plot for the oxidation of 1,3-butadiene catalyzed by MoO_x/TiO_2(CLD 782,unwashed) catalysts prepared by the impregnation method. ○, B;□, MA; △,CO_x.⊘,⊠,◬ for monolayer catalyst prepared by $MoOCl_4$ method.

6.4 References

1. I.R. Beattie and T.R. Gilson, J. Chem. Soc. (A) 2322 (1969); Proc. Roy. Soc. London Ser. A, 307, 407 (1968).
2. D.S. Zingg, L.E. Makovsky, R.E. Tischer, F.R. Brown and D.M. Hercules, J. Phys. Chem., 84, 2898 (1980).
3. G.C. Bond and S. Flamerz, unpublished work.
4. G.C. Bond, J. Perez Zurita, S. Flamerz, P.J. Gellings, H. Bosch, J.G. van Ommen and B.J. Kip, Appl. Catal., 22, 361 (1986).
5. A.J. van Hengstum, J. Pranger, J.G. van Ommen and P.J. Gellings, Appl. Catal., 11, 317 (1984).
6. A.J. van Hengstum, Ph.D. Thesis, Twente University of Technology, Enschede, The Netherlands (1984).
7. P. Dufresne, E. Payen, J. Grimblot and J.P. Bonnelle, J. Phys. Chem., 85, 2344 (1981).
8. L. van Wijk, Dissertation, Brunel University, Uxbridge, United Kingdom (1985).
9. F.J. Gil-Llambías, A.M. Escudey, J.L.G. Fierro and A. López Agudo, J. Catal., 95, 520 (1986).
10. L. Wang and W.K. Hall, J. Catal., 66, 251 (1980).
11. R. Thomas, E.M. van Oers, V.H.J. de Beer, J. Medema and J.A. Moulijn, J. Catal., 76, 241 (1982).
12. R. Thomas, V.H.J. de Beer and J.A. Moulijn, Bull. Soc. Chim. Belg., 90, 1349 (1981).
13. P. Arnoldy, M.C. Franken, B. Scheffer and J.A. Moulijn, J. Catal., 96, 381 (1985).
14. C.V. Caceres, J.L.G. Fierro, A.L. Agudo, M.N. Blanco and H.J. Thomas, J. Catal., 95, 501 (1985).
15. R. Burch and A. Collins, Appl. Catal., 18, 389 (1985).

16. M. Akimoto and E. Echigoya, J. Catal., 29, 191 (1973).

17. F. Roozeboom, A.J. van Dillen, J.W. Geus and P.J. Gellings, Ind. Eng. Chem. Proc. Res. Dev., 20, 304 (1981).

18. F. Roozboom, P.D. Cordingly and P.J. Gellings, J. Catal., 68, 464 (1981).

19. G.K. Boreskov, Kinet. Katal., 14, 7 (1973).

20. M. Ai, Bull. Chem. Soc. Jap., 49, 1328 (1976).

21. D. Vanhove, S.R. Op, A. Fernandez and M. Blanchard, J. Catal., 57, 253 (1979).

22. A.A. Balandin and N.P. Sokolova, Probl. Kinet. Katal., 363 (1960).

CHAPTER 7

GENERAL DISCUSSION AND CONCLUSIONS

In this Chapter a general survey of the experimental results will be presented. As mentioned in the Introduction, the main objective of the work presented in this thesis was to collect knowledge about some aspects concerning the preparation and characterisation of the supported vanadium and molybdenum oxide catalysts for the selective oxidation of 1,3-butadiene and the decomposition of isopropanol, and the structural chemistry of these catalysts in relation to their catalytic behaviour.

It was shown that an oxidic support can be uniformly covered with the active phase without the formation of crystalline material by the reaction of metal oxychlorides or alkoxide with the surface hydroxyl groups of the support (Chapter 3). Strong indications for the presence of a monolayer were obtained from the XPS results and the catalytic measurements in the case of vanadium catalysts (Chapter 4) and from the XPS results in the case of molybdenum catalysts (Chapter 6). Neither laser Raman spectroscopy nor TPR could provide direct evidence for this. Aqueous impregnation and multiple treatments with $VOCl_3$ or $VO(O^iBu)_3$ methods were intended to produce more than one monolayer. These may lead to the formation of metal oxide crystallites.

Large effects of the impurities (phosphorus and potassium) on (or in) the TiO_2 support on the properties of the active phase were detected even when the impurities were present only in relatively small amounts (Chapters 4 and 5).

Potassium reacts with VO_x monolayer species forming potassium-containing vanadium oxide (see Structure D, Discussion Section, Chapter 4) which has low reducibility and low activity in the butadiene oxidation and isopropanol decomposition. Reaction of potassium-containing vanadium oxide with excess VO_x species forms another type of potassium-containing vanadium oxide which has a low amount of potassium and this compound has high reducibility. Increasing the amount of potassium forms more potassium-salt which strongly reduces the activity.

Phosphorus has no or only a slightly effect on the VO_x species. It may form the structure E with VO_x species (see Discussion Section, Chapter 4) because the chemistry of both are similar. Phosphorus increases the acidity of the catalyst. The effect of additives decreases with increasing the V_2O_5 loading.

Although the reducibility of an oxidic catalyst was an important parameter, it is certainly not the only factor determining its catalytic activity. Acidity or basicity of the catalyst surface strongly influences the adsorption and desorption of reactants and products, and consequently also the activity and selectivity of the reaction.

The results of this thesis show a general correlation between the catalytic and the chemical/physical properties of the catalysts.

Appendices

Appendix I

A. Vanadium content of the theoretical monolayer

A calculation of the theoretical monolayer is performed as follows. Assuming the monolayer to be composed of a two-dimensional array of V_2O_5 "molecules" similar to a lamella of the three-dimensional crystal.

Date:

Surface area of TiO_2 = $9.6\ m^2 g^{-1}$

Density of V_2O_5 = $3.36\ g\ cm^{-3}$

Molecular weight of V_2O_5 = $181.88\ g\ mol^{-1}$

* Surface occupied by one molecule of V_2O_5

$$\text{Density } (\rho) = \frac{\text{Mass}(M)}{\text{Volume}(V)}$$

$$V = \frac{M}{\rho}$$

$$V = \frac{181.88\ g\ mol^{-1}}{3.36\ g\ cm^{-3}} \times \frac{1\ mol}{6.02 \times 10^{23}\ molecule} \times \frac{1\ m^3}{10^6\ cm^3}$$

$$V = 8.99 \times 10^{-29}\ m^3/molecule$$

$$V = (Side)^3$$

$$Side(l) = V^{1/3}$$

$$l = 4.5 \times 10^{-10}\ m$$

Assuming V_2O_5 a cubic molecule:

$$Surface = l^2$$

$$Surface = 20.07 \times 10^{-20}\ m^2/molecule$$

* Number of molecules of V_2O_5 needed to cover the TiO_2 surface.

$$\text{No. of molecules} = 9.6\ m^2 g^{-1} \times \frac{\text{molecule}}{20.07 \times 10^{-20}\ m^2}$$

$$= 4.88 \times 10^{19}\ \text{molecule/g}$$

* Number of mol

$$\text{No. of mole} = 4.88 \times 10^{19} \text{ molecule/g} \times \frac{1 \text{ mol}}{6.02 \times 10^{23} \text{ molecule}}$$

$$= 8.11 \times 10^{-5} \text{ mol /g}$$

* Weight of V_2O_5

$$\text{wt.} = 8.11 \times 10^{-5} \text{ mol /g} \times \frac{181.88 \text{ g}}{1 \text{ mol}}$$

$$\text{wt.} = 1.48 \times 10^{-2} \text{ g/g}$$

* Wt.% of V_2O_5 for the monolayer

$$\text{wt.\%} = \frac{1.48 \times 10^{-2}}{1 + 1.48 \times 10^{-2}} \times 100$$

$$\text{wt.\%} = 1.45$$

B. Molybdenum content of the theoretical monolayer

A calculation of the theoretical monolayer is performed as follows.

Data:

Surface area of TiO_2 = $9.6 \text{ m}^2\text{g}^{-1}$

Density of MoO_3 = 4.69 g cm^{-3}

Molecular weight of MoO_3 = $143.94 \text{ g mol}^{-1}$

* Surface occupied by one molecule of MoO_3

$$V = \frac{M}{\rho}$$

$$V = \frac{143.94 \text{ g mol}^{-1}}{4.69 \text{ g cm}^{-3}} \times \frac{1 \text{ mol}}{6.02 \times 10^{23} \text{ molecule}} \times \frac{1 \text{ m}^3}{10^6 \text{ cm}^3}$$

$$= 5.096 \times 10^{-29} \text{ m}^3\text{/molecule}$$

$$l = V^{1/3}$$

$$l = 3.707 \times 10^{-10} \text{ m}$$

Assuming MoO_3 a cubic molecule:

Surface = l^2

Surface = 1.374×10^{-19} m^2/molecule

* Number of molecules of MoO_3 needed to cover the TiO_2 surface:

$$\text{No. of molecules} = 9.6\ m^2 g^{-1} \times \frac{\text{molecule}}{1.374 \times 10^{-19}\ m^2}$$

$$= 6.987 \times 10^{19}\ \text{molecule/g}$$

* Number of mol

$$\text{No. of mol} = 6.987 \times 10^{19}\ \text{molecule/g} \times \frac{1\ \text{mol}}{6.02 \times 10^{23}\ \text{molecule}}$$

$$= 1.16 \times 10^{-4}\ \text{mol /g}$$

* Weight of MoO_3

$$\text{wt.} = 1.16 \times 10^{-4}\ \text{mol /g} \times \frac{143.94\ \text{g}}{1\ \text{mol}}$$

$$= 1.67 \times 10^{-2}\ \text{g/g}$$

* Wt.% of MoO_3 for the monolayer

$$\text{wt.\%} = \frac{1.67 \times 10^{-2}}{1 + 1.67 \times 10^{-2}} \times 100$$

wt.% = 1.64

Appendix II

Monolayer capacity calculated from the number of OH groups nm^{-2} on the surface of TiO_2.

A. Vanadium oxide (VO_x)

The number of OH groups on the surface of TiO_2 corresponds to about 4.9 OH nm^{-2} or 4.9×10^{18} OH m^{-2}. For a 9.6 $m^2 g^{-1}$ TiO_2, there are $9.6 \times 4.9 \times 10^{18}$ surface OH groups g^{-1}. Assuming a surface Ti-OH:V ratio of unity, there are: $9.6 \times 4.9 \times 10^{18}$ V atoms g^{-1}.

$$1/2 \text{ Mol. wt. of } V_2O_5 = \frac{181.88 \text{ g mol}^{-1}}{2}$$

$$\text{wt.\% } V_2O_5 = \frac{9.6 \times 4.9 \times 10^{18}}{6.02 \times 10^{23}} \times \frac{181.88}{2} \times 100$$

$$= 0.71$$

B. Molybdenum oxide (MoO_X)

Assuming a surface Ti-OH:Mo ratio of unity, there are: $9.6 \times 4.9 \times 10^{18}$ Mo atoms g^{-1}

Mol. wt. of MoO_3 = 143.94 g mol^{-1}

$$\text{wt.\% } MoO_3 = \frac{9.6 \times 4.9 \times 10^{18}}{6.02 \times 10^{23}} \times 143.94 \times 100$$

$$= 1.12$$

Appendix III

Monolayer capacity calculated from the number of Ti atoms nm^{-2}:

A. Vanadium oxide (VO_X)

The density of Ti atoms on the (010) anatase surface corresponds to about 6.25 Ti nm^{-2} or 6.25×10^{18} Ti m^{-2}. For a 9.6 m^2g^{-1} TiO_2, there are $9.6 \times 6.25 \times 10^{18}$ surface Ti atoms g^{-1}. Assuming a surface Ti:V ratio of unity, there are: $9.6 \times 6.25 \times 10^{18}$ V atoms g^{-1}

$$1/2 \text{ Mol. wt. of } V_2O_5 = \frac{181.88 \text{ g mol}^{-1}}{2}$$

$$\text{wt.\% } V_2O_5 = \frac{9.6 \times 6.25 \times 10^{18}}{6.02 \times 10^{23}} \times \frac{181.88}{2} \times 100$$

$$= 0.91$$

B. Molybdenum oxide (MoO_X)

Assuming a surface Ti:Mo ratio of unity, there are: $9.6 \times 6.25 \times 10^{18}$ Mo atoms g^{-1}

Mol. wt. of MoO_3 = 143.94 g mol^{-1}

$$wt.\% \ MoO_3 = \frac{9.6 \times 6.25 \times 10^{18}}{6.02 \times 10^{23}} \times 143.94 \times 100$$

$$= 1.43$$

Appendix IV

XPS calculation

Let the fraction of the surface of the monolayer covered by the "towers" be given by x = 1/Y, where x represents the surface coverage by the layer in the tower, Y represents the number of layers in the tower. Let m denote the number of monolayer equivalents to which the V_2O_5 concentration corresponds. If all the "towers" are of uniform height, the number of layers n in each is given by

$$n = [(m - 1)/x] + 1$$

Thus for example if x = 0.25 and the V_2O_5 concentration corresponds to m = 2, the value of n is five, since the "tower" is formed above the monolayer (Figure 4.88). The expressions for the intensities of the emitted electrons as a function of x, n and d/λ (denoted as f_1 for Ti and f_2 for V) above the monolayer point are as follows:

$$I(Ti) = (1 - x)[\exp(-f_1)] + x\,[\exp(-nf_1)]$$
$$I(V) = (1 - x)[1 - \exp(-f_2)] + x\,[1 - \exp(nf_2)]$$

The value of the intensity ratio may then easily be calculated as a function of the variable terms. Initially

the escape depths for electrons in TiO_2 and in V_2O_5 are assumed equal (1.5 nm) and the values of d also equal (0.5 nm): thus $f_1 = f_2 = 0.\dot{3}$. The above expressions suppose that only those electrons reach the detector which are emitted through the monolayer or the top of the "towers". This is likely to be approximately true if the "towers" are not too high and for that part of the sample exposed to the incident X-rays and hence sensed by the measurements.

The expression for the I(Ti) shows two terms. The first term $(1 - x)[\exp(-f_1)]$ represents those electrons emitted from the TiO_2 under the surface covered only by the VO_x monolayer. The second term $x\ [\exp(-nf_1)]$ represents the electrons emitted from the TiO_2 which is covered by VO_x towers and passing perpendicularly through them. The value of this term decreases with increasing number of layers in the towers.

The expression for the I(V) also shows two terms. The first term $(1 - x)[1 - \exp(-f_2)]$ represents the electrons emitted from the VO_x monolayer. The second term $x\ [1 - \exp(-nf_2)]$ represents the electrons emitted from the top of the VO_x "towers".